

**Validation of Laboratory Cracking Tests for Field Top-down Cracking Performance**

by

Chen Chen

A dissertation submitted to the Graduate Faculty of  
Auburn University  
in partial fulfillment of the  
requirements for the Degree of  
Doctor of Philosophy

Auburn, Alabama  
May 2, 2020

Keywords: Top-down Cracking, Laboratory Cracking Tests, Field Cracking Performance,  
Critical Loose Mixture Aging, Correlation

Copyright 2020 by Chen Chen

Approved by

Randy West, Chair, Director, National Center for Asphalt Technology  
Nam Tran, Assistant Director, National Center for Asphalt Technology  
Fan Yin, Assistant Research Professor, National Center for Asphalt Technology  
Benjamin Bowers, Assistant Professor, Civil Engineering  
Maria Auad, Director and Professor, Chemical Engineering

## ABSTRACT

Top-down cracking (TDC) has been widely reported as a primary mode of distress in asphalt pavements. Currently there is no consensus on a practical laboratory cracking test that can reliably predict an asphalt mixture's resistance to TDC. Age hardening of asphalt binder has been identified as a critical factor that contributes to the development of TDC. Thus, laboratory specimens should be conditioned prior to testing to simulate the aging of pavements in-service. However, there is insufficient guidance on an appropriate aging protocol to simulate the critical field aging condition when TDC starts to develop. To address these needs regarding TDC, this study had two objectives: 1) identify the field aging condition when TDC starts to develop, then determine a laboratory aging protocol to condition asphalt mixtures for TDC evaluations; 2) evaluate the ability of laboratory cracking tests to identify mixtures resistant to TDC based on measured cracking performance in the real pavements using real loading conditions.

In 2015, National Center for Asphalt Technology (NCAT) initiated an experiment on the NCAT Test Track (hereinafter referred to as the NCAT TDC experiment). Seven surface mixtures with a range of cracking susceptibilities were designed and constructed as a 1.5-inch surface layer on top of highly modified base and binder layers. After construction, truck traffic was applied to the test sections. Field cracking has been monitored weekly throughout the experiment. Six laboratory cracking tests were selected by the experiment sponsors: Energy Ratio (ER), the Texas Overlay Test (TX-OT), the NCAT Modified Overlay Test (NCAT-OT), the Semi-Circular Bend test (SCB), the Illinois Flexibility Index Test (I-FIT), and the indirect tensile asphalt cracking test (IDEAL-CT).

A literature review was first conducted to determine the field aging condition for evaluating TDC. Data from a number of existing pavements showed that TDC typically initiated

after approximately 70,000 cumulative degree-days (CDD). Both plant loose mixtures and field cores from five field projects in three states were used to determine an aging protocol that was representative of this critical CDD. The loose mixtures from each project were conditioned using four loose mixture aging protocols, including a 6-hour, 135°C protocol, a 12-hour, 135°C protocol, a 24-hour, 135°C protocol, and a 5-day, 95°C protocol. Asphalt binder extracted from conditioned loose mixtures and field cores were tested using a dynamic shear rheometer (DSR), a bending beam rheometer (BBR), and Fourier Transform Infrared Spectroscopy (FT-IR). Test results showed that the 5-day, 95°C protocol was most representative of 70,000 CDD of field aging, and an 8-hour, 135°C and 5-day, 95°C protocol was likely to achieve an equivalent aging level. Thus, the more practical 8-hour, 135°C protocol was selected for the remaining study to simulate 70,000 CDD of field aging.

Two candidate critical aging (CA) protocols for loose mixture aging, 5 days at 95°C and 8 hours at 135°C, were further evaluated using four NCAT TDC experimental mixtures. For each mixture, the plant loose mixtures were conditioned using both protocols. Field cores were also collected annually after construction. Mixture and binder properties of the conditioned loose mixtures and field cores were tested and compared using I-FIT, IDEAL-CT, small-specimen Asphalt Mixture Performance Tester (AMPT) cyclic fatigue, linear amplitude (LAS), double-edge-notched tension (DENT), DSR, BBR, and FT-IR tests. Test results showed inconsistent trends when comparing two candidate CA protocols. Only I-FIT results indicated no significant difference between two protocols. Most of the asphalt binder and mixture properties indicated that two candidate CA protocols yielded a more severe aging level than 4 years field aging in Alabama.

Seven NCAT TDC mixtures, including both plant-produced and laboratory-prepared mixtures, were conditioned and tested using the six selected cracking tests. Test results were utilized to conduct comparison, sensitivity, and correlation analyses. No significant differences were identified between plant mixture and laboratory mixture results after critical aging for all the mixture cracking test parameters. In addition, all the cracking test parameters of I-FIT, IDEAL-CT, and both OT tests were sensitive to aging for plant and laboratory mixtures. ER and  $J_c$  were not sensitive to aging for both plant mixtures and laboratory mixtures. Some cracking test parameters were found to be sensitive to air voids, recycled asphalt mixture, and modified binder for certain conditions, but not in every case considering combinations of plant- and lab-produced mixtures with short-term and critically aged conditioning. Based on mean value analysis, only NCAT- $\beta$  was sensitive to all the influence factors for plant mixture at both aging conditions. The cracking test parameters of both OT tests were sensitive to all the influence factors for laboratory mixtures. Strong positive linear correlations exist among NCAT- $N_f$ , TX- $N_f$ , FI, and  $CT_{Index}$  results, and there are strong power relationships between the  $N_f$  and  $\beta$  parameters for both OT tests.

The field cracking performance of seven test sections were utilized to evaluate the laboratory cracking test results. After approximately 15 million ESALs and 73,728 CDD, sections N1, N2, N5, and N8 exhibited a range of cracking severity and extent. Section N8 with 5% RAS had the highest cracking percentage of 70.7% of the lane area. No measurable cracks were found in sections S5, S6 or S13. The Pearson's correlation coefficient ( $r_p$ ) results indicated that NCAT- $\beta$  and TX- $\beta$  generally have a very strong linear correlation with the field cracking performance for both plant mixtures and laboratory mixtures at both aging conditions.  $DCSE_{Min}$ , TX- $N_f$ , TX- $\beta$ , NCAT- $N_f$ , NCAT- $\beta$ , FI, and  $CT_{Index}$  correctly identified mixture N8 as the most

susceptible to TDC for both plant mixtures and laboratory mixtures at both aging conditions. ER did not identify mixture N8 as the most susceptible to TDC. No cracking test parameter discriminated uncracked sections from cracked sections for both plant mixture and laboratory mixture at both aging conditions.

The test sections will remain in place for additional trafficking and environmental aging on the NCAT Test Track. This ongoing work will help further validate the aging protocols and identify the best test for determining the TDC susceptibility of asphalt mixtures for possible use in mix design and quality assurance.

## ACKNOWLEDGMENTS

I would like to sincerely thank my advisor and committee chair, Dr. Randy West, for his guidance and support during my Ph.D. period. I really appreciated the opportunity he provided to study at NCAT and have a great life experience at Auburn. I still remembered that he spent few hours to introducing the cracking group project and my courses schedule in detail when we first met. His diligent and well-organized working style deeply impress and influence me throughout my research and study. He always gave me meticulous guidance for my academical writing and career planning, and provided thoughtful assistance during the research and study. I am very grateful and honored to have been his student.

Secondly, I would like to thank Dr. Nam Tran, Dr. Fan Yin, Dr. Benjamin Bowers, and Dr. Maria Auad for serving as my committee members. I greatly appreciated their patience and assistance for giving me valuable comments to improve my dissertation and research ability. Special acknowledgements should go to Dr. Fan Yin for his guidance and suggestion regarding analyzing data, academical writing and presentation, and experimental planning throughout my research.

Thirdly, I would like to thank Adam Taylor for his assistance with laboratory tests, he was always patient to give me training and provide great suggestions for my research. I would also like to thank Jason Moore and Nathan Moore for their assistance during my laboratory work. The completion of my dissertation would not have been possible without the assistance of Pamela Turner and Tina Ferguson, and I acknowledged their incredible work for conducting binder and mixture tests. Additionally, I would also like to thank Jason Nelson, Matt Sasser, and many other lab technicians and co-op students for assisting me with data collection and laboratory work.

Next, I would like to express my sincere appreciation to the NCAT family, and I am very honored and grateful to be a member of NCAT family. NCAT family not only provided professional knowledge and guidance throughout my study, but also made me feel at home because the tremendous support and care they gave. I would also like to thank Dr. Fan Gu for his assistance and suggestion regarding academic writing and professional skills throughout my study. Special thanks to Vickie Adams and her family for sharing their wonderful southern life experience, including rodeo competition, wagon train, horse adventure, and lots of family activities.

I wish to thank all my friends for their continuous and unconditional care and support during these years. It was impossible for me to have such a wonderful research and life experience without their accompany, and it was their encouragement and recognition that kept me working hard and being a better person.

Finally, I want to thank my parents, brother, sister-in-law, and little niece for their priceless support and love, and I could not have completed this dissertation without them.

## TABLE OF CONTENTS

ABSTRACT .....	2
ACKNOWLEDGMENTS .....	6
LIST OF TABLES .....	14
LIST OF FIGURES .....	16
CHAPTER 1 INTRODUCTION .....	21
1.1 Problem Statement.....	21
1.2 Objectives.....	23
1.3 Scope.....	23
1.4 Organization of this Dissertation .....	24
CHAPTER 2 LITERATURE REVIEW .....	26
2.1 Mechanisms of Top-down Cracking.....	26
2.2 Influence Factors for Top-down Cracking .....	28
2.3 Long Term Oven Aging.....	30
2.4 Laboratory Mixture Cracking Tests.....	34
2.4.1 Energy Ratio .....	34
2.4.2 Texas Overlay Test.....	35
2.4.3 NCAT Modified Overlay Test .....	38
2.4.4 Semi-circular Bend Test .....	40
2.4.5 Illinois Flexibility Index Test.....	42
2.4.6 Indirect Tensile Asphalt Cracking Test (a.k.a, IDEAL-Cracking Test).....	44

CHAPTER 3 RESEARCH METHODOLOGY .....	46
3.1 Experimental Plan.....	46
3.1.1 Construction of NCAT TDC Experimental Test Sections .....	46
3.1.2 Determination of the Critical Aging Protocol for NCAT TDC Experiment .....	47
3.1.3 Laboratory Cracking Tests of NCAT TDC Experiment .....	48
3.2 Materials.....	50
3.2.1 Materials used to Select the Preliminary Critical Aging Protocol .....	50
3.2.2 NCAT TDC Experimental Mixtures.....	50
3.3 Laboratory Binder Tests .....	53
3.3.1 Dynamic Shear Rheometer .....	53
3.3.2 Bending Beam Rheometer .....	55
3.3.3 Double-Edge-Notched Tension (DENT) Test .....	57
3.3.4 Fourier Transform Infrared Spectroscopy .....	59
3.4 Laboratory Mixture Cracking Tests .....	61
3.4.1 Energy Ratio .....	61
3.4.2 Texas Overlay Test .....	63
3.4.3 NCAT Modified Overlay Test.....	66
3.4.4 Semi-Circular Bend Test.....	67
3.4.5 Illinois Flexibility Index Test.....	70
3.4.6 Indirect Tensile Asphalt Cracking Test.....	72

3.4.7 Small-Specimen AMPT Cyclic Fatigue Test.....	74
3.4.8 Summary.....	76
CHAPTER 4 SELECTING A PRELIMINARY CRITICAL AGING PROTOCOL.....	78
4.1 Identification of Critical Field Aging for TDC .....	78
4.2 Experimental Design.....	81
4.3 Tests Results and Data analysis.....	84
4.3.1 Comparisons of Laboratory Aging Protocols .....	84
4.3.2 Correlation of Field Aging with Laboratory Aging Protocols.....	94
4.3.3 Selection of Alternative Aging Protocol at 135°C .....	96
4.4 Summary .....	98
CHAPTER 5 PRELIMINARY VALIDATION OF THE CRITICAL AGING PROTOCOL ...	100
5.1 Experimental Design.....	100
5.2 Comparison of Two Candidate Critical Aging Protocols .....	102
5.2.1 I-FIT Results .....	103
5.2.2 IDEAL-CT Results.....	104
5.2.3 Small-Specimen AMPT Cyclic Fatigue Test Results .....	105
5.2.4 Glover-Rowe Parameter Results .....	106
5.2.5 LAS Test Results.....	107
5.2.6 $\Delta T_c$ Results .....	108
5.2.7 DENT Test Results.....	109

5.3 Evolution of Asphalt Binder and Mixtures Properties with Field Aging .....	110
5.3.1 I-FIT Results .....	111
5.3.2 Continuous PG Results.....	112
5.3.3 Glover-Rowe Parameter Results .....	113
5.3.4 $\Delta T_c$ Results .....	114
5.3.5 LAS Results .....	115
5.3.6 FT-IR Results.....	116
5.4 Correlation between Laboratory Critical Aging Protocols and Field Aging .....	117
5.5. Summary .....	120
CHAPTER 6 LABORATORY MIXTURE CRACKING TEST RESULTS.....	123
6.1 Experimental Design.....	123
6.1.1 Sensitivity Groups .....	124
6.1.2 Sample Preparation.....	125
6.1.3 Statistical Analysis .....	126
6.2 Comparison Analysis between Plant Mixtures and Laboratory Mixtures .....	127
6.2.1 Energy Ratio .....	128
6.2.2 Texas Overlay Test.....	132
6.2.3 NCAT Modified Overlay Test .....	135
6.2.4 Semi-Circular Bend Test .....	137
6.2.5 Illinois Flexibility Index Test.....	139

6.2.6 Indirect Tensile Asphalt Cracking Test .....	140
6.2.7 Summary of Comparison Analysis between Plant mixtures and Laboratory Mixtures .....	142
6.3 Sensitivity Analyses.....	144
6.3.1 Aging Sensitivity.....	144
6.3.2 Air Voids Sensitivity .....	158
6.3.3 Recycled Asphalt Materials Sensitivity.....	162
6.3.4 Modified Binder Sensitivity.....	166
6.4 Correlations between Different Laboratory Cracking Tests .....	170
6.5 Summary .....	173
CHAPTER 7 PRELIMINARY VALIDATION OF LABORATORY CRACKING TESTS.....	176
7.1 Preliminary Field Cracking Performance.....	176
7.2 Correlations between Field Cracking Performance and Laboratory Cracking Test Results .....	178
7.2.1 Analysis of Pearson’s Correlation Coefficient.....	178
7.2.2 Identification of the most Susceptible Mixture to TDC .....	179
7.2.3 Discrimination between Cracked Sections and Uncracked Sections .....	181
7.3 Summary .....	182
CHAPTER 8 CONCLUSIONS AND RECOMMENDATIONS.....	185
8.1 Determination of a Critical Aging Protocol .....	185
8.2 Preliminary Evaluation of Laboratory Cracking Tests .....	186

8.3 Recommendations for Future Research .....	188
REFERENCES .....	190

## LIST OF TABLES

Table 1. 1 Summary of Laboratory Load-related Cracking Tests .....	22
Table 3. 1 Summary of Field Projects.....	50
Table 3. 2 Mix Design and Quality Control Properties of the NCAT TDC Experimental Test Sections .....	52
Table 3. 3 Summary of Laboratory Cracking Tests.....	77
Table 4. 1 Summary of Construction and Coring Dates .....	82
Table 5. 1 Summary of Representative CDD (x 1,000) Values for CA1 Protocol of Loose Mixture Aging for 5 days at 95°C.....	119
Table 5. 2 Summary of Representative CDD (x 1,000) Values for CA2 Protocol of Loose Mixture Aging for 8 hours at 135°C .....	120
Table 6. 1 <i>p-value</i> Summary of Comparison Analysis .....	143
Table 6. 2 Summary of Mixtures showing Statistical Difference during <i>t-test</i> .....	143
Table 6. 3 Summary of Aging Sensitivity Analysis .....	158
Table 6. 4 Summary of Air Voids Sensitivity Analysis for Plant Mixtures.....	161
Table 6. 5 Summary of Air Voids Sensitivity Analysis for Laboratory Mixtures.....	162
Table 6. 6 Summary of Recycled Asphalt Materials Sensitivity Analysis for Plant Mixtures ...	165
Table 6. 7 Summary of Recycled Materials Sensitivity Analysis for Laboratory Mixtures .....	166
Table 6. 8 Summary of Modified Binder Sensitivity Analysis for Plant Mixtures .....	169
Table 6. 9 Summary of Modified Binder Sensitivity Analysis for Laboratory Mixtures .....	170
Table 6. 10 Summary of Pearson Correlation Coefficients.....	171
Table 7. 1 Preliminary Field Cracking Performance Summary .....	177
Table 7. 2 Summary of $r_p$ between Cracking test parameter and Field Cracking Performance ..	179

Table 7. 3 Identification Results of the Most Susceptible Mixture to TDC.....180

Table 7. 4 Discrimination Results between Cracked and Uncracked Sections.....182

## LIST OF FIGURES

Figure 1. 1 Typical TDC and a Corresponding Field Core .....	21
Figure 2. 1 Mechanisms of TDC Initiation Process; (a) Bending Mechanism, (b) Near-tire Mechanism.....	27
Figure 3. 1 Pavement Structure of NCAT TDC Experimental Test Sections .....	47
Figure 3. 2 Experimental Plan .....	49
Figure 3. 3 DSR Test; (a) DSR Equipment, (b) Sample Preparation .....	53
Figure 3. 4 BBR Test; (a) Test Equipment, (b) Loading Frame.....	56
Figure 3. 5 BBR Sample Preparation.....	56
Figure 3. 6 Nicolet 6700 FT-IR Spectrometer and Mechanism of ATR .....	59
Figure 3. 7 Illustration of FT-IR Analysis; (a) Full Spectrum, (b) FT-IR Carbonyl Area.....	60
Figure 3. 8 Energy Ratio Test Specimen Setup.....	62
Figure 3. 9 Energy Ratio Concept; .....	63
Figure 3. 10 TX-OT Specimen Setup .....	64
Figure 3. 11 Illustration of the New Analysis Methodology of TX-OT; (a) $W_c$ , (b) $\beta$ .....	66
Figure 3. 12 Determination of the failure point for NCAT-OT vs. TX-OT.....	67
Figure 3. 13 SCB Specimen and Test Setup; (a) Notched Specimens, (b) Test Setup.....	68
Figure 3. 14 Methodology of SCB Analysis; .....	69
Figure 3. 15 I-FIT Test Setup and Specimen; (a) Test Setup, (b) I-FIT Specimen .....	70
Figure 3. 16 Illustration of I-FIT Analysis .....	71
Figure 3. 17 IDEAL-CT Test Setup.....	73
Figure 3. 18 Illustration of IDEAL-CT Analysis.....	74
Figure 4. 1 Wheel-path Longitudinal Crack Survey Results;.....	80

Figure 4. 2 A Map showing the Number of Years to Reach 70,000 CDD.....	81
Figure 4. 3 Research Methodology for Laboratory Aging .....	82
Figure 4. 4 HPG Results of Plant Production Mixtures; (a) HPG Results before and after Storage, (b) Correlation between Change in HPG with the Storage Time .....	83
Figure 4. 5 Continuous PG Results of Extracted Asphalt Binders with Various Loose Mixture Aging Protocols; (a) High-Temperature, (b) Low-Temperature .....	86
Figure 4. 6 G-R Parameter Results in Black Space Diagram; (a) Mix 1, (b) Mix 2, (c) Mix 3, (d) Mix 4, (e) Mix 5.....	89
Figure 4. 7 BBR $\Delta T_c$ Results of Extracted Asphalt Binders with Various Loose Mixture Aging Protocols.....	90
Figure 4. 8 FT-IR CA Results of Extracted Asphalt Binders with Various Loose Mixture Aging Protocols.....	91
Figure 4. 9 G-R HS Results; (a) Mix 1, (b) Mix 2, (c) Mix 3, (d) Mix 4, (e) Mix 5 .....	93
Figure 4. 10 Comparison of Field Aging and Laboratory Loose Mixture Aging Protocols; (a) 5- day, 95°C, (b) 6-hour, 135°C, (c) 12-hour, 135°C, (d) 24-hour, 135°C .....	95
Figure 4. 11 Determination of Equivalent Aging Time at 135°C; (a) Example of Mix 2 FT-IR CA Results, (b) Summary of All Results .....	98
Figure 5. 1 Aging Validation Experimental Design .....	102
Figure 5. 2 I-FIT Results of PMLC Specimens with Different Aging Conditions.....	104
Figure 5. 3 IDEAL-CT Test Results of PMLC Specimens with Different Aging Conditions....	105
Figure 5. 4 AMPT Cyclic Fatigue Test Results of PMLC Specimens with Different Aging Conditions.....	106

Figure 5. 5 G-R Parameter Results of Extracted Binders from PMLC Specimens with Different Aging Conditions .....	107
Figure 5. 6 LAS-N <sub>f</sub> (5.0%) Parameter Results of Extracted Binders from PMLC Specimens with Different Aging Conditions .....	108
Figure 5. 7 ΔT <sub>c</sub> Results of Extracted Binders from PMLC Specimens with Different Aging Conditions.....	109
Figure 5. 8 DENT Test Results of Extracted Binders from PMLC Specimens with Different Aging Conditions .....	110
Figure 5. 9 I-FIT Results of Reheated PMLC Specimen and Post-Construction Field Cores ....	111
Figure 5. 10 Continuous PG Results of Extracted Binders from Reheated Plant Mixture and Post-Construction Field Cores; (a) High-Temperature, (b) Low-Temperature.....	113
Figure 5. 11 Glover-Rowe Parameter Results of Extracted Binders from Reheated Plant Mixture and Post-Construction Field Cores .....	114
Figure 5. 12 ΔT <sub>c</sub> Results of Extracted Binders from Reheated Plant Mixture and Post-Construction Field Cores.....	115
Figure 5. 13 LAS-N <sub>f</sub> Results of Extracted Binders from Reheated Plant Mixture and Post-Construction Field Cores.....	116
Figure 5. 14 FT-IR Carbonyl Area Results of Extracted Binders from Reheated Plant Mixture and Post-Construction Field Cores .....	117
Figure 5. 15 An Example to Illustrate the Determination of the Representative CDD for the Two Candidate CA Protocols using the I-FIT Results of Mix S6.....	118
Figure 6. 1 Research Methodology for Laboratory Cracking Tests .....	124

Figure 6. 2 ER Test Results of PMLC-RH and LMLC-STOA; (a) $DCSE_{HMA}$ Results, (b) $DCSE_{Min}$ Results, (c) ER Results.....	130
Figure 6. 3 ER Test Results of PMLC-CA and LMLC-CA; (a) $DCSE_{HMA}$ Results, (b) $DCSE_{Min}$ Results, (c) ER Results.....	132
Figure 6. 4 TX-OT Test Results of PMLC-RH and LMLC-STOA; (a) $TX-N_f$ Results, (b) $TX-\beta$ .....	134
Figure 6. 5 TX-OT Test Results of PMLC-CA and LMLC-CA; (a) $TX-N_f$ Results, (b) $TX-\beta$ ..	135
Figure 6. 6 NCAT-OT Test Results of PMLC-RH and LMLC-STOA; (a) NCAT- $N_f$ Results, (b) NCAT- $\beta$ .....	136
Figure 6. 7 NCAT-OT Test Results of PMLC-CA and LMLC-CA; (a) NCAT- $N_f$ Results, (b) NCAT- $\beta$ .....	137
Figure 6. 8 SCB Test Results of PMLC-RH and LMLC-STOA.....	138
Figure 6. 9 SCB Test Results of PMLC-CA and LMLC-CA.....	138
Figure 6. 10 I-FIT Test Results of PMLC-RH and LMLC-STOA.....	140
Figure 6. 11 I-FIT Test Results of PMLC-CA and LMLC-CA.....	140
Figure 6. 12 IDEAL-CT Test Results of PMLC-RH and LMLC-STOA.....	141
Figure 6. 13 IDEAL-CT Test Results of PMLC-CA and LMLC-CA .....	142
Figure 6. 14 Aging Sensitivity Results of ER Test to Laboratory Mixtures; (a) $DCSE_{HMA}$ Results, (b) $DCSE_{Min}$ Results, (c) ER Results .....	146
Figure 6. 15 Aging Sensitivity Results of ER Test to Plant Mixtures; (a) $DCSE_{HMA}$ Results, (b) $DCSE_{Min}$ Results, (c) ER Results.....	148
Figure 6. 16 Aging Sensitivity Results of TX-OT Test to Laboratory Mixtures; (a) $TX-N_f$ Results, (b) $TX-\beta$ Results .....	149

Figure 6. 17 Aging Sensitivity Results of TX-OT Test to Plant Mixtures; (a) TX- $N_f$ Results, (b) TX- $\beta$ Results .....	151
Figure 6. 18 Aging Sensitivity Results of NCAT-OT Test to Laboratory Mixtures; (a) NCAT- $N_f$ Results, (b) NCAT- $\beta$ Results .....	152
Figure 6. 19 Aging Sensitivity Results of NCAT-OT Test to Plant Mixtures; (a) NCAT- $N_f$ Results, (b) NCAT- $\beta$ Results .....	153
Figure 6. 20 Aging Sensitivity of SCB Test to Laboratory Mixtures .....	154
Figure 6. 21 Aging Sensitivity of SCB Test to Plant Mixtures .....	155
Figure 6. 22 Aging Sensitivity of I-FIT Test to Laboratory Mixtures .....	156
Figure 6. 23 Aging Sensitivity of I-FIT Test to Plant Mixtures .....	156
Figure 6. 24 Aging Sensitivity of IDEAL-CT Test to Laboratory Mixtures.....	157
Figure 6. 25 Aging Sensitivity of IDEAL-CT Test to Plant Mixtures.....	157
Figure 6. 26 Examples of Air Voids Sensitivity; (a) ER Results, (b) $CT_{Index}$ Results .....	160
Figure 6. 27 Examples of Recycled Asphalt Materials Sensitivity; .....	164
Figure 6. 28 Examples of Modified Binder Sensitivity; .....	168
Figure 6. 29 OT $N_f$ versus $\beta$ Correlations; (a) NCAT-OT Results, (b) TX-OT Results.....	172
Figure 7. 1 Cracks on Section N8 and Field Core .....	177
Figure 7. 2 Example of Discrimination between Cracked and Uncracked Sections .....	181

## CHAPTER 1 INTRODUCTION

### 1.1 Problem Statement

Top-down cracking (TDC) has been widely reported as a common mode of distress in asphalt pavements (Hugo and Kennedy, 1985; Gerritsen et al., 1987; Myers et al., 1998). Different from traditional bottom-up fatigue cracking, TDC initiates at the surface of an asphalt pavement in or near the wheel-path and propagates downward through the asphalt layers (Myer et al., 1998).

Figure 1.1 shows typical TDC in the wheel-path and a corresponding field core.



**Figure 1. 1 Typical TDC and a Corresponding Field Core**

Several mechanisms of TDC development have been proposed, including high bending-induced surface tension, shear-induced near-surface tension due to tire-pavement interactions (Hugo and Kennedy, 1985; Gerritsen et al., 1987; Zou and Roque, 2011). Factors that have been identified that contribute to the development of TDC include traffic loading, pavement structure, and mixture properties (Myers et al., 1998; Myers and Roque, 2002; Roque et al., 2004).

Additionally, aging of asphalt binder in the surface layer has also been identified as a critical

factor (Myers et al., 1998; Matsuno and Nishizawa, 1992; Hugo and Kennedy, 1985). Age hardening of asphalt binder stiffens and embrittles surface mixtures resulting in greater thermal stresses and higher potential of cracking initiation on the pavement surface (Myers and Roque, 2002; Roque et al., 2004). TDC results in the need for pavement rehabilitation, such as milling and placing a new surface layer. If mixtures susceptible to TDC can be identified during the mixture design process, the occurrence of premature surface distress would be avoided or mitigated. Therefore, there is an urgent need to select a suitable laboratory cracking test for TDC as part of mixture design and quality assurance. Over the last few decades, several cracking tests have been developed by various researchers, although only a few of the tests have been implemented for projects by a small number of highway agencies. Load-related cracking tests, such as those listed in Table 1.1, have been used by researchers to evaluate the cracking resistance of asphalt mixtures. However, there is no consensus regarding the most appropriate cracking test to predict TDC.

**Table 1. 1 Summary of Laboratory Load-related Cracking Tests**

<b>Test Name</b>	<b>References</b>
Energy Ratio (ER)	Roque et al., 2004
Texas Overlay Test (TX-OT)	Tex-248-F
NCAT Modified OT (NCAT-OT)	Ma, 2014
Semi-circular Bend Test (SCB)	Mull et al., 2002
Illinois Flexibility Index Test (I-FIT)	AASHTO TP 124
Indirect Tensile Asphalt Cracking Test (IDEAL-CT)	ASTM D 8255-19
Bending Beam Fatigue Test (BBFT)	AASHTO T 321
Simplified Viscoelastic Continuum Damage Test (S-VECD)	AASHTO TP 107

Considering the importance of aging in the development of TDC in asphalt pavement surface layers, it is logical to include appropriate short-term and long-term laboratory aging prior

to testing to simulate the aging that occurs during mixture production and the first few years of service, respectively.

According to AASHTO R 30, the standard method for laboratory short-term oven aging (STOA) is to condition loose mixtures for four hours at 135°C. For long-term oven aging (LTOA), AASHTO R 30 calls for conditioning of compacted specimens for five days at 85°C. Instead of conditioning compacted specimens, a number of loose mixture oven aging protocols have been used to simulate field aging using different times and oven temperatures (Braham et al., 2009; Reinke et al., 2015; Elwardany et al., 2017). However, these aging protocols have not been adequately related to in-service field aging. In addition, the traditional expectation of LTOA to simulate seven to ten years of field aging may not be appropriate to evaluate TDC, since most of these cracks have been reported to develop within a significantly shorter period (i.e., three to five years) (Myers et al., 1998; Uhlmeier et al., 2000; Dauzats and Rampal, 1987).

## **1.2 Objectives**

Based on the problems described above, the objectives of this study were set to:

- (1) Identify the critical field aging condition when TDC starts to develop, then determine a critical aging (CA) protocol to condition asphalt mixtures for TDC evaluation.
- (2) Validate laboratory cracking tests by establishing correlations between the test results and measured cracking performance of test sections on the NCAT Test Track.

## **1.3 Scope**

In 2015, the National Center for Asphalt Technology (NCAT) initiated a study to gain more understanding about TDC and to evaluate laboratory cracking tests for their suitability in identifying mixtures susceptible to TDC (hereinafter referred to as the NCAT TDC experiment).

Seven surface mixtures with a range of expected cracking potential were designed and constructed on the NCAT Test Track. Each mixture was constructed as a 1.5-inch surface layer on top of highly polymer modified base and binder layers. Six laboratory cracking tests were selected by the experiment sponsors: ER, TX-OT, NCAT-OT, SCB, I-FIT, and IDEAL-CT.

Prior to laboratory testing of the mixtures in the NCAT TDC experiment, materials from five projects were utilized to determine a preliminary critical aging protocol. The NCAT TDC experimental materials were subsequently used to validate the preliminary critical aging protocol by comparing the mixture and binder properties between critically aged plant mixtures and field cores. Furthermore, six laboratory cracking tests were conducted to evaluate the cracking resistance of seven NCAT TDC experimental mixtures. Lastly, the laboratory cracking tests can be validated through examining the correlations between laboratory test results and measured field cracking performance.

#### **1.4 Organization of this Dissertation**

This dissertation consists of eight chapters. Chapter 1 describes the problems related to TDC evaluation and states the objectives and overall scope of this study. Chapter 2 contains a literature review of the mechanism and influence factors for the development of TDC, long-term oven aging methods, and six laboratory mixture cracking tests. Chapter 3 explains the research methodology and summarizes the materials, laboratory binder tests and mixture cracking tests used in this study. Chapter 4 presents the process of determining the preliminary critical aging protocol, and the critical field aging condition is identified in this section. Chapter 5 describes the validation of the preliminary aging protocol using the NCAT TDC experimental mixtures. Chapter 6 summarizes the laboratory cracking test results and analyses of seven mixtures, including comparison, sensitivity, and correlation analyses. Chapter 7 presents the preliminary

findings of the correlations between field cracking performance and six laboratory cracking tests.

Chapter 8 presents the conclusions and recommendations of this study.

## CHAPTER 2 LITERATURE REVIEW

This chapter conducts a literature review regarding the proposed mechanisms and influence factors of TDC. Meanwhile, the studies of long-term oven aging methods and six laboratory cracking tests were also reviewed and summarized in this section.

### 2.1 Mechanisms of Top-down Cracking

TDC is commonly longitudinal or transverse crack that initiates at the pavement surface and propagates downward (Baladi et al., 2003). The formation of TDC consists of two phases: initiation and propagation. The most widely accepted hypothesis for cracking initiation proposes that cracks are generated by micro-fracture damage (Lytton et al., 1993; Li, 1999), then the cracks propagate through the whole asphalt layer (Little et al., 2001). Over the last decades, two mechanisms have been proposed to explain the initiation of longitudinal TDC (Roque et al., 2010; Zou and Roque, 2011), which included: 1) bending mechanism: bending-induced surface tension away from the tire; and 2) near-tire mechanism: shear-induced surface tension at the edge of the tire, as shown in Figure 2.1. The study of Zou and Roque (2011) implied that the bending mechanism was primarily used to explain the TDC initiation in pavements with thin to medium (2.5 to 5.0 inches) asphalt layers, and the near-tire mechanism was appropriate for the pavements with thick (7.5 to 10.0 inches) asphalt layers. However, the studies about the initiation of transverse TDC were limited (Baladi et al., 2003; Gu et al., 2018). Gu et al. (2018) developed a three-dimensional finite element model to simulate the critical responses of asphalt pavement. The simulation results indicated that the near tire-front surface in longitudinal direction was compressed, and the maximum longitudinal tensile stress near the load center (around 0.6 m) could induce the transverse TDC. In addition, the study of Baladi et al. (2003) indicated that the

short transverse TDC might be caused by the thermal stress and asphalt aging based on the field investigation.

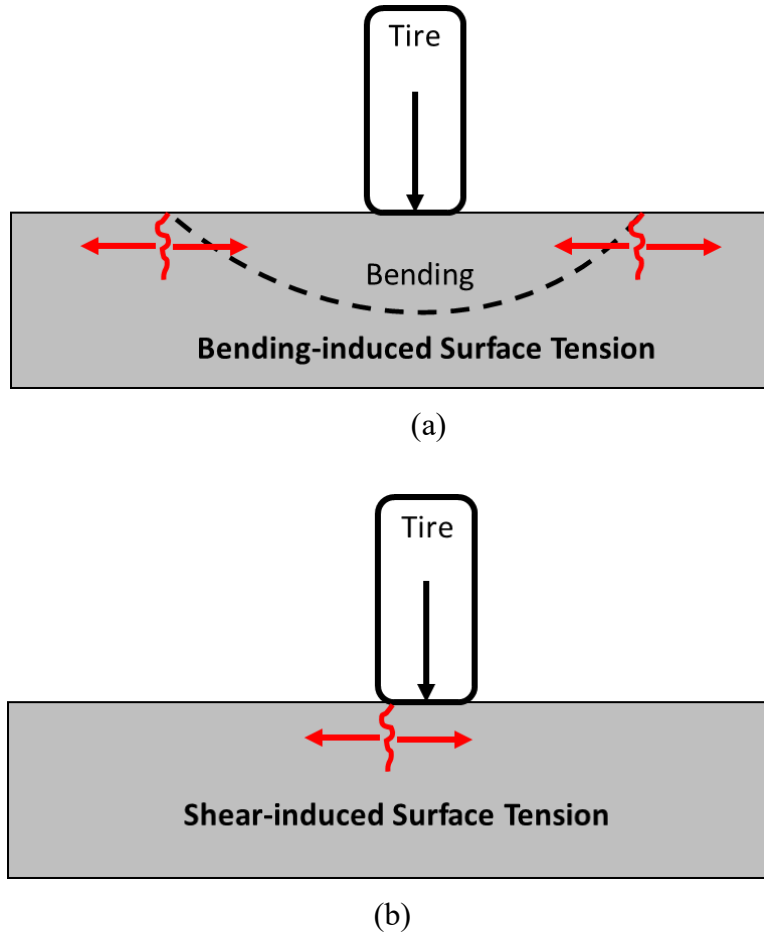


**Figure 2. 1 Mechanisms of TDC Initiation Process; (a) Bending Mechanism, (b) Near-tire Mechanism**

After crack initiation, the cracks propagate downward into the pavement. The mechanisms of crack propagation are different than crack initiation and are highly dependent on load magnitudes and positions, stiffness gradients in asphalt layers (induced by temperature gradients and aging), and pavement structure (Myers, 2000). Based on the study of Myers (2000), the TDC propagation mechanism was primarily a Mode I tensile mechanism, and the propagation speed depends on the crack length, pavement thickness, and mixture gradation. In general, thinner pavements and coarser gradations are expected to have faster propagation speeds

(Myers, 2000; Zou and Roque, 2011). In contrast, Nesnas and Nunn (2004) indicated that the TDC propagation mechanism was mainly in shear mode for composite pavements, which was significantly affected by binder aging and pavement structure.

## **2.2 Influence Factors for Top-down Cracking**

TDC has received increasing attention in recent years. Some research has been devoted to explaining the cause of TDC and the critical factors that contribute to it (Myers, 2000; Roque et al., 2004; Min Baek, 2010; Zou and Roque, 2011; Wu and Muhunthan, 2018). Critical factors include:

- Age hardening of asphalt binder
- Climate conditions (e.g., temperature)
- Pavement structure (e.g., layer thickness)
- Mixture properties (e.g., air voids, binder type, and aggregate gradation)
- Traffic loading (e.g., traffic volume, loading magnitude and position)
- Construction quality (e.g., mixture segregation and compaction)

Age hardening stiffens and embrittles asphalt binder in mixtures resulting in greater thermal stresses and higher potential of cracking initiation on the pavement surface (Myers and Roque, 2002; Roque et al., 2004). Additionally, stiffness gradients induced by aging also significantly increased the chance of TDC initiation and propagation (Myers, 2000; Zou and Roque, 2011). The effects of aging on TDC development was confirmed by several field projects where excessive aging was observed in cracked areas (Dauzats and Linder, 1982; Gerritsen et al., 1987; Matsuno and Nishizawa, 1992).

TDC has been reported in different climates, and temperature was identified as a critical factor for the development of TDC. Stiffness gradients induced by temperature gradients with depth affected propagation of TDC (Myers, 2000; Myers and Roque, 2002). Other studies indicated that pavements in higher temperature climates are more susceptible to TDC due to high tensile strains in the pavement surface at the tire edge (Matsuno and Nishizawa, 1992; Freitas et al., 2005; Wang et al., 2003). However, Zou and Roque (2011) argued that the effects of temperature on TDC were not significant because its effects on thermal-induced damage and load-induced damaged appeared to offset.

Pavement structure is also believed to have a strong influence on the development of TDC. Myers (2000) implied that pavements with lower stiffness base layers were more susceptible to TDC. In addition, Zou and Roque (2011) also demonstrated that pavements with thick asphalt structures had better cracking resistance, and the crack propagation speed was faster in a thinner asphalt layer. Similar results were also obtained by Nesnas and Nunn (2004).

Mixture properties also play an important role in cracking performance, including air voids, binder type, aggregate gradation, and mixture strength. Several laboratory and field studies indicated that asphalt layers with higher in-place density have better cracking resistance by increasing stiffness and possibly reducing the rate of aging (Harvey et al., 1996; Fisher et al., 2010; Tran et al., 2016). In addition, the use of polymer-modified binder was shown to improve the cracking performance (Bahia et al., 2001; Kim et al., 2003; Yildirim, 2007; Kök and Çolak, 2011). Myers (2000) indicated that mixtures with coarser gradations yielded faster cracking propagation speed than mixtures with finer gradations. Meanwhile, several studies implied that TDC would more likely initiate on pavements with low strength surface mixtures (Gerritsen et al., 1987; Malan et al., 1989; Wang et al., 2003).

Traffic loading is also recognized as a primary factor for TDC. Myers (2000) indicated that both load magnitude and tire position dramatically affected the initiation and propagation of TDC. A similar result was also found by Myers and Roque (2002). Zou and Roque (2011) also presented that worse cracking performance was observed on pavements with higher traffic levels.

In addition to factors associated with mixture properties and traffic loading, the construction quality of pavement also affects cracking performance. Freitas et al. (2003) investigated the causes of TDC and found that in addition to traffic loading and mixture properties affecting TDC, construction quality as evident with segregation and in-place density were also important. A field project in Colorado found that segregation was the primary cause of TDC (Harmelink and Aschenbrener, 2003).

### **2.3 Long Term Oven Aging**

Long-term oven aging (LTOA) of asphalt mixtures is used to simulate the oxidative aging that occur throughout pavement's service life (Petersen, 2009). In general, there are two commonly used laboratory LTOA protocols: (1) conditioning of compacted specimens in an oven, and (2) conditioning of loose mixtures in an oven prior to compaction (Airey, 2003; Kim et al., 2018). The NCHRP 9-6(1) project was one of the first studies that recommended conditioning compacted specimens in a forced-draft oven at 60°C for 2 days, followed by 3 days at 107°C (Von Quintus et al., 1991). Since then, several similar aging protocols have been developed, requiring the conditioning of compacted specimens at a wide range of temperatures (i.e. 60°C to 100°C) for varying durations (i.e. days to months) (Bell et al., 1994a; Bell et al., 1994b; Brown and Scholz, 2000; Morian et al., 2011; Safaei et al., 2014). The SHRP-A-003A project found that conditioning of compacted specimens for 5 days at 85°C simulated 15 years of field aging in a Wet-No-Freeze climate and 7 years of field aging in a Dry-Freeze climate (Harrigan et al., 1994;

Bell et al., 1994a). This finding was later verified by Brown and Scholz (2000) based on mixture stiffness results. More recently, Harrigan (2007) tested the dynamic modulus of compacted specimens conditioned for 5 days at 80°C, 85°C, and 90°C, and concluded that the 5-day, 95°C protocol was representative of seven to ten years of field aging. This aging protocol was adopted as the standard LTOA procedure for mixture performance testing in AASHTO R 30.

The NCHRP 9-52 project evaluated the validity of this LTOA protocol using over 40 different asphalt mixtures with a wide variety of material components and production parameters. The resilient modulus and Hamburg wheel-tracking test (HWTT) results indicated that conditioning of compacted specimens for 5 days at 85°C was representative of approximately one year of field aging in warmer climates and two years of field aging in colder climates (Newcomb et al., 2015). Similar findings were also reported by Islam et al. (2015) based on bending beam fatigue tests and Howard and Doyle (2015) based on Cantabro tests. Sirin et al. (2018) compared the dynamic modulus of laboratory-produced specimens aged at 85°C for a wide range of durations (i.e. 5 days to 120 days) versus 7-year old field cores, and found that the AASHTO standard LTOA protocol was not severe enough to represent long-term field aging in the hot climate of Qatar. To address this issue, Sirin et al. (2018) recommended extending the aging duration from 5 days to 45 days for base mixtures and 75 days for surface mixtures. In addition to these disparities in aging between the standard LTOA procedure and the field, there are two other concerns regarding specimen integrity due to the use of compacted specimens for LTOA: (1) changes in air voids and geometry caused by specimen softening and slumping and (2) presence of both radial and vertical oxidation gradients within the specimen volume (Houston et al., 2005; Reed, 2010; Elwardany et al., 2017).

Compared to conditioning compacted specimens, loose mixture aging typically yields a more severe level of asphalt aging due to the increased exposure to oxygen and elevated temperature. Additionally, the loose mixture aging process can be accelerated using higher temperatures without concerns of the aforementioned specimen integrity issues. Thus, loose mixture aging has recently been recognized as a more user-friendly alternative for simulating the long-term field aging of asphalt pavements in terms of time efficiency and cost (Sirin et al., 2018). Over the last decade, several loose mixture aging protocols had been used by different researchers with a wide range of temperatures and durations (Roche et al., 2009; Arega et al., 2013; Reinke et al., 2015; Elwardany et al., 2017). Some of these aging protocols, however, were mainly used to prepare artificial reclaimed asphalt pavement (RAP) materials in the laboratory rather than to simulate the long-term field aging of asphalt pavements (Van den Bergh, 2011; Partl et al., 2012). Braham et al. (2009) conditioned the loose mixture at 135°C for 6 to 48 hours and evaluated its effect on mixture fracture energy measured in the Disk-shaped Compact Tension (DCT) test. Meanwhile, the six-year field cores were also collected and used to characterize the effects of field aging on mixture fracture energy. Test results indicated that 24 hours loose mixture aging protocol was representative of approximately 6 years of field aging in Minnesota through interpolation. In a study conducted by Reinke et al. (2015), loose mixtures collected from three test sections on the Minnesota Department of Transportation's Road Research facility (MnROAD) were conditioned at 135°C for 12 and 24 hours. Based on the binder delta T<sub>c</sub> results, the aging protocol of 18 hours at 135°C was found equivalent to 8 years of field aging in Minnesota.

Mensching et al. (2017) explored the impact of short-term aging and two loose mixture aging protocols (i.e., 5 days at 85°C and 24 hours at 135°C) on mixtures with varying levels of

re-refined engine oil bottoms. Cracking resistance indicators for the mixture and binder indicated that the 24-hour, 135°C protocol yielded higher stiffness and lower relaxation properties than the 5-day, 85°C aging protocol. Rahbar-Rastegar et al. (2018) investigated the effect of aging on the viscoelastic and fracture properties of asphalt mixtures using three loose mixture aging protocols: 5 days at 95°C, 12 days at 95°C, and 24 hours at 135°C. Test results indicated that the 135°C aging protocol yielded reduced mixture fracture properties compared to the two 95°C aging protocols. Chen et al. (2018) conditioned loose mixtures with four aging protocols, including 5 days at 95°C, 6 hours at 135°C, 12 hours at 135°C, and 24 hours at 135°C. Based on the binder rheological and chemical test results, the aging temperature did not show a significant effect on the oxidation kinetics of the five asphalt binders tested. Furthermore, the two loose mixture aging protocols of 5 days at 95°C and 8 hours at 135°C were found equivalent and expected to simulate approximately 4 to 5 years of field aging in Alabama. Considering the non-uniform aging of asphalt mixtures with depth (Turner, 2008; Yin et al., 2017a; Elwardany et al., 2017), only the top one inch of the field cores was tested.

In the NCHRP 9-54 project, materials collected from 18 projects with a wide range of material components and characteristics were evaluated in order to develop a mixture LTOA protocol for performance testing and prediction (Kim et al., 2018). The logarithm of the binder complex shear modulus ( $\log |G^*|$ ) and total absorbance area under the carbonyl and sulfoxide peaks in the Fourier transform infrared (FT-IR) spectrum were used to quantify the aging level of laboratory-aged mixtures and field cores. The project evaluated both compacted specimen and loose mixture aging approaches with or without pressure and finally recommended using loose mixture aging without pressure as the most appropriate aging procedure with the consideration of specimen integrity, efficiency, and versatility. The project also compared loose mixture aging at

95°C and 135°C and found that the 135°C aging protocol significantly reduced the dynamic modulus and fatigue resistance of asphalt mixtures. Thus, loose mixture aging at 95°C was recommended as the LTOA procedure for laboratory performance evaluation. Finally, a rheology-based kinetics model was developed to predict the field aging of asphalt pavements, which was also used to determine the loose mixture aging durations for projects with different climates, depths, and pavement in-service times.

## **2.4 Laboratory Mixture Cracking Tests**

### *2.4.1 Energy Ratio*

The Energy Ratio (ER) method was developed by researchers at the University of Florida to assess the TDC resistance of asphalt mixtures (Roque et al., 2004). The ER approach uses an HMA Fracture Mechanics Model that was also developed at the University of Florida (Zhang et al., 2001). Recognizing that no single mixture property was able to accurately and consistently correlate to TDC, Roque et al. (2004) combined the results of three tests used in the HMA Fracture Mechanics Model to form a more comprehensive measurement of TDC susceptibility. ER results accurately distinguished between cracked and uncracked sections in 19 of the 22 pavements studied in Florida and led to the development of ER criteria. In subsequent studies, the ER method has been used to evaluate and predict the cracking resistance of mixtures using field cores, laboratory testing, and mechanistic-empirical (M-E) design (Wang et al., 2007; Shu et al., 2008; Wills et al., 2009; Moore, 2016; Song et al., 2018). Wang et al. (2007) incorporated the Florida cracking model into M-E design using ER concept to develop a new M-E pavement design tool for TDC. The new design tool could be used to conduct pavement thickness design and pavement life prediction regarding to TDC in Florida. The Florida Department of Transportation (FDOT) sponsored two research sections at the NCAT Test Track during the

summer of 2006 to validate the ER design concept. The same aggregate source and pavement structure were used for these two sections, but two different binder types were selected (PG 67-22 versus PG 76-22) to provide different ER values. As expected, the section designed with higher ER proved to be more resistant to TDC (Willis et al., 2009). Shu et al. (2008) evaluated the fatigue properties of mixtures using ER and beam fatigue tests. The plant mixtures used in this study included RAP contents ranging from 0 % to 30 %. The results indicated that both ER and beam fatigue tests agreed with each other in ranking the fatigue resistance of mixtures. A similar laboratory study was conducted by Zhao et al. (2012) using warm-mix asphalt (WMA) with high RAP contents. Though ER and beam fatigue tests yielded similar ranking results, the cracking resistance of WMA increased with the higher RAP content. The suitability of ER test to predict cracking resistance was evaluated using four NCAT Test Track sections by correlating the laboratory test results with actual field cracking performance (Willis et al., 2016). The test results indicated that the ER parameter didn't correlate with the field cracking performance well, but the dissipated creep strain energy measured during ER test had a good correlation with field cracking performance. A similar study was conducted by West et al. (2016) using seven NCAT Test Track sections constructed in 2006. All sections included similar pavement structure and the surface-layer mixtures with various RAP contents and virgin binder grades. The virgin binder PG was found to affect the field cracking performance significantly, and the creep strain rate measured as part of ER method matched the field performance of the test sections.

#### *2.4.2 Texas Overlay Test*

The Texas Overlay Test (TX-OT) method was developed by the Texas A&M Transportation Institute (TTI) in the late 1970's to simulate reflective cracking of asphalt overlays on concrete pavements. The original TTI small overlay tester was upgraded to a fully computer-controlled

system by Zhou and Scullion (2003), and four field projects on US 175 in Dallas were used to validate the upgraded tester. The results indicated that the upgraded tester was able to effectively identify asphalt mixtures with different cracking resistance. The method was refined in the early 2000's by Zhou and Scullion (2005) who demonstrated that the test was sensitive to testing temperature, maximum opening displacement (MOD), and asphalt binder content and type. The test's sensitivity to the mixture components was also investigated by Zhou et al. (2017a) using five mixtures with a wide range of material characterizations. The results indicated that TX-OT was sensitive to the RAP, reclaimed asphalt shingles (RAS), and binder content and type. A more in-depth sensitivity study was performed by Walubita et al. (2012) that reviewed the current state of the TX-OT in a number of laboratories in the United States. High variability (coefficient of variation (COV) > 30%) was reported by many of the laboratories participating in the study. Walubita et al. (2012) indicated that a significant proportion of the variability could be caused by the sample drying method, glue quantity, number of replicates, air voids, aging condition of samples, and temperature variation. Garcia and Miramontes (2015) also demonstrated that the amount of torque applied to attach OT specimens, the amount of glue, the curing time of glue, and the elapsed time between preparation and testing could also result in higher variability. In addition, OT specimens with more uniform air void distributions had less variability compared with specimens with greater air void distributions (Kassem et al., 2011).

Numerous studies have used the TX-OT to evaluate the cracking resistance of asphalt mixtures. Estakhri et al. (2009) used the TX-OT to compare cracking resistance between WMA and HMA using both field cores and plant mixtures. The results showed WMA and HMA were comparable, which was also confirmed by the field performance. The effects of recycled materials (RAP or RAS), modified binders, and rejuvenators on the mixture cracking resistance

were investigated by many researchers (Mogawer et al., 2011; Mogawer et al., 2013; Im et al., 2014; Luo et al., 2015; Tran et al., 2016; Xie et al., 2017). In general, the use of modified binders and rejuvenators to mitigate the negative impacts of recycled mixtures could increase the mixture cracking resistance. Zhou et al. (2005) utilized TX-OT as part of a mixture design process to characterize the reflective cracking resistance of mixture. A new mixture design method for asphalt mixtures containing RAP and rejuvenators was developed by Im et al. (2016), and the TX-OT was used to address the potential cracking issues caused by RAP and further to determine the optimum asphalt content and rejuvenator content. The correlation between TX-OT and field cracking performance was investigated using actual pavements and full-scale test pavement sections. The study of Zhou and Scullion (2003) indicated that TX-OT test results matched the field reflective cracking performance using four Texas projects. TX-OT results also had good correlations with field fatigue cracking and low temperature cracking performance (Zhou and Scullion, 2005; Zhou et al., 2005; Zhou et al., 2007). Similar conclusions were also obtained using experimental sections at NCAT Test Track (West et al., 2016; Willis et al., 2016; Xie et al., 2017). Zhou and Scullion (2005) recommended a TX-OT pass/fail criterion of number of cycles to failure ( $N_f$ ) greater than 300 for reflective cracking, and  $N_f > 750$  for reflective cracking with the presence of a rich bottom layer. The  $N_f > 300$  criterion was initially intended to address reflective cracking, but it also worked well for predicting fatigue cracking (Zhou et al., 2007). The TX-OT is also used in New Jersey since 45% of the New Jersey Department of Transportation (NJDOT) roads are asphalt overlays on Portland cement concrete (Bennert and Maher, 2008). In 2013, the NJDOT specified  $N_f > 150$  for surface mixtures with high RAP contents ( $> 20\%$ ) and a performance grade (PG) 64-22 binder, and  $N_f > 175$  for surface mixtures with high RAP contents ( $> 20\%$ ) and a PG 76-22 binder (Sheehy, 2013).

To address the high variability issue of the original TX-OT analysis method ( $N_f$  parameter), new analysis methodologies were developed to characterize the healing and fracture properties of asphalt mixtures (Koohi et al., 2013; Gu et al., 2015; Garcia et al., 2017; Cao et al., 2019). Koohi et al. (2013) proposed a novel analysis method to predict the actual crack growth rate in asphalt mixtures based on viscoelastic fracture mechanics and finite-element modeling, which was further used to characterize the fracture and healing properties. The study indicated that new test method provided more repeatable results than the previous method. Gu et al. (2015) also developed a new methodology for the TX-OT using viscoelastic force equilibrium and finite-element simulations to determine the crack growth function of asphalt mixtures. Furthermore, a modified Paris law was employed to evaluate the fracture behavior of asphalt mixtures, and two new parameters ( $A$  and  $n$ ) was defined based on the theoretical equations. Garcia et al. (2017) utilized a power equation to fit the normalized load-displacement curve, and the fitting coefficient ( $\beta$ ) was defined as cracking resistance index. In addition, the area under the hysteresis loop at the maximum peak load in the first loading cycled was defined as critical fracture energy ( $G_c$ ), which indicated the energy required to initiate a crack. These two new parameters were proven to satisfactorily discriminate the cracking resistance of mixtures and also had much lower variabilities than the previous  $N_f$  parameter. Cao et al. (2019) further modified the analysis method proposed by Garcia et al. (2017) through incorporating the viscoelastic relaxation effects. The test results indicated that the adjusted analysis method had a good correlation with the field cracking performance and comparable variability with  $G_c$  and  $\beta$ .

#### *2.4.3 NCAT Modified Overlay Test*

The NCAT-OT method was developed in 2014 (Ma, 2014). Specimen preparation and test setup are the same as the TX-OT method described in Tex-248-F with two exceptions: 1) maximum

opening displacement and 2) loading frequency. Originally, TTI researchers selected the MOD at 0.635 mm to simulate the thermal expansion and contraction of concrete pavement joints in Texas. Tran et al. (2012) and Ma (2014) proposed smaller MOD values to better simulate reflection cracking in flexible pavements. Therefore, a MOD of 0.381 mm was selected for the NCAT-OT method. Ma (2014) also found that at the lower MOD, the resulting  $N_f$  values at a loading frequency of 0.1 Hz were very similar to the results obtained at 1 Hz. Therefore, the faster loading frequency of 1 Hz was adopted in the NCAT-OT method to reduce testing time. It is also important to note that the NCAT-OT method uses a different method to determine cycles to failure than the TX-OT method. The NCAT-OT was further evaluated using the field performance of five base-layer mixtures of NCAT Test Track (Ma et al., 2015). The test results showed that NCAT-OT yielded similar ranking of these five mixtures with the four-point bending beam fatigue test, and a good correlation between NCAT-OT and field fatigue performance was also observed. Castro (2017) utilized both NCAT-OT and TX-OT methods to evaluate the effects of a bio-based rejuvenator on the laboratory properties and field cracking performance of asphalt mixtures. The test results indicated that NCAT-OT method showed a same statistical group ranking of mixture properties with TX-OT method, but with a lower variability. Meanwhile, both OT tests showed a good correlation with the field cracking performance. West et al. (2017) also utilized NCAT-OT method to evaluate the relationship between laboratory results and fatigue cracking of ten Federal Highway Administration's (FHWA) Accelerated Loading Facility (ALF) test lanes. NCAT-OT results showed a weak correlation with field fatigue performance and failed to discriminate good and poor field fatigue performance.

#### *2.4.4 Semi-circular Bend Test*

The SCB test, although originally used to characterize fracture mechanisms of rocks (Chong and Kuruppu, 1988), has been used by researchers to measure fracture properties of asphalt mixtures for over a decade. The SCB test has been used to evaluate low-temperature fracture resistance, and load-related cracking resistance at intermediate temperatures of asphalt mixtures (Li and Marasteanu, 2004; Arabani and Ferdowsi, 2009; Huang et al., 2009; Kim et al., 2012). Each of these studies used slightly different specimen geometries to determine the fracture properties. Intermediate temperature cracking potential has been estimated by calculating the critical strain energy release rate, or the J-integral ( $J_c$ ). The  $J_c$  concept was first used to evaluate asphalt mixtures containing with crumb rubber by Mull et al. (2002). Since then, the J-integral has been used extensively in Louisiana to assess fatigue resistance of asphalt mixtures (Kim et al., 2012). Kim et al. (2012) evaluated asphalt mixtures using both SCB and indirect tensile (IDT) tests and found a good correlation between the SCB  $J_c$  and IDT Toughness Index for lab produced mixtures. The field cracking performance was collected from nine field projects, which were trafficked with 1-12 million ESALs during various in-service time of 7-11 years. Four types of cracking pattern were collected using the automated road analyzer system, including transverse, longitudinal, alligator, and random cracking. Note that only the fracture-related cracking patterns of transverse and alligator cracking were used to correlate with the laboratory results (Kim et al., 2012). The study determined that  $J_c$  correlated well with field cracking data despite an average COV of 20% from 86 test mixtures. Mohammad et al. (2012) utilized asphalt mixtures from nine rehabilitation field projects throughout Louisiana state to further validate SCB test. These field projects have been trafficked for approximately ten years when the field cracking measurements were performed. Analysis of the results indicated that there was a good correlation with  $J_c$  results

and the field cracking rate. Zhou et al. (2017a) also demonstrated that the SCB  $J_c$  ranking matched the measured field fatigue and reflective cracking performance using six accelerated pavement test (APT) sections in Texas. However, a poor or fair correlation between SCB test results and field cracking performance was also observed by other researchers (West et al., 2016; Willis et al., 2016; Castro, 2017; West et al., 2017; Xie et al., 2017; Cao et al., 2018; Cao et al., 2019). The SCB test was used to evaluate the cracking resistance of four surface mixtures containing various contents of recycled materials and rejuvenator at NCAT Test Track. The SCB- $J_c$  results were poorly correlated with the field cracking performance (Castro, 2017). Similar conclusions were also obtained by other researchers using the measured field cracking performance from NCAT Test Track (Willis et al., 2016; Xie et al., 2017). The cracking resistance of ten mixtures from 2013 FHWA ALF experiment was assessed using SCB test, and the results indicated that there was essentially no relationship between  $J_c$  results and measured field cracking (West et al., 2017). Similar conclusions were also obtained by other studies (Cao et al., 2018; Cao et al., 2019). Wu et al. (2005) analyzed the sensitivity of  $J_c$  to a wide variety of mixture variables and found significant effects due to nominal maximum aggregate size (NMAS), binder type, and the number of gyrations ( $N_{design}$ ). Many studies have also demonstrated that the SCB test is sensitive to mixture aging, binder content, binder type (PG grade and polymer modification), and additives (e.g., rejuvenator and emulsifier) (Mohammad et al., 2004; Elseifi et al., 2012; Kim et al., 2012; Zhou et al., 2017a; Song et al., 2018; Chen et al., 2018; Jahanbakhsh et al., 2019). In addition, SCB test was proved to successfully discriminate mixtures with temperature segregation, which indicated that samples with temperature segregation generally yielded lower cracking resistance than control samples (Kim et al., 2017). However, some researchers found that SCB test was not sensitive to recycled asphalt materials

(RAP or RAS), which indicated that the cracking resistance of asphalt mixtures increased with the higher content of recycled asphalt materials (Kim et al., 2012; Chitragar and Singh, 2016; Willis et al., 2016; Singh et al., 2017; Castro, 2017; Zhou et al., 2017a). This unexpected trend might be caused by the absence of relaxation time, materials variability, and unaccountability of post-peak behavior (Singh et al., 2017). Seven asphalt mixtures from three projects were utilized to assess the effects of mix reheating and loading rate on the  $J_c$  results (Yin et al., 2017b). The test results indicated an insignificant effect of mix reheating on the  $J_c$  results, and mixtures with a higher loading rate showed higher  $J_c$  results than those mixtures tested with a lower rate.

#### *2.4.5 Illinois Flexibility Index Test*

Researchers at the University of Illinois developed another SCB test to screen out potentially poor performing mixtures with high amounts of RAP and RAS. The Illinois Flexibility Index Test (I-FIT) was found to be repeatable, and had a good field correlation and a significant spread of test results, and correlated well to other current cracking tests (Ozer et al., 2016). The sensitivity of I-FIT to different mixture design variables were investigated by many researchers (Ling et al., 2017; Zhou et al., 2017a; Kim et al., 2018; Zhu et al., 2019; Mohammed-Ali et al., 2019). The sensitivity of I-FIT to key asphalt mixture components was investigated using five different mixtures by Zhou et al. (2017a), the results indicated that the I-FIT was sensitive to asphalt content, recycled materials content (RAP and RAS), and softer binder. The cracking resistance of eight plant-produced mixtures in Georgia was evaluated using I-FIT test, and the results indicated that mixture design parameters had significant effects on the Flexibility Index (FI), including RAP contents, NMAAS, binder types and contents (Kim et al., 2018). In addition, the I-FIT was also proven to be sensitive to mixture additives, including fiber filler, rejuvenator, and sulfur (Castro, 2017; Ling et al., 2017; Espinoza-Luque et al., 2018; Mohammed-Ali et al.,

2019). Additionally, the effects of specimen configuration were explored in many studies, including specimen thickness, air voids, notch length, and notch width. In general, the FI decreased with the increasing specimen thickness and notch width, and the specimens with the higher air voids and notch length were expected to yield greater FI value width (Barry, 2016; Kim et al., 2018; Rivera-Perez et al., 2018; Batioja-Alvarez et al., 2019). Ozer et al. (2017) and Barber et al. (2018) examined the effects of testing configuration (spring or bearing rollers) and loading system (hydraulic or screw-driven) on the I-FIT, which were proved to be insignificant. Nsengiyumva and Kim (2019) investigated the effect of I-FIT testing configuration on the test results and their variability using six different load-support fixtures. Generally, the test results measured with six load-support fixtures were comparable, but the roller springs could increase the testing variability. Furthermore, the effects of loading rate and testing temperature were inspected by some researchers, the I-FIT results generally decreased with the loading rate and increased with the test temperature (Haslett, 2018; Son et al., 2019; Chen and Solaimanian, 2019). The correlation between I-FIT with field performance was validated using FHWA's ALF, NCAT Test Track, and in-service roads in Illinois, and the results indicated that I-FIT results had a good correlation with field cracking performance (Castro, 2017; Xie et al., 2017; Al-Qadi et al., 2017; Safi et al., 2019; Al-Qadi et al., 2019). Kaseer et al. (2018) developed a new cracking test parameter, called the cracking resistance index (CRI), which was derived from the load-displacement curve of I-FIT. The calculation of CRI was similar with FI by replacing the slope at the inflection point with peak load. In general, the CRI had lower variability and showed greater distinction between different asphalt mixtures, which was validated using Indian asphalt mixtures by Batioja-Alvarez et al. (2019). Meanwhile, the CRI was also sensitive to the binder PG, recycled materials content, and the presence of recycling agents (Kaseer et al., 2018).

#### *2.4.6 Indirect Tensile Asphalt Cracking Test (a.k.a, IDEAL-Cracking Test)*

The indirect tensile asphalt cracking test, more commonly known as the IDEAL-CT, was developed by Zhou et al. (2017b) to evaluate the cracking resistance of asphalt mixtures for use in mix design and quality assurance testing. The IDEAL-CT was found to be sensitive to materials and volumetric parameters including RAP and RAS contents, binder grade, binder content, air voids, and aging condition (Zhou et al., 2017b; Im and Zhou, 2017). NJDOT conducted a comprehensive comparison study among different cracking tests to identify a suitable test for fatigue cracking during mixture design and quality control, and the results indicated that the IDEAL-CT test was sensitive to asphalt mixture volumetrics, composition, binder grade and aging condition (Bennert et al., 2018). Lee et al. (2019) utilized IDEAL-CT to evaluate the cracking resistance of mixtures with rejuvenators, and the results indicated that the cracking test index ( $CT_{\text{Index}}$ ) was sensitive to rejuvenator additive. The cracking resistance of cold recycling mixtures with varying emulsion and cement contents was evaluated using IDEAL-CT, and the results indicated that IDEAL-CT was sensitive to the varying emulsion and cement contents (Dong and Charmot, 2018). Meanwhile, a ruggedness experiment found that the IDEAL-CT was considered as rugged with the specified ranges of specimen thickness, loading rate, test temperature, and air voids (Zhou et al., 2017b). The IDEAL-CT can be performed with common IDT strength test equipment without the need for specimen trimming or notching. Many studies showed that IDEAL-CT was simple and practical with respect to equipment, sample preparation, and analysis, and it was also efficient with time and cost investment on equipment (Zhou et al., 2017b; Im and Zhou, 2017; Bennert et al., 2018; Diefenderfer and Bowers, 2019). In addition, the IDEAL-CT was observed to have a lower variability than other cracking tests (Zhou et al., 2017b; Im and Zhou, 2017; Bennert et al., 2018; Diefenderfer and Bowers, 2019).

The correlations between IDEAL-CT and other cracking tests were investigated using ten mixtures with different binder contents, binder PG, and recycled materials contents (RAP and RAS) (Zhou et al., 2019). The test results presented that the  $CT_{Index}$  had a similar trend with TX-OT and I-FIT results, and there was a good linear relationship existing among the results of these three tests. Bowers et al. (2019) and Diefenderfer et al. (2019) also observed a good correlation between IDEAL-CT and the  $N_{flex}$  Factor test using both plant-produced and laboratory-prepared cold recycled mixtures, and IDEAL-CT provided greater discrimination than the  $N_{flex}$  Factor test (Diefenderfer et al., 2019). In addition, NJDOT found a strong relationship between IDEAL-CT and TX-OT, and the corresponding criteria of IDEAL-CT were established based on the previous TX-OT criteria (Bennert et al., 2018). The correlation between IDEAL-CT with field performance was further validated using FHWA's ALF, full-scale test sections at MnROAD, and in-service roads in Texas, and the results indicated that IDEAL-CT results had a good correlation with fatigue cracking, reflective cracking, and thermal cracking (Zhou et al., 2019).

## CHAPTER 3 RESEARCH METHODOLOGY

This chapter describes the experimental plan for this study, which includes: 1) determining the critical aging (CA) protocol for TDC evaluation, and 2) validating the laboratory cracking tests with the field cracking performance using real loading conditions. The materials and laboratory tests used in this study are also summarized. For the critical aging protocol, materials from five projects were used to select a preliminary aging protocol which was then validated with NCAT TDC experimental mixtures. For the cracking test validation experiment, seven mixtures with a wide range of cracking susceptibilities were designed and constructed on 2015 NCAT Test Track. The field cracking performance of the seven test sections have been monitored weekly during traffic loading. Six laboratory cracking tests were selected to evaluate the cracking resistance of the seven mixtures.

### 3.1 Experimental Plan

#### *3.1.1 Construction of NCAT TDC Experimental Test Sections*

In 2015, seven experimental mixtures were designed and constructed on the NCAT Test Track for the TDC experiment. Figure 3.1 illustrates the pavement structure of the seven test sections. As can be seen, each mixture was constructed as a 1.5-inch surface layer on top of highly polymer-modified asphalt base layer designed to be highly elastic to mitigate the occurrence of bottom-up cracking (Moore, 2016; West et al., 2019). After construction, traffic was applied on the test sections using the Test Track's fleet of five heavily loaded trucks. Field cracking performance was monitored weekly throughout the traffic cycle.

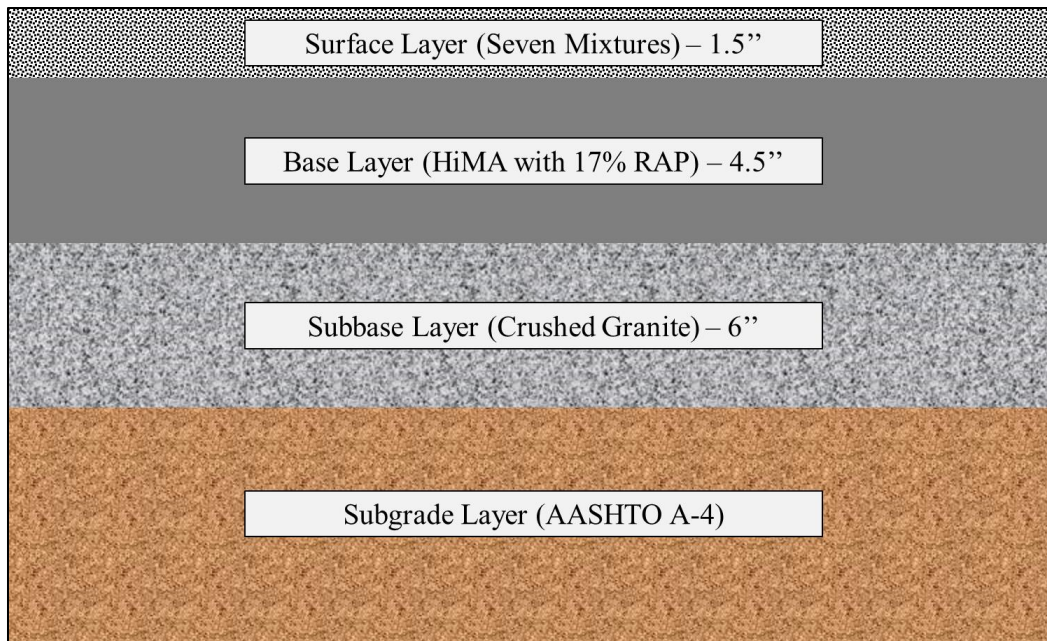


**Figure 3. 1 Pavement Structure of NCAT TDC Experimental Test Sections**

### *3.1.2 Determination of the Critical Aging Protocol for NCAT TDC Experiment*

As described previously, mixture properties, environmental aging, pavement structure, and traffic loading have been identified as factors that contribute to the development of TDC. In the NCAT TDC experiment, test sections with different materials had the same pavement structure and sustained the same traffic loading. Thus, the material properties and environmental aging were the primary influence factors on the cracking resistance in this study. Considering the importance of aging of asphalt mixtures in the development of TDC, an experiment was devised to simulate the environmental aging of the mixtures prior to laboratory testing.

To determine an aging protocol for the NCAT TDC experiment, materials from five field projects that covered a wide range of pavement age, climatic conditions, and mixture components were selected. For each field project, loose plant mixtures were conditioned with four different loose mixture aging protocols of 5 days at 95°C, 6 hours at 135°C, 12 hours at 135°C, and 24 hours at 135°C. Asphalt binders extracted from the conditioned loose mixtures and field cores were tested with the dynamic shear rheometer (DSR), bending beam rheometer

(BBR), and Fourier transform infrared spectroscopy (FT-IR). The preliminary aging protocol was determined by comparing the binder properties from the conditioned loose mixtures and field cores. For validation of the aging protocol, the plant mixtures from the NCAT TDC experiment were conditioned using this preliminary aging protocol, and field cores from each section were collected annually after 2016. Several mixture and binder tests were used to compare mixture and binder properties of the laboratory-aged plant mixtures and field cores.

### *3.1.3 Laboratory Cracking Tests of NCAT TDC Experiment*

In this study, six laboratory cracking tests were selected by the experiment sponsors to evaluate the cracking resistance of seven NCAT TDC experimental mixtures, including ER, TX-OT, NCAT-OT, SCB, I-FIT, and IDEAL-CT. During the construction of 2015 NCAT Test Track, the plant-produced mixtures of each section were sampled and stored in five-gallon buckets.

Laboratory-prepared mixtures of each section were also prepared based on the corresponding mixture designs. For each mixture, both plant-produced samples and laboratory-prepared samples were aged at 135 °C for 8 hours prior to compaction. After aging, the loose mixtures were compacted with an SGC and then fabricated in accordance with the requirements of different cracking tests. Analyses of the laboratory cracking test results included:

- Comparisons of corresponding plant mixtures and laboratory mixtures.
- Sensitivity of six cracking test results to aging, air voids, recycled asphalt materials, and modified binder.
- Correlations among the cracking test parameters of six laboratory cracking tests.
- Assessment of how well the laboratory cracking test results correlate to measured cracking in the test sections.

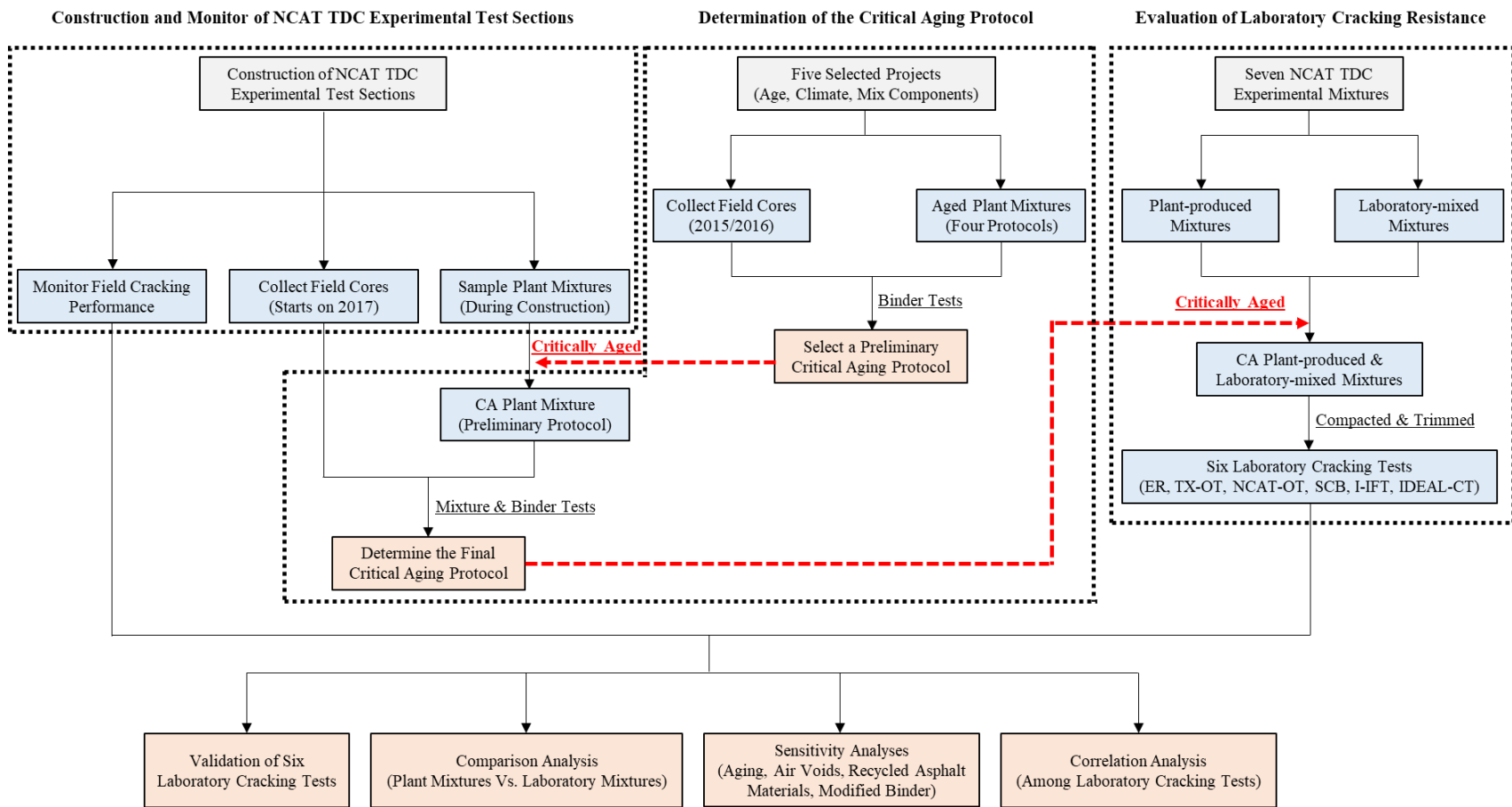


**Figure 3. 2 Experimental Plan**

## 3.2 Materials

### 3.2.1 Materials used to Select the Preliminary Critical Aging Protocol

Materials used to develop the preliminary aging protocol were from five field projects that covered a range of pavement age, climatic conditions, and mixture components. These projects were selected based on the availability of plant loose mixtures sampled during production. Two projects were from NCHRP project 09-47A; one was on US-12 in Walla Walla, Washington, and the other was on County Road 513 near Rapid River, Michigan. The other three projects were from test sections on the NCAT Test Track, but they were constructed in different research cycles. For each project, both plant mixtures and field cores were collected. All of the mixtures were constructed as surface layers on the projects/test sections. Table 3.1 provides a brief summary of mixture components for the five field projects.

**Table 3. 1 Summary of Field Projects**

Mix ID	Mix 1	Mix 2	Mix 3	Mix 4	Mix 5
Location	Rapid River, Michigan	Walla Walla, Washington	Auburn, Alabama	Auburn, Alabama	Auburn, Alabama
Mixture Type	HMA	HMA	HMA	HMA	HMA
Virgin Binder	PG 52-34	PG 64-28	PG 76-22 (SBS)	PG 67-22	PG 67-22
NMAS	12.5 mm	12.5 mm	9.5 mm	12.5 mm	12.5 mm
Gradation	Dense-Graded	Dense-Graded	Dense-Graded	Dense-Graded	Dense-Graded
RAP	17%	20%	0%	20%	0%

### 3.2.2 NCAT TDC Experimental Mixtures

In the NCAT TDC experiment, seven surface mixtures were designed and constructed on the NCAT Test Track with a range of air voids ( $V_a$ ), binder type, and recycled materials, summarized as follows:

- Mix N1(control mix): PG 67-22 asphalt binder with 20% RAP (93.6% in-place density);

- Mix N2: the same mix as N1 with a higher density (96.1% in-place density);
- Mix N5: a similar mix as N1 with a lower density (90.3% in-place density) and lower asphalt content;
- Mix N8: PG 67-22 asphalt binder with 20% RAP and 5% RAS;
- Mix S5: PG 58-28 styrene-butadiene-styrene (SBS)-modified binder with 35% RAP material;
- Mix S6: a similar mix as N1 with a highly polymer modified asphalt (HiMA) binder. Note that HiMA refers to the asphalt mix that contains an asphalt binder with 7.5% styrene-butadiene-styrene polymer;
- Mix S13: a gap-graded 12.5 mm mixture with PG 67-22 modified with 20% ground tire rubber.

Table 3.2 summarizes mix design and as-produced properties of the seven experimental mixtures.

**Table 3. 2 Mix Design and Quality Control Properties of the NCAT TDC Experimental Test Sections**

Sieve Size	N1 Control		N2 Control w/ High Density		N5 Control w/ Low Dens. & AC		N8 Control w/ 5% RAS		S5 35% RAP PG 58-28		S6 Control w/ HiMA		S13 Gap-Graded Asphalt-Rubber*	
	Design	QC	Design	QC	Design	QC	Design	QC	Design	QC	Design	QC	Design	QC
12.5 mm (1/2")	100	99	100	100	100	100	100	99	100	99	100	100	95	96
9.5 mm (3/8")	99	97	99	98	98	99	99	98	98	96	99	98	77	85
4.75 mm (#4)	74	67	74	70	74	73	70	66	74	73	74	67	38	35
2.36 mm (#8)	51	52	51	54	52	54	45	51	52	56	51	52	23	22
1.18 mm (#16)	39	41	39	43	41	42	35	41	41	44	39	42	18	19
0.60 mm (#30)	26	28	26	28	27	28	23	30	27	29	26	28	12	14
0.30 mm (#50)	15	15	15	15	15	15	14	17	15	16	15	15	7	8
0.15 mm (#100)	9	9	9	9	10	9	9	11	10	10	9	9	5	5
0.075 mm (#200)	6.2	5.4	6.2	5.6	6.3	5.7	6.1	7.1	6.3	6.3	6.2	5.4	3.3	3.6
Tot. Binder Content (P <sub>b</sub> )	5.7	5.4	5.7	5.4	5.2	5.1	5.5	5.3	5.7	5.8	5.9	5.8	7.4	7.4
Eff. Binder Content (P <sub>bce</sub> )	5.0	4.7	5.0	4.7	5.0	4.4	5.0	4.8	5.0	5.1	5.2	5.0	6.6	6.6
RAP Binder Ratio	0.19	0.20	0.19	0.20	0.21	0.21	0.20	0.20	0.33	0.33	0.18	0.19	0.07	0.07
RAS Binder Ratio	--	--	--	--	--	--	0.14	0.14	--	--	--	--	--	--
Dust/Binder Ratio	1.2	1.1	1.2	1.2	1.4	1.3	1.2	1.5	1.2	1.2	1.2	1.1	0.6	0.5
Rice Sp. Gravity (G <sub>mm</sub> )	2.474	2.469	2.474	2.468	2.493	2.478	2.483	2.492	2.481	2.472	2.470	2.459	2.418	2.402
Bulk Sp. Gravity (G <sub>mb</sub> )	2.375	2.375	2.375	2.372	2.355	2.348	2.383	2.415	2.382	2.393	2.371	2.384	2.273	2.319
Air Voids (V <sub>a</sub> ), %	4.0	3.8	4.0	3.9	5.5	5.3	4.0	3.1	4.0	3.2	4.0	3.1	6.0	3.4
Agg. Bulk Gravity (G <sub>sb</sub> )	2.654	2.634	2.654	2.631	2.665	2.633	2.668	2.672	2.665	2.656	2.654	2.634	2.647	2.631
Avg. VMA, %	15.6	14.7	15.6	14.7	15.9	15.4	15.5	14.4	15.7	15.1	16.0	14.7	19.9	18.4
Avg. VFA, %	75	74	75	73	65	66	74	79	75	79	75	79	71	81
Layer thickness (in.)	1.5	1.6	1.5	1.5	1.5	1.3	1.5	1.5	1.5	1.6	1.5	1.5	1.5	1.6
Mat Density (%G <sub>mm</sub> )	94.0	93.6	97.0	96.1	91.0	90.3	94.0	91.5	94.0	92.2	94.0	91.8	94.0	92.7
Virgin Binder Grade	PG 67 -22		PG 67 -22		PG 67 -22		PG 67 -22		PG 58 -28		PG 94 -22		67-22 +20% CR	
Rec. Binder True Grade (Plant Mixtures)	88.6 -16.6		89.9 -15.9		88.0 -18.5		107.3 -5.4		82.8 -23.0		101.4 -21.5		Not. Avail.	

\*50-blow Marshall Hammer compaction used for mix design and QC

### 3.3 Laboratory Binder Tests

#### 3.3.1 Dynamic Shear Rheometer

A DSR was used to characterize the rheological properties of asphalt binders by measuring the complex shear modulus ( $G^*$ ) and phase angle ( $\delta$ ) at a specific temperature and frequency. Figure 3.3 shows the DSR equipment and the sample preparation.

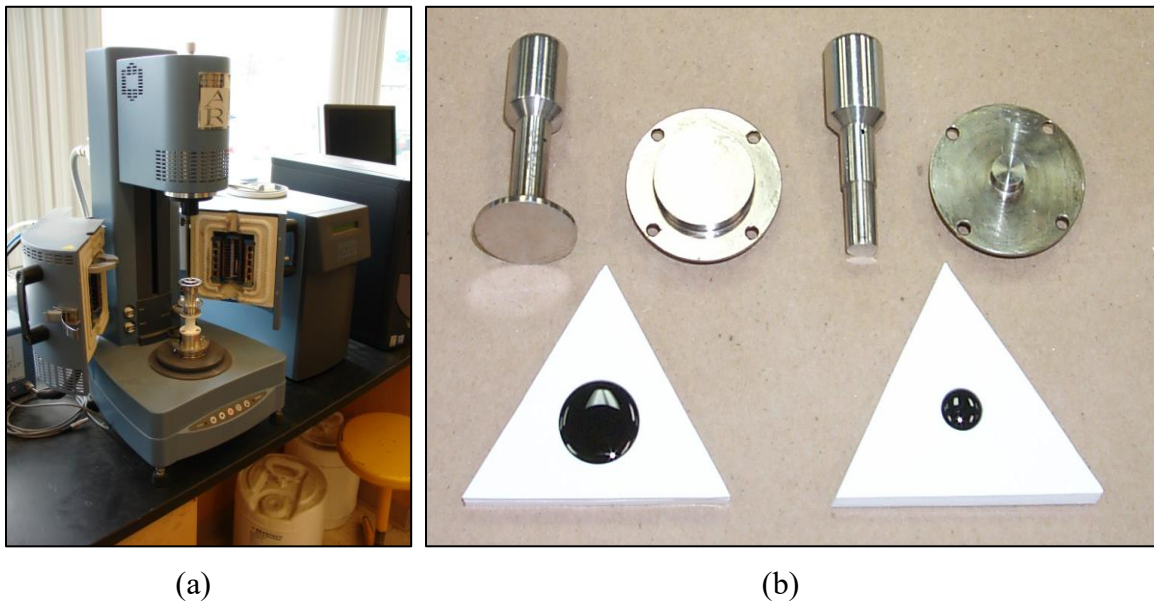


**Figure 3. 3 DSR Test; (a) DSR Equipment, (b) Sample Preparation**

Extracted asphalt binders were first tested to determine the continuous high-temperature performance grade (HPG) per AASHTO R 29 and M 320. In addition, the limited DSR frequency sweep test was conducted at 20, 30, and 40°C and with an angular frequency range of 0.1 to 10 rad/s. The maximum oscillation strain was controlled at one percent to ensure the asphalt binder was in the linear viscoelastic range. For data analysis,  $G^*$  and  $\delta$  master curves were constructed by fitting the individual  $G^*$  and  $\delta$  results at each temperature and frequency to the Christensen-Anderson-Marasteanu (CAM) model (Santagata et al., 1996), as expressed in Equation (3.1). The master curves were then utilized to calculate the Glover-Rowe (G-R) parameter using Equation (3.2) (Glover et al., 2005; Rowe, 2011). The G-R parameter considers

both binder stiffness and embrittlement and offers an indication of the cracking potential at intermediate temperatures. Asphalt binders with higher G-R parameters are expected to have experienced a greater level of aging than those with lower G-R parameters. A damage zone between 180 kPa and 600 kPa was proposed for G-R parameter to evaluate the block cracking susceptibility of asphalt binder, and the threshold values of this damage zone indicated the onset damage and visible damage in pavements (Rowe, 2011). However, this damage zone was developed using limited unmodified binder sources in one climate zone (Rowe, 2011). Thus, this damage zone may not be appropriate for TDC evaluation.

$$G^* = G_g \left[ 1 + \left( \frac{\omega}{\omega_c} \right)^v \right]^{-\frac{w}{v}}$$

$$\delta = \frac{90w}{\left[ 1 + \left( \frac{\omega}{\omega_c} \right)^v \right]}$$
(3.1)

Where:

$G_g$  = glass modulus, assumed equal to 1 GPa;

$\omega_c$  = crossover frequency;

$\omega$  = reduced frequency;

$v$  and  $w$  = model coefficients.

$$G-R \text{ Parameter} = \left\{ \frac{G^* [\cos(\delta)^2]}{\sin(\delta)} \right\}_{T=15^\circ C, f=0.005 \text{ rad/s}}$$
(3.2)

The DSR linear amplitude sweep (LAS) test was conducted to evaluate the fatigue resistance of extracted binders per AASHTO TP 101. The test consisted of two steps: a frequency sweep test and an amplitude sweep test. In the first part of the LAS procedure, an initial 100 cycles were applied at small strain (0.1%) to determine undamaged linear viscoelastic properties.

The second part of the procedure consisted of ramping up the strain amplitude, beginning at 0.1% and ending at 30% applied strain, over 3,100 cycles of loading at 10 Hz. Once the strain sweep was applied to the sample, damage accumulation was then determined using Viscoelastic Continuum Damage (VECD) analysis, resulting in the fatigue power law damage model (Equation 3.3), and the corresponding coefficients,  $A$  and  $B$ .

$$N_f = A(\gamma_{\max})^{-B} \quad (3.3)$$

$N_f$  is the traffic volume failure criteria and defines the number of cycles to fatigue failure at a user-defined damage level.  $\gamma_{\max}$  is the maximum tensile strain expected in the binder phase under traffic loading, which will be a function of pavement structure.  $A$  is the LAS power-law parameter representing the intercept at 1% strain.  $B$  is the LAS power-law parameter representing the slope of the  $N_f$ -strain curve. The logarithmic slope of the storage modulus  $[G'(\omega)]$  as a function of angular frequency is used to calculate the damage accumulation, quantified as the  $B$ -parameter. Safaei et al. (2014) recommended that the LAS test temperatures be selected such that linear dynamic shear moduli corresponding to the test temperature and frequency were within the range of 12 to 60 MPa to avoid confounding effects of flow or adhesion loss (Safaei et al., 2014; Safaei et al., 2016). In this study, for all the evaluated asphalt binders, the LAS test was performed using the 8 mm parallel plate geometry and at a temperature of 28°C.

### 3.3.2 Bending Beam Rheometer

A BBR was used to characterize the resistance of asphalt binders to thermal cracking at low temperatures. Figure 3.4 presents the BBR equipment and the loading frame, and Figure 3.5 shows the sample preparation.



(a)

(b)

**Figure 3. 4 BBR Test; (a) Test Equipment, (b) Loading Frame**

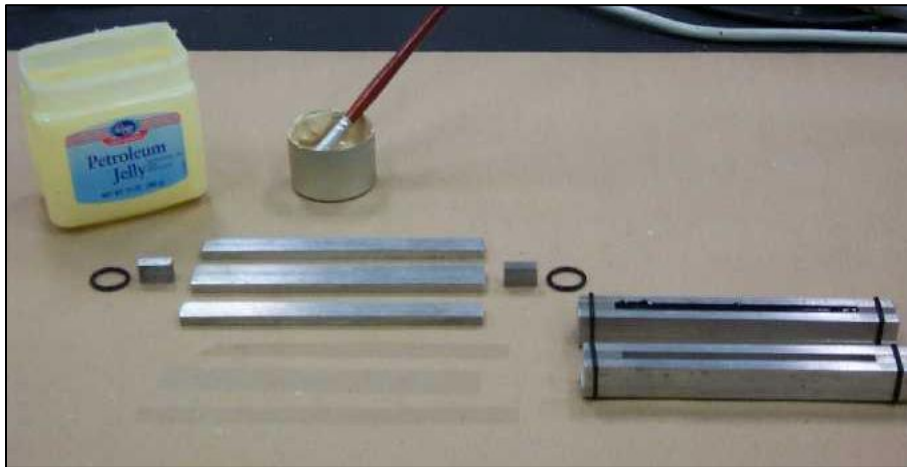


**Figure 3. 5 BBR Sample Preparation**

The test was conducted to determine the low-temperature performance grade (LPG) based on the creep stiffness ( $S$ ) and m-value results per AASHTO T 313. The performance grade determined with  $S$  ( $T_{c,s}$ ) was reported as the continuous LPG, and the numerical difference between  $T_{c,s}$  and performance grade determined with m-value ( $T_{c,m}$ ) was defined as  $\Delta T_c$  (Anderson et al., 2011), as shown in Equation 3.4. The  $\Delta T_c$  parameter is indicative of the

environmental-related cracking potential of asphalt binders; specifically, binders with a more negative  $\Delta T_c$  are more likely susceptible to block cracking than those with a less negative  $\Delta T_c$ .

$$\Delta T_c = T_{c,S} - T_{c,m} \quad (3.4)$$

### 3.3.3 Double-Edge-Notched Tension (DENT) Test

The DENT test was performed according to AASHTO TP 113, where three specimens with different ligament lengths (5, 10 and 15 mm) were loaded in monotonic, direct tension mode with a rate of 100 mm/min. at 25°C until failure. Ductile failure can be assessed by visually observing failed samples at the end of the test. During the failure process, the load versus displacement curves were recorded and total energy of failure was calculated. The failure process consisted in a continuous flow of energy through the plastic deformation region to the failure region, with energy being partitioned between a plastic “outer” zone and an autonomous “inner” zone. Therefore, there was a progressive reduction of the energy release rate in the failure zone as the two new surfaces of material were created. The work performed to create new surfaces of material in the crack end region was defined by Cotterell and Reddel (1977) as the “essential work”. Therefore, the total energy of ductile failure was composed of two parts: (I) “the essential work performed in the end region” and (II) “the non-essential work performed in the screening plastic region.”

The essential work of fracture ( $W_e$ ) is proportional to the failure area [i.e. ligament length ( $l$ ) multiplied by sample thickness ( $B$ )], while the non-essential work ( $W_p$ ), or the plastic work, is proportional to the volume of the plastic zone [i.e. failure area ( $l \times B$ ) multiplied by ligament length and a  $\beta$  factor]. The  $\beta$  factor depends on the shape of the plastic zone. Because the ligament length holds significance in determining the extent of plastic deformation it can be distinctly incorporated as ( $l \times \beta$ ) and multiplied with the surface area to express the volume

dependence of the plastic work of fracture,  $W_p$ . The mathematical expression for the total work of fracture ( $W_f$ ) is given by Equation 3.5:

$$W_f = W_e + W_p = lBw_e + \beta l^2 Bw_p \quad (3.5)$$

Where:

$w_e$  and  $w_p$  are the corresponding specific terms for  $W_e$  and  $W_p$ .

This equation represents a thermodynamic approach to the failure process. Written in specific terms, total work of fracture divided by the failure area ( $l \times B$ ), becomes the total specific work of fracture ( $w_f$ ) (Equation 3.6):

$$w_f = w_e + \beta l w_p \quad (3.6)$$

The plot of the total specific work of fracture ( $w_f$ ) versus the ligament length ( $l$ ) results in a straight line, having an intercept equal to the essential work of fracture ( $w_e$ ) and a slope equal to the specific plastic work of fracture multiplied by the shape factor ( $\beta \times w_p$ ). Cotterell and Reddel (1977) also observed that “the screening plastic zone vanishes for small ligaments” and defined critical tip opening displacement (CTOD or  $\delta$ ) as the ultimate elongation for zero ligament length. As a result, they defined the value of essential work per Equation 3.7:

$$w_e = \delta \times \sigma \quad (3.7)$$

Where:

( $\sigma$ ) represents the yield stress in tension.

A minimum of three specimens with various ligament lengths (e.g. 5 mm, 10 mm and 15 mm) can provide enough information for the approximate calculation of the CTOD or strain tolerance of the material. The essential work of fracture can be determined as the intercept of the

plot of the total specific work of fracture versus the ligament length, while the peak stress of the sample with the smallest ligament length (5 mm) can be used to approximate the yield stress of the material. Finally, the CTOD can be calculated as the ratio between the specific work of fracture and the peak stress for the smallest ligament length sample (in this case, 5 mm). The capacity of CTOD parameter to predict fatigue failure was validated during the 2002 Accelerating Loading Facility (ALF) experiment at Turner Fairbank Highway Research Center and on other testing sites in North America.

### 3.3.4 Fourier Transform Infrared Spectroscopy

An FT-IR measures the infrared light absorbed by the material, and the absorption depends on the constituents and chemical function groups in the material. In this study, FT-IR was used to measure the infrared spectrum of asphalt binders extracted and recovered from the laboratory and field aged mixtures to determine their compositional changes with aging. The test was conducted using a Nicolet 6700 FT-IR spectrometer with attenuated total reflectance (ATR) setup, as shown in Figure 3.6.

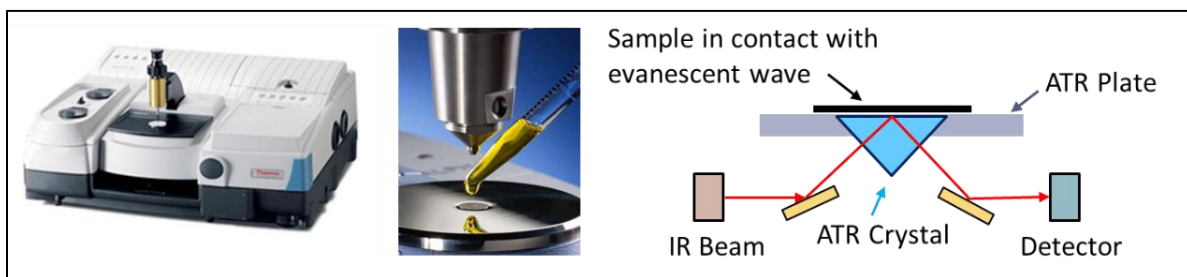
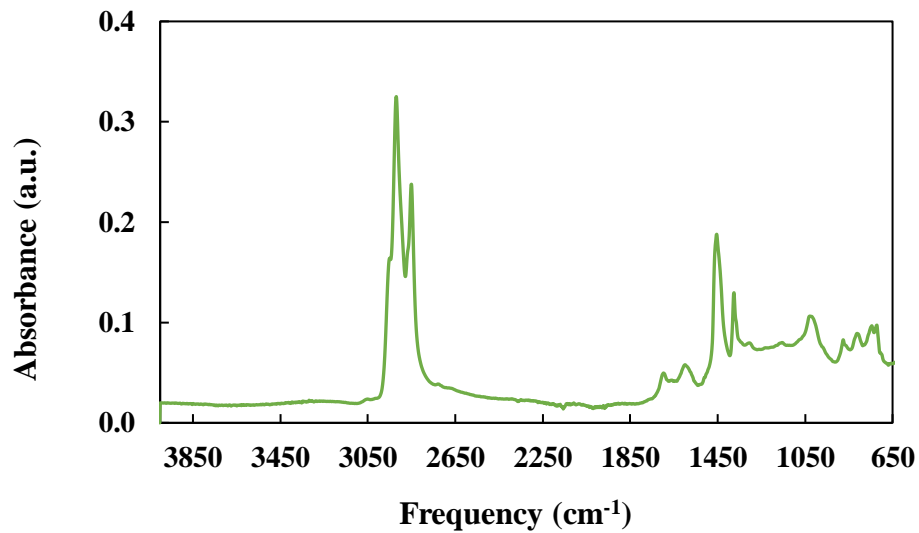


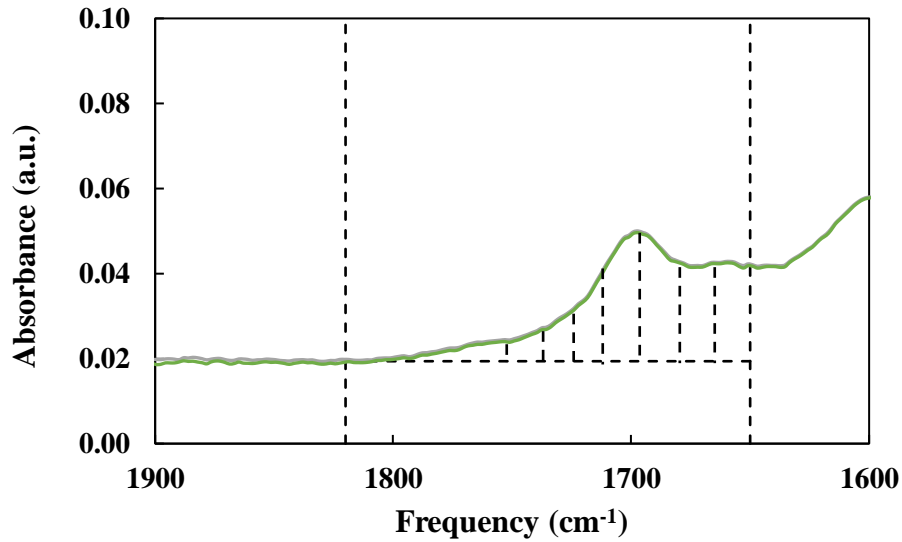
**Figure 3. 6 Nicolet 6700 FT-IR Spectrometer and Mechanism of ATR**

As shown in Figure 3.6, the asphalt samples were prepared and placed on the ATR crystal area to assure the contact with the evanescent wave. During the spectrum collection, the absorbance value and corresponding frequency were recorded at region of  $4000\text{-}650\text{ cm}^{-1}$ . The scanning resolution was set to be  $0.5\text{ cm}^{-1}$ , and the measured spectrum was saved after 64 scans

for each replicate. The FT-IR carbonyl area (FT-IR CA), defined as the integrated peak area for the wavelength range from 1820 to 1650  $\text{cm}^{-1}$  (Liu et al., 1998), was used to characterize the oxidation level of asphalt binders extracted from mixtures with various aging levels. Figure 3.7 shows an example of a full spectrum and the illustration of FT-IR CA. Asphalt binders with higher FT-IR CA are expected to have experienced a greater level of oxidative aging than those with lower FT-IR CA.



(a)



(b)

**Figure 3. 7 Illustration of FT-IR Analysis; (a) Full Spectrum, (b) FT-IR Carbonyl Area**

The FT-IR test procedure is summarized as follows:

- Prepare the following items: asphalt sample, heat gun, paper tissues, plastic spatula, metal spatula, towel, thick gloves, and chemical solvent (Big Orange-E, and Acetone).
- Preheat the asphalt sample at 135°C prior to FT-IR testing.
- Use a metal spatula to blend/stir the heated asphalt sample to achieve homogeneity.
- Collect FT-IR background spectrum.
- Apply a thin film of asphalt sample on the ATR crystal with a plastic spatula.
- Collect FT-IR spectrum (two replicates per sample).
- Apply a few drops of chemical solvent (Big Orange-E) and use a plastic spatula to remove the asphalt sample (Be cautious not to damage the ATR crystal).
- Apply a few drops of Acetone on the ATR crystal between samples.
- Repeat above steps for the next replicate or sample.

### **3.4 Laboratory Mixture Cracking Tests**

#### *3.4.1 Energy Ratio*

For each mixture, three specimens, 150 mm in diameter by 38 to 50 mm thick, cut from gyratory compacted samples, were prepared. The air voids for these samples were the target air void content  $\pm 0.5\%$ . The specimens were fitted with extensometers both vertically (in the loading direction) and horizontally (perpendicular to the load) to measure deformation on both faces of the specimen, as shown in Figure 3.8. The ER is determined from results of the resilient modulus ( $M_R$ ) (ASTM D7369), creep compliance (AASHTO T322), and IDT strength (ASTM D6931). All three individual tests were performed at 10°C using a servo-hydraulic testing device.

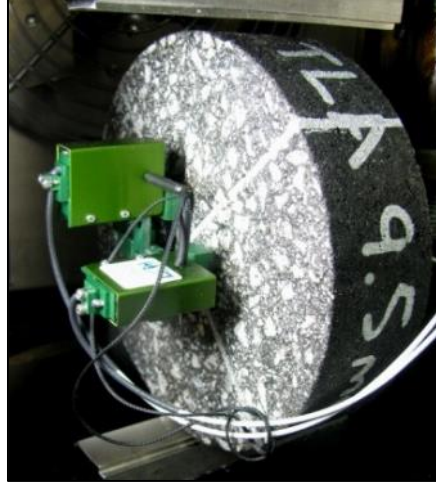


**Figure 3. 8 Energy Ratio Test Specimen Setup**

The creep compliance test is used to determine viscoelastic parameters,  $D_1$  and  $m$ , which are shown in Figure 3.9(b). Dissipated creep strain energy threshold ( $DCSE_{HMA}$ ) is an intrinsic property of an asphalt mixture at which it will form a micro-crack. In other words, the  $DCSE_{HMA}$  is the amount of energy required beyond the elastic region of a mixture to initiate cracking. As illustrated in Figure 3.9(c), the tensile strength ( $S_t$ ) and  $DCSE_{HMA}$  are determined from resilient modulus and IDT strength tests. The  $DCSE_{Min}$  is defined as the dissipated creep strain energy accumulated after 6,000 cycles in the HMA fracture mechanics model (Roque et al., 2004).  $DCSE_{Min}$  is an indicator of pavements with good TDC resistance, which can be calculated with Equation (3.8):

$$DCSE_{Min} = \frac{m^2 D_1}{0.0299 \times \sigma^{-3.10} (6.36 - S_t) + 2.46 \times 10^{-8}} \quad (3.8)$$

Where:

$m$  and  $D_1$  are the creep compliance parameters;

$\sigma$  is the applied tensile stress;

$S_t$  is the tensile strength.

ER is defined as the ratio of  $DCSE_{HMA}$  to  $DCSE_{Min}$ , as shown in Equation (3.9). Mixtures with a higher ER are expected to have a better cracking resistance than those with a lower ER.

$$ER = \frac{DCSE_{HMA}}{DCSE_{Min}} \quad (3.9)$$

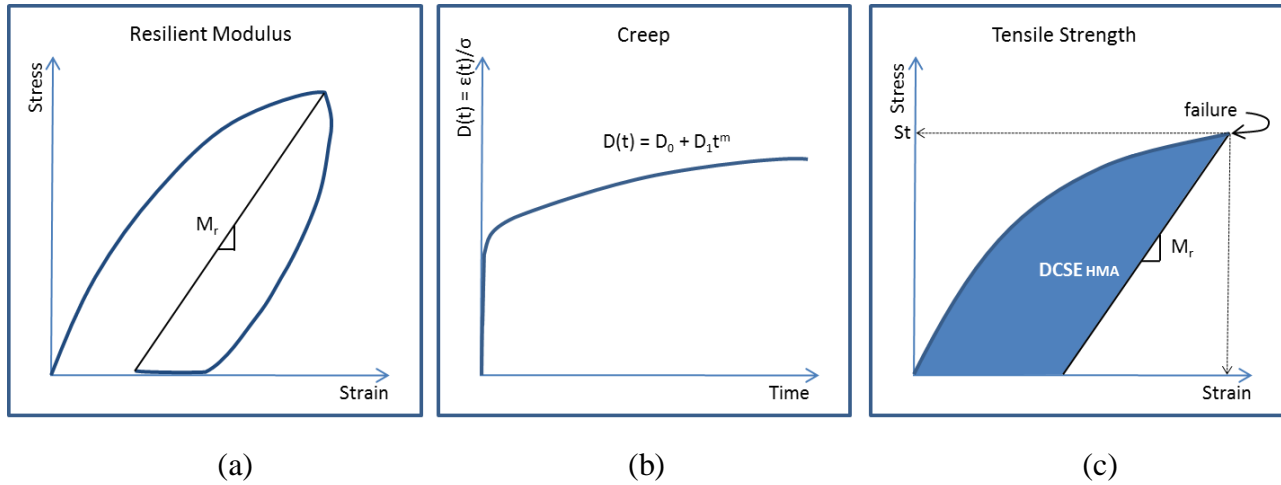


**Figure 3. 9 Energy Ratio Concept;**  
**(a) Resilient Modulus, (b) Creep Compliance, (c) Strength Tests (West et al., 2016)**

### 3.4.2 Texas Overlay Test

TX-OT tests were conducted in accordance with Tex-248-F. TX-OT specimens were compacted in an SGC to a target height of 125 mm. Although Tex-248-F requires that only one OT specimen be made from each gyratory pill, a sensitivity analysis performed by Walubita (2012) recommended using two specimens per gyratory pill to improve efficiency. In this study, two specimens per pill were trimmed to the following dimensions: 150 mm x 76 mm x 38 mm. The air voids for the cut specimens were selected as the target in-place air void content  $\pm 1.0\%$ . The fabricated test specimens were glued to the OT fixture for testing in the Asphalt Mixture Performance Tester (AMPT). Figure 3.10 shows an example of OT specimen setup.



**Figure 3. 10 TX-OT Specimen Setup**

During the test, one side of the fixture remains fixed while the other side moves in a displacement-controlled mode applying a sawtooth wave form once per 10 second cycle (5 seconds of loading, 5 seconds for unloading). Testing was performed at 25°C with a maximum displacement of 0.635 mm per cycle. The peak load of each cycle was measured, and the test reached failure when the peak load reached 93% of the initial peak load and the number of cycles to failure (TX-N<sub>f</sub>) was recorded.

Garcia et al. (2017) proposed a new analysis methodology for the TX-OT test that requires the calculation of two parameters: critical fracture energy ( $G_c$ ) and crack resistance index ( $\beta$ ). In the first loading cycle, the area under the hysteresis loop at the maximum peak load is used to determine the  $G_c$ , as presented in Figure 3.11(a) and Equation (3.10).  $G_c$  indicates the energy required to initiate a crack at the first loading cycle. Note that  $G_c$  is a stiffness indicator, not cracking test parameter, thus, it is not included in this study.

$$G_c = \frac{W_c}{b \times h} \quad (3.10)$$

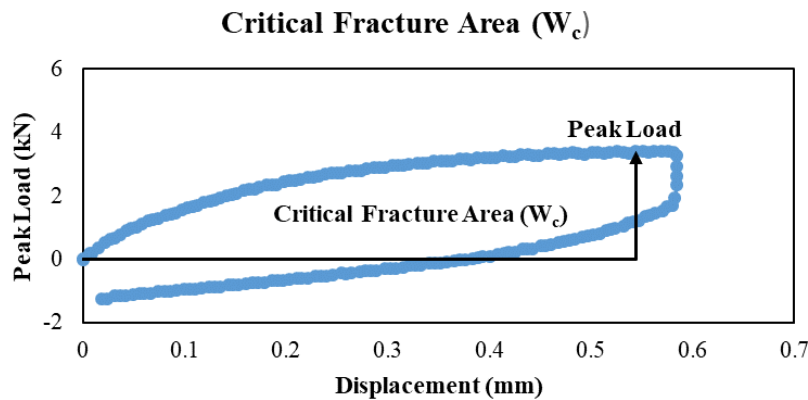
Where:

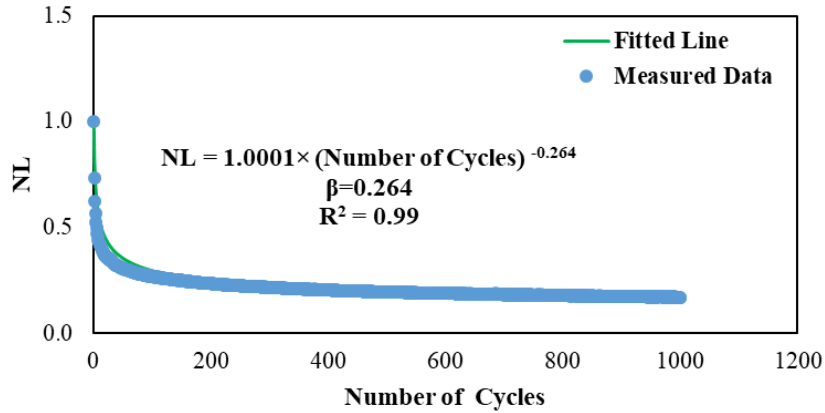
$W_c$  is the fracture area (lb.-inch);

$b$  is the specimen width (inch);

$h$  is the specimen height (inch).

In addition, the crack driving force (maximum peak load) of each loading cycle is measured and utilized to develop the load reduction curve. The load reduction curve is normalized by the maximum peak load of the first loading cycle in order to compare the results among different mixtures. The normalized load (NL) reduction curve is fitted with a power equation, and the power coefficient (absolute value) of the power equation is determined as the cracking test parameter  $\beta$ , as shown in Figure 3.11(b). The coefficient of regression (i.e.,  $R^2$ ) of the fitted line is usually higher than 0.9.  $\beta$  is indicative of the flexibility and fatigue behavior of mixtures during the crack propagation phase. Mixtures with lower  $\beta$  values are expected to have better cracking resistance than those with higher  $\beta$  values.





(b)

**Figure 3. 11 Illustration of the New Analysis Methodology of TX-OT; (a)  $W_c$ , (b)  $\beta$**

### 3.4.3 NCAT Modified Overlay Test

As noted previously, the NCAT method differs from the TX-OT in three ways: 1) a smaller maximum displacement, 2) a faster load frequency, and 3) a different method of determining specimen failure. The NCAT-OT failure definition uses the concept proposed by Rowe and Bouldin (2000) for the bending beam fatigue test (Ma, 2014). This approach uses the peak of the “normalized load x cycle” (NLC) curve to identify the transition from micro-crack formation to macro-crack formation and thus, failure. A comparison between the failure definitions of the two OT methods is shown in Figure 3.12.

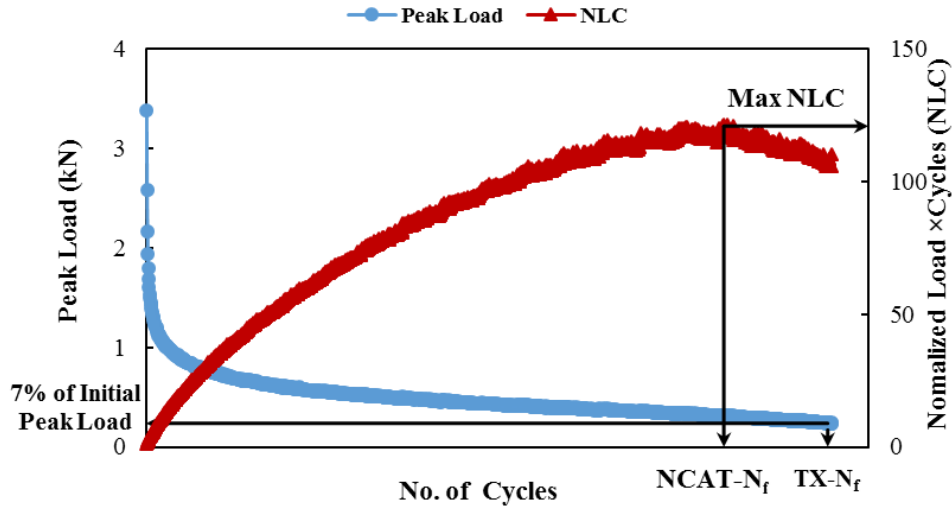


**Figure 3. 12 Determination of the failure point for NCAT-OT vs. TX-OT**

The cycle that corresponds to the maximum product of the load and the cycle is reported as the  $NCAT-N_f$  for the test. Ma (2014) reported significantly lower coefficient of variation (COV) values for this method compared to the Tex-248-F method. Furthermore, the NLC failure definition more closely matched the point at which cracks propagated completely through the specimen as evidenced in video analysis. The new analysis methodology illustrated in Figure 3.11 can also be used to determine the critical fracture energy ( $NCAT-G_c$ ) and crack resistance index ( $NCAT-\beta$ ) from results using the NCAT-OT method.

#### 3.4.4 Semi-Circular Bend Test

The SCB test was performed in accordance with a draft specification developed by the Louisiana Transportation Research Center (LTRC). This procedure uses SCB specimens with three different notch depths: 25.4, 31.8, and 38.1 mm (Cooper III et al., 2016), as shown in Figure 3.13 (a). For each mixture, six gyratory specimens were prepared and then cut in half to produce 12 semi-circular specimens. The gyratory specimens were compacted to a target height of 57 mm tall and a target air void content  $\pm 0.5\%$ . A notch was then cut to the specified depth along the center axis of the semi-circular specimen. The target notch width was  $3.0 \pm 0.5$  mm. Four

specimens were prepared and tested for each notch depth. These specimens were conditioned in an environmental chamber at  $25 \pm 0.5^\circ\text{C}$  for two hours prior to being tested. The notched test specimens were tested using an AMPT, as shown in Figure 3.13 (b).

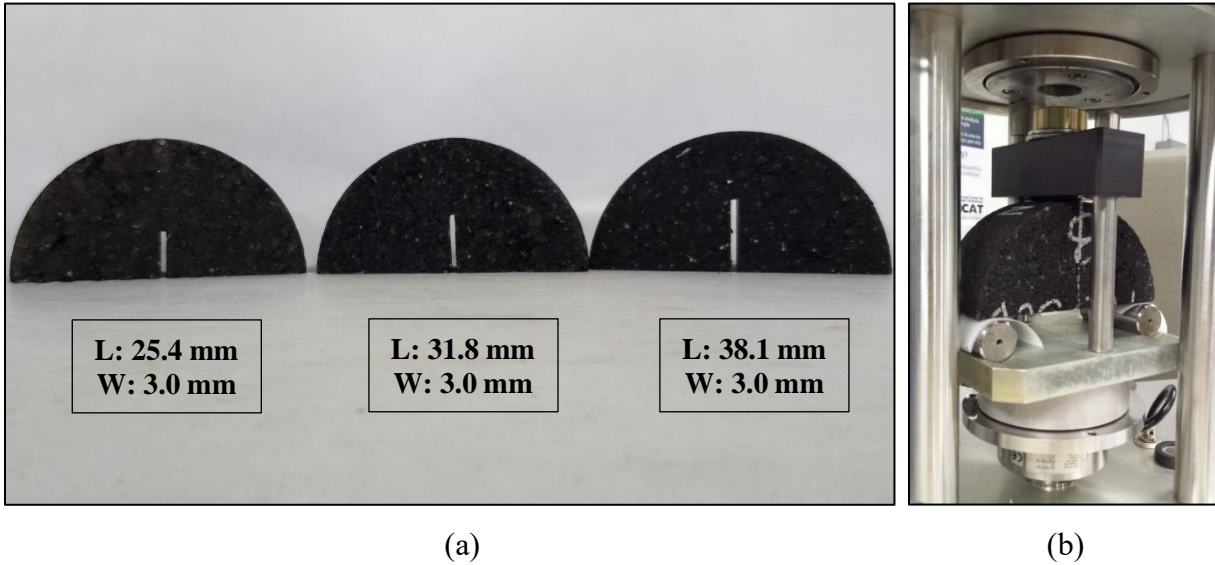


**Figure 3. 13 SCB Specimen and Test Setup; (a) Notched Specimens, (b) Test Setup**

During the test, SCB specimens were loaded at a rate of 0.5 mm/min. Strain energy to failure,  $U$ , was recorded from the test results by measuring the area under the load-displacement curve to the peak load, as shown in Figure 3.14(a). Figure 3.14(b) demonstrates how the strain energy values are then plotted against notch depth for each of the specimen replicates to create a negative linear regression line where the slope,  $dU/da$ , is used to calculate the  $J_c$  value. The J-integral, or  $J_c$ , is calculated as shown in Equation (3.11).

$$J_c = -\left(\frac{1}{b}\right) \frac{dU}{da} \quad (3.11)$$

Where:

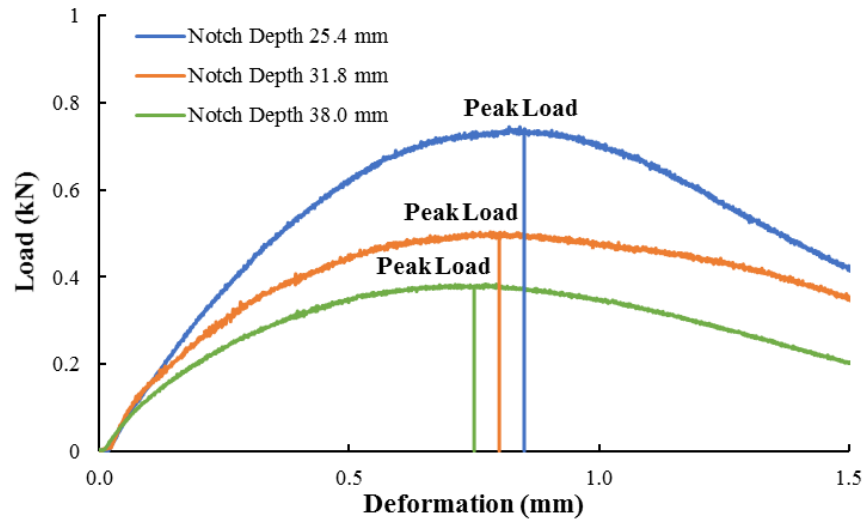
$J_c$  is the critical strain energy release rate ( $\text{kJ}/\text{m}^2$ );

$b$  is the sample thickness (mm);

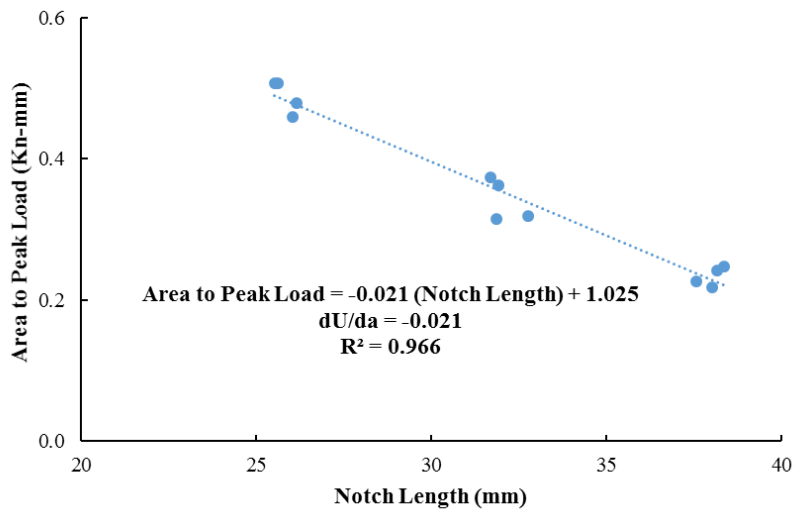
$a$  is the notch depth (mm);

$U$  is the strain energy to failure (N-mm);

$dU/da$  is the change of strain energy with notch depth.



(a)



(b)

**Figure 3. 14 Methodology of SCB Analysis;**  
**(a) Load vs. Displacement, (b) Area under load-displacement curve vs. Notch depth**

### 3.4.5 Illinois Flexibility Index Test

The I-FIT was performed in accordance with AASHTO TP 124 using a standalone, servo-hydraulic I-FIT test device, as shown in Figure 3.15 (a). I-FIT specimens were prepared to the target air voids  $\pm 0.5\%$  after trimming. A minimum of six replicates were prepared for this study. Each specimen was trimmed from a larger 160 mm tall by 150 mm diameter gyratory specimen. Four replicates were obtained per specimen, and the thickness is required to be  $50 \pm 1$  mm. A notch was then cut into each specimen at a target depth of 15 mm and width of 1.5 mm along the center axis of the specimen, as shown in Figure 3.15 (b). Tests were conducted at  $25.0 \pm 0.5^\circ\text{C}$  after being conditioned in an environmental chamber for 2 hours.

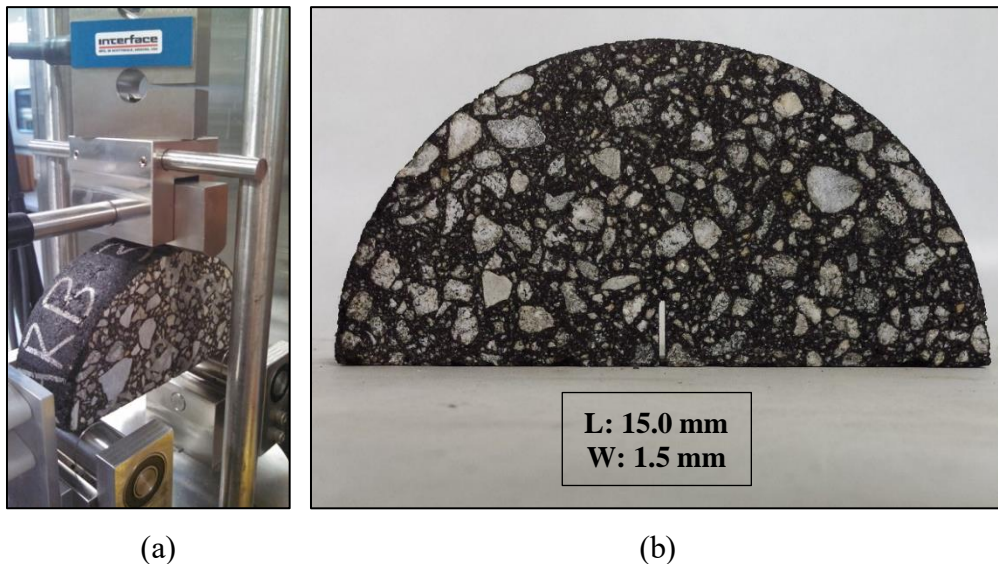


**Figure 3. 15 I-FIT Test Setup and Specimen; (a) Test Setup, (b) I-FIT Specimen**

During the test, specimens were loaded over two rollers at a rate of  $50 \pm 2.0$  mm/min, and the load and corresponding displacement were recorded at a rate of 50 Hz by the computer system. The load versus displacement curve was plotted and used to determine the slope at inflection point ( $m$ ) and the area under the curve, defined as fracture work ( $W_f$ ), as shown in

Figure 3.16. Flexibility index (FI) was calculated from the slope and fracture work, as shown in Equation (3.12).

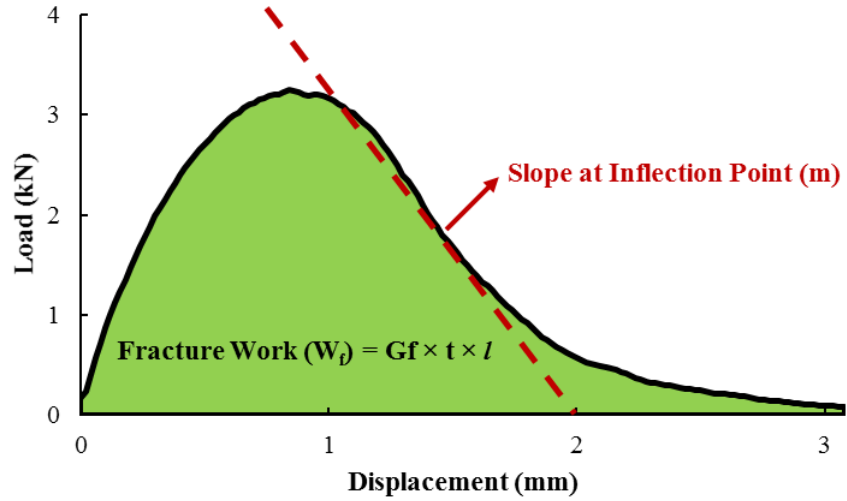


**Figure 3. 16 Illustration of I-FIT Analysis**

$$G_f = \frac{W_f}{t * l} \tag{3.12}$$

$$FI = A \times \frac{G_f}{|m|}$$

Where:

*FI* is the unit-less flexibility index;

*G<sub>f</sub>* is the fracture energy in J/m<sup>2</sup>;

*m* is the slope of the inflection point;

*t* is the specimen thickness, mm;

*l* is the ligament length, mm;

*A* is a scaling factor of 0.01.

In this study, I-FIT was also used to test the field cores collected from test sections for the validation of the preliminary critical aging protocol. However, because the field cores had

inconsistent thickness and air voids, their results were adjusted by applying a thickness correction factor and a density correction factor to the *FI* values, as shown in Equation 3.13 (Rivera-Perez, 2017). In this study, post-construction field cores collected from the NCAT Test Track had thicknesses ranging between 30 and 40 mm and air voids between 7.0 to 10.0 percent.

$$\text{Corrected } FI = \text{Measured } FI \times \frac{t_F}{50} \times \frac{0.0651}{V_a - V_a^2} \quad (3.13)$$

Where:

$t_F$  is the thickness of field cores, mm;

$V_a$  is the air voids of field cores (%).

#### 3.4.6 Indirect Tensile Asphalt Cracking Test

The IDEAL-CT test was performed using a stand-alone, servo-hydraulic device and in accordance with ASTM D 8255-19. IDEAL-CT specimens were compacted to a target height of 57 mm and a target air void content  $\pm 0.5\%$  using an SGC. A minimum of six replicates were prepared for each mixture. The specimens were tested at  $25.0 \pm 0.5^\circ\text{C}$  after being conditioned in an environmental chamber for 2 hours. The IDEAL-CT was performed using a common IDT test fixture loaded at a rate of 50 mm/min, as presented in Figure 3.17.



**Figure 3. 17 IDEAL-CT Test Setup**

During the test, load and displacement were recorded at a rate of 50 Hz. The load vs. displacement curve was plotted and used to determine the post-peak slope corresponding to 75% of the peak load ( $P_{75}$ ) and the total area under the curve, defined as fracture work ( $W_f$ ), as shown in Figure 3.18. The interval slope ( $m$ ) is the slope between  $P_{85}$  and  $P_{65}$  when the load is reduced to 85% and 65% of the peak load, respectively. The corresponding loads ( $P_{85}$ ,  $P_{65}$ ) and displacements ( $l_{85}$ ,  $l_{65}$ ) were utilized to calculate the absolute value of the interval slope ( $|m|$ ), as presented in Figure 3.18. The cracking test index ( $CT_{Index}$ ) is computed based on  $|m|$  and  $G_f$  and  $l_{75}$ , as shown in Equation (3.14).

$$G_f = \frac{W_f}{t * D} \tag{3.14}$$

$$CT_{Index} = \frac{t}{62} \times \frac{G_f}{|m|} \times \frac{l_{75}}{D}$$

Where:

$CT_{Index}$  is the unit-less cracking index;

$G_f$  is the fracture energy in  $J/m^2$ ;

$m$  is the slope at post-peak point ( $P_{75}$ ) when the load is reduced to 75% of peak load;

$t$  is the specimen thickness, mm;

$l_{75}$  is the displacement when the load is reduced to 75% of the peak load, mm;

$D$  is the specimen diameter, mm.

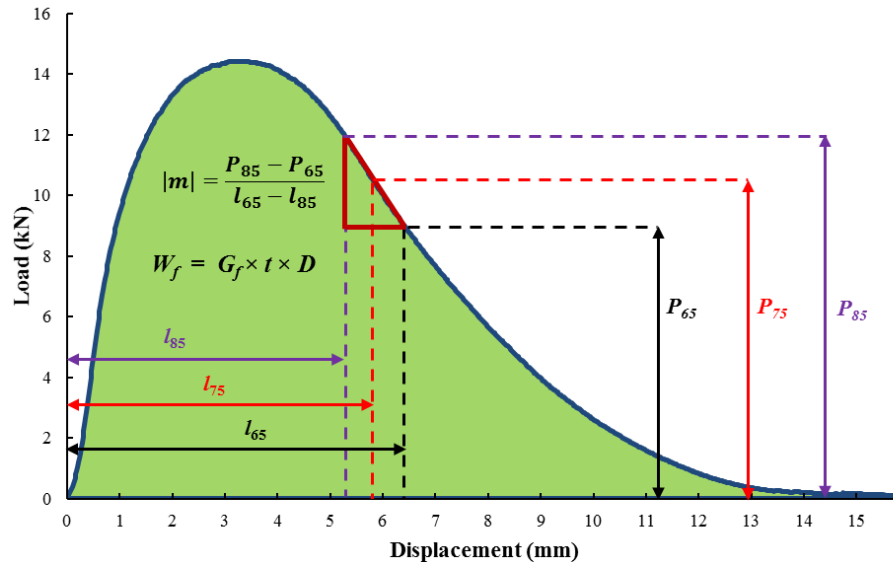


**Figure 3. 18 Illustration of IDEAL-CT Analysis**

### 3.4.7 Small-Specimen AMPT Cyclic Fatigue Test

The small-specimen AMPT cyclic fatigue test was performed in accordance with AASHTO TP 133. For each mix evaluated in the study, sufficient quantities of loose mixture were conditioned in a forced-draft oven for 8 hours at 135°C and for 5 days at 95°C to produce three to four- 180-mm tall gyratory-compacted specimens. Four small-scale (38-mm diameter and 110-mm height) specimens were cored and sawed from the larger gyratory specimens. The volumetric data for each test specimen was determined and the average Voids in Mineral Aggregate (VMA) and Voids Filled with Asphalt (VFA) were recorded.

Each fatigue test includes a tension-compression dynamic modulus fingerprint (FP) and a direct tension cyclic fatigue loading program. During the FP test, the specimen is subjected to a

non-damaging strain amplitude that produces a target on-specimen strain ranging between 50 and 75  $\mu\text{m}$ . Strain on the specimen are measured using three LVDTs with a 70-mm gauge length attached to steel targets that are glued to the specimen with a quick-cure epoxy. The FP is carried out at a single frequency of 10 Hz and a single temperature. The specimens are then subjected to a direct tension cyclic fatigue test at 10 Hz, in actuator displacement control mode. The target on-specimen strain level for the test is determined per the AASHTO TP 133 guidance. After completing the test, data from three specimens were used to construct a dynamic modulus master curve and three additional specimens were used for the determination of fatigue characteristics using continuum damage theory. The on-specimen strain amplitude increases gradually as the specimen is damaged and the ability of the specimen to resist displacement is diminished. Data from both dynamic modulus and AMPT cyclic fatigue tests were analyzed using the FlexMAT<sup>TM</sup> spreadsheet.

The damage capacity index,  $S_{app}$ , is the latest development for simplified-viscoelastic continuum damage mixture performance analysis. It is derived from the representative fatigue damage parameter that corresponds to  $C_{avg}$  (average pseudo stiffness of the material during fatigue testing) on the damage characteristic curve (Etheridge et al., 2019). The  $S_{app}$  value is calculated using Equation 3.15. In this study, the  $S_{app}$  at 21°C was used to compare the fatigue resistance of plant-mixed, lab-compacted (PMLC) specimens with different laboratory aging protocols.

$$S_{app} = 1000^{\frac{\alpha}{2}-1} \frac{a_T^{\frac{1}{\alpha+1}} \left( \frac{D^R}{C_{11}} \right)^{\frac{1}{C_{12}}}}{|E^*|^{\frac{\alpha}{4}}} \quad (3.15)$$

Where:

$a_T$  is the time-temperature shift factor computed at the reference temperature;

$C_{11}$  and  $C_{12}$  are power law coefficients to fit the damage characteristic curve;

$\alpha$  is the damage growth rate in the governing evolution law;

$|E^*|$  is the dynamic modulus at 10 Hz and the temperature of interest;

$D^R$  is the average reduction in pseudo stiffness up to failure.

### 3.4.8 Summary

Table 3.3 summarizes the test details of six laboratory cracking tests, including test equipment, loading condition, test temperature, time to complete steps, and the typical test variability (i.e., COV). For each cracking test, the equipment listed in the table were used in the NCAT laboratory; other agencies might use different equipment. The time to complete each test consisted of four parts, which included cutting time, preparation time, condition time, and test time. The cutting time only considered the process of trimming the compacted gyratory samples to specimens of required configuration using the cutting equipment at the NCAT laboratory. The preparation work included bulking, drying, measuring dimensions, and instrumentation (e.g., gluing samples). The test time only counted the testing process using the test equipment in NCAT laboratory for the number of specimens representing one test. Note that the all of the times listed were estimated based on the average NCAT operation speed for one set of specimens. In addition, the COV value for each cracking test was summarized based on the limited literature review (Ma, 2014; Moore, 2016; Zhou et al., 2016).

**Table 3. 3 Summary of Laboratory Cracking Tests**

Test Name		Test Equipment	Loading Condition	Test Temperature	Time				Test Variability
					Cutting	Preparation	Condition	Test	
ER	M <sub>R</sub>	MTS	Five cyclic haversine waveform loading to horizontal 100-200 $\mu\epsilon$ (0.1s loading followed by 0.9s relaxing)	10 °C	10-15 min	0.5 days	Overnight	1 day	Not Available
	IDT		Monotonic vertical axis loading at 50 mm/min						
	Creep		Static loading for 1000s Controlling horizontal $\epsilon_{100s}$ (100-150 micro-inch) and $\epsilon_{1000s}$ (< 750 micro-inch)						
TX-OT		AMPT	Displacement-controlled cyclic loading to 0.635 mm using sawtooth waveform at 0.1 Hz	25 °C	1-1.5 hours	0.5 days (overnight curing)	2 hours	Varies (hours-days)	30-50% COV
NCAT-OT		AMPT	Displacement-controlled cyclic loading to 0.381 mm using sawtooth waveform at 1.0 Hz	25 °C	1-1.5 hours	0.5 days (overnight curing)	2 hours	Varies (hours-days)	20-30% COV
SCB		AMPT	Monotonic three-point bending at 0.5 mm/min	25 °C	3-4 hours	3-4 hours	2 hours	1.5-2 hours	Not Available
I-FIT		Stand-alone servo hydraulic	Monotonic three-point bending at 50 mm/min	25 °C	1.5-2 hours	1.5-2.5 hours	2 hours	10-15 min	10-20% COV
IDEAL-CT		Stand-alone servo hydraulic	Monotonic vertical axis loading at 50 mm/min	25 °C	No Need	1 hour	2 hours	10-15 min	10-20% COV

## **CHAPTER 4 SELECTING A PRELIMINARY CRITICAL AGING PROTOCOL**

Considering the importance of age hardening of asphalt mixtures in the development of TDC, laboratory specimens should be short-term conditioned and long-term aged prior to testing. Although some long-term aging protocols have been proposed for use in mixture design and performance testing, their correlations with field aging have not been identified. In addition, the traditional expectation of long-term aging has been to simulate seven to ten years of field aging, but that length of time may not be appropriate to evaluate TDC which more commonly occurs in the first five years of service. In this chapter, the critical field aging condition was first identified using cumulative degree-days (CDD) instead of pavement in-service time. Furthermore, a preliminary critical aging protocol was selected through correlating field aging with four laboratory loose mixture aging protocols in terms of their effects on the rheological and oxidation properties of asphalt binders.

### **4.1 Identification of Critical Field Aging for TDC**

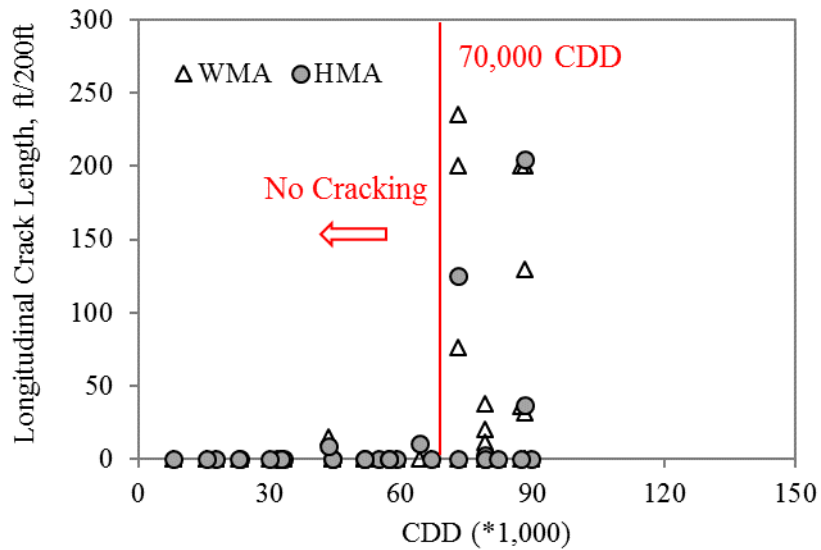
Pavement in-service time (e.g. months or years) at the time of coring is commonly used to quantify field aging of asphalt mixtures. Time, however, fails to differentiate the aging of pavements in different climates and construction seasons. Generally, for the same amount of time, field aging is more severe in warmer climates than in colder climates. In NCHRP project 09-52, the CDD parameter was proposed to overcome this shortcoming (Newcomb et al., 2015). As expressed in Equation (4.1), CDD was defined as the accumulation of the daily high temperature above freezing for all the days being considered from the time of construction to the time of coring or field inspection. Compared to in-service time, CDD takes into account both temperature and time in characterizing the field aging of asphalt pavements.

$$CDD = \begin{cases} \sum (T_{dmax} - 32), & \text{if } T_{dmax} \geq 32 \\ 0, & \text{if } T_{dmax} < 32 \end{cases} \quad (4.1)$$

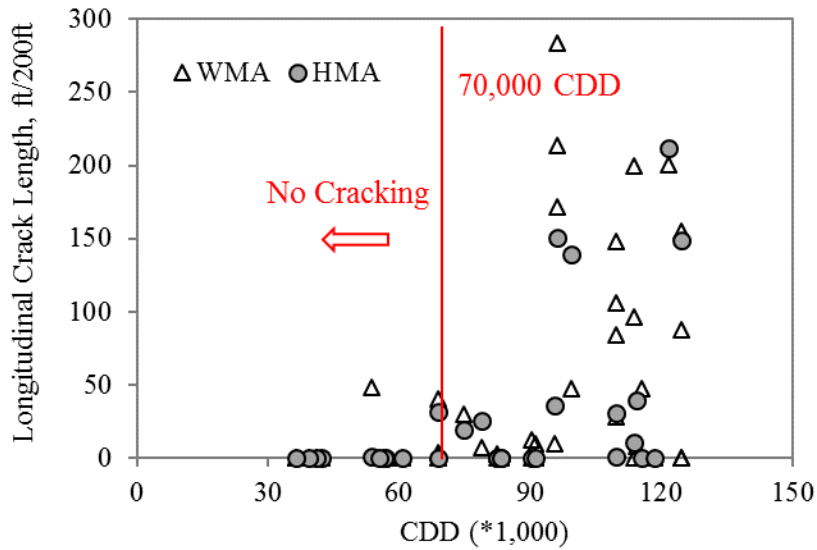
Where:

$T_{dmax}$  = daily max temperature, °F.

In NCHRP project 09-49A, the long-term field performance of 53 warm mix asphalt (WMA) and 30 HMA pavement sections were monitored (Shen et al., 2013). Two rounds of pavement inspections were conducted in 2012/2013 and 2014/2015 to collect field distresses, including rutting, transverse cracking, and wheel-path longitudinal cracking. Figure 4.1 presents the wheel-path longitudinal crack length versus the corresponding pavement CDD at the time of pavement inspections.



(a)



(b)

**Figure 4. 1 Wheel-path Longitudinal Crack Survey Results;**  
**(a) First Survey in 2012/2013, (b) Second Survey in 2014/2015 (Shen et al., 2017)**

For the first survey results shown in Figure 4.1(a), pavements with less than 70,000 CDD showed no cracking, while some with over 70,000 CDD had measurable cracking (crack length over 20 feet). A similar trend was also observed for the second survey results, as shown in Figure 4.1(b). Examination of field cores sampled from pavements with wheel-path longitudinal cracks showed that these cracks initiated from the pavement surface and stopped within the surface layer, which was indicative of top-down fatigue cracking (Shen et al., 2013). Based on these results in Figure 4.1, TDC seemed to develop in most of the asphalt pavements with approximately 70,000 CDD or more of field aging. Thus, 70,000 CDD was proposed as a preliminary critical field aging condition to evaluate TDC. Figure 4.2 presents a map showing the number of years required by different states to reach this preliminary CDD value. Note that the CDD values shown for each state are based on weather data for the state’s capital city. In general, warm climate states (e.g., Alabama, Florida, Texas, etc.) need approximately 4 years to

achieve 70,000 CDD while a significantly longer time of up to 8 years is required for states in cold climates (e.g., Michigan, Minnesota, Wisconsin, etc.).

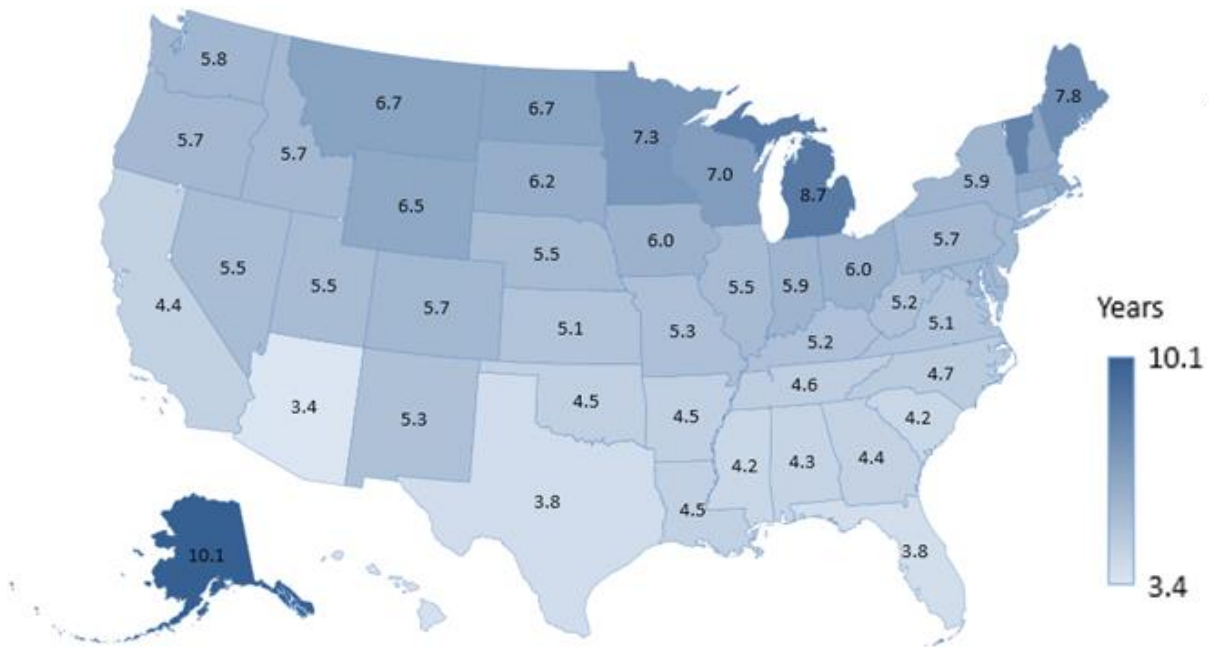


**Figure 4. 2 A Map showing the Number of Years to Reach 70,000 CDD**

## 4.2 Experimental Design

Figure 4.3 presents the research methodology used to select a laboratory aging protocol to simulate 70,000 CDD of field aging. Materials used in the experiment were from five field projects in Washington, Michigan, and Alabama. Specific details about the mixture components were presented in Table 3.1. For each field project, plant produced mixtures and post-construction field cores were sampled and tested to characterize field aging, and the dates of construction and coring were presented in Table 4.1. Based on the construction and coring dates, the CDD number of each project was calculated using Equation (4.1), which was also summarized in Table 4.1.

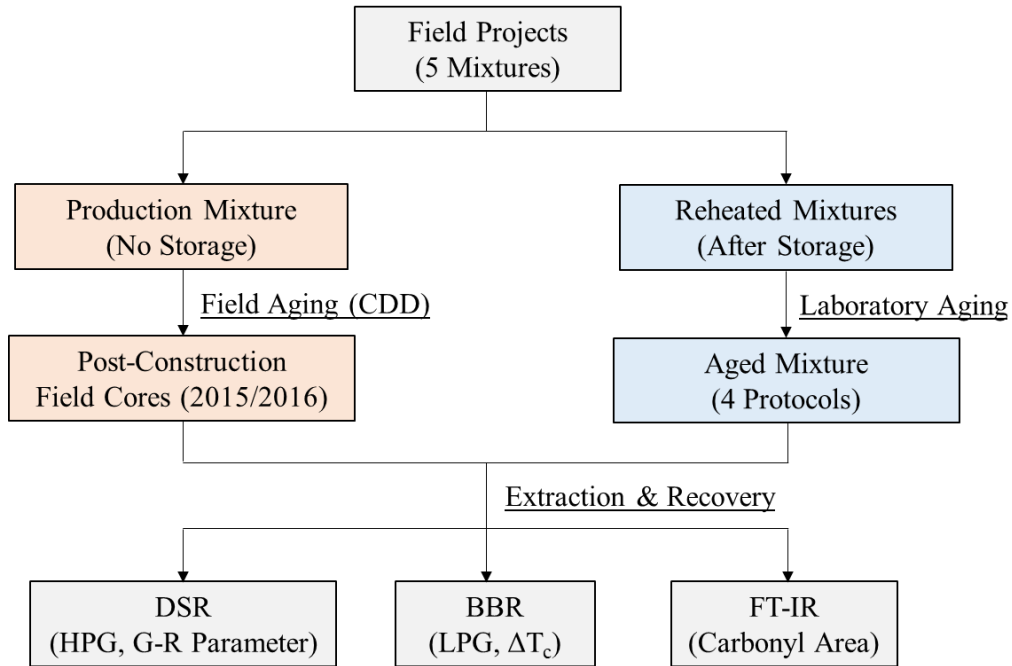


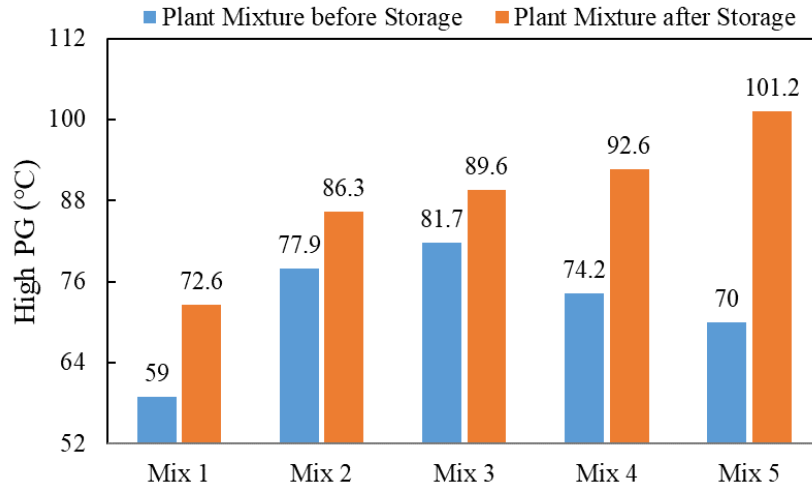
**Figure 4. 3 Research Methodology for Laboratory Aging**

**Table 4. 1 Summary of Construction and Coring Dates**

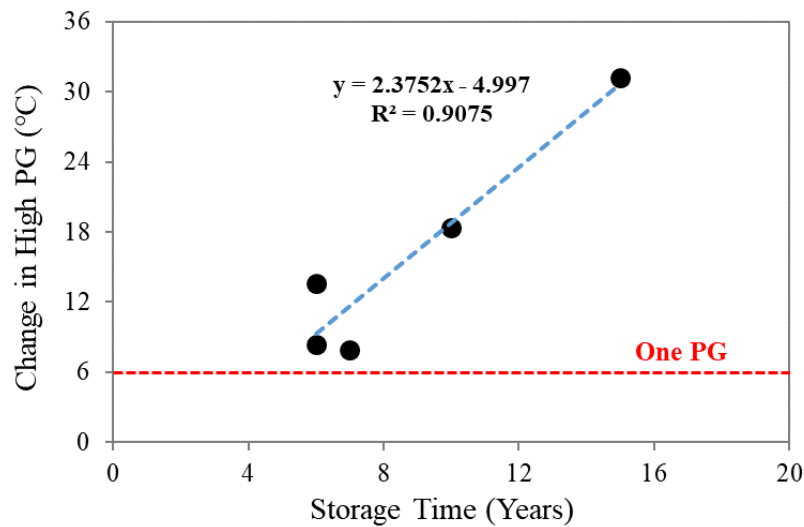
Mix ID	Mix 1	Mix 2	Mix 3	Mix 4	Mix 5
Location	Rapid River, Michigan	Walla Walla, Washington	Auburn, Alabama	Auburn, Alabama	Auburn, Alabama
Construction Date	07/2010	04/2010	07/2009	09/2006	07/2000
Post- Construction Coring Date	09/2016	10/2016	10/2016	10/2016	01/2015
In-Service Time	6 years, 2 months	6 years, 6 months	7 years, 3 months	10 years, 1 month	14 years, 6 months
CDD	48,000	80,000	114,000	157,000	235,000

It should be noted that the storage of plant mixtures was not climate-controlled, thus, the plant mixtures aged during the storage. Figure 4.4 (a) presents the HPG results of the binders extracted from the plant mixtures before and after storage. It could be seen that, for all five mixtures, the HPG results increased dramatically after storage. Furthermore, the change in HPG for five mixtures was plotted against the corresponding storage time, and a linear equation was used to fit the results, as shown in Figure 4.4 (b). In general, the change in HPG ranged between

7.9 to 31.2°C, and it increased with the storage time. Note that the linear relationship between storage time and the change in HPG is limited for these five mixtures, which might not be appropriate for other mixtures.



(a)



(b)

**Figure 4. 4 HPG Results of Plant Production Mixtures; (a) HPG Results before and after Storage, (b) Correlation between Change in HPG with the Storage Time**

The plant mixtures from each project were conditioned with four loose mixture aging protocols of 5 days at 95°C, 6 hours at 135°C, 12 hours at 135°C, and 24 hours at 135°C. To

prepare loose mixture samples, buckets of each plant mixture were first placed in an oven at 150°C for approximately three hours. Afterwards, the reheated mixture was batched into individual samples of approximately 2,500 grams, which were then spread out in shallow pans and placed back in the oven for further aging at the four conditions noted above. Mixture samples aged for 5 days at 95°C were stirred once every 24 hours to ensure aging uniformity. As mentioned previously, post-construction field cores were included in the experiment to represent field aging. Considering the non-uniform aging of asphalt pavements with depth (Elwardany et al., 2017; Turner, 2008; Yin et al., 2017a), only the top one inch of the field cores was tested. Asphalt binders were extracted and recovered from reheated plant mixtures, laboratory aged mixtures, and post-construction field cores in accordance with AASTHO T164 and ASTM D 5404, respectively. The extracted and recovered binders were then subjected to DSR, BBR, and FT-IR testing without additional aging using the rolling thin-film oven (RTFO) or pressure aging vessel (PAV).

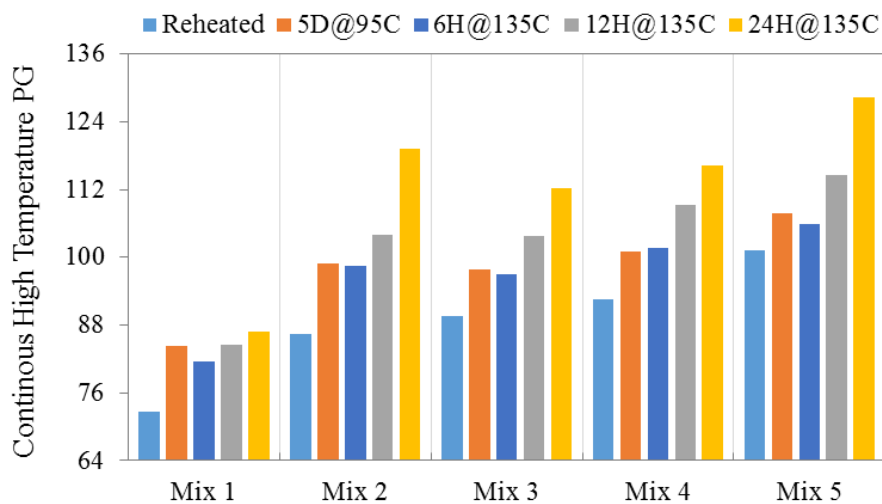
### **4.3 Tests Results and Data analysis**

This section presents the DSR, BBR, and FT-IR results of asphalt binders extracted from laboratory aged mixtures and pavement cores. Test results were analyzed to evaluate the effects of laboratory loose mixture aging on binder rheological and oxidation properties. Additionally, the correlation of field aging with these aging protocols was explored. Finally, protocols that were representative of 70,000 CDD of field aging were preliminarily selected for the NCAT TDC experiment.

#### *4.3.1 Comparisons of Laboratory Aging Protocols*

##### (1) Continuous PG Results

Figure 4.5 presents the continuous HPG and LPG results of asphalt binders extracted from reheated and laboratory aged mixtures. As shown in Figure 4.5(a), for all five mixtures, asphalt binders from laboratory aged mixtures showed consistently higher HPG than those from the corresponding reheated mixtures, which indicated that the aging protocols evaluated in this study yielded significant levels of asphalt aging. The average increase in the continuous HPG for different aging protocols varied from 8.4 to 24.1°C. As expected, longer aging times at 135°C showed greater increases in the continuous HPG. For all mixtures except Mix 4, the 5-day, 95°C protocol yielded a slightly higher increase in the HPG than the 6-hour, 135°C protocol. The average difference in the continuous HPG between these two aging protocols was approximately 1.1°C, which was not considered practically significant. Similar trends were also observed for the continuous LPG results shown in Figure 4.5(b). In general, the 24-hour, 135°C protocol yielded the greatest increase in both HPG and LPG, followed by the 12-hour, 135°C protocol, 5-day, 95°C protocol, and 6-hour, 135°C protocol, respectively.



(a)

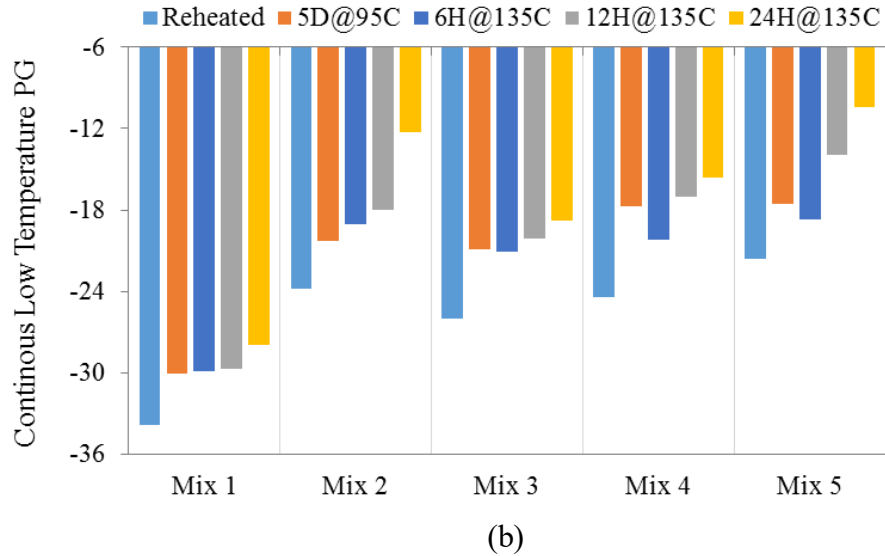
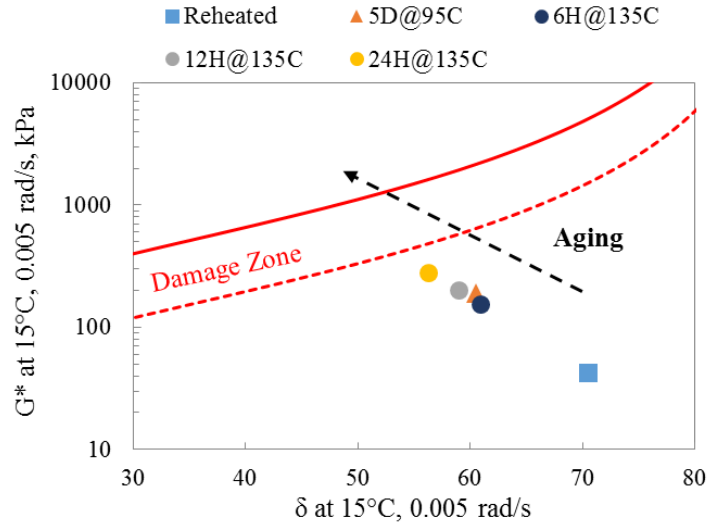


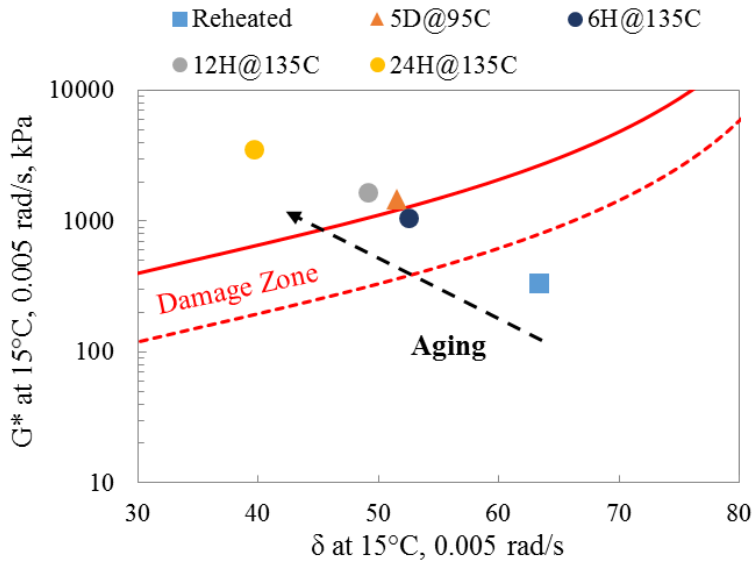
**Figure 4. 5 Continuous PG Results of Extracted Asphalt Binders with Various Loose Mixture Aging Protocols; (a) High-Temperature, (b) Low-Temperature**

(2) Cracking test parameter Results

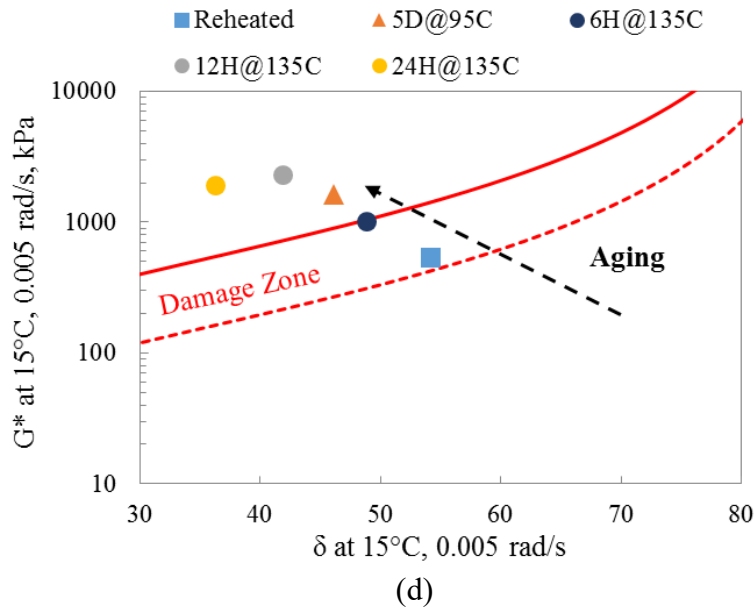
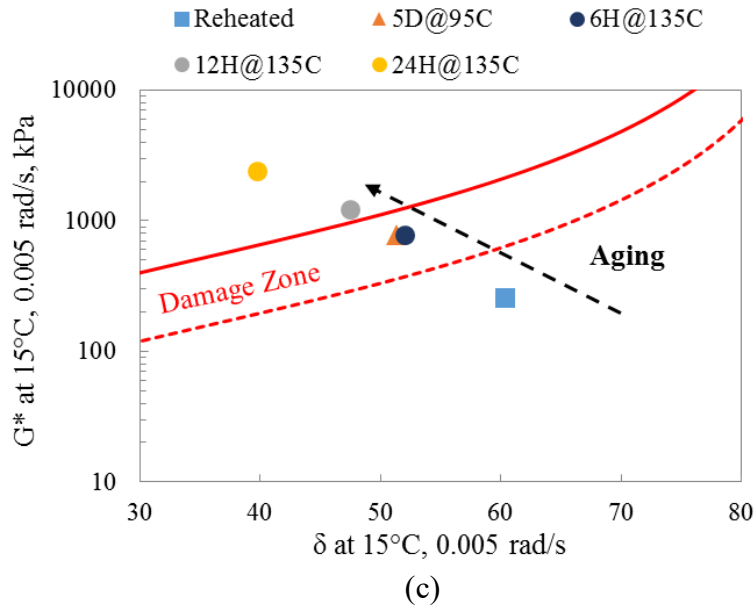
Figure 4.6 presents the  $G-R$  parameter results in Black space diagrams, where the  $G^*$  at 15°C and 0.005 rad/s of extracted asphalt binders were plotted against the corresponding  $\delta$  values. A consistent trend was observed for all mixtures that asphalt binders extracted from laboratory aged mixtures were located closer to the upper left corner on the Black space diagram than those from the reheated mixtures, which indicated that asphalt binders after aging had increased stiffness and a loss of relaxation properties. Based on the “travelled” distances on the Black space diagram, the 24-hour, 135°C protocol produced the highest level of asphalt aging, followed by the 12-hour, 135°C protocol, then the 5-day, 95°C protocol, and finally the 6-hour, 135°C protocol, respectively. These results were in agreement with the continuous PG results in Figure 4.4.



(a)



(b)



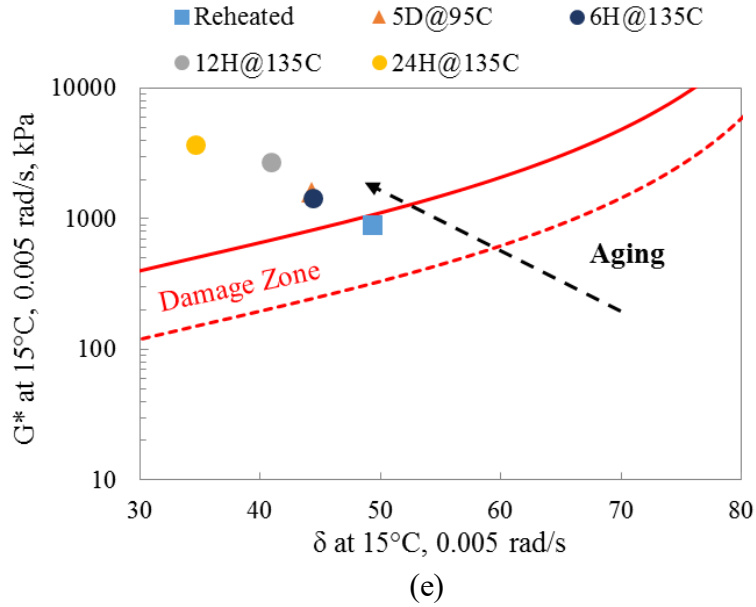


**Figure 4. 6 G-R Parameter Results in Black Space Diagram; (a) Mix 1, (b) Mix 2, (c) Mix 3, (d) Mix 4, (e) Mix 5**

Figure 4.7 presents the BBR  $\Delta T_c$  results of asphalt binders extracted from reheated and laboratory aged mixtures. As mentioned previously, asphalt binders with a more negative  $\Delta T_c$  are more susceptible to cracking due to reduced relaxation properties. As can be seen, the  $\Delta T_c$  of asphalt binders from laboratory aged mixtures was consistently lower (i.e., more negative) than those of the corresponding reheated mixtures. The 12-hour and 24-hour, 135°C protocols exhibited the two lowest  $\Delta T_c$  values for all mixtures. No consistent trend was found for the  $\Delta T_c$  comparisons between the 5-day, 95°C and 6-hour, 135°C protocols; but in most cases, the difference in the  $\Delta T_c$  between these two aging protocols was less than 1.0.

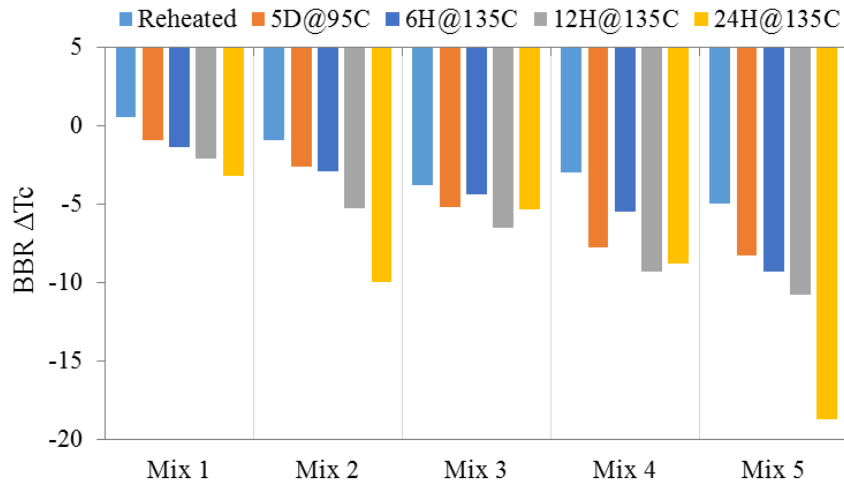


**Figure 4. 7 BBR  $\Delta T_c$  Results of Extracted Asphalt Binders with Various Loose Mixture Aging Protocols**

### (3) FT-IR CA Results

Figure 4.8 presents the FT-IR *CA* results of asphalt binders extracted from reheated and laboratory aged mixes. In general, the results were consistent with the continuous PG and *G-R* parameter results shown in Figure 4.5 and Figure 4.6, respectively. Asphalt binders extracted from 135°C mixtures showed a consistent increase in FT-IR *CA* with longer aging times, which indicated that more polar oxygen-containing functional groups were formed during the laboratory aging processes. For all mixtures except Mix 4, extracted binders from the 5-day, 95°C mix had a FT-IR *CA* that was between those of binders from the 6-hour and 12-hour, 135°C mixtures. Based on the FT-IR *CA* results, the four loose mixture aging protocols were ranked in the following order in terms of the resultant aging level: 6-hour, 135°C < 5-day, 95°C < 12-hour, 135°C < 24-hour, 135°C.

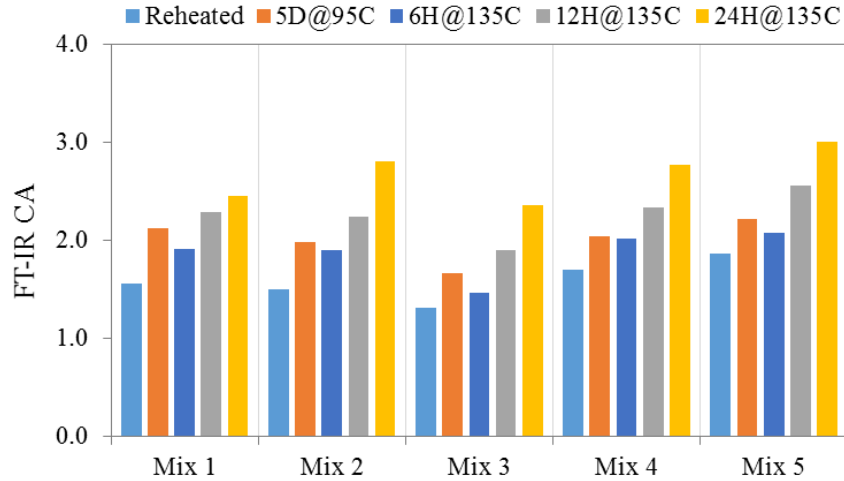


**Figure 4. 8 FT-IR CA Results of Extracted Asphalt Binders with Various Loose Mixture Aging Protocols**

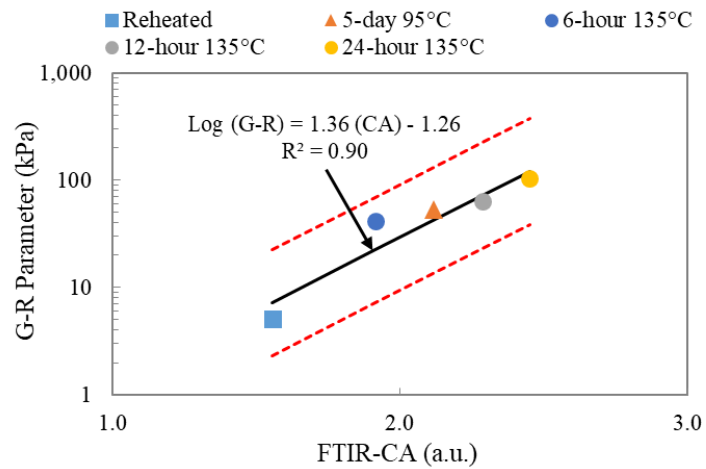
#### (4) Hardening Susceptibility Results

Previous research reported that aging at 135°C could change the relationship between chemical oxidation and physical hardening of asphalt binders due to the physicochemical disruption of its microstructure at such an elevated temperature (Peterson, 2009). This oxidation-hardening relationship was typically referred to as hardening susceptibility (Glover et al., 2005; Domke et al., 1999). In this study, the Glover-Rowe hardening susceptibility (*G-R HS*) parameter was used to explore the impact of loose mixture aging on the oxidation-hardening relationship of asphalt binders. As expressed in Equation (4.2), the *G-R HS* was defined as the ratio of change in the logarithm of the *G-R* parameter over the change in the FT-IR *CA* with aging (Yin et al, 2017c).

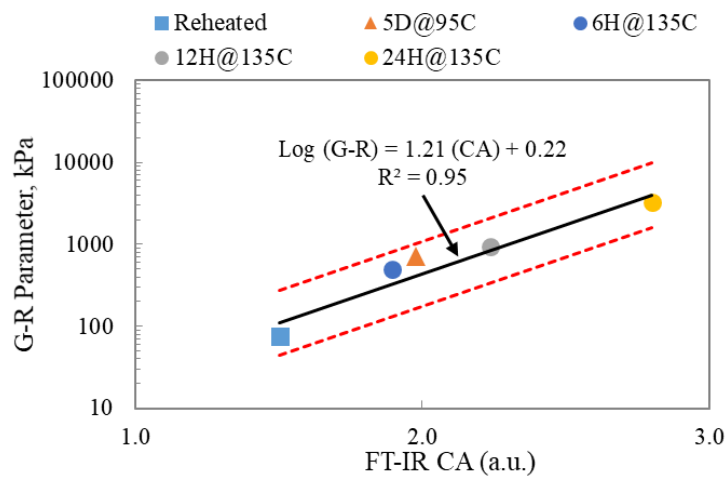
$$G-R HS = \frac{d[\log(G-R)]}{d(CA)} \quad (4.2)$$

Figure 4.9 presents the *G-R HS* results of all five mixtures. In the figure, the *G-R* parameter and FT-IR *CA* results were fitted using a semi-log linear relationship and the slope of the trendline represented the *G-R HS*. The solid line represented the trendline determined based

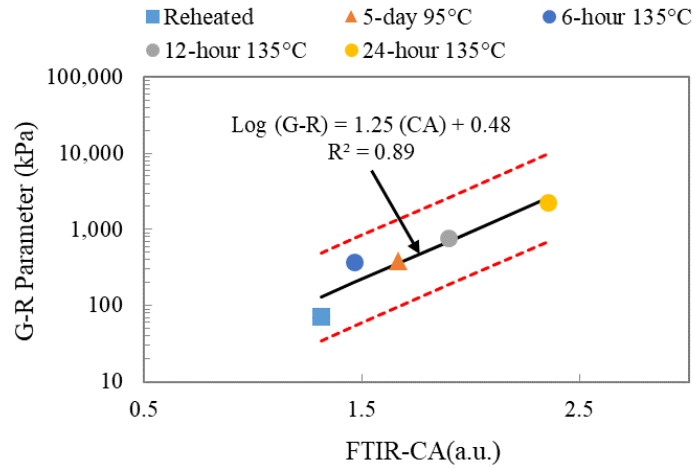
on the aging protocols at 135°C, and the dashed lines represented the 95% confidence interval for the trendline. For all five mixtures, the coefficient of determination (i.e.,  $R^2$ ) of the trendline was very close to or greater than 0.9, indicating a high goodness of the fit for the relationship. As shown in the Figure 4.9, for all five mixtures, the results of 95°C aging protocol was always located within the 95% confidence interval of the trendline determined based on aging protocols at 135°C, indicating no significant difference in the oxidation-hardening relationship of asphalt binders aged at 95°C versus 135°C.



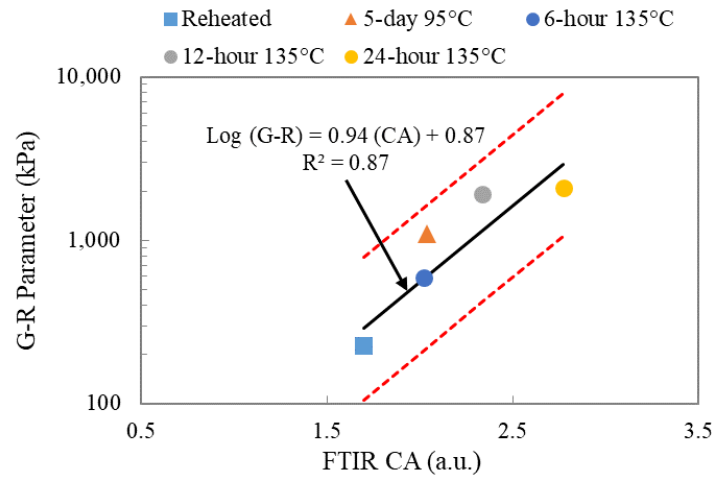
(a)



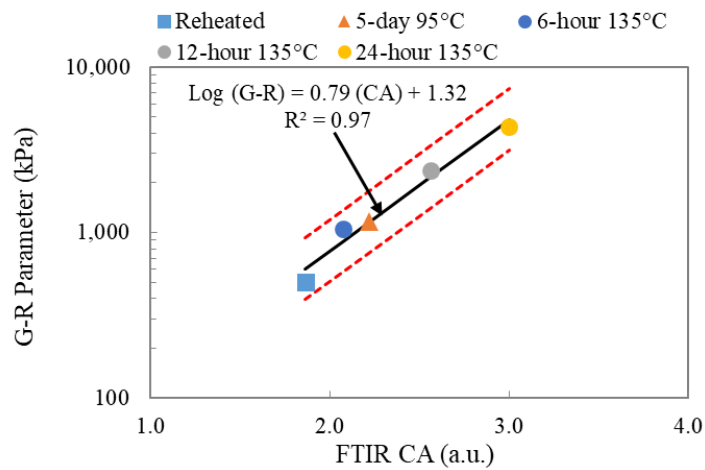
(b)



(c)



(d)

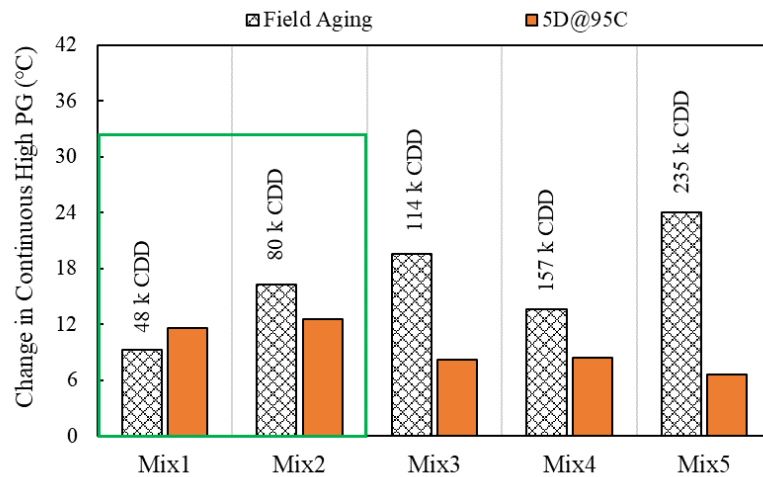


(e)

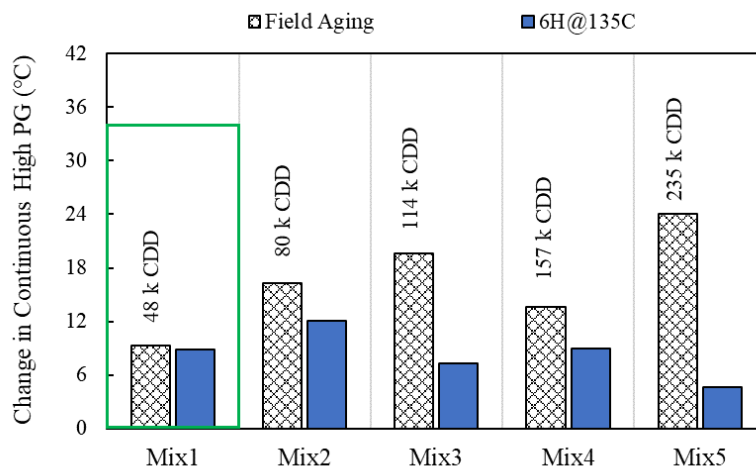
**Figure 4. 9 G-R HS Results; (a) Mix 1, (b) Mix 2, (c) Mix 3, (d) Mix 4, (e) Mix 5**

### 4.3.2 Correlation of Field Aging with Laboratory Aging Protocols

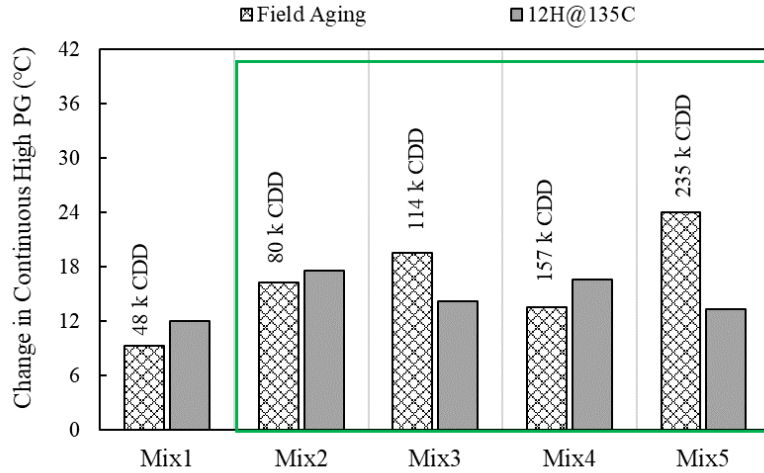
Figure 4.10 presents the continuous HPG results to determine the correlation of field aging with laboratory loose mixture aging protocols. The pattern-filled bars represent the difference in the continuous HPG of asphalt binders extracted from post-construction field cores versus the corresponding plant mixtures that were tested immediately after sampling. The solid-filled bars represent the difference between the laboratory aged mixtures and reheated mixtures after storage.



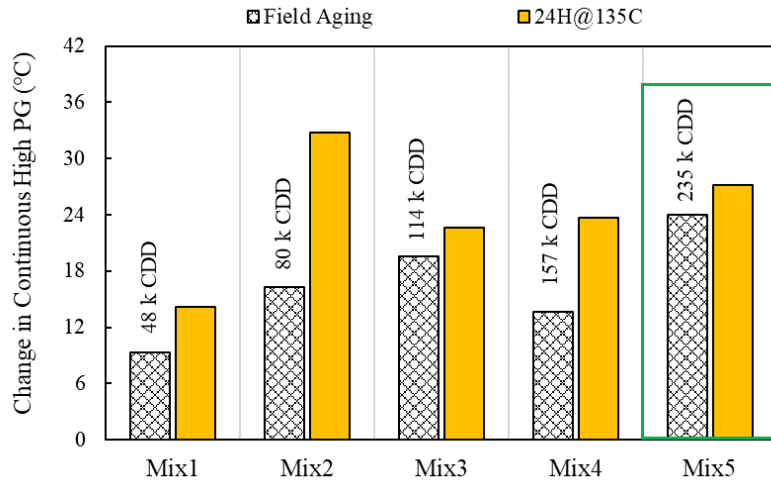
(a)



(b)



(c)



(d)

**Figure 4. 10 Comparison of Field Aging and Laboratory Loose Mixture Aging Protocols; (a) 5-day, 95°C, (b) 6-hour, 135°C, (c) 12-hour, 135°C, (d) 24-hour, 135°C**

As shown in Figure 4.10(a), the 5-day, 95°C protocol was more severe than field aging of approximately 48,000 CDD (Mix 1), as indicated by a greater increase in the continuous HPG. The opposite trend, however, was shown for the other mixtures with field aging of approximately 80,000, 157,000, and 235,000 CDD, respectively. These results indicated that the 5-day, 95°C protocol yielded asphalt aging that was representative of field aging between 48,000 and 80,000 CDD. The same approach was applied for the other three loose mixture aging protocols [Figure

4.10(b) to Figure 4.10(d)], and their representative CDD ranges are summarized as follows. For 12-hour, 135°C protocol, an expected trend existed where this protocol showed higher aging level than 157,000 CDD, but lower aging level than 114,000 CDD. This unexpected situation might be caused by the testing errors or the different aging characteristics of SBS modified binder used in Mix 3 (Sun et al., 2014; Ruan et al., 2003; Ouyang et al., 2006). Thus, the representative CDD range of 12-hour, 135°C protocol was identified as 80,000 – 235,000.

- 5-day, 95°C protocol: 48,000 to 80,000 CDD
- 6-hour, 135°C protocol: approximately 48,000 CDD
- 12-hour, 135°C protocol: 80,000 to 235,000 CDD
- 24-hour, 135°C protocol: greater than 235,000 CDD

As discussed previously, 70,000 CDD was identified as a preliminary critical field aging condition for evaluating TDC. Therefore, based on the data shown in Figure 4.10, loose mixture aging of 5 days at 95°C was the most representative aging protocol.

#### *4.3.3 Selection of Alternative Aging Protocol at 135°C*

Although loose mixture aging of 5 days at 95°C was identified as the most appropriate protocol to simulate 70,000 CDD of field aging, this protocol is not practical for implementation.

Therefore, test results were further analyzed to determine an alternative aging protocol at 135°C that yielded an equivalent level of aging as the 5-day, 95°C protocol. Figure 4.11(a) presents an example of the FT-IR *CA* results of Mix 2. To determine the alternative aging protocol, the fast-rate-constant-rate oxidation kinetic model (Jin et al., 2011), described in Equation (4.3), was first used to fit the FT-IR *CA* results of laboratory aged mixtures at 135°C. Once the model coefficients were determined, the equivalent aging time at 135°C was then calculated based on

the measured FT-IR  $CA$  of the 5-day,  $95^{\circ}\text{C}$  protocol [Figure 4.11(a)]. For the continuous HPG and  $G-R$  results, linear and semi-log linear models were used to determine the equivalent aging times, respectively. As shown in Figure 4.11(b), for both oxidation and rheological parameters, similar level of asphalt aging was achieved by loose mixture aging protocols of 5 days at  $95^{\circ}\text{C}$  and approximately 8 hours at  $135^{\circ}\text{C}$ . Thus, the 8-hour,  $135^{\circ}\text{C}$  protocol was recommended as an alternative loose mixture aging protocol to simulate 70,000 CDD of field aging. In order to differentiate this aging protocol from short-term and other long-term aging protocols, NCAT researchers termed it the “critical aging” protocol to specifically associate it with the point at which surface cracking typically occurs.

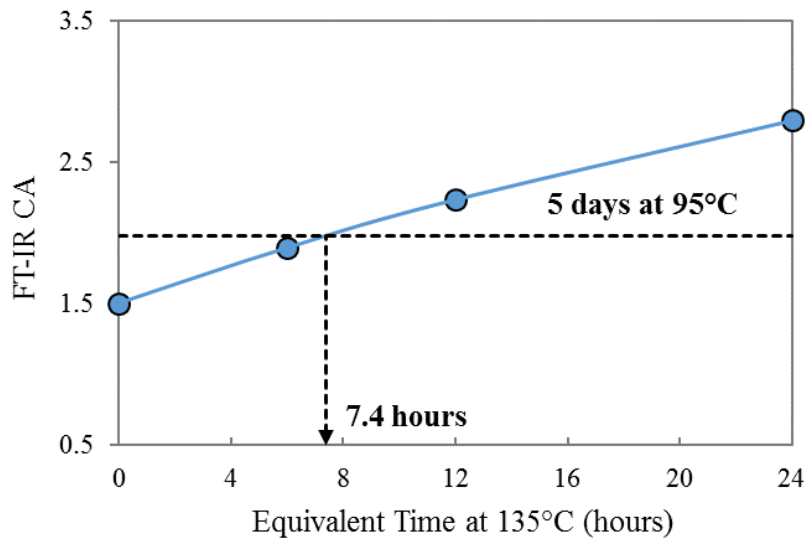
$$CA = CA_0 + k_c t + M(1 - e^{-k_f t}) \quad (4.3)$$

Where:

$CA_0$  = carbonyl area of asphalt binder extracted from the reheated mixture;

$t$  = aging time at  $135^{\circ}\text{C}$ ;

$k_c$ ,  $k_f$ , and  $M$  = model coefficients.



(a)

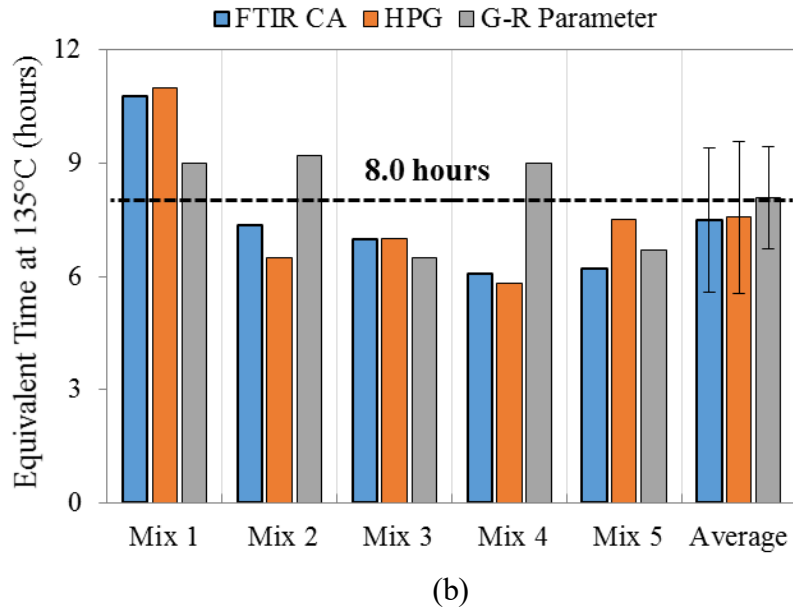


**Figure 4. 11 Determination of Equivalent Aging Time at 135°C; (a) Example of Mix 2 FT-IR CA Results, (b) Summary of All Results**

#### 4.4 Summary

The objective of this chapter was to select a preliminary mixture aging protocol for the NCAT TDC experiment. Four different loose mix aging protocols were evaluated in terms of their effects on rheological and oxidation properties of asphalt binders. In addition, their correlations with field aging were investigated based on the concept of CDD. Based on the results of this study, the following conclusions were obtained:

(1) TDC was found to develop in asphalt pavements with over approximately 70,000 CDD; thus, this CDD value was identified as the critical field aging condition for evaluating TDC.

(2) Based on the rheological and oxidation results, the 24-hour, 135°C protocol yielded the greatest amount of asphalt aging, followed by the 12-hour, 135°C protocol, 5-day, 95°C, protocol, and 6-hour, 135°C protocol, respectively.

(3) The *G-R HS* parameter was used to explore the effect of loose mixture aging on the oxidation-hardening relationship of asphalt binders. For the five mixtures evaluated in this study,

no significant difference in the *G-R HS* results was shown for mixtures aged at 95°C versus 135°C.

(4) Among the four loose mixture aging protocols evaluated in this study, the 5-day, 95°C protocol was most representative of 70,000 CDD of field aging.

(5) Based on the HPG, *G-R* parameter, and FT-IR *CA* results, the loose mixture aging protocol of 8 hours at 135°C was anticipated to yield an equivalent level of aging as that of 5 days at 95°C. Therefore, the 8-hour, 135°C loose mix protocol has been termed the “critical aging protocol” and recommended it as a practical method to simulate 70,000 CDD of field aging.

## **CHAPTER 5 PRELIMINARY VALIDATION OF THE CRITICAL AGING PROTOCOL**

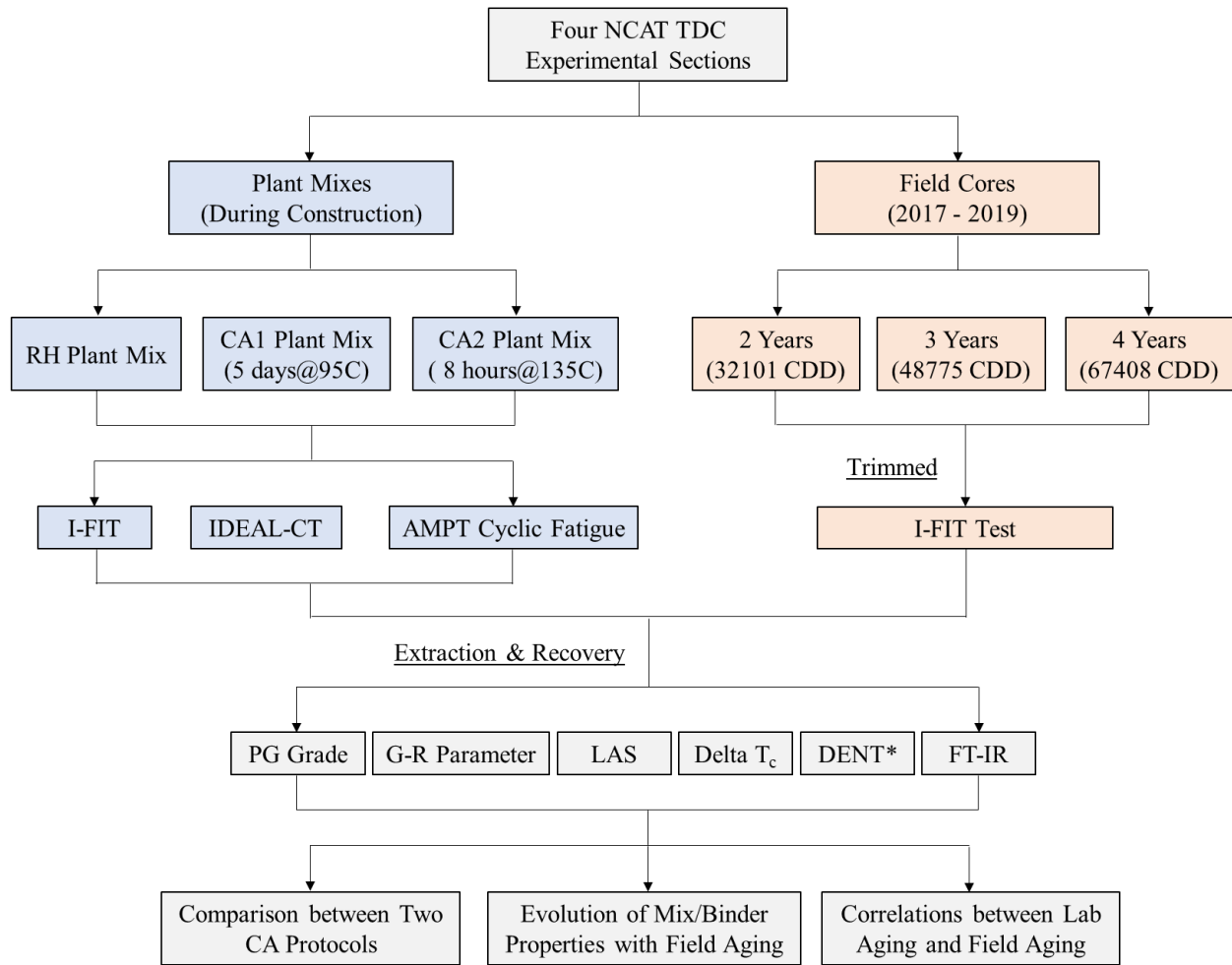
Since the preliminary critical aging protocol was based on a limited number of asphalt mixtures, additional work was conducted to validate it with the NCAT TDC experimental mixtures prior to conducting the laboratory cracking tests. The overall objective of this chapter was to validate the two candidate critical aging (CA) protocols with up to 4 years of field aging data that has been collected for the NCAT TDC experiment. Specifically, this chapter sought to (1) compare the impacts of two candidate CA protocols on the fatigue and cracking resistance of asphalt binders and mixtures, (2) characterize the evolution of asphalt binder and mixture properties with field aging on the NCAT Test Track, and (3) evaluate the correlation between the two laboratory CA protocols and field aging.

### **5.1 Experimental Design**

Figure 5.1 presents the experimental approach used to validate if the preliminary critical aging protocol is appropriate for the NCAT TDC experimental mixtures. Both plant mixtures and field cores of all seven experimental sections were supposed to be included in the validation process. However, section S13 was excluded because the asphalt-rubber binder of mixture S13 cannot be extracted and recovered due to the existence of rubber particles. As mentioned previously, the mixture components of sections N1, N2, and N5 were almost same except that section N5 had a 0.3% lower binder content, and the primary difference among these three sections was the compacted density. In this study, the field cores of each section were collected from the pavement shoulder, which were not compacted to a same density level with the testing lane area. Meanwhile, the density of shoulders was similar among sections N1, N2, and N5, so only section

N1 was used from these three test sections. Consequently, sections N1, N8, S5, and S6 were selected to validate the preliminary critical aging protocol.

For these four sections, plant mixture was sampled during construction of the test sections on the NCAT Test Track. For each mix, three sets of PMLC specimens with different aging protocols were prepared. The first set was compacted right after the mixture was reheated to the field compaction temperature and is referred to RH-PMLC specimens. The other two sets of specimens were prepared using the two candidate CA protocols of loose mixture aging for 5 days at 95°C and 8 hours at 135°C, which are referred to as CA1-PMLC and CA2-PMLC specimens, respectively. All PMLC specimens were tested in the I-FIT, the IDEAL-CT test, and the small-specimen AMPT cyclic fatigue test to determine the mixture cracking and fatigue resistance. In addition, post-construction field cores after 2 to 4 years in-service were sampled from the NCAT Test Track. The top 1.5-inch of the field cores was tested in the I-FIT. After the I-FIT testing was completed, asphalt binders were extracted and recovered from each set of PMLC specimens and post-construction field cores and tested to characterize their rheological properties. The asphalt binder tests used include the Superpave performance grading, delta T<sub>c</sub>, DSR linear amplitude sweep (LAS), DSR frequency sweep, DENT, and FT-IR. Finally, data analyses were conducted to (1) compare the two CA protocols in terms of their impacts on the fatigue and cracking resistance of asphalt binders and mixtures, (2) characterize the evolution of asphalt binder and mixture properties with field aging on the NCAT Test Track, and (3) determine the correlation between the two CA protocols and field aging.



Note: \* on plant mixtures only

**Figure 5. 1 Aging Validation Experimental Design**

## 5.2 Comparison of Two Candidate Critical Aging Protocols

This section presents the comparison of mixture cracking test (i.e., I-FIT, IDEAL-CT test, and small-specimen AMPT cyclic fatigue test) and binder cracking test (i.e., *G-R* parameter, LAS,  $\Delta T_c$ , and DENT) results for the reheated versus two critically aged PMLC specimens. The Games-Howell post-hoc test at a significance level of 0.05 was conducted for each mix with different aging levels to evaluate the impacts of the two CA protocols on the I-FIT, IDEAL-CT, and LAS test results and determine if a statistically significant difference exists between the two CA protocols.

### 5.2.1 I-FIT Results

Figure 5.2 presents the I-FIT results of the four mixes included in the study, where the bars denote the average *FI* values and the whiskers represent plus and minus one standard deviation. The statistical analysis results are also included in the figure using the capital letters located above the bars; for each mix, the *FI* results of PMLC specimens sharing a same letter are not significantly different. As expected, for all four mixes, the two critically aged specimens had significantly lower *FI* than the reheated specimens. These results indicate the effect of the two CA protocols on reducing mixture cracking resistance. Based on the statistical analyses, for all four mixes, the *FI* of the two critically aged specimens were categorized into the same group, which indicates that the two candidate CA protocols have no significant difference in terms of their impacts on the I-FIT results. In comparing the reheated specimens, mix S5 showed the highest *FI*, and thus, had the best cracking resistance, followed by mixes S6, N1, and N8, respectively. However, a different trend was observed for the results of the two critically aged specimens, where mix S6 had higher *FI* than mix S5. For all three aging conditions, mix N8 consistently showed the lowest *FI*, which is likely due to use of high RAP and RAS contents. Among the four mixes, S6 had the smallest relative change in *FI* after CA, which possibly demonstrates better aging resistance of the HiMA binder relative to the PG 67-22 neat and PG 58-28 SBS binders used in the other three mixes.

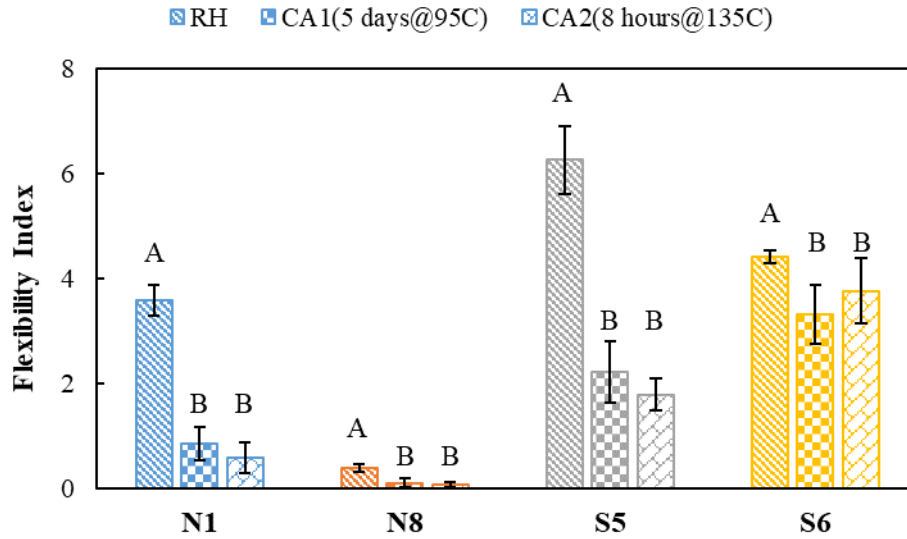


**Figure 5. 2 I-FIT Results of PMLC Specimens with Different Aging Conditions**

### 5.2.2 IDEAL-CT Results

Figure 5.3 presents the IDEAL-CT results of the four mixes for both reheated and two critically aged PMLC specimens. For all four mixes, the critically aged specimens had significantly lower  $CT_{index}$  results, indicating reduced cracking resistance, which is consistent with the I-FIT results in Figure 5. According to the Games-Howell post hoc test, the  $CT_{index}$  of CA1 specimens (aged for 5 days at 95°C) were statistically higher than CA2 specimens (aged for 8 hours at 135°C) for mixes N1, N8, and S5. Nevertheless, the difference in average  $CT_{index}$  between the two sets of CA specimens varied only from 0.9 to 4.1, which may not be practically different. It should be noted that the IDEAL-CT test is relatively new and its precision and bias statement has not yet been established. The CA1 specimens of mix S6 had slightly higher  $CT_{index}$  than the corresponding CA2 specimens, but the difference was not statistically significant considering the variability of the test results. Among the four mixes, S5 and S6 had the highest  $CT_{index}$  for all three aging conditions, followed by N1 and then N8. These results indicate the effect of polymer modification on improving mixture cracking resistance.

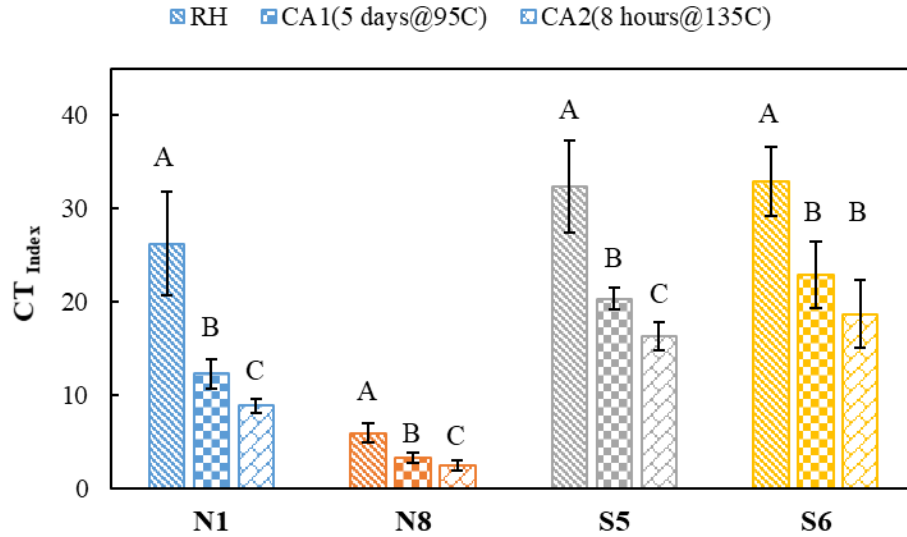


**Figure 5. 3 IDEAL-CT Test Results of PMLC Specimens with Different Aging Conditions**

### 5.2.3 Small-Specimen AMPT Cyclic Fatigue Test Results

Figure 5.4 presents the damage capacity index,  $S_{app}$ , results of the four mixes. Statistical analysis was not conducted due to material quantity limitations; thus, the analysis of  $S_{app}$  results was based on the mean values. Among these four mixes, the trends are similar for both reheated and critically aged PMLC specimens, where mix S6 showed the highest  $S_{app}$ , indicating the best fatigue resistance, followed by mixes S5, N1 and N8, respectively. This trend is expected and reflects the impacts on mixture fatigue due to polymer modification and use of RAP and RAS materials. For mixes N8, S5, and S6, the critically aged specimens had lower  $S_{app}$  results than reheated specimens, indicating reduced cracking resistance. However, for mix N1, the reheated specimens yielded same  $S_{app}$  results with CA2 specimens, which was unexpected. In comparing the two aging protocols, the  $S_{app}$  results showed a different trend from the I-FIT and IDEAL-CT results. For mixes N1, N8 and S5, CA1 (aged for 5 days at 95°C) resulted in more damage capacity loss than CA2 (aged for 8 hours at 135°C). However, the opposite trend was observed for mix S6, where the CA1 specimens had a higher  $S_{app}$  value, and thus, better fatigue resistance,

than the CA2 specimens. This trend was also found when the respective recovered binders were tested for stain tolerance in the DENT test.

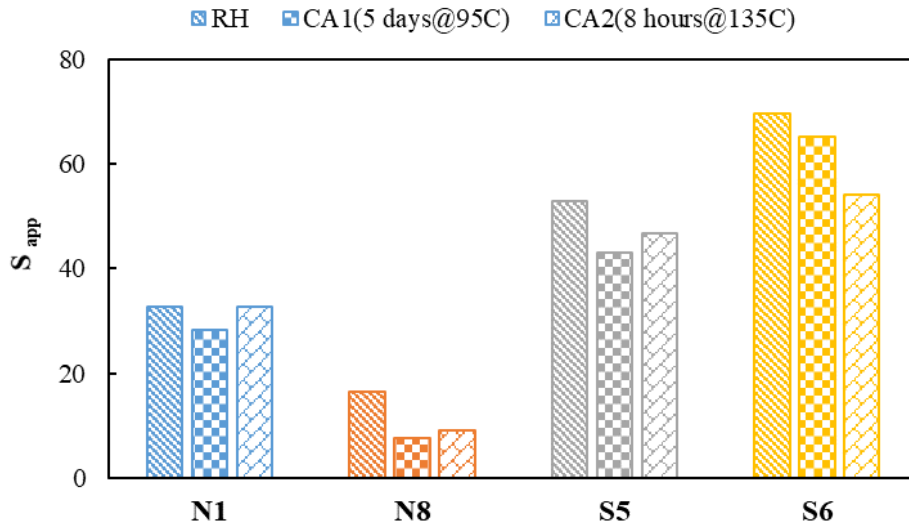


**Figure 5. 4 AMPT Cyclic Fatigue Test Results of PMLC Specimens with Different Aging Conditions**

#### 5.2.4 Glover-Rowe Parameter Results

Figure 5.5 presents the  $G-R$  parameter results of asphalt binders extracted from the reheated and critically aged plant mixtures. For all four mixes, extracted binders from the two critically aged mixtures had significantly higher  $G-R$  parameters than the reheated mixture, indicating the effect of CA protocols on reducing the cracking resistance of asphalt binders. For mixes N1, N8, and S6, the extracted binder from the CA2 mixture had a higher  $G-R$  parameter than the CA1 mixture. These results indicated that the 8-hour, 135°C aging protocol yielded a more severe level of asphalt aging than the 5-day, 95°C protocol. When compared to the preliminary  $G-R$  parameter threshold of 600 kPa for significant cracking, mix N8 reached the cracking “damage zone” for all three aging conditions. Mix N1, with a PG 67-22 binder and 20% RAP, reached the  $G-R$  parameter threshold after critical aging, while mixes S5 and S6 containing polymer-

modified binders did not reach the cracking “damage zone” for all aging conditions. It should be noted that the preliminary *G-R* parameter threshold of 600 kPa was based on a limited number of unmodified binders and a PG 58-28 climate in Pennsylvania, and thus, its applicability to polymer-modified binders and other climates remains unknown and needs further investigation.

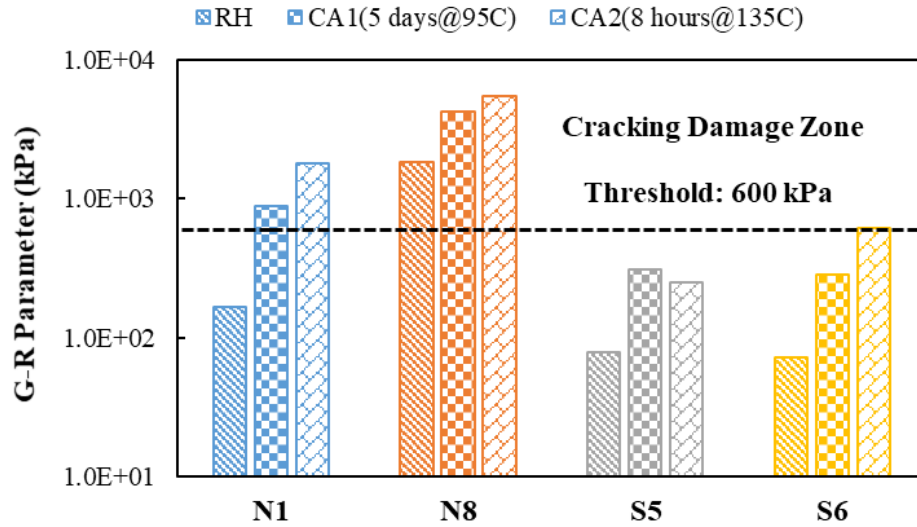


**Figure 5. 5 G-R Parameter Results of Extracted Binders from PMLC Specimens with Different Aging Conditions**

### 5.2.5 LAS Test Results

Figure 5.6 presents the LAS- $N_f$  (5.0%) results of the extracted binders from reheated and critically aged specimens, where the bars denote the average LAS- $N_f$  values and the error bars represent plus and minus one estimated standard deviation. The Games-Howell post-hoc test analysis results are also included in the figure using the capital letters located above the bars, and labels A, B, and C represent groupings that have statistically different  $N_f$ -parameter values resulting from the three aging protocols. Based on the statistical analysis, for mixes N1 and N8, the reheated specimens yielded significantly greater results than two critically aged specimens, indicating reduced fatigue resistance. However, no significant difference was observed between

reheated specimens and CA1 specimens for mixes S5 and S6. LAS- $N_f$  results showed a different trend from G-R parameter results when comparing two critically aged protocols. For mixes N1 and S6, the 8-hour, 135°C aging protocol yielded lower LAS- $N_f$  values than the 5-day, 95°C protocol, which indicated higher aging level. However, there was no significant difference between two aging protocols for mixes N8 and S5.

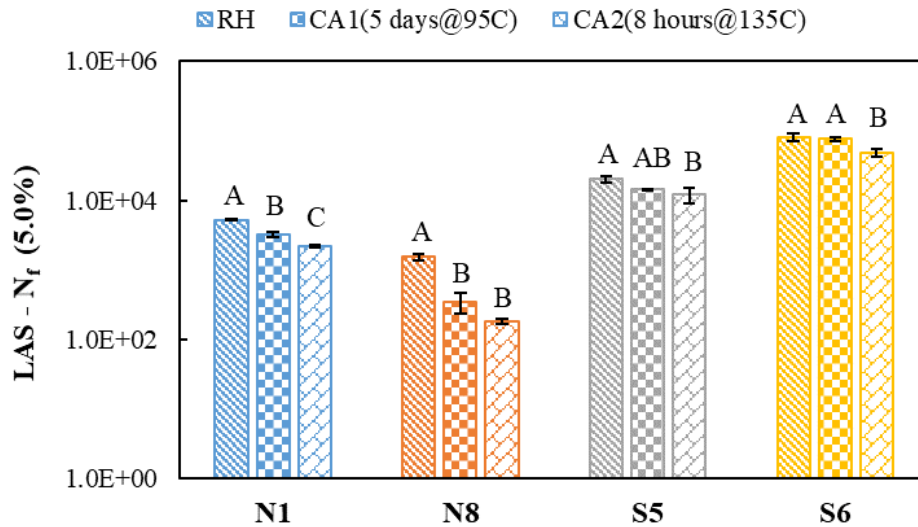


**Figure 5. 6 LAS- $N_f$  (5.0%) Parameter Results of Extracted Binders from PMLC Specimens with Different Aging Conditions**

### 5.2.6 $\Delta T_c$ Results

Figure 5.7 presents the  $\Delta T_c$  results of asphalt binders extracted from both reheated and two critically aged plant mixtures. As mentioned previously, asphalt binders with lower (i.e., more negative)  $\Delta T_c$  are more susceptible to cracking due to reduced relaxation properties. For all four mixes, the extracted binders from the two critically aged mixtures had lower  $\Delta T_c$  than the reheated mixture. Except for N1, the extracted binders from the CA2 had a lower  $\Delta T_c$  than binders from CA1, which indicated that the 8-hour, 135°C protocol was more severe than the 5-

day, 95°C protocol. For mix N1, the extracted binders from the two CA protocols had a difference in  $\Delta T_c$  of approximately 0.3°C, which was not considered practically different.

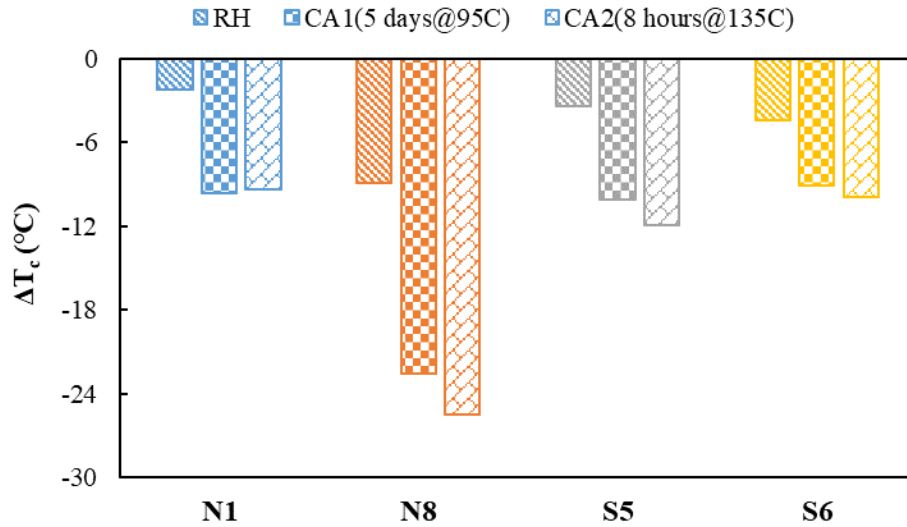


**Figure 5. 7  $\Delta T_c$  Results of Extracted Binders from PMLC Specimens with Different Aging Conditions**

### 5.2.7 DENT Test Results

Figure 5.8 presents the CTOD results (expressed in millimeters) of the recovered binders from both reheated and critically aged mixtures. Note that statistical analysis using the Games-Howell post-hoc test was not possible since CTOD is a computed parameter from all tested samples and that limited quantities of material recovered did not allow repeating the testing multiple times.

The binder recovered from N8 after CA1 experienced brittle failure during the test, so the CTOD value could not be calculated. Nevertheless, this indicates that this material had the worst (smallest) CTOD among all the binders tested. For all four mixes, the trends were similar for the reheated and the two critically aged samples, where mix S6 fared the best, followed by S5, N1 and N8, respectively. This trend is expected and reflects the effects of polymer or RAP and RAS. In comparing the CA protocols, results for mixes N1 and N8 indicate that CA1 (aged for 5 days

at 95°C) was more severe than CA2 (aged for 8 hours at 135°C). Mix S6, however, showed the opposite trend. The CTOD results of the two critically aged mixtures were almost identical for mix S5. In general, the DENT test captures the changes in the binders with aging as the magnitude of the CTOD drop after the CA procedures is higher than the one observed with  $S_{app}$  values from the AMPT cyclic fatigue test (Figure 5.4).

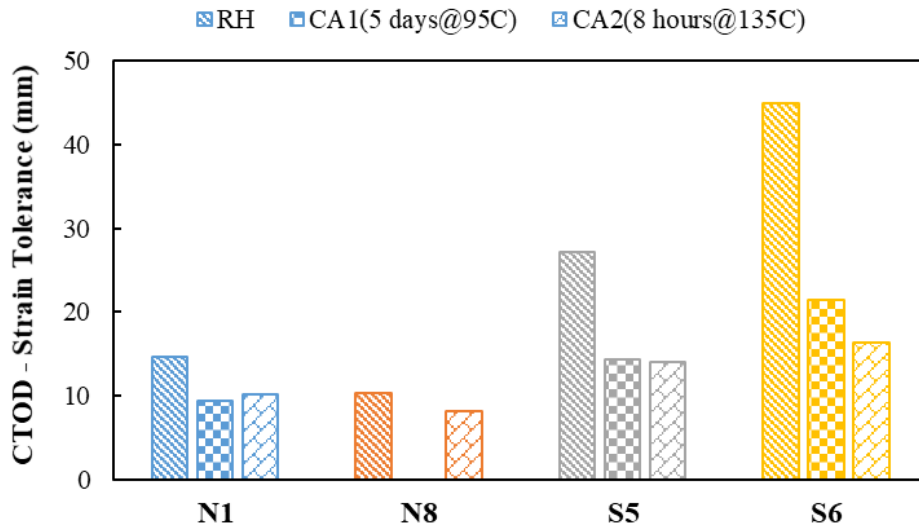


**Figure 5. 8 DENT Test Results of Extracted Binders from PMLC Specimens with Different Aging Conditions**

### 5.3 Evolution of Asphalt Binder and Mixtures Properties with Field Aging

This section presents the I-FIT results of post-construction field cores collected from the NCAT Test Track after 2 years in-service, as well as the DSR (including HPG,  $G-R$  parameter, and LAS), BBR (including LPG and  $\Delta T_c$ ), DENT, and FT-IR test results of the extracted binders. Data analyses were conducted to determine the evolution of asphalt binder and mixture properties with field aging. In this study, field aging was quantified using the CDD parameter, which was calculated based on the construction date of the test section and coring date of the field cores. It should be noted that because field cores at construction were not available, the

reheated PMLC specimens were used as the beginning of the field aging curve, which was assigned with a CDD of zero.

5.3.1 I-FIT Results

Figure 5.9 presents the I-FIT results of the reheated PMLC specimens and post-construction field cores, where the dots represent the average corrected *FI* values and the error bars represent plus and minus one estimated standard deviation. For all mixes except N1, the field cores showed a gradual decrease in the corrected *FI* with increasing CDD, which indicated that the cracking resistance of the mixtures deteriorated with field aging. For mix N1, the 3-year cores had a slightly higher *FI* than the 2-year cores, but the difference was not significant considering the variability of the test results. For all field aging conditions, mix S5 consistently had the highest *FI* and thus, the best cracking resistance, followed by mixes S6, N1, and N8, respectively.

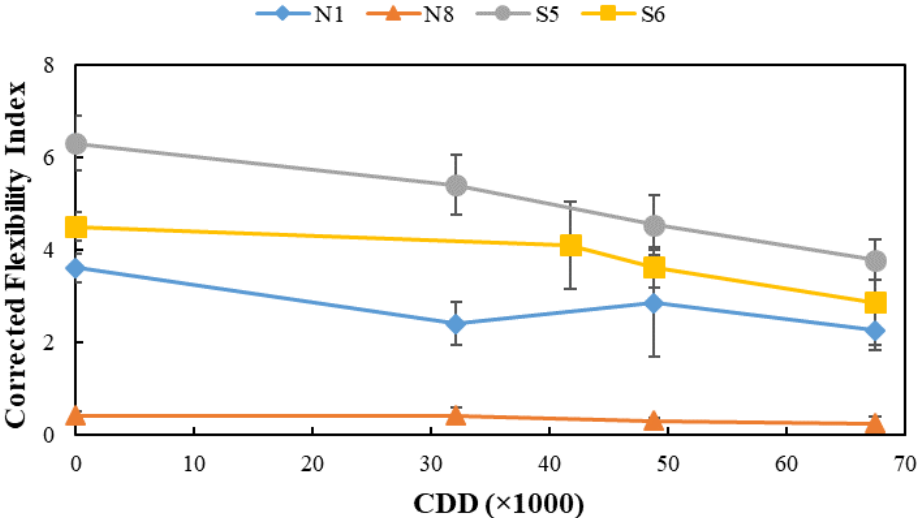
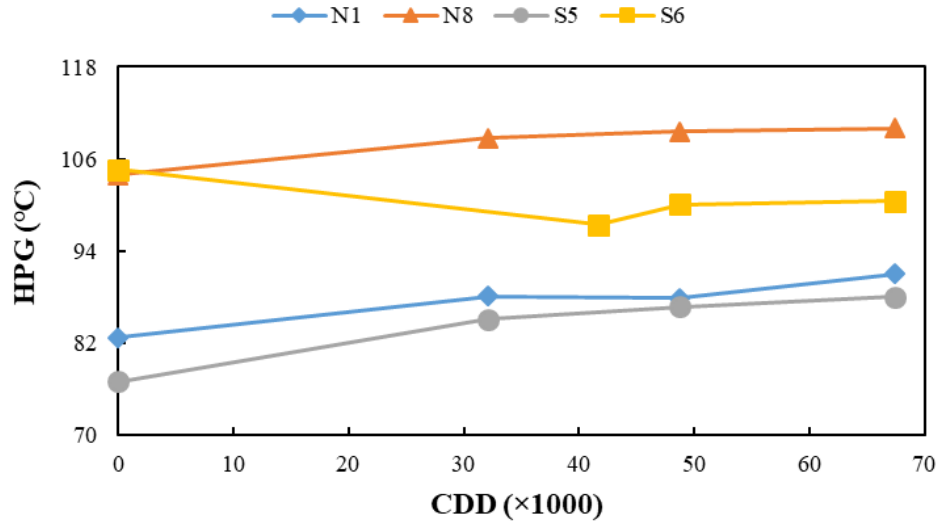


Figure 5. 9 I-FIT Results of Reheated PMLC Specimen and Post-Construction Field Cores

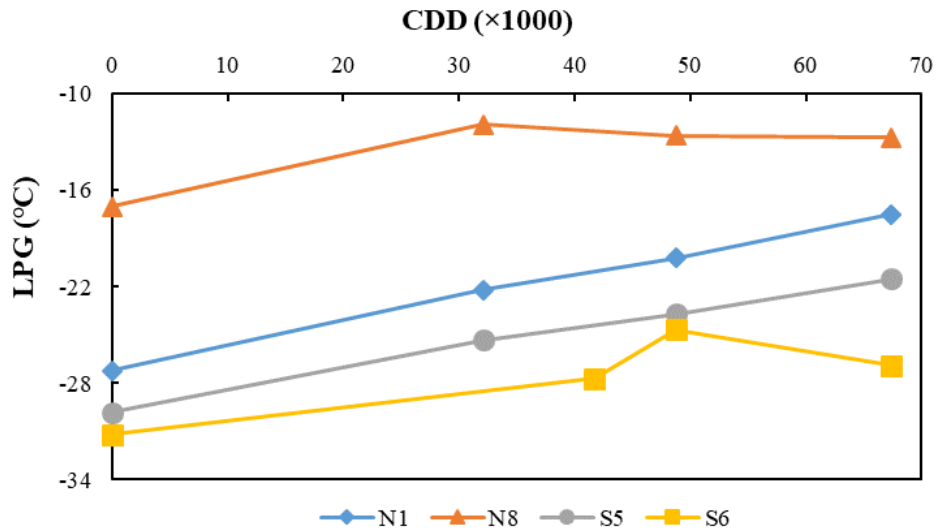
### 5.3.2 Continuous PG Results

Figure 5.10 presents the continuous HPG and LPG results of extracted binders from the reheated plant mixtures and post-construction field cores. As shown in Figure 5.10 (a), the HPG of extracted binders for mixes N1, N8, and S5 increased with increasing CDD, indicating the binder stiffening effect as a result of field aging. For mix S6, the extracted binders from all field cores yielded lower HPG than the extracted binder from reheated plant mixture, which was not expected and could be due to errors in recovering or testing the binder. In addition, the HPG of extracted binders from field cores increased with increasing CDD, indicating the binder became stiffer during field aging.

As presented in Figure 5.10 (b), the continuous LPG of extracted binders for mixes N1 and S5 increased (i.e., became less negative) with CDD, which indicate that the binders were more susceptible to thermal cracking after field aging. For mix N8, the extracted binders from all three sets of post-construction field cores had similar LPG (with a maximum difference of  $0.8^{\circ}\text{C}$ ) of around  $-12.5^{\circ}\text{C}$ , which was considerably higher than that of the extracted binder from the reheated plant mixture. For mix S6, the results of the 2.5-year and 4-year field cores showed an expected trend where the LPG of the extracted binders gradually increased with field aging. However, the extracted binder from the 3-year field core had a higher LPG than the 4-year field core, which is possibly due to testing errors and thus, needs to be reverified.



(a)



(b)

**Figure 5. 10 Continuous PG Results of Extracted Binders from Reheated Plant Mixture and Post-Construction Field Cores; (a) High-Temperature, (b) Low-Temperature**

### 5.3.3 Glover-Rowe Parameter Results

Figure 5.11 presents the *G-R* parameter results of extracted binders from the reheated plant mixture and post-construction field cores. For all mixes except N8, the *G-R* parameter increased with increasing CDD, indicating increased binder stiffness and reduced cracking resistance due to field aging. For mix N8, the *G-R* parameter increased first and then decreased slightly with

field aging where the highest  $G-R$  parameter corresponded to the 3-year field core with approximately 49,000 CDD. When comparing the results to the preliminary  $G-R$  parameter threshold of 600 kPa for significant cracking, mix N8 reached the cracking “damage zone” right after construction for the reheated plant mixture. The poor cracking resistance of this mix was likely due to the inclusion of 20% RAP and 5% RAS. Mix N1 with a PG 67-22 binder and 20% RAP reached the cracking “damage zone” after approximately 2 years of field aging with 32,000 CDD, while the two mixes with polymer-modified binders (i.e., S5 and S6) did not reach the cracking “damage zone” after 4 years of field aging with 67,000 CDD. These results further highlight the effect of polymer modification in improving the long-term cracking resistance of asphalt binders.

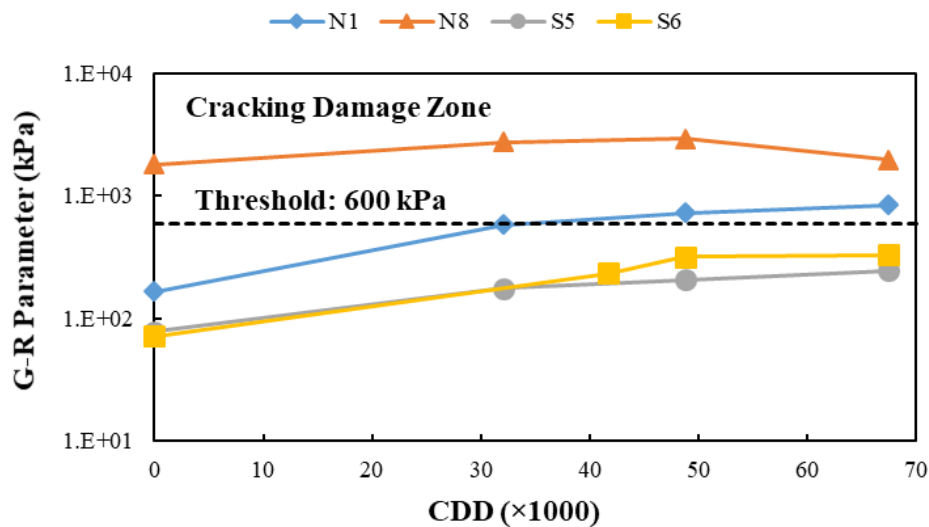


**Figure 5. 11 Glover-Rowe Parameter Results of Extracted Binders from Reheated Plant Mixture and Post-Construction Field Cores**

#### 5.3.4 $\Delta T_c$ Results

Figure 5.12 presents the  $\Delta T_c$  results of extracted binders from the reheated plant mixture and post-construction field cores. The  $\Delta T_c$  results of all mixes showed a general decrease with

increasing CDD, which indicate that the binders became more susceptible to cracking with field aging. However, an unexpected trend was observed for the 3-year field core of mix S6, where the extracted binder had a more negative  $\Delta T_c$  than the 4-year field core. This abnormality, which is also observed in the LPG results in Figure 5.10 (b), was possibly caused by the testing errors and thus, needs to be reverified.

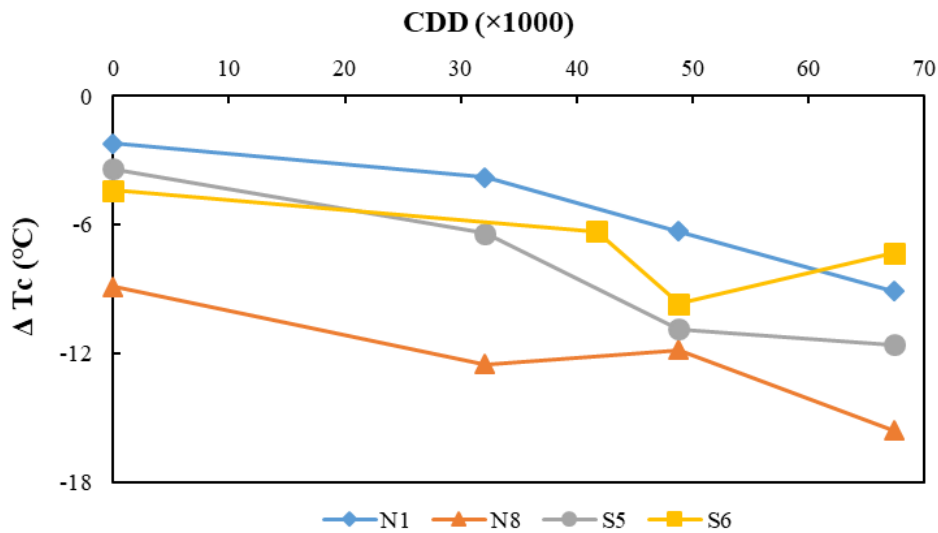


**Figure 5. 12  $\Delta T_c$  Results of Extracted Binders from Reheated Plant Mixture and Post-Construction Field Cores**

### 5.3.5 LAS Results

Figure 5.13 presents the LAS- $N_f$  results of extracted binders from the reheated plant mixture and post-construction field cores, and the error bars represent plus and minus one estimated standard deviation. Note that the LAS- $N_f$  results of 4-year field cores were not available currently. As shown in Figure 5.13, the LAS- $N_f$  results of all mixes showed a decreasing trend with increasing CDD, which indicate that the binders became less resistant to fatigue with field aging.

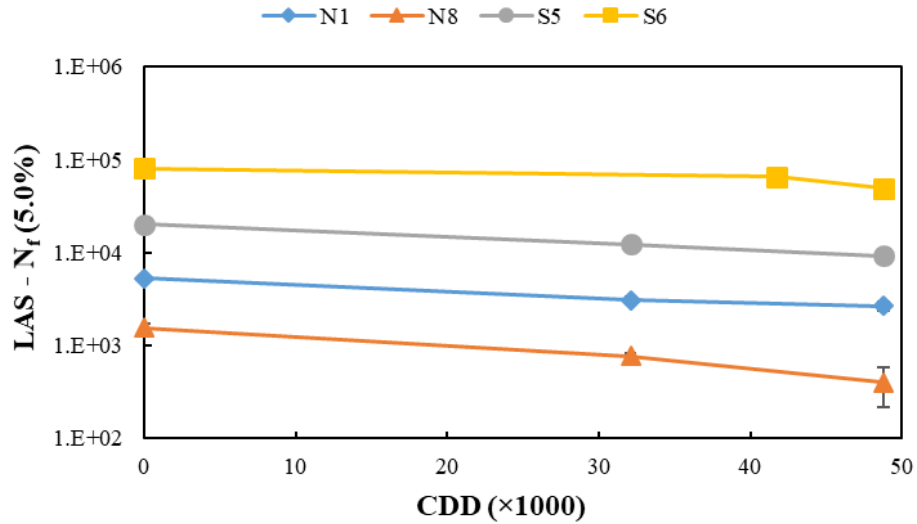


**Figure 5. 13 LAS-N<sub>f</sub> Results of Extracted Binders from Reheated Plant Mixture and Post-Construction Field Cores**

### 5.3.6 FT-IR Results

Figure 5.14 presents the FT-IR carbonyl area results of extracted binders from the reheated plant mixture and post-construction field cores, and the error bars represent plus and minus one estimated standard deviation. Note that the FT-IR results of 4-year field cores were not available currently. As shown in Figure 5.14, for mixes N8 and S6, the FT-IR carbonyl area results increased with increasing CDD, which indicate that the binders experience more oxidation aging with field aging. However, for mixes N1 and S5, the FT-IR carbonyl area results increased first and then decreased slightly with field aging where the highest carbonyl area results corresponded to the 2-year field core with approximately 32,000 CDD, which was unexpected and might be caused by testing errors.

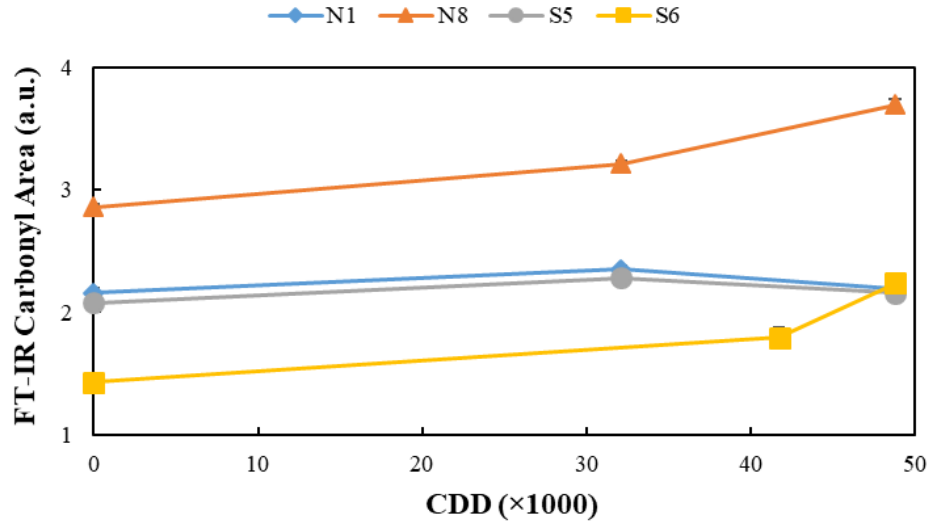


**Figure 5. 14 FT-IR Carbonyl Area Results of Extracted Binders from Reheated Plant Mixture and Post-Construction Field Cores**

#### 5.4 Correlation between Laboratory Critical Aging Protocols and Field Aging

This section presents the analysis results for evaluating the correlation between the two candidate CA protocols and field aging on the NCAT Test Track. The representative CDD of the two CA protocols of loose mixture aging for 5 days at 95°C and 8 hours at 135°C was determined by comparing the test results of critically aged plant mixtures and the corresponding field cores. Note that this comparison was conducted separately for all binder and mixture properties discussed in Section 5.3. Figure 5.15 presents an example of the data analysis for the I-FIT results of mix S6, where the solid line represents the corrected *FI* of post-construction field cores at various field in-service times (expressed in CDD) and the two dashed lines represent the *FI* of the two critically aged PMLC specimens. Based on linear interpolation of the *FI* results, the two candidate CA protocols of loose mixture aging for 5 days at 95°C and 8 hours at 135°C were estimated to simulate approximately 46,600 and 56,100 CDD of field aging, respectively.

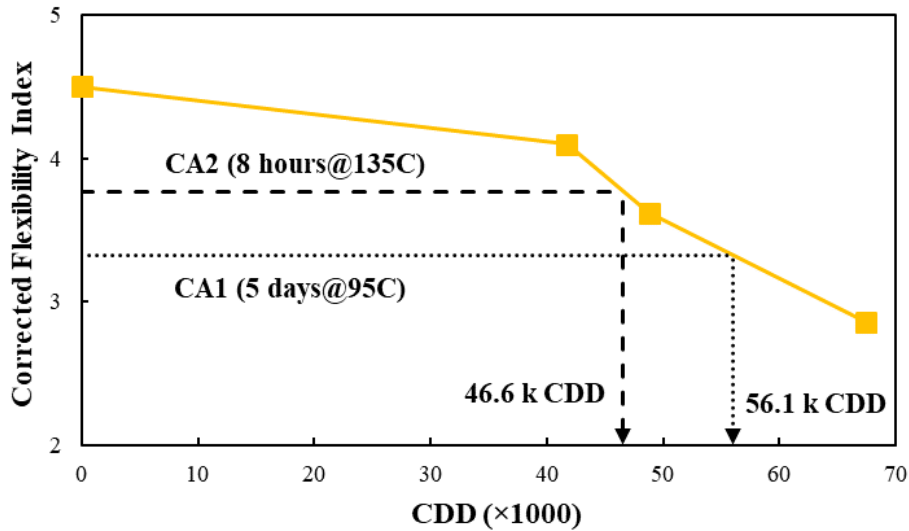


**Figure 5. 15 An Example to Illustrate the Determination of the Representative CDD for the Two Candidate CA Protocols using the I-FIT Results of Mix S6**

Table 5.1 and Table 5.2 summarize the representative CDD of the two candidate CA protocols of loose mixture aging for 5 days at 95°C and 8 hours at 135°C, respectively. Because of the unexpected trends of the continuous PG and  $\Delta T_c$  results for mix S6 (Figure 5.10 and Figure 5.12), their representative CDD could not be determined, and thus, are shown as “not available (N/A)”. It should also be noted that in cases where the CA protocol yielded more severe asphalt aging than the corresponding 4-year field cores, additional field aging data is needed to determine the representative CDD without data extrapolation. In such cases, the projected representative CDD values are greater than 67,400, and thus, are shown as “> 67.4” in Table 2 and Table 3.

As shown in Table 5.1, for mixes N1, N8, and S5, the representative CDD of the 5-day, 95°C aging protocol was consistently higher than 67,400 for the majority of the binder and mixture properties evaluated. The binder LPG and *G-R* parameter of mix N1 and binder  $\Delta T_c$  of mix S5 had a representative CDD of between 46,000 and 67,400. The LAS- $N_f$  of mixes N1 and S5 and carbonyl area of mix N8 had a representative CDD ranging between 23,500 to 47,700.

For LAS-N<sub>f</sub> of mix N8 and carbonyl area of mixes N1 and S5, the representative CDD was higher than 48,800. For mix S6, the loose mixture aging protocol of 5 days at 95°C had a representative CDD of 56,100, 47,900, and 10,900 for mixture *FI*, binder *G-R* parameter, and LAS-N<sub>f</sub>, respectively. In general, a similar trend was observed for the other CA protocol in Table 5.2, where the 8-hour, 135°C aging protocol had a representative CDD of over 67,400 for mixture *FI*, HPG, LPG,  $\Delta T_c$ , *G-R* parameter. For the two exceptional cases, mix S5 showed a representative CDD of 64,000 for the binder *G-R* parameter and mix S6 showed a representative CDD of 46,600 for mixture *FI*. The representative CDD of LAS-N<sub>f</sub> and carbonyl area was greater than 48,800 for most of the mixtures. The only three exceptions were the LAS-N<sub>f</sub> of mix S5, and carbonyl area of mixes N8 and S6, which had a representative CDD of between 33,900 and 48,400. In summary, the two candidate CA protocols of loose mixture aging for 5 days at 95°C and 8 hours at 135°C appear to yield a more severe level of asphalt aging than 4 years of field aging on the NCAT Test Track.

**Table 5. 1 Summary of Representative CDD (x 1,000) Values for CA1 Protocol of Loose Mixture Aging for 5 days at 95°C**

Binder/Mixture Property	N1	N8	S5	S6
Flexibility Index	> 67.4	> 67.4	> 67.4	56.1
HPG	> 67.4	> 67.4	> 67.4	N/A
LPG	> 67.4	> 67.4	> 67.4	N/A
$\Delta T_c$	> 67.4	> 67.4	46.0	N/A
Glover-Rowe Parameter	63.0	> 67.4	> 67.4	47.9
LAS-N <sub>f</sub> (5.0%)	29.2	> 48.8	23.5	10.9
FT-IR Carbonyl Area	> 48.8	47.7	> 48.8	> 48.8

**Table 5. 2 Summary of Representative CDD (x 1,000) Values for CA2 Protocol of Loose Mixture Aging for 8 hours at 135°C**

Binder/Mixture Property	N1	N8	S5	S6
Flexibility Index	> 67.4	> 67.4	> 67.4	46.6
HPG	> 67.4	> 67.4	> 67.4	N/A
LPG	> 67.4	> 67.4	> 67.4	N/A
$\Delta T_c$	> 67.4	> 67.4	> 67.4	N/A
Glover-Rowe Parameter	> 67.4	> 67.4	64.0	> 67.4
LAS-N <sub>f</sub> (5.0%)	> 48.8	> 48.8	33.9	> 48.8
FT-IR Carbonyl Area	> 48.8	48.4	> 48.8	44.5

### 5.5. Summary

The objective of this chapter was to validate the two candidate CA protocols of loose mixture aging for 5 days at 95°C and 8 hours at 135°C for the NCAT TDC experiment. Four surface mixes placed on the NCAT Test Track were evaluated, which were representative of several levels of binder modification, performance grades, recycled material contents, and field cracking performance. For each mix, three laboratory aging protocols (i.e., reheating and with the two proposed CA protocols) were used to prepare specimens for the I-FIT, the IDEAL-CT test, and the small-specimen AMPT cyclic fatigue test. Cores from the test sections were also obtained at various points in time through four years of service and tested in following the I-FIT test. In addition, asphalt binders extracted from each set of the PMLC specimens and field cores were tested in DSR, BBR, and DENT, and the FT-IR tests to determine their PG, *G-R* parameter,  $\Delta T_c$ , LAS-N<sub>f</sub> (5.0%) parameter, CTOD strain tolerance, and carbonyl area. Finally, data analyses were conducted to (1) compare the two candidate CA protocols in terms of their impacts on the fatigue and cracking resistance of asphalt binders and mixtures, (2) characterize the evolution of asphalt binder and mixture properties with field aging on the NCAT Test Track, and (3) evaluate the

correlation between the two CA protocols and field aging. Based on the analysis results, the following conclusions are made:

(1) The two candidate CA protocols of loose mixture aging for 5 days at 95°C and 8 hours at 135°C showed a significant impact on reducing the fatigue and cracking resistance of asphalt binders and mixtures.

(2) Comparisons of the two candidate CA protocols yielded different results depending on the binder and mixture properties evaluated. The I-FIT results showed no significant difference between the two CA protocols. The IDEAL-CT test, *G-R* parameter, LAS test, and  $\Delta T_c$  results all indicated that the 8-hour, 135°C protocol was more severe than the 5-day, 95°C protocol. However, the opposite trend was generally observed for small-specimen AMPT cyclic fatigue test results.

(3) The AMPT cyclic fatigue and DENT test results showed greater deterioration in the fatigue and cracking resistance of mix S6 (containing the HiMA binder) due to the 8-hour, 135°C protocol than the 5-day, 95°C protocol. These results support the hypothesis in literature that SBS polymers are more susceptible to thermal degradation when exposed to higher conditioning temperatures.

(4) In general, the I-FIT, PG, *G-R* parameter,  $\Delta T_c$ , LAS- $N_f$  (5.0%), and carbonyl area results of post-construction field cores showed an expected trend of increased stiffness and reduced cracking resistance with field aging. Although the LPG and  $\Delta T_c$  results for mix S6 extracted binders indicate that 3-year field cores were aged more than that from the 4-year field cores, those results are spurious. In addition, the HPG results of extracted binder from mix S6 indicate that reheated specimens yielded higher aging level than all the field cores, which could be caused by the errors in recovering or testing the binder.

(5) The majority of the asphalt binder and mixture properties indicate that the two candidate CA protocols of loose mixture aging for 5 days at 95°C and 8 hours at 135°C yield a more severe level of asphalt aging than 4 years of field aging on the NCAT Test Track. Therefore, additional field aging data is needed to help determine the representative CDD of these two CA protocols.

(6) Virtually all the binder and mixture results identified mixes S5 and S6 as having the best fatigue and cracking resistance, followed by N1, and N8, respectively, which agrees with their field performance on the NCAT Test Track through more than four years of heavy traffic. These results highlight the effects of polymer modification and recycled materials on the cracking resistance of asphalt binders and mixtures.

## **CHAPTER 6 LABORATORY MIXTURE CRACKING TEST RESULTS**

To evaluate laboratory cracking tests for their suitability in identifying mixtures susceptible to TDC, seven mixtures were designed and constructed on the NCAT Test Track with a range of characteristics including air voids, binder type, and recycled materials. For each mixture, both plant-produced and laboratory-mixed mixtures were tested with six sponsor-selected laboratory cracking tests, including ER, TX-OT, NCAT-OT, SCB, I-FIT, and IDEAL-CT.

### **6.1 Experimental Design**

The approach of the laboratory mixture cracking tests is illustrated in Figure 6.1. For each mixture, both plant-produced mixtures and laboratory-mixed mixtures were prepared and critically aged at 135 °C for 8 hours prior to compaction. The laboratory cracking tests results were utilized to conduct: (1) comparison analysis between plant and laboratory mixtures; (2) sensitivity analyses of the test results to aging, air voids, recycled asphalt materials, and modified binder; (3) correlation analyses among the six laboratory cracking tests.

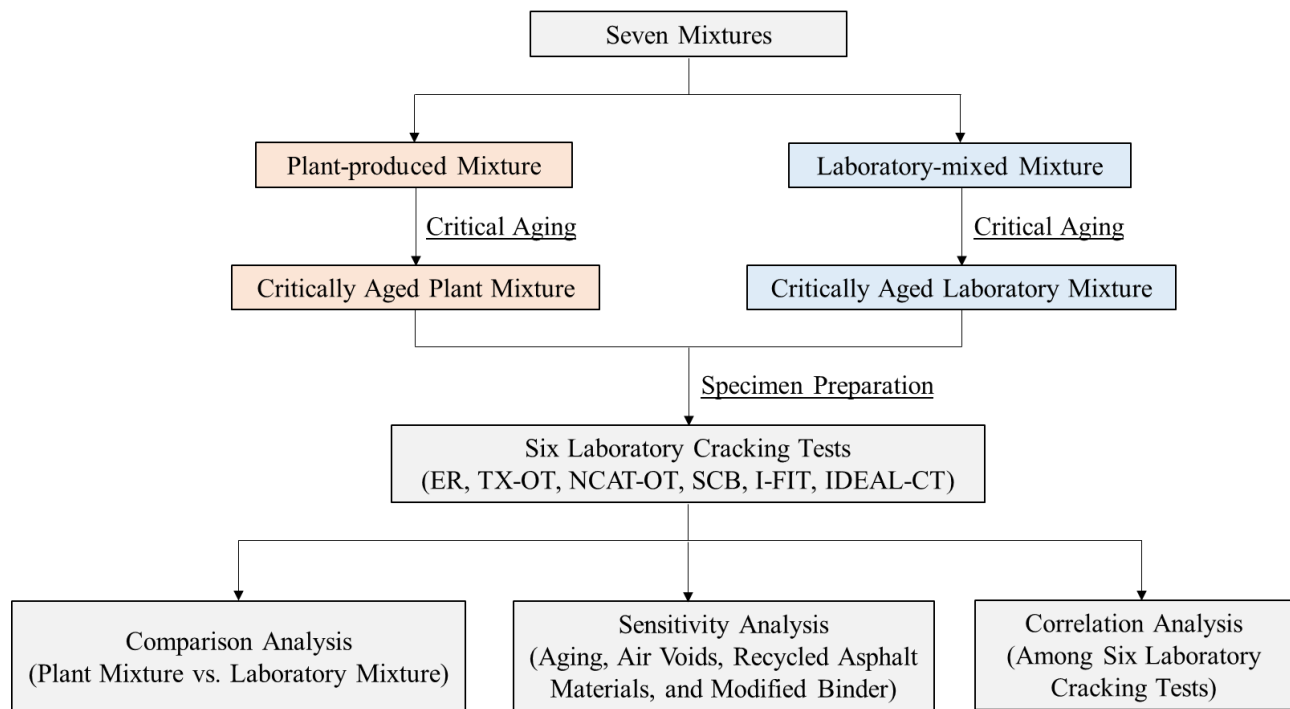


**Figure 6. 1 Research Methodology for Laboratory Cracking Tests**

### 6.1.1 Sensitivity Groups

Table 3.2 summarizes the key distinguishing properties of the seven experimental mixtures. N1 mixture was identified as the “control mixture” with 20% RAP and a PG 67-22 binder. N2 was identical to the control mixture but was compacted in the field to a higher density. Therefore, mixtures N1 and N2, with lab air void samples of 7.0 and 4.0%, respectively, were grouped to analyze the sensitivity of air voids on TDC resistance. Similarly, another group of mixtures were analyzed to determine the sensitivity of recycled asphalt materials, and a third group was analyzed to evaluate the sensitivity to modified binders on TDC resistance. The three sensitivity groups are summarized as follows:

- Air Voids Group: N1 (7.0% air voids), N2 (4.0% air voids).
- Recycled Asphalt Materials Group: N1 (20% RAP), N8 (20% RAP + 5% RAS), and S5 (35% RAP + Softer Binder).

- Modified Binder Group: N1 (PG 67-22), S6 (highly polymer-modified binder (HiMA)).

Mixture N5 was not categorized in the air voids group due to its lower asphalt content. Mixture S13 was not grouped with any other mixtures due to its unique properties: it had a lower RAP content (15%), a larger NMAS, and coarser gradation, and used an asphalt-rubber binder. Additionally, the total binder content was more than 1.5% higher than any other mixtures in the experiment.

### *6.1.2 Sample Preparation*

In this study, both plant-produced and laboratory-mixed mixtures were utilized to evaluate six laboratory cracking tests. During the construction of 2015 NCAT Test Track, the seven plant-produced mixtures were sampled and placed in five-gallon buckets. The mixtures were later reheated at 150 °C for two hours to prepare loose mixtures for additional critical aging of 8 hours at 135 °C. For laboratory mixtures, the seven mixtures were mixed in accordance with the corresponding mixture designs and then STOA per AASHTO R 30 for 4 hours at  $135 \pm 3$  °C prior to the following critical aging. For the STOA process, the loose mixtures were stirred every hour to ensure the uniform conditioning. After critical aging, the loose mixtures were compacted with a Superpave Gyratory Compactor (SGC); the specifics of this process are summarized as follows:

- Separate reheated plant mixtures and STOA laboratory mixtures into a loose state as for Rice specific gravity samples.
- Weight 2500-2700g loose mixtures onto a Rice pan and spread them to an even thickness.
- Critically age the loose mixtures for 8 hours at 135 °C.

- After 8 hours, transfer the loose mixtures to small pans and heat them to the corresponding compaction temperature.
- Compact specimens after the mixture reached the compaction temperature.

The reheated plant-mixed, lab-compacted test specimens are abbreviated as PMLC-RH; the short-term oven aged laboratory-mixed, lab-compacted test specimens are abbreviated as LMLC-STOA; the critically-aged plant-mixed lab-compacted test specimens are abbreviated as PMLC-CA, and the critically-aged lab-mixed, lab-compacted test specimens are abbreviated as LMLC-CA. Each of the seven mixtures were tested using the six asphalt mixture cracking tests previously described. The lab compacted specimens were compacted to the target in-place air void contents of the respective test sections. Thus, all PMLC-CA and LMLC-CA specimens were compacted to a target of 7.0% air voids, except for mixtures N2 and N5 which had target air voids of 4.0% and 10.0%, respectively.

### *6.1.3 Statistical Analysis*

All test results except the Energy Ratio were checked for outliers in accordance with ASTM E178-08. All results that failed ASTM E178-08 at a significance level of 0.10 were eliminated from further analysis. TX-OT, NCAT-OT, I-FIT, and IDEAL-CT results were analyzed to obtain the mean value and standard deviation.

Energy Ratio results are a product of a pooled analysis of three tests that have trimmed means applied to the results of the tests and the average is used to calculate the ER. For each specimen, the results are calculated for each instrumented specimen face (left and right), giving two results per specimen. For a set of three specimens, this gives six specimen faces from which the high and low value are removed to determine the trimmed mean for the individual properties.

Although there are replicates for each component test in the ER, a single ER value is calculated from the average results from the component test replicates.

For the SCB test results, regression analyses were performed to estimate of the error of the  $dU/da$  slopes. The standard error of the regression slope coefficient was used to estimate the standard deviation of the slope. The standard deviation of the  $dU/da$  slope was estimated by dividing the estimate of the total model deviation ( $s_e$ ) by the sum of squared differences between the  $x$  values ( $S_{xx}$ ), in this case, notch lengths. This provided an isolated estimate for the error in the model pertaining only to the slope (Devore and Farnum, 2005). A more detailed explanation of this analysis is available elsewhere (Moore, 2016). Since the thickness of the specimens was constant in this experiment, the slope of the strain energy vs. notch depth line was the only variable in  $J_c$  calculation, so the standard deviation of the  $dU/da$  slope was multiplied by the thickness constant to estimate the variability of  $J_c$  results.

As mentioned above, only a single value is obtained from ER and SCB tests without any replicates for each mixture. Thus, the *paired-t* test was conducted to compare ER and SCB test results and analyze the effects of aging and group sensitivities. For TX-OT, NCAT-OT, I-FIT, and IDEAL-CT tests, different statistical analyses were applied for the following comparison and sensitivity analysis, such as *t*-test, two-way analysis of variance (ANOVA) test, and the Games-Howell post hoc test.

## **6.2 Comparison Analysis between Plant Mixtures and Laboratory Mixtures**

As mentioned previously, the cracking resistance of both plant-produced and laboratory-mixed mixtures was evaluated at both aging conditions for the six laboratory cracking tests. For each laboratory cracking test, the comparison between plant mixtures and laboratory mixtures was conducted with a two-way ANOVA at a significance level of 0.05 except for ER and SCB results.

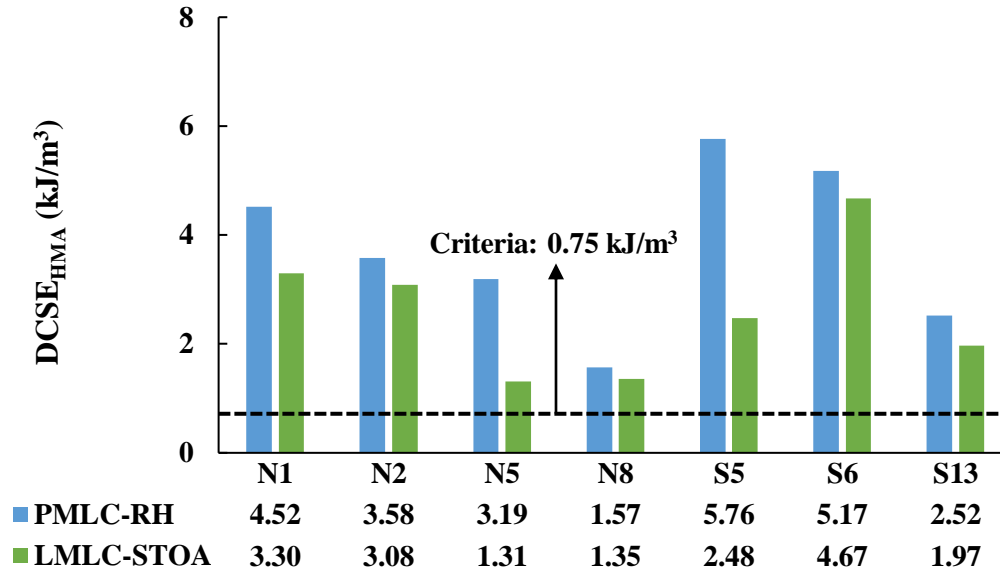
Additionally, for each mixture, *t*-test was also executed at a significance level of 0.05 to compare plant mixtures results with the corresponding laboratory mixtures results of each cracking test. For ER and SCB results, the *paired-t* test was conducted at a significant level of 0.05 to examine the difference between plant mixtures and laboratory mixtures at both aging conditions.

### 6.2.1 Energy Ratio

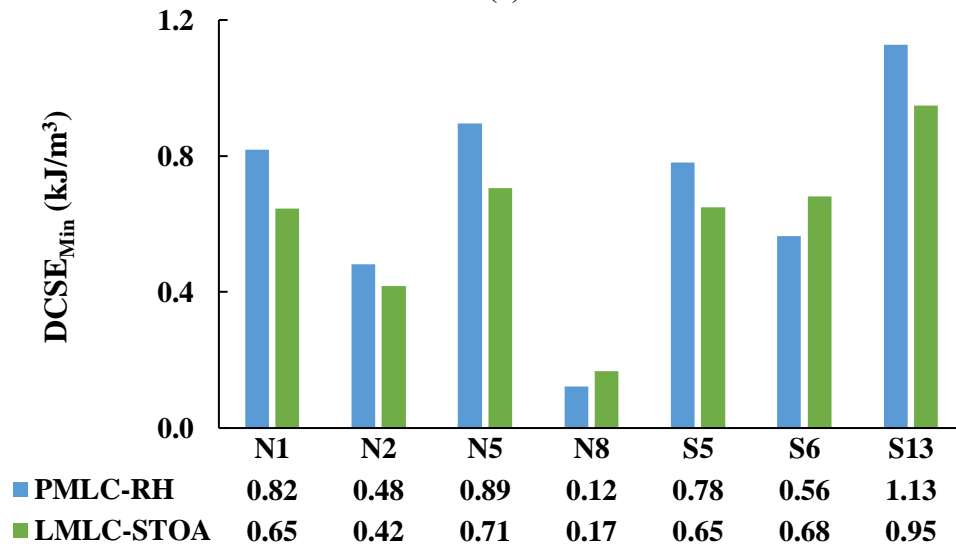
Figure 6.2 and Figure 6.3 present the comparison results of  $DCSE_{HMA}$ ,  $DCSE_{Min}$  and ER before and after critical aging, respectively.  $DCSE_{HMA}$  is the amount of energy required to initiate cracking, and a minimum  $DCSE_{HMA}$  criteria of  $0.75 \text{ kJ/m}^3$  was proposed to screen out extremely stiff mixtures (Roque et al., 2004). In addition, minimum ER criteria were also proposed for different traffic levels, and the highest criteria was 1.95 for a traffic level of 1 million ESALs per year. However, seven experimental mixtures were exposed to 5 million ESALs per year, a much higher traffic level than the validated range.

Figure 6.2 presents the  $DCSE_{HMA}$ ,  $DCSE_{Min}$  and ER results of PMLC-RH and LMLC-STOA specimens. As shown in Figure 6.2 (a), all the  $DCSE_{HMA}$  results exceeded the minimum criteria of 0.75. In addition, the PMLC-RH specimens consistently yielded higher  $DCSE_{HMA}$  values than the corresponding LMLC-STOA specimens, which indicates that the standard AASHTO STOA procedure yielded a higher aging level than the actual plant-produced process. As shown in Figure 6.2 (b), the  $DCSE_{Min}$  results displayed the same trend with the  $DCSE_{HMA}$  results for all mixtures except for mixtures N8 and S6. Figure 6.2 (c) shows all the ER results are greater than the highest ER criteria of 1.95 except for LMLC-STOA specimens of N8. Meanwhile, the ER results of PMLC-RH are consistently higher than the LMLC-STOA results, which is in agreement with  $DCSE_{HMA}$  results. Additionally, the *paired-t* test results indicate that the  $DCSE_{HMA}$  and ER results of PMLC-RH specimens are statistically higher than the

corresponding LMLC-STOA specimens ( $p$ -value < 0.05), but there is no significant difference between PMLC-RH and LMLC-STOA for  $DCSE_{Min}$  results.



(a)



(b)

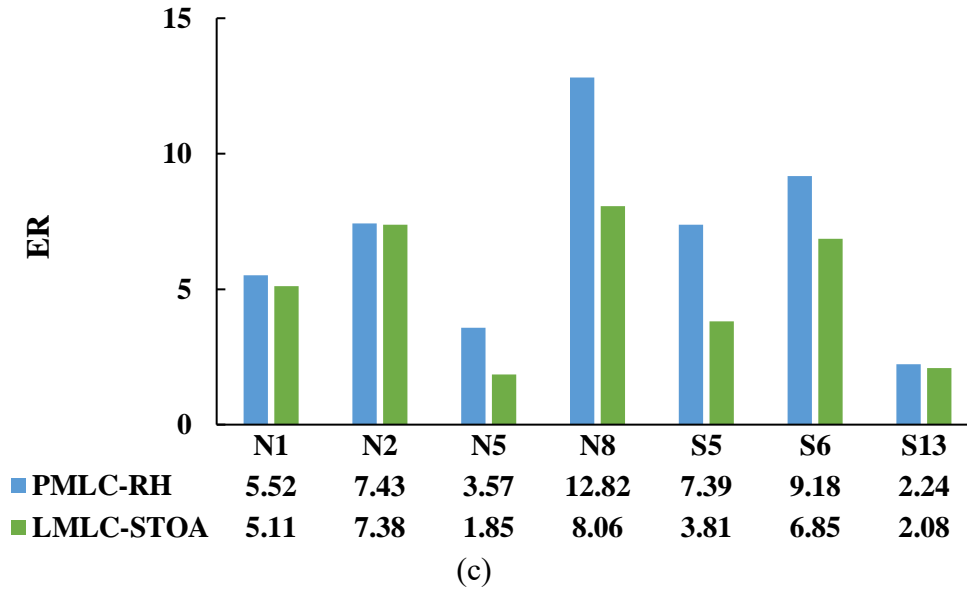
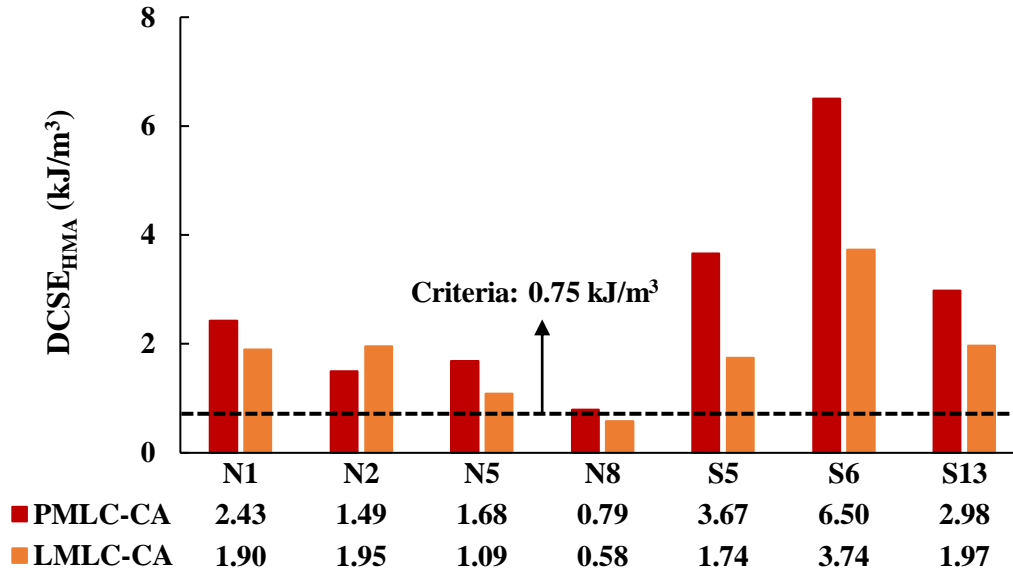


**Figure 6. 2 ER Test Results of PMLC-RH and LMLC-STOA; (a) DCSE<sub>HMA</sub> Results, (b) DCSE<sub>Min</sub> Results, (c) ER Results**

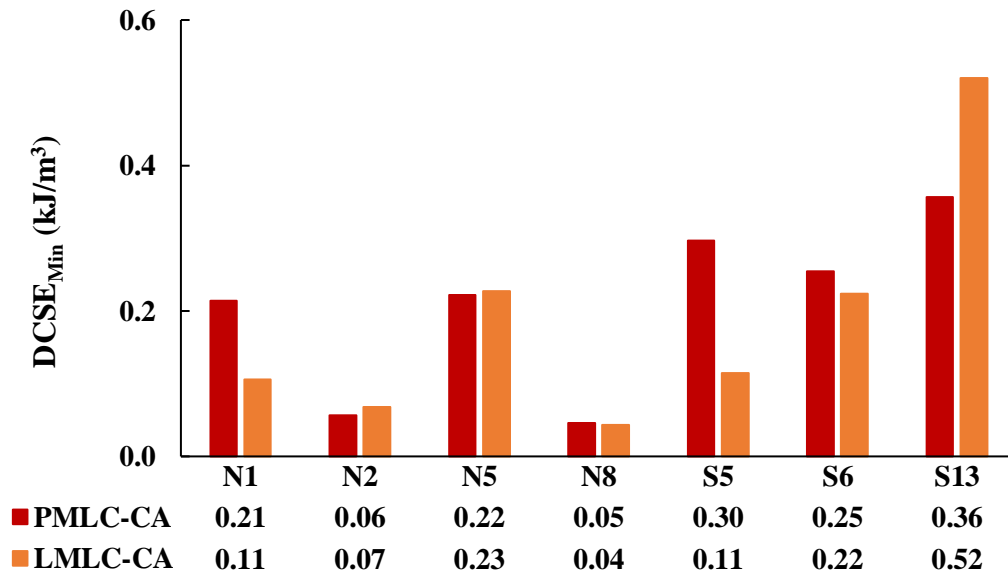
Figure 6.3 presents the DCSE<sub>HMA</sub>, DCSE<sub>Min</sub> and ER results of critically aged test specimens. Figure 6.3 (a) shows that the DCSE<sub>HMA</sub> results of all mixtures meet the criteria except for the laboratory mixture N8. It can also be seen that the DCSE<sub>HMA</sub> results of PMLC-CA mixtures are greater than their LMLC-CA results except for mixture N2. These results indicated that the LMLC-CA mixtures required less energy to initiate cracking. This might be explained by a higher aging level for laboratory STOA than plant production aging. Among seven experimental mixtures, for both PMLC-CA and LMLC-CA samples, N8 yielded the lowest DCSE<sub>HMA</sub> value, which has highest content of recycled materials.

Figure 6.3 (b) shows that the DCSE<sub>Min</sub> results of PMLC-CA and LMLC-CA are similar for N2, N5, N8, and S6, whereas N1 and S5 had much higher DCSE<sub>Min</sub> for the plant mixtures than the corresponding lab prepared mixtures, but S13 has the opposite trend. Figure 6.3 (c) shows that no consistent trend exists when comparing the ER results between PMLC-CA and LMLC-CA mixtures, and all of the ER results are greater than the highest ER criteria 1.95. The

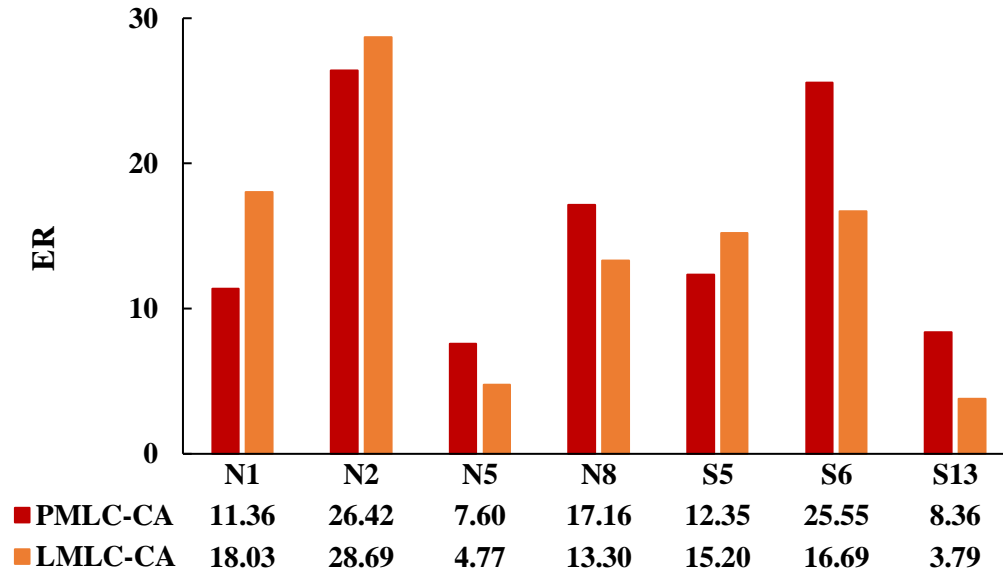
*paired-t* test results showed there was no significant difference between PMLC-CA and LMLC-CA among these three cracking test parameters (*p-value* > 0.05).



(a)



(b)



(c)

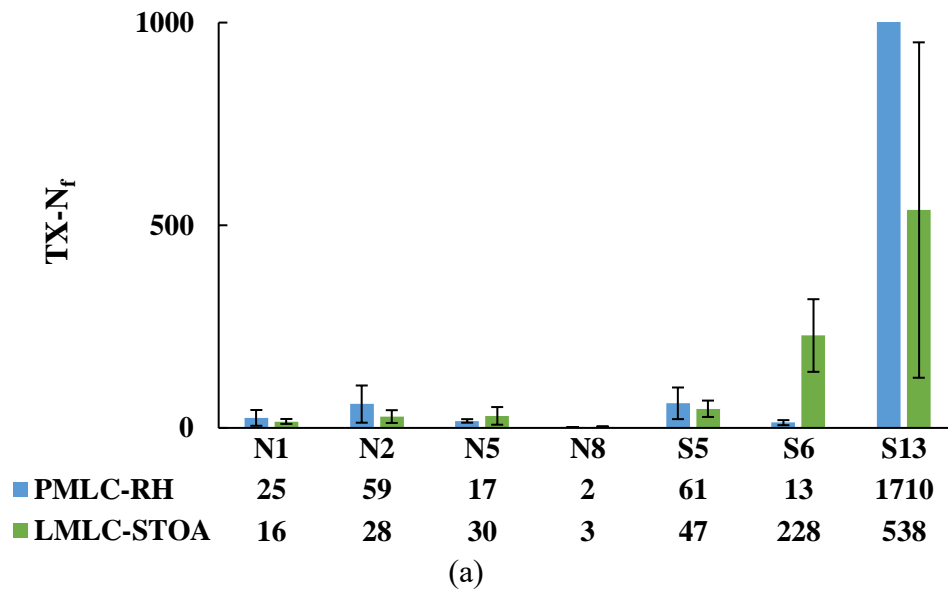
**Figure 6. 3 ER Test Results of PMLC-CA and LMLC-CA; (a) DCSE<sub>HMA</sub> Results, (b) DCSE<sub>Min</sub> Results, (c) ER Results**

### 6.2.2 Texas Overlay Test

Figure 6.4 presents the comparison results of TX- $N_f$  and TX- $\beta$  between PMLC-RH and LMLC-STOA specimens. The error bars in the figure represent plus and minus one standard deviation. As shown in Figure 6.4 (a), for both PMLC-RH and LMLC-STOA specimens, mixture N8 with 20% RAP and 5% RAS yielded the lowest TX- $N_f$  value, which failed at two and three cycles, respectively. Mixture S13 containing higher binder content and 20% ground tire rubber obtained the highest TX- $N_f$  value for both plant-produced and laboratory-prepared mixtures. Two-way ANOVA results indicated that no significant difference existed between PMLC-RH and LMLC-STOA specimens. However, *t-test* results showed that statistical differences existed between plant mixtures and laboratory mixtures for mixtures S6 and S13. As shown in Figure 6.4 (b), mixtures N8 and S13 yielded the highest and lowest TX- $\beta$  value, respectively, which indicated the worst and best cracking resistance, respectively. Two -way ANOVA results indicated that

there was a significant difference between PMLC-RH and LMLC-STOA specimens, and statistical difference was also observed for mixtures N8 and S13 using *t-test*.

Figure 6.5 presents the comparison results of TX- $N_f$  and TX- $\beta$  for the critically aged specimens. The error bars in the figure represent plus and minus one standard deviation. As shown in Figure 6.5, both TX- $N_f$  and TX- $\beta$  results indicated that mixture N8 and S13 had the lowest and highest cracking resistance, respectively, which were attributed to the compositions of these mixtures. In addition, both two-way ANOVA and *t-test* results indicated there was no statistically significant difference between PMLC-CA and LMLC-CA specimens for both TX-OT cracking test parameters.



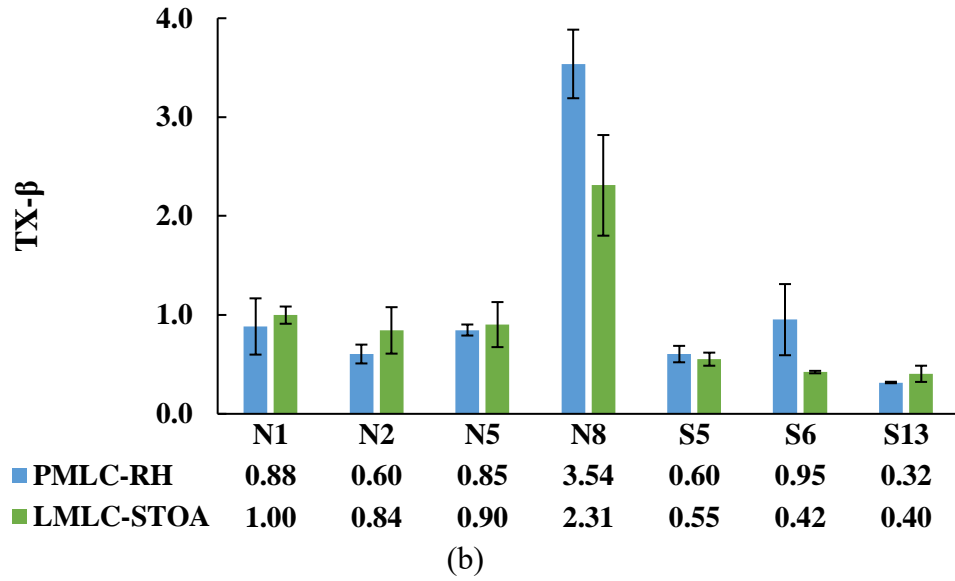
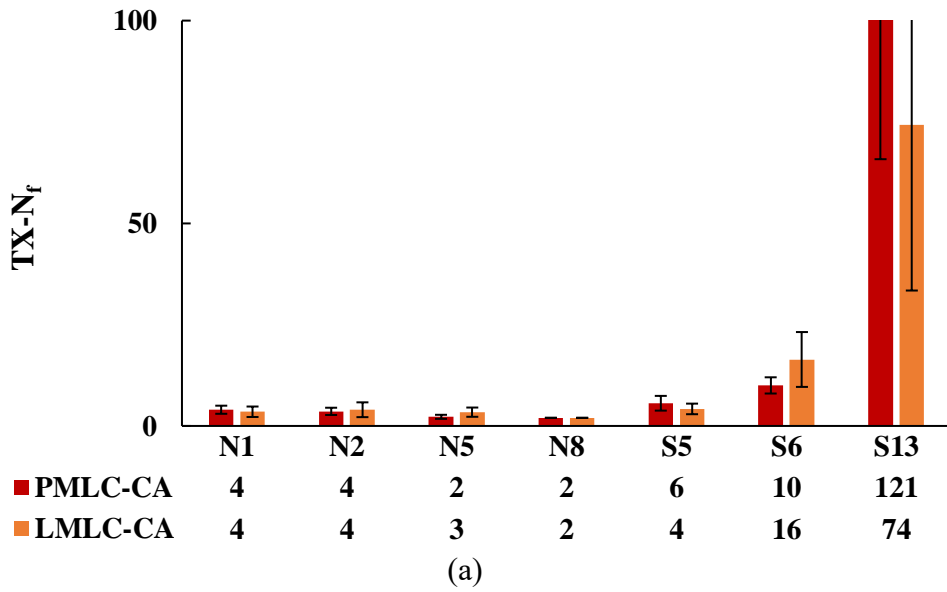
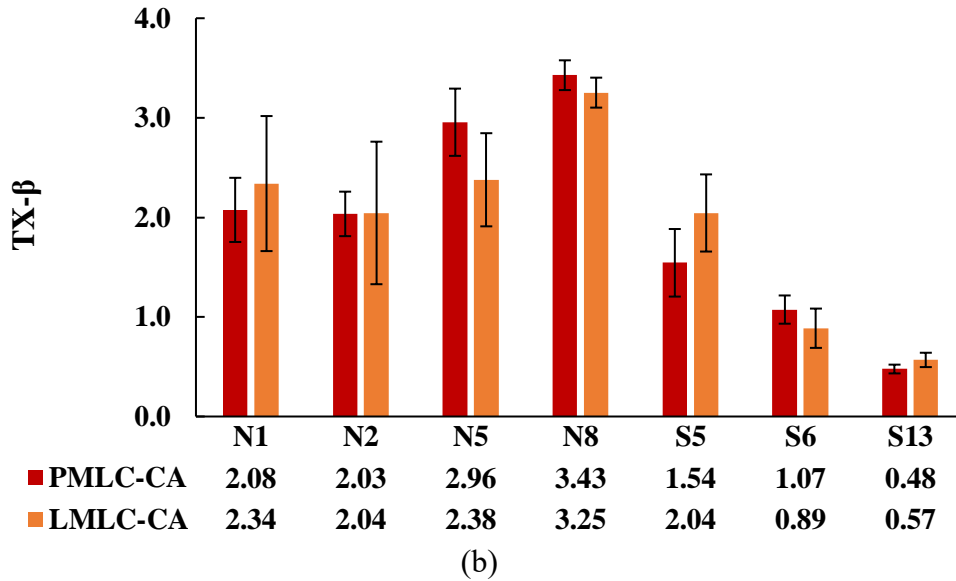


Figure 6. 4 TX-OT Test Results of PMLC-RH and LMLC-STOA; (a) TX- $N_f$  Results, (b) TX- $\beta$

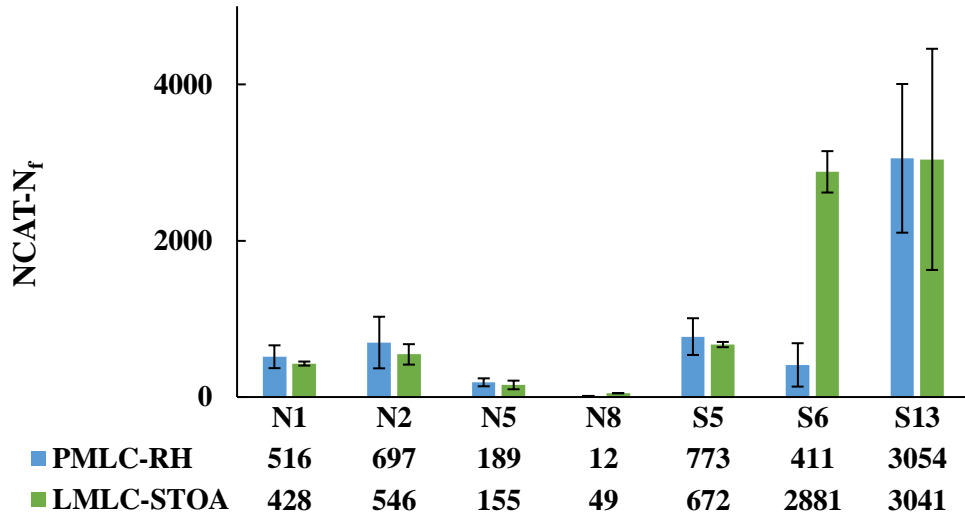




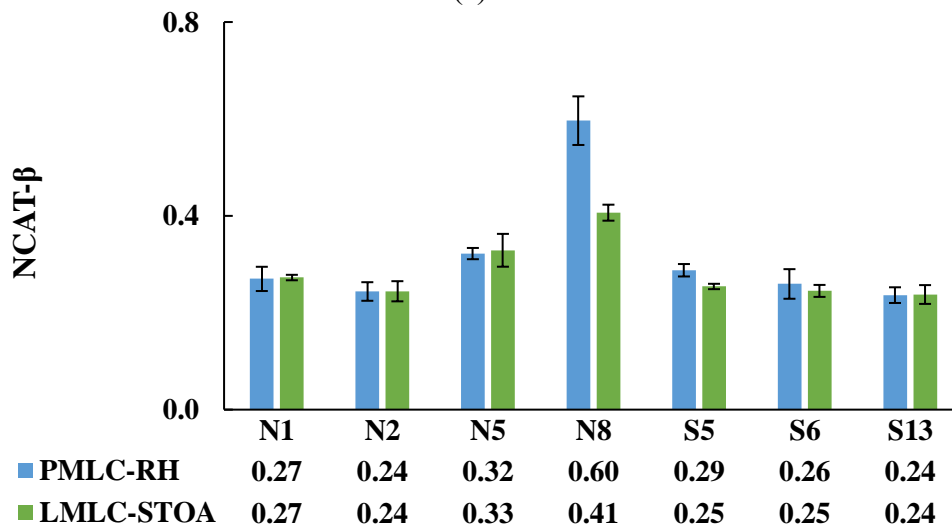
**Figure 6. 5 TX-OT Test Results of PMLC-CA and LMLC-CA; (a) TX- $N_f$  Results, (b) TX- $\beta$**

### 6.2.3 NCAT Modified Overlay Test

Figure 6.6 presents the comparison results of NCAT- $N_f$  and NCAT- $\beta$  between PMLC-RH and LMLC-STOA specimens. As shown in the Figure 6.6 (a), mixture N8, which contained 20% RAP and 5% RAS yielded the lowest NCAT- $N_f$  value for both plant-produced and laboratory-prepared mixtures. Meanwhile, mixture S13 had the highest NCAT- $N_f$  value for both plant-produced and laboratory-prepared mixtures, which indicated the best cracking resistance. Two-way ANOVA results indicated that no significant difference existed between PMLC-RH and LMLC-STOA for NCAT- $N_f$  results. However, *t-test* results showed that a statistical difference existed between PMLC-RH and LMLC-STOA specimens for mixtures N8 and S6. As shown in Figure 6.6 (b), NCAT- $\beta$  results showed the similar trend with NCAT- $N_f$  results; mixtures N8 and S13 yielded the worst and best cracking resistance for both plant mixtures and laboratory mixtures, respectively. Two-way ANOVA results implied that there was a significant difference existing between PMLC-RH and LMLC-STOA, and statistical difference was also observed for mixtures N8 and S5 based on the *t-test* results.



(a)



(c)

**Figure 6. 6 NCAT-OT Test Results of PMLC-RH and LMLC-STOA; (a) NCAT- $N_f$  Results, (b) NCAT- $\beta$**

Figure 6.7 presents the NCAT- $N_f$  and NCAT- $\beta$  results of critically aged test specimens. For both plant mixtures and laboratory mixtures, mixtures N8 had the lowest NCAT- $N_f$  result and the highest NCAT- $\beta$  result, which indicated the worst cracking resistance. In addition, mixture S13 yielded the highest NCAT- $N_f$  result and the lowest NCAT- $\beta$  result, which represented the best cracking resistance. For both NCAT- $N_f$  and NCAT- $\beta$  results, two-way ANOVA results indicated that there was no significant difference between PMLC-CA and LMLC-CA specimens,

although the *t*-test indicated a statistical difference between plant mixtures and laboratory mixtures for mixture S5.

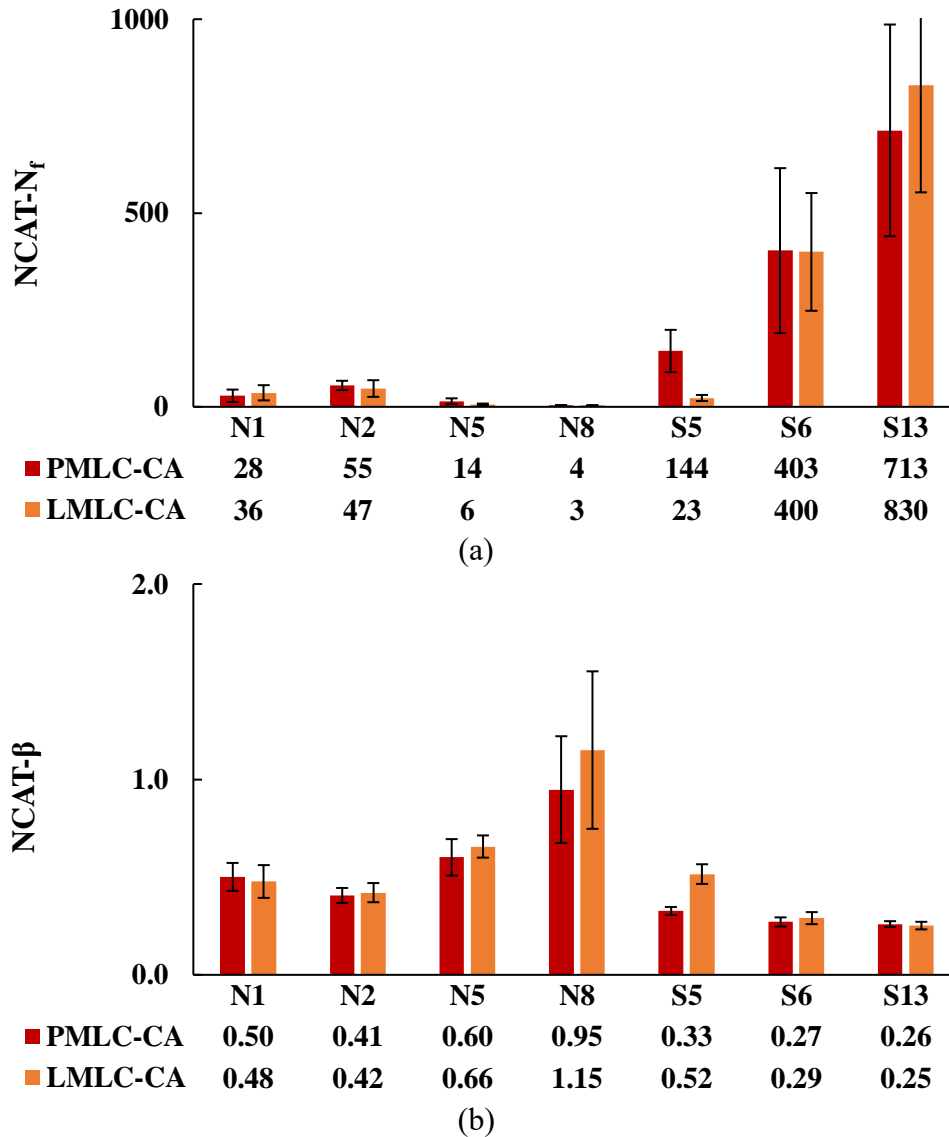
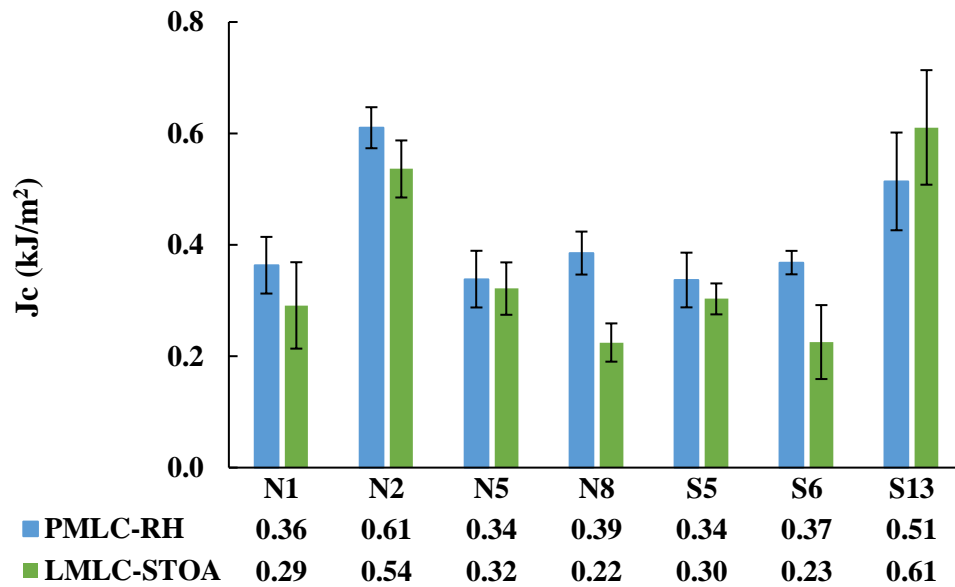


**Figure 6. 7 NCAT-OT Test Results of PMLC-CA and LMLC-CA; (a) NCAT-N<sub>f</sub> Results, (b) NCAT-β**

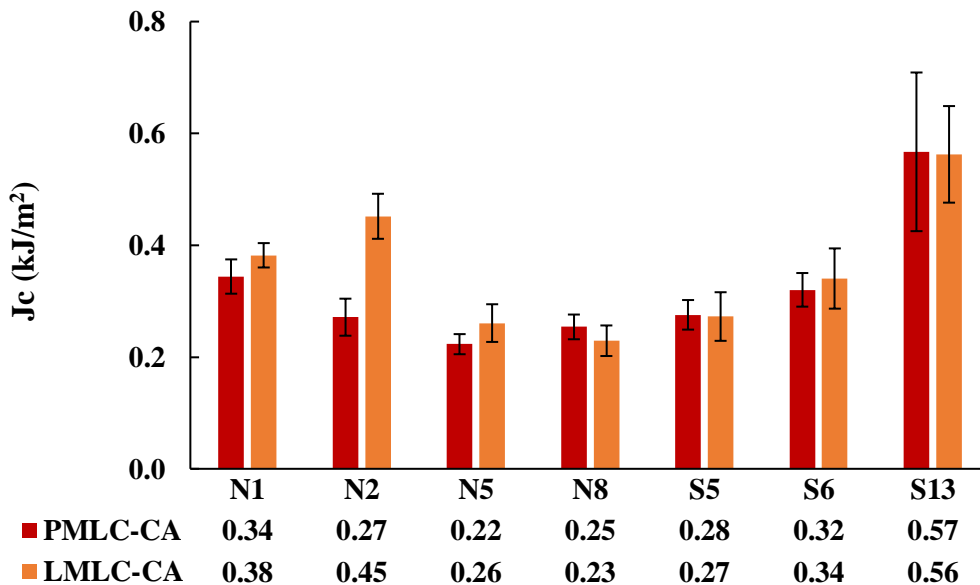
#### 6.2.4 Semi-Circular Bend Test

Figure 6.8 and Figure 6.9 present the comparison results of SCB-J<sub>c</sub> before and after critical aging, respectively. The error bars in the figures represent plus and minus one estimated standard deviation. As shown in Figure 6.8, the PMLC-RH specimen showed greater J<sub>c</sub> results than the

corresponding LMLC-STOA specimens except for mixture S13. Figure 6.9 shows that the LMLC-CA specimens yielded greater  $J_c$  results for mixtures N1, N2, and N5, whereas mixtures N8, S5, S6, and S13 had similar  $J_c$  results for PMLC-CA and LMLC-CA specimens with an average difference of 0.015. *Paired-t* test results indicated there was no significant difference between plant mixtures and laboratory mixtures at both aging conditions.



**Figure 6. 8 SCB Test Results of PMLC-RH and LMLC-STOA**

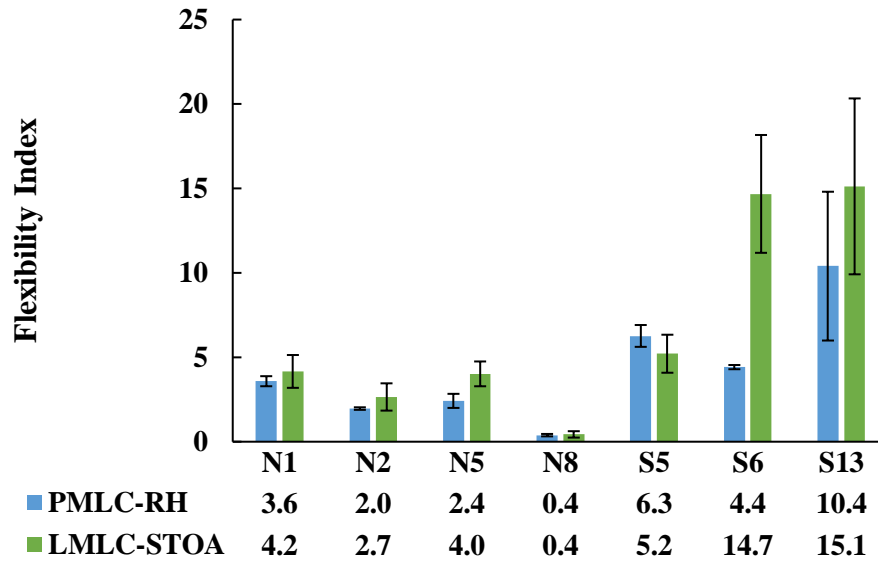


**Figure 6. 9 SCB Test Results of PMLC-CA and LMLC-CA**

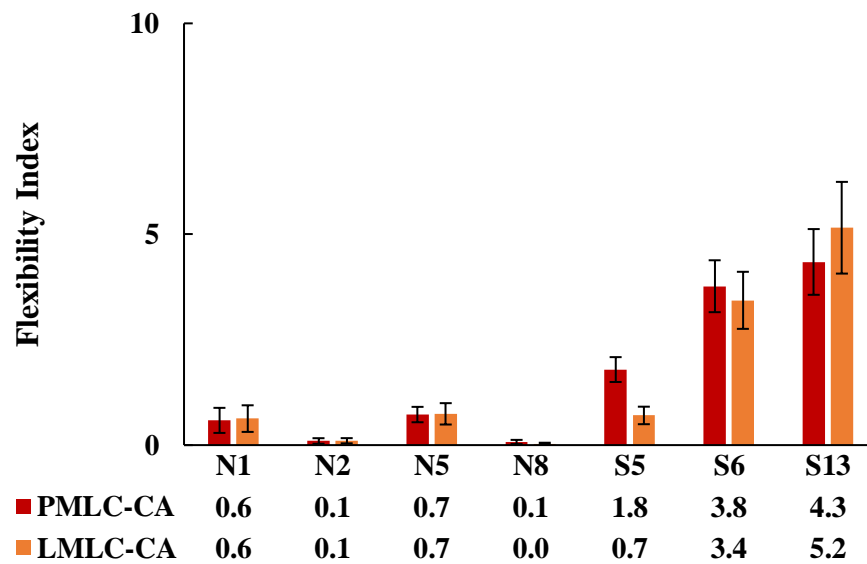
### 6.2.5 Illinois Flexibility Index Test

Figure 6.10 and Figure 6.11 present the comparison results of FI before and after critical aging, respectively. As shown in Figure 6.10, mixture N8 containing 20% RAP and 5% RAS yielded the lowest FI value for both PMLC-RH and LMLC-STOA specimens, which indicated the worst cracking resistance. LMLC-STOA specimens had greater FI results than the corresponding PMLC-RH specimens except for mixture S5. Two-way ANOVA results indicated that there was a significant difference in FI between PMLC-RH and LMLC-STOA specimens, implying that a higher aging level occurred during the plant production compared to the laboratory STOA protocol. Furthermore, statistical differences in FI were also observed for mixtures N2, N5, and S6 based on *t-test* results.

Figure 6.11 shows that plant mixtures had similar FI results with laboratory mixtures after critical aging; the differences varied from 0.0 to 1.1. In addition, two-way ANOVA results indicated that no significant difference in FI existed between plant mixtures and laboratory mixtures after critical aging. Although, *t-test* results showed that a statistical difference existed in FI between PMLC-CA and LMLC-CA for mixture S5, a difference of only 1.1 for FI is probably not practically significant.



**Figure 6. 10 I-FIT Test Results of PMLC-RH and LMLC-STOA**



**Figure 6. 11 I-FIT Test Results of PMLC-CA and LMLC-CA**

### 6.2.6 Indirect Tensile Asphalt Cracking Test

Figure 6.12 and Figure 6.13 present the comparison results of  $CT_{Index}$  before and after critical aging, respectively. As shown in Figure 6.12, LMLC-STOA specimens had higher  $CT_{Index}$  values than the corresponding PMLC-RH specimens except for mixture S13. Mixture N8 had the lowest  $CT_{Index}$  value, which indicated the worst cracking resistance. Although there was no significant

difference in  $CT_{Index}$  between PMLC-RH and LMLC-STOA specimens based on the two-way ANOVA, statistical differences were observed for mixtures N5, N8, S5, S6, and S13 using the *t*-test.

Figure 6.13 presents the IDEAL-CT results after critical aging. The two-way ANOVA results indicated that there was no significant difference in  $CT_{Index}$  results between PMLC-CA and LMLC-CA mixtures. However, *t*-test results showed that a statistical difference existed between plant mixtures and laboratory mixtures for mixtures N1, N2, N5, and S5 (*p*-value < 0.05). The differences in  $CT_{Index}$  between PMLC-CA and LMLC-CA specimens for these four mixtures can be attributed to the low variability of these sets of specimens; the differences are probably not significant in the practical sense.

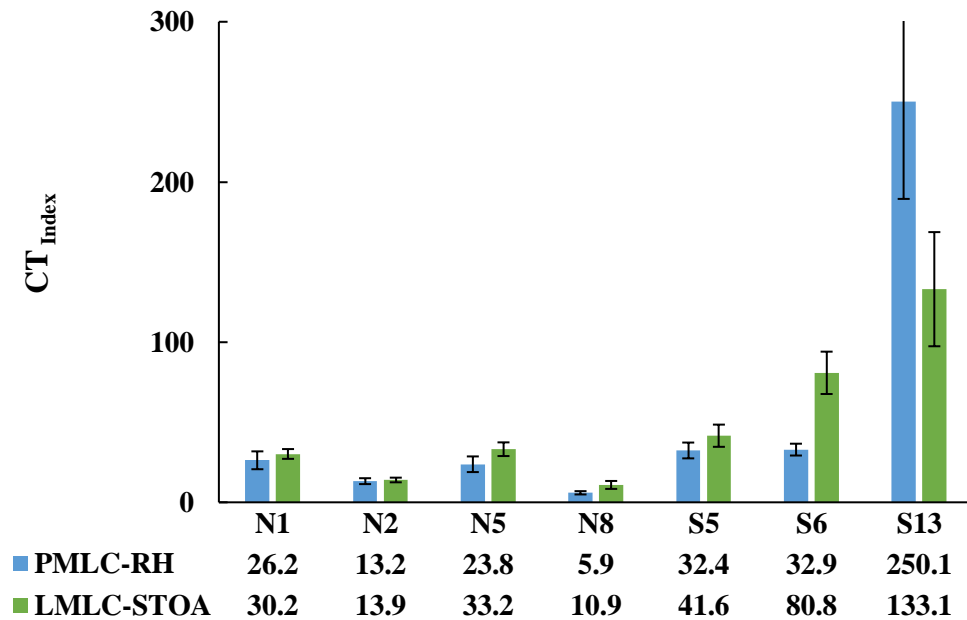


**Figure 6. 12 IDEAL-CT Test Results of PMLC-RH and LMLC-STOA**

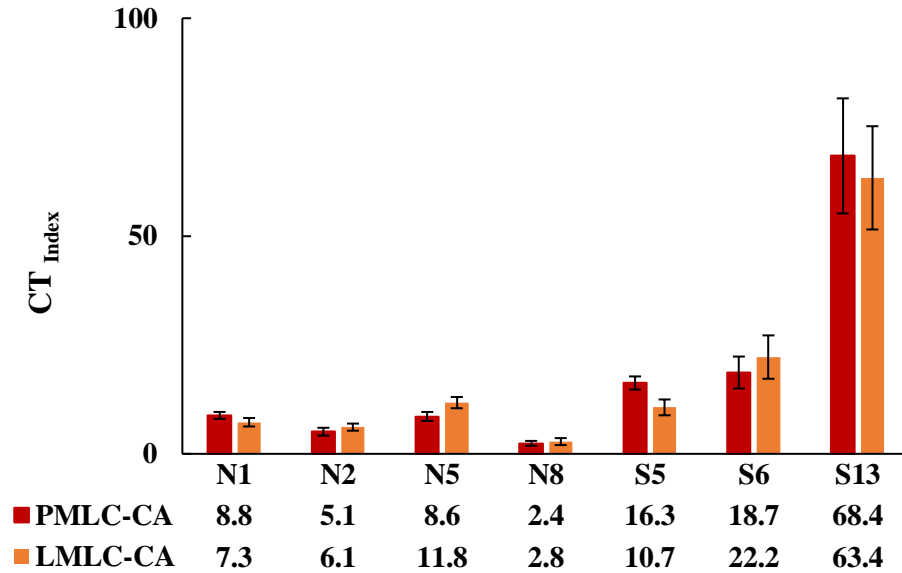


**Figure 6. 13 IDEAL-CT Test Results of PMLC-CA and LMLC-CA**

*6.2.7 Summary of Comparison Analysis between Plant mixtures and Laboratory Mixtures*

Two-way ANOVA tests and *paired-t* tests were conducted to compare results for plant mixtures and laboratory mixtures at both aging conditions for the six laboratory cracking tests. Table 6.1 summarizes the *p-values* of *paired-t* test and two-way ANOVA test for the comparison analysis at both aging conditions. Cells highlighted with yellow indicate that a significant difference exists between plant mixtures and laboratory mixtures (*p-value* < 0.05). As shown in Table 6.1, there was a significant difference between plant mixtures and laboratory mixtures before critical aging for DCSE<sub>HMA</sub>, ER, TX-N<sub>f</sub>, NCAT-N<sub>f</sub>, and FI. After critical aging, no statistical difference was observed between plant mixtures and laboratory mixtures among all the cracking test parameters.

In addition, *t-tests* also detected statistical differences between some, but not all plant mixtures and laboratory mixtures at both aging conditions for TX-OT, NCAT-OT, I-FIT, and IDEAL-CT tests. The mixtures having statistical differences are summarized in Table 6.2; “NA” indicated that there was no statistical difference between plant mixtures and laboratory mixtures for all seven mixtures. As shown in Table 6.2, the *t-test* statistical differences between plant

mixtures and laboratory mixtures were observed in different mixtures and different cracking test parameters. There was no consistent trend regarding the statistical differences before critical aging. After critical aging, no statistical differences were found for TX-OT test, and only mixture S5 showed statistical difference for NCAT-OT, I-FIT, and IDEAL-CT tests.

**Table 6. 1 *p*-value Summary of Comparison Analysis**

	PMLC-RH Vs. LMLC-STOA	PMLC-CA Vs. LMLC-CA	Statistical Test
DCSE <sub>HMA</sub>	0.03	0.07	<i>Paired-t</i> test
DCSE <sub>Min</sub>	0.12	0.60	<i>Paired-t</i> test
ER	0.04	0.58	<i>Paired-t</i> test
TX-N <sub>f</sub>	0.06	0.28	Two-way ANOVA
TX-β	0.04	0.92	Two-way ANOVA
NCAT-N <sub>f</sub>	0.28	0.99	Two-way ANOVA
NCAT-β	0.02	0.08	Two-way ANOVA
J <sub>c</sub>	0.13	0.23	<i>Paired-t</i> test
FI	0.00	0.37	Two-way ANOVA
CT <sub>Index</sub>	0.63	0.64	Two-way ANOVA

**Table 6. 2 Summary of Mixtures showing Statistical Difference during *t*-test**

	PMLC-RH Vs. LMLC-STOA	PMLC-CA Vs. LMLC-CA
TX-N <sub>f</sub>	S6, S13	NA
TX-β	N8, S13	NA
NCAT-N <sub>f</sub>	N8, S6	S5
NCAT-β	N8, S5	S5
FI	N2, N5, S6	S5
CT <sub>Index</sub>	N5, N8, S5, S6, S13	N1, N2, N5, S5

### 6.3 Sensitivity Analyses

According to the NCHRP 9-57 project (Zhou et al., 2017), an ideal test for evaluating the cracking resistance of asphalt mixtures should be sensitive to common mix design factors (e.g., aggregate, binder, RAP/RAS), have low variability and a good correlation with field cracking performance. This section presents a sensitivity analysis of the six selected cracking tests to four mix design factors: aging, air voids, recycled asphalt materials, and binder type. For ER and SCB tests, the aging sensitivity analysis was conducted using *paired-t* test at a significant level of 0.05, and the mean value analysis was used to evaluate their sensitivities to air voids, recycled asphalt materials, and modified binders. For TX-OT, NCAT-OT, I-FIT, and IDEAL-CT results, aging sensitivity analyses were conducted using both mean values and a two-way ANOVA at a significance level of 0.05. The Games-Howell post hoc test at a significance level of 0.05 was utilized to evaluate sensitivities to air voids, recycled asphalt materials, and modified binders.

#### 6.3.1 Aging Sensitivity

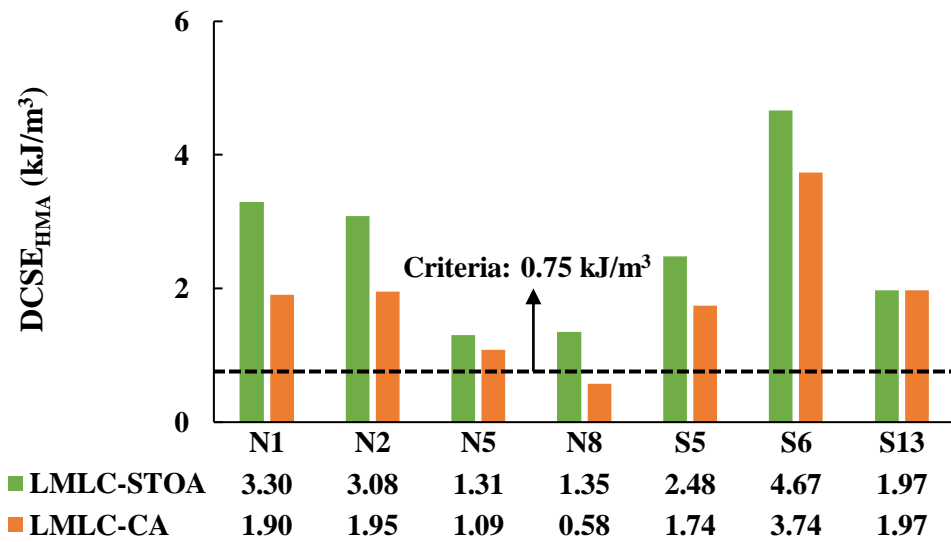
Asphalt aging has a significant effect on the development of TDC; after aging, mixtures are expected to be more brittle and less resistant to crack initiation (Rahbar-Rastegar et al., 2018). Each of the six cracking tests were conducted on reheated and critically aged PMLC specimens. All the cracking test results, except for  $\beta$ , were expected to decrease with aging. If the cracking test parameter showed the expected trend, this parameter was considered sensitive to aging.

##### (1) Energy Ratio

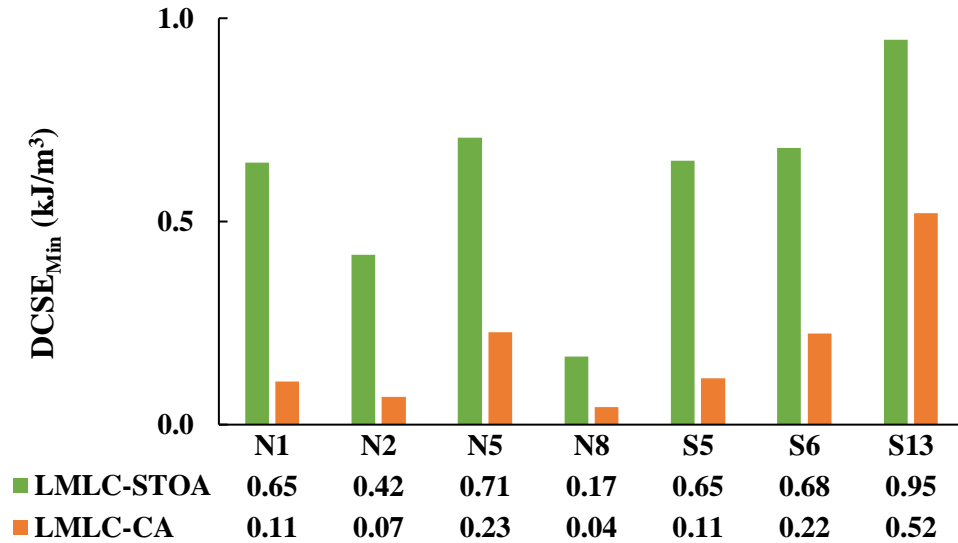
Figure 6.14 and Figure 6.15 present the aging sensitivity results of  $DCSE_{HMA}$ ,  $DCSE_{Min}$ , and ER for laboratory mixtures and plant mixtures, respectively. Based on the study of Roque et al. (2004), the ER was calibrated and validated over the  $DCSE_{HMA}$  range from 0.75 to 2.5 kJ/m<sup>3</sup>,

and a minimum  $DCSE_{HMA}$  criterion of  $0.75 \text{ kJ/m}^3$  was recommended to screen out mixtures with extremely high stiffness. In addition, minimum ER criteria were also proposed for different traffic levels, and the highest criteria was 1.95 for a traffic level of 1 million ESALs per year. However, seven experimental mixtures were exposed to a much higher traffic level than the validated range.

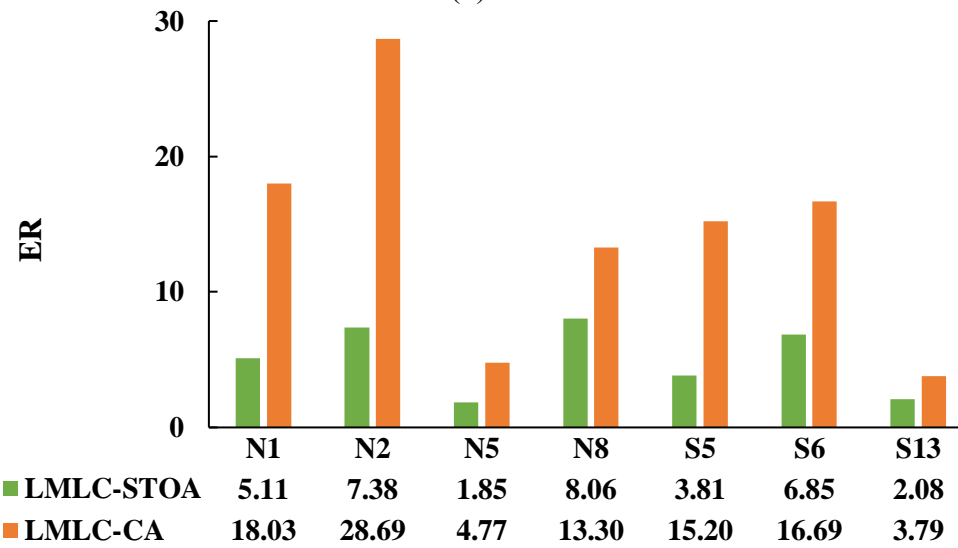
As shown in the Figure 6.14 (a), the  $DCSE_{HMA}$  of laboratory mixtures at both aging conditions met the minimum criteria of  $0.75 \text{ kJ/m}^3$  except for the mixture N8 containing 20% RAP and 5% RAS after critical aging. In addition, the  $DCSE_{HMA}$  decreased after critical aging for all mixtures except for mixture S13, which included ground tire rubber modified binder. Figure 6.14 (b) shows that the  $DCSE_{Min}$  decreased after critical aging for all seven mixtures, which was expected. However, as shown in Figure 6.14 (c), the ER increased after critical aging for all seven mixtures, which was not consistent with the expected trend. Furthermore, *paired-t* test results indicated that aging had significant effects on all these three parameters.  $DCSE_{HMA}$  and  $DCSE_{Min}$  both decreased with aging as expected, but ER displayed the opposite trend.



(a)



(b)

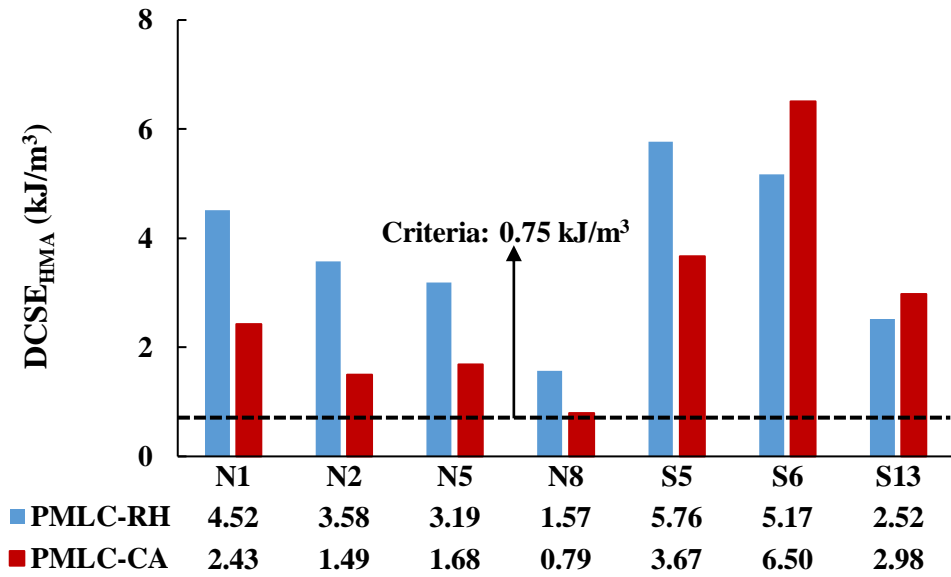


(c)

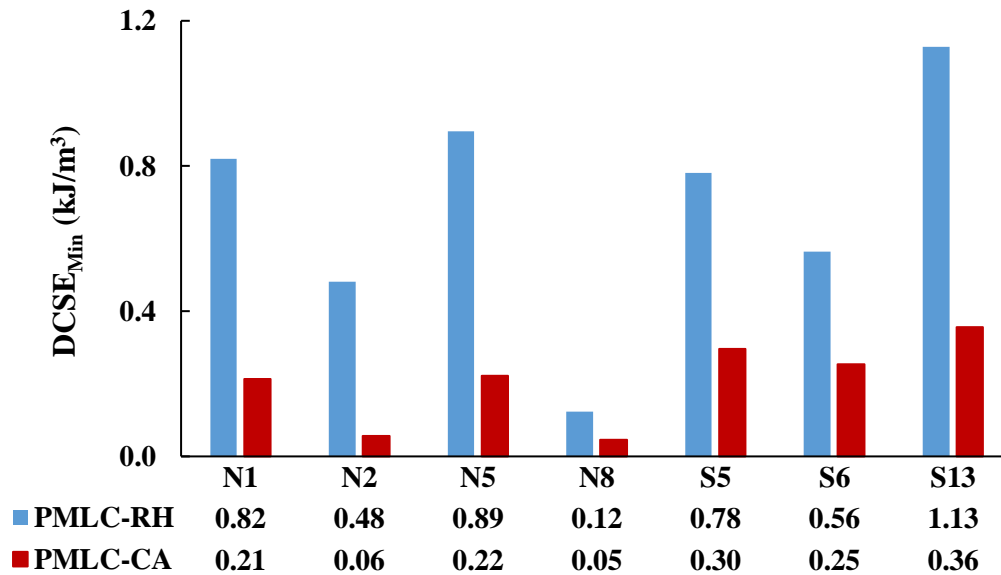
**Figure 6. 14 Aging Sensitivity Results of ER Test to Laboratory Mixtures; (a)  $DCSE_{HMA}$  Results, (b)  $DCSE_{Min}$  Results, (c) ER Results**

Figure 6.15 (a) shows that all PMLC-RH mixtures except N8 had  $DCSE_{HMA}$  results within the validated range of 0.75 to 2.5  $\text{kJ/m}^3$ . However, only three PMLC-CA mixtures were within the validated range, including S5, S6, and S13. As expected, for most mixtures, the  $DCSE_{Min}$  for PMLC-CA mixtures were lower than their PMLC-RH results. The two exceptions were S6 and S13, which have a HiMA binder and a rubber modified binder, respectively. These results may indicate that these modified binders require more energy to initiate cracking after

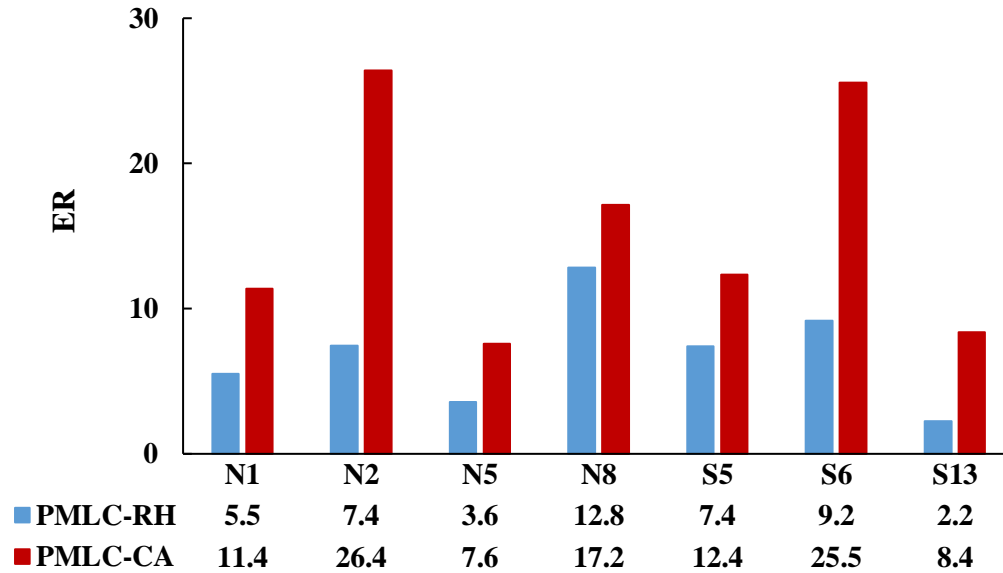
aging. Figure 6.15 (b) shows that the  $DCSE_{Min}$  results of all mixes decreased significantly with aging. However, in Figure 6.15 (c), all seven mixtures had higher ER values after aging, which is not consistent with the expected trend. Based on the *paired-t* test results,  $DSCE_{HMA}$  was not sensitive to aging,  $DCSE_{Min}$  was sensitive to aging in the expected direction, and ER was sensitive to aging but the direction did not follow the expected trend.



(a)



(b)



(c)

**Figure 6. 15 Aging Sensitivity Results of ER Test to Plant Mixtures; (a) DCSE<sub>HMA</sub> Results, (b) DCSE<sub>Min</sub> Results, (c) ER Results**

(2) Texas Overlay Test

Figure 6.16 presents the TX-OT results of laboratory mixtures at both aging conditions, including TX-N<sub>f</sub> and TX-β. The error bars shown in figures represent plus and minus one standard deviation of the results for each mixture, and the mean values are shown below each respective mixture. As shown in Figure 6.16 (a), TX-N<sub>f</sub> decreased after critical aging for all seven mixtures, indicating a lower cracking resistance after aging. Mixtures S6 and S13 had much higher TX-N<sub>f</sub> results than other five mixtures at both aging conditions, which might be explained by the use of HiMA binder and a rubber modified binder, respectively. Mixture N8, which contained 20% RAP and 5% RAS, had the lowest TX-N<sub>f</sub> values among all the mixtures at both aging conditions. As shown in Figure 6.16 (b), all LMLC-CA mixtures had greater TX-β results than the corresponding LMLC-STOA mixtures, which implied that the cracking resistance of mixtures decreased after aging. In addition, mixtures N8 and S13 yielded the highest and lowest TX-β results, respectively, which indicated the worst and best cracking

resistance, respectively. Two-way ANOVA results indicated that both parameters were significantly affected by aging.

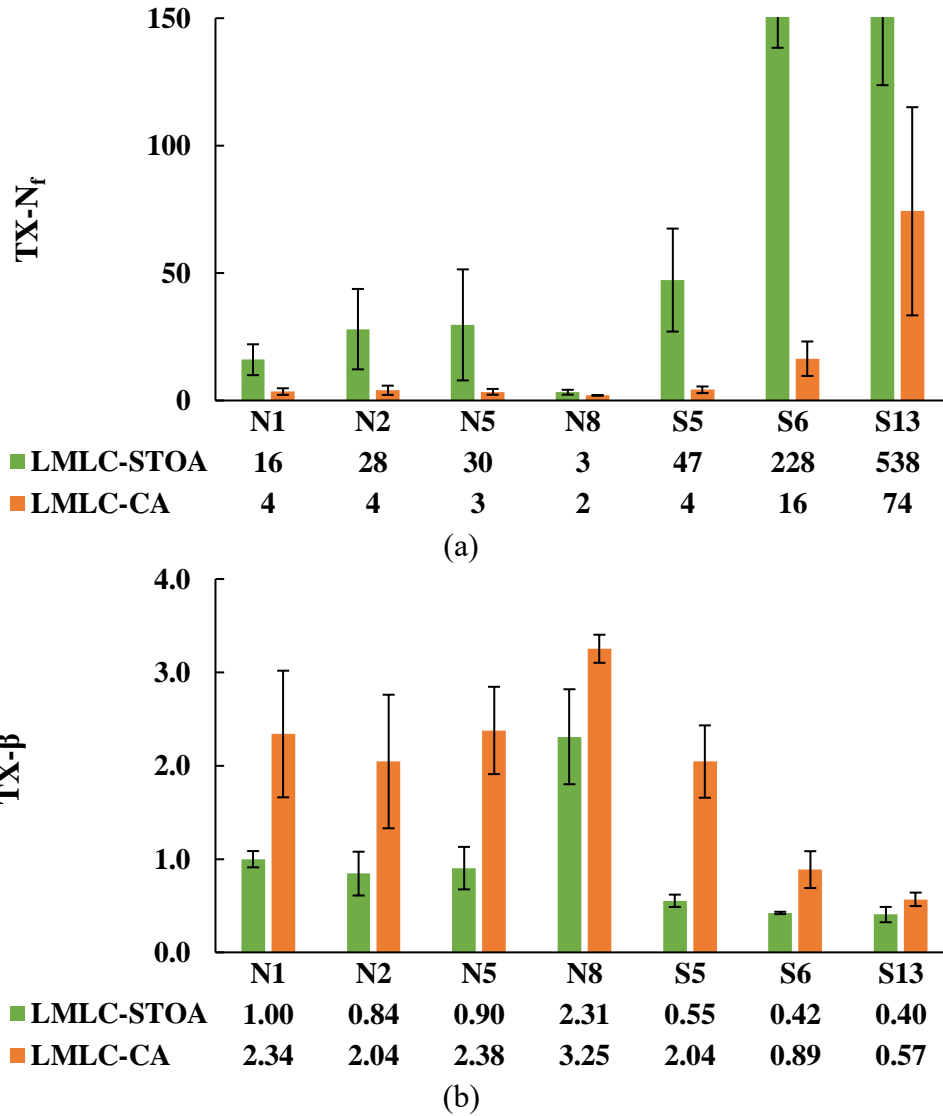
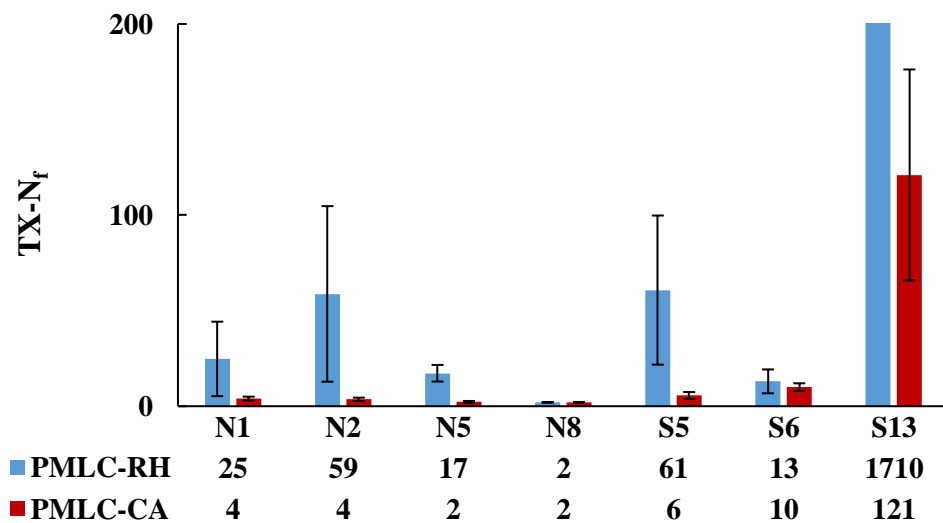


**Figure 6.16 Aging Sensitivity Results of TX-OT Test to Laboratory Mixtures; (a) TX- $N_f$  Results, (b) TX- $\beta$  Results**

Figure 6.17 presents the TX-OT results of plant mixtures, including TX- $N_f$  and TX- $\beta$ . The error bars shown in figures represent plus and minus one standard deviation of the results for each mixture. The mean values are shown below each respective mixture. As shown in Figure 6.17 (a), for all seven mixtures, the mean TX- $N_f$  of tests on critically aged mixtures were

substantially lower than those of reheated mixtures, indicating increased susceptibility to cracking after aging. Mixture N8, which contained 20% RAP and 5% RAS, failed at two cycles for both reheated and critically aged conditions, which indicated that this mixture had almost no cracking resistance in this extremely high strain test. The mean  $N_f$  of mixture S13 greatly exceeded the other mixtures, which were more than 28 times and 12 times higher than other reheated and critically aged mixtures, respectively.

Similar trends were also observed for the TX- $\beta$  results shown in Figure 6.17 (b). The RAP/RAS mixture, N8, yielded the highest TX- $\beta$  values for both reheated and critically aged conditions, which indicated the worst cracking resistance. The GTR mixture, S13, had the lowest TX- $\beta$  values indicating better cracking resistance than the other six mixtures. As expected, for all mixtures except N8, the TX- $\beta$  results on critically aged samples were higher than results of reheated samples. For mixture N8, the difference in TX- $\beta$  results between reheated and critically aged samples was only 0.11. For both parameters of the TX-OT test, the *p-values* of the aging factor were less than 0.005 based on a two-way ANOVA analysis. The results indicated that the effect of aging on TX-OT results was significant, with both parameters sensitive to aging.



(a)

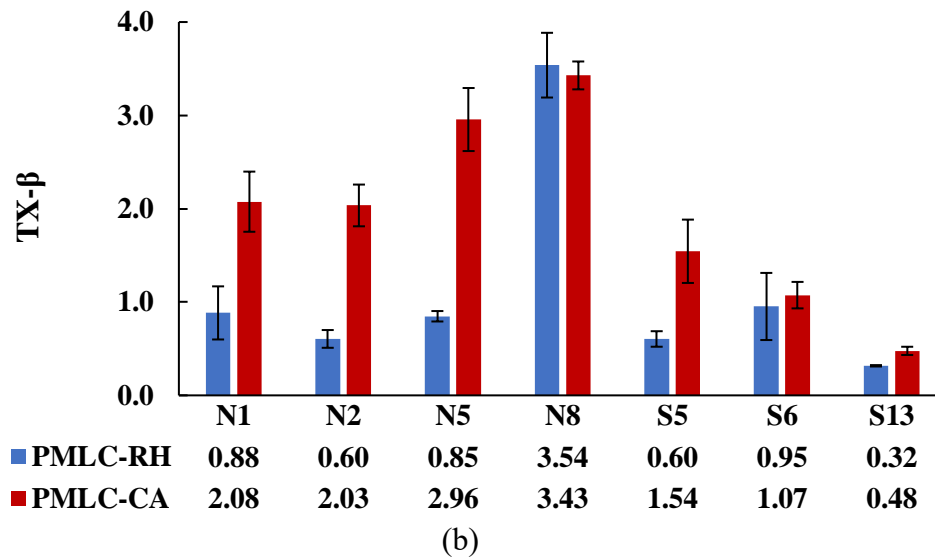


**Figure 6. 17 Aging Sensitivity Results of TX-OT Test to Plant Mixtures; (a) TX- $N_f$  Results, (b) TX- $\beta$  Results**

### (3) NCAT Modified Overlay Test

Figure 6.18 presents the NCAT- $N_f$  and NCAT- $\beta$  results of laboratory mixtures at both aging conditions. The error bars represent plus and minus one standard deviation from the mean values. As shown in Figure 6.18 (a), all LMLC-STOA mixtures had much higher NCAT- $N_f$  results than the corresponding LMLC-CA mixtures, which indicated a substantial decline in cracking resistance after aging. A similar trend was also observed in Figure 6.18 (b), the TX- $\beta$  results increased after critical aging, indicating a decrease in cracking resistance after aging. However, the changes after aging were very small for mixtures S6 and S13, which indicated the HiMA binder and GTR modified binder had good aging resistance. In addition, the two-way ANOVA results indicated that both NCAT-OT parameters were significantly influenced by aging.

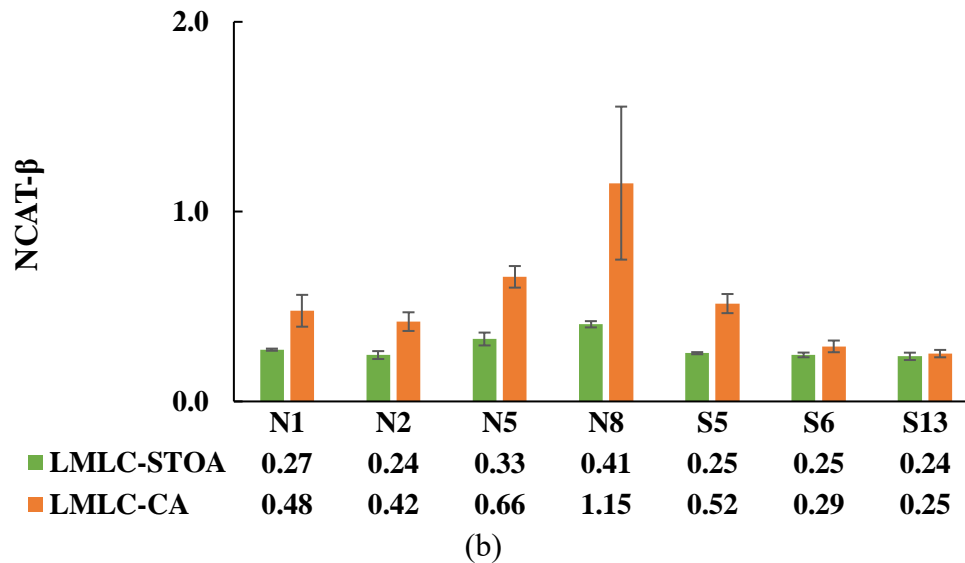
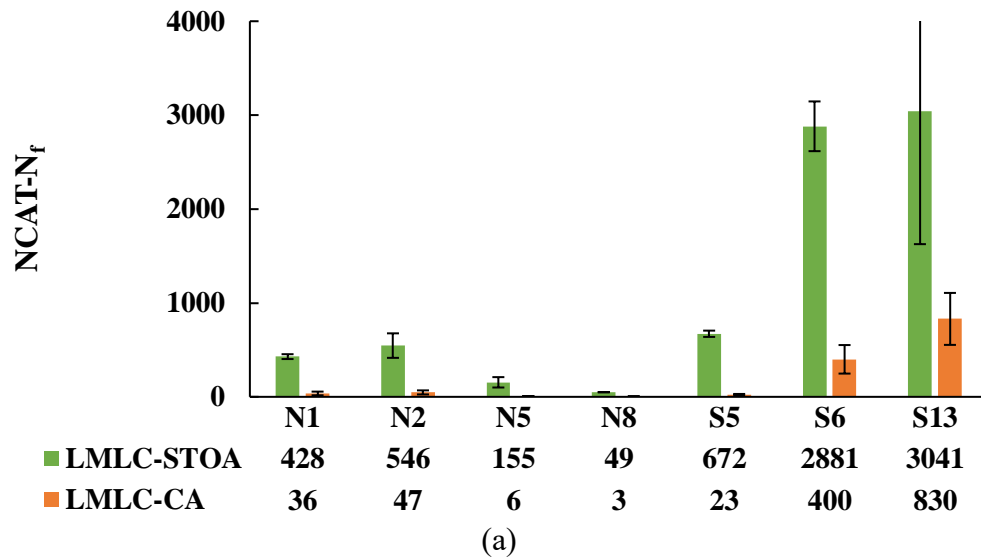


**Figure 6. 18 Aging Sensitivity Results of NCAT-OT Test to Laboratory Mixtures; (a) NCAT- $N_f$  Results, (b) NCAT- $\beta$  Results**

Figure 6.19 presents the NCAT- $N_f$  and NCAT- $\beta$  results of plant mixtures at both aging conditions. The error bars represent plus and minus one standard deviation from the mean values. As shown in Figure 6.19 (a), most mixtures had much lower NCAT- $N_f$  results for critically aged samples than for reheated samples. The one exception was the mixture with a HiMA binder, S6. As shown in Figure 6.19 (b), the NCAT- $\beta$  results increased for all of the critically aged samples compared to the corresponding reheated samples, however the differences were very small for

S5, S6, and S13. Meanwhile, the statistical analysis results also indicated that aging had significant effects on both parameters, which was consistent with the mean values analysis. This was the expected trend for aging. Overall, for both laboratory and plant mixtures, both parameters showed the expected trend, which indicate that NCAT-OT parameters are sensitive to aging.

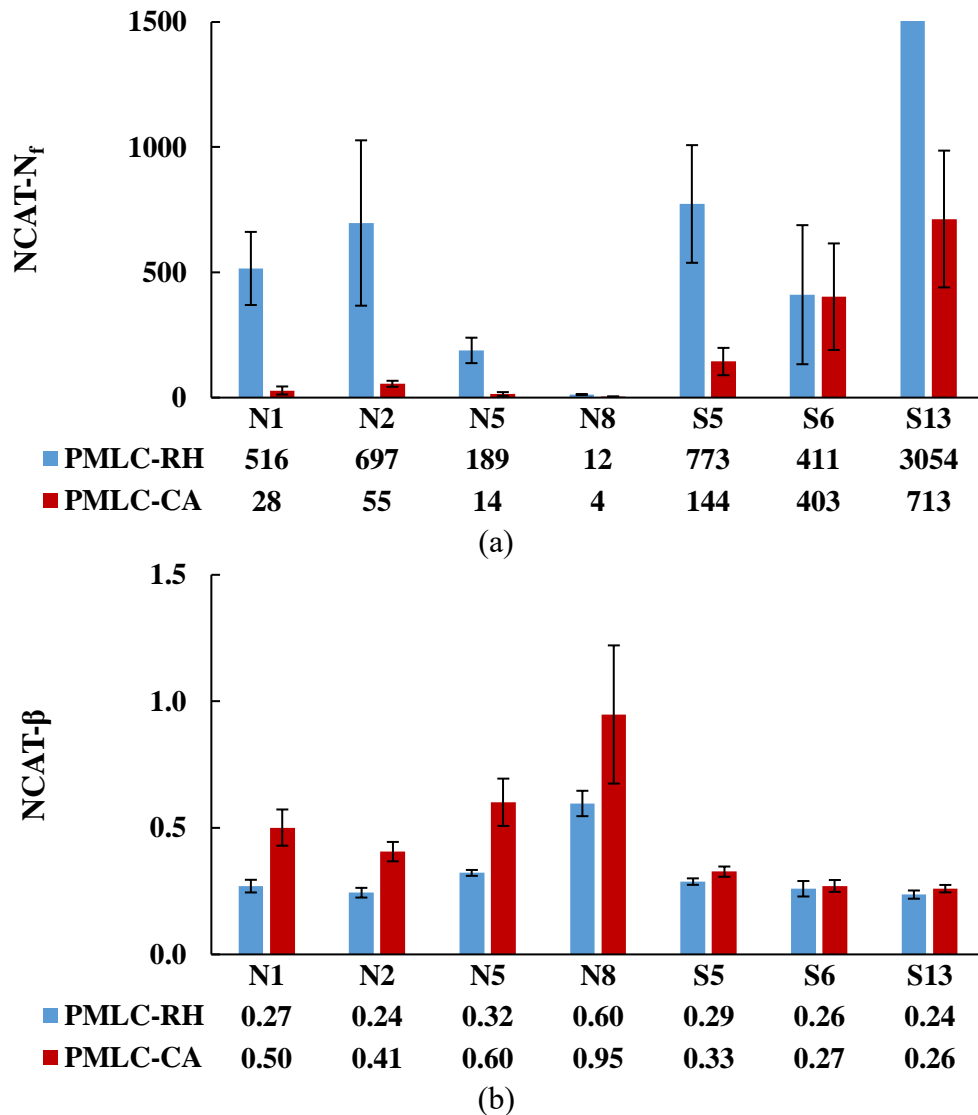


**Figure 6. 19 Aging Sensitivity Results of NCAT-OT Test to Plant Mixtures; (a) NCAT- $N_f$  Results, (b) NCAT- $\beta$  Results**

#### (4) Semi-Circular Bend Test

Figure 6.20 and Figure 6.21 present the  $J_c$  results of laboratory mixtures and plant mixtures at both aging conditions, respectively. The error bars in the figures represent plus and minus one estimated standard deviation. As shown in Figure 6.20, the  $J_c$  results of laboratory mixtures decreased after aging for four of the seven mixtures, but increased after aging for the other three mixtures. Figure 6.21 shows, for all plant mixtures except for the GTR modified mixture, S13, the critically aged  $J_c$  results were substantially lower than the corresponding results on reheated samples. The *paired-t* test results indicated that aging did not significantly affect the  $J_c$  results for both laboratory and plant mixtures.

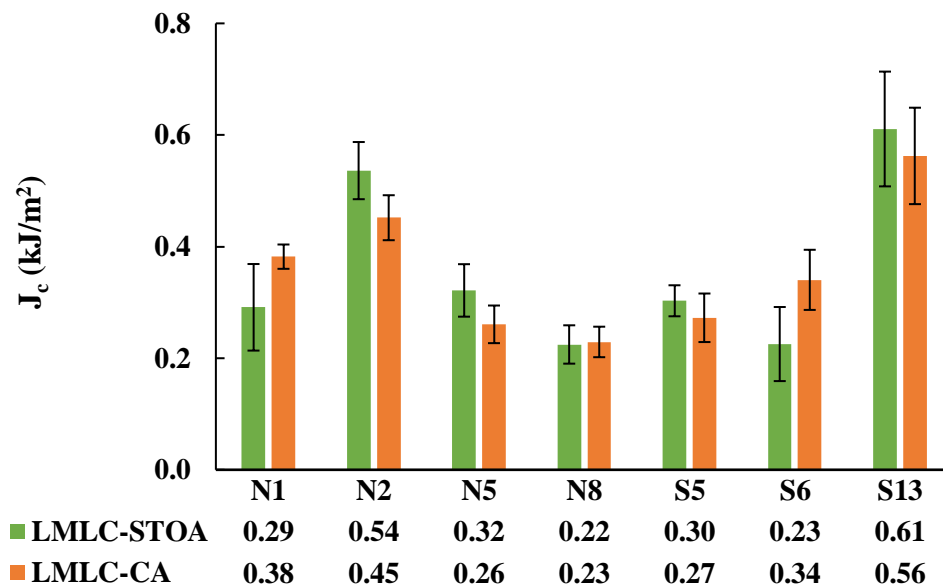


**Figure 6. 20 Aging Sensitivity of SCB Test to Laboratory Mixtures**

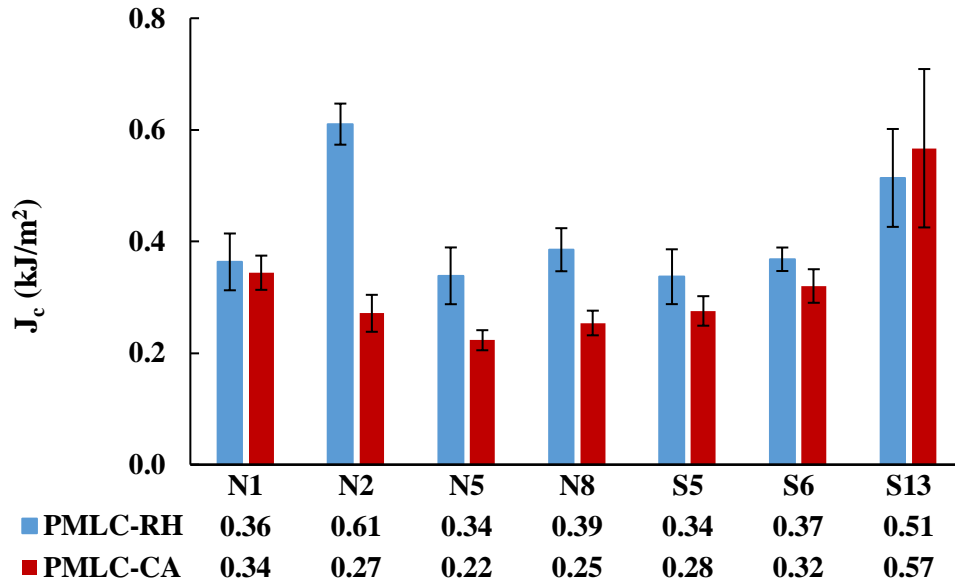


**Figure 6. 21 Aging Sensitivity of SCB Test to Plant Mixtures**

(5) Illinois Flexibility Index Test

Figure 6.22 and Figure 6.23 present the FI results of laboratory mixtures and plant mixtures at both aging conditions, respectively. The error bars in the figures represent plus and minus one estimated standard deviation. As shown in following figures, for both laboratory and plant mixtures, the FI reduced after aging, which indicated decreasing cracking resistance after aging. In addition, mixture N8 containing 20% RAP and 5% RAS consistently yielded the lowest FI value for both laboratory and plant mixtures at both aging conditions. Both the mean value and two-way ANOVA analyses indicated that FI results were significantly affected by aging for both laboratory and plant mixtures.

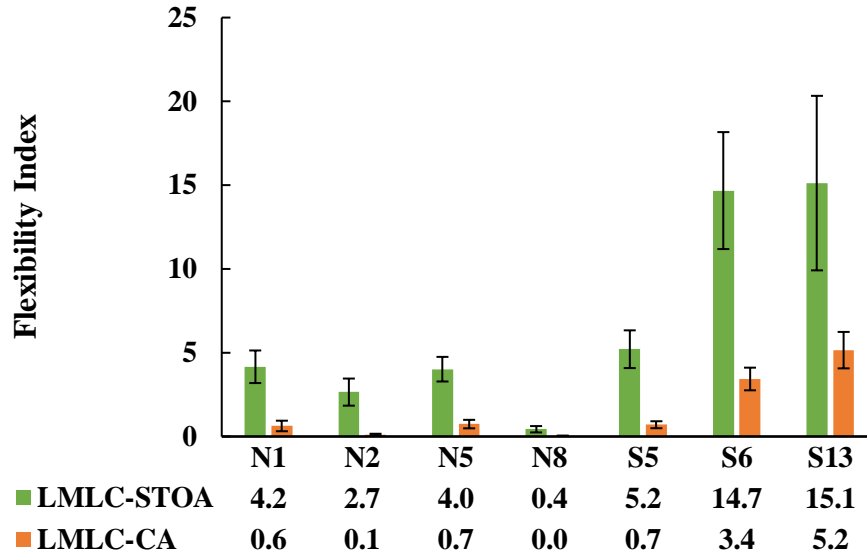


Figure 6. 22 Aging Sensitivity of I-FIT Test to Laboratory Mixtures

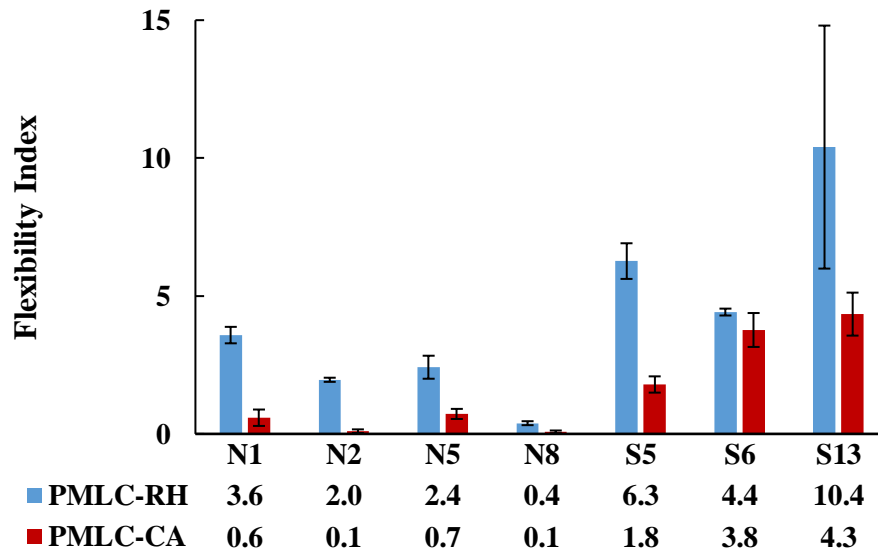


Figure 6. 23 Aging Sensitivity of I-FIT Test to Plant Mixtures

(6) Indirect Tensile Asphalt Cracking Test

Figure 6.24 and Figure 6.25 present the  $CT_{Index}$  results of laboratory mixtures and plant mixtures at both aging conditions, respectively. The error bars in the figures represent plus and minus one estimated standard deviation. As shown in following figures, mixtures N8 and S13 showed the worst and the best cracking resistance for both laboratory and plant mixtures at both aging

conditions, respectively, which was consistent with TX-OT, NCAT-OT, and I-FIT results. In addition, for both laboratory and plant mixtures, the  $CT_{Index}$  results of critically aged samples were statistically lower than the corresponding STOA or reheated samples, which indicated decreasing cracking resistance after aging.

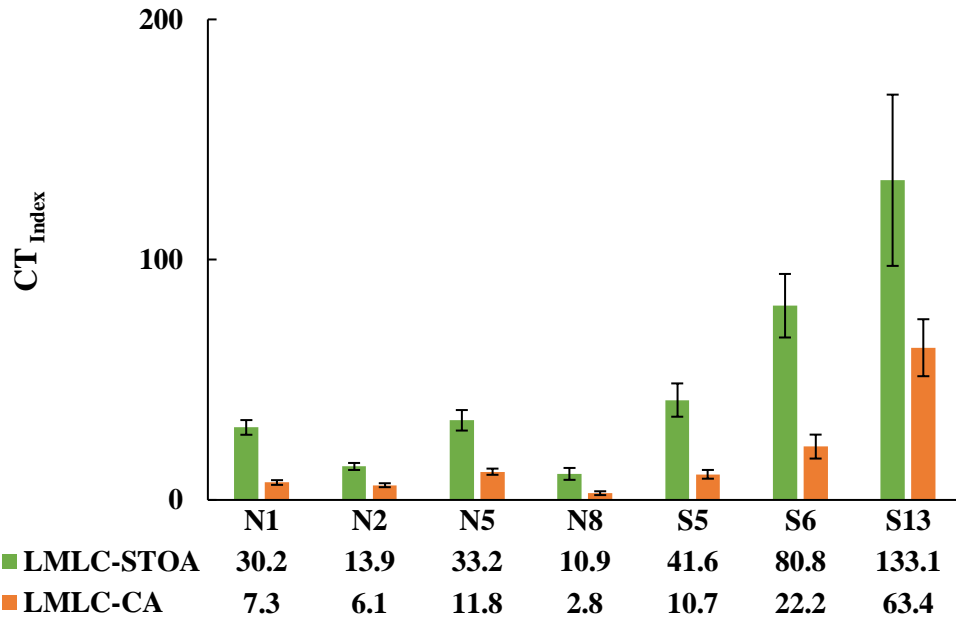


Figure 6. 24 Aging Sensitivity of IDEAL-CT Test to Laboratory Mixtures

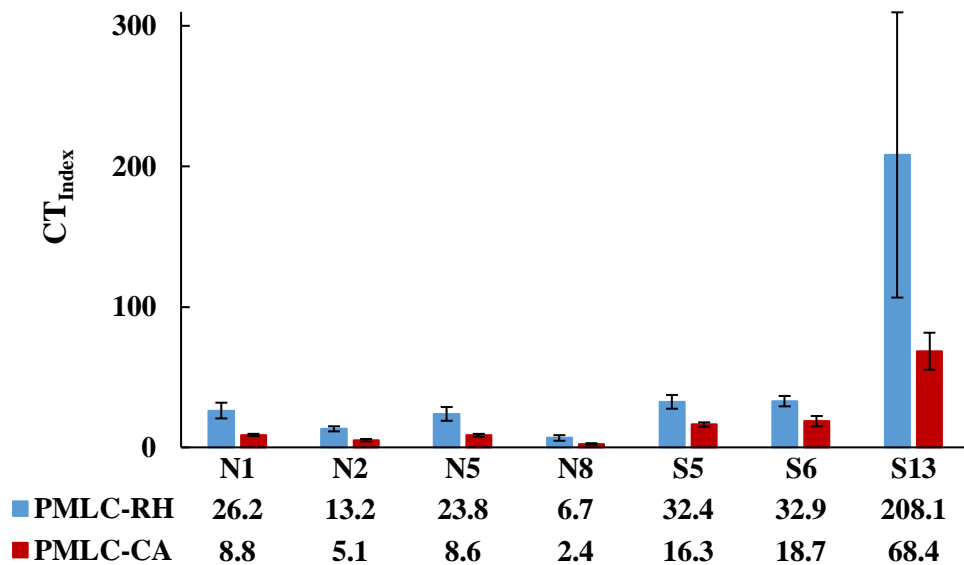


Figure 6. 25 Aging Sensitivity of IDEAL-CT Test to Plant Mixtures

### (7) Summary of Aging Sensitivity Analysis

The aging sensitivity analysis were conducted using *paired-t* test and two-way ANOVA for both plant mixtures and laboratory mixtures, which was summarized in Table 6.3. A “+” indicates that the parameter is sensitive to aging; a “-” indicates that the parameter is not sensitive to aging. As it can be seen, most of the cracking test parameters are sensitive to aging for both plant and laboratory mixtures, including DCSE<sub>Min</sub>, TX-N<sub>f</sub>, TX-β, NCAT-N<sub>f</sub>, NCAT-β, FI, and CT<sub>Index</sub>. In addition, ER and J<sub>c</sub> are not sensitive to aging for both plant and laboratory mixtures, and DCSE<sub>HMA</sub> is only sensitive to aging for laboratory mixtures.

**Table 6. 3 Summary of Aging Sensitivity Analysis**

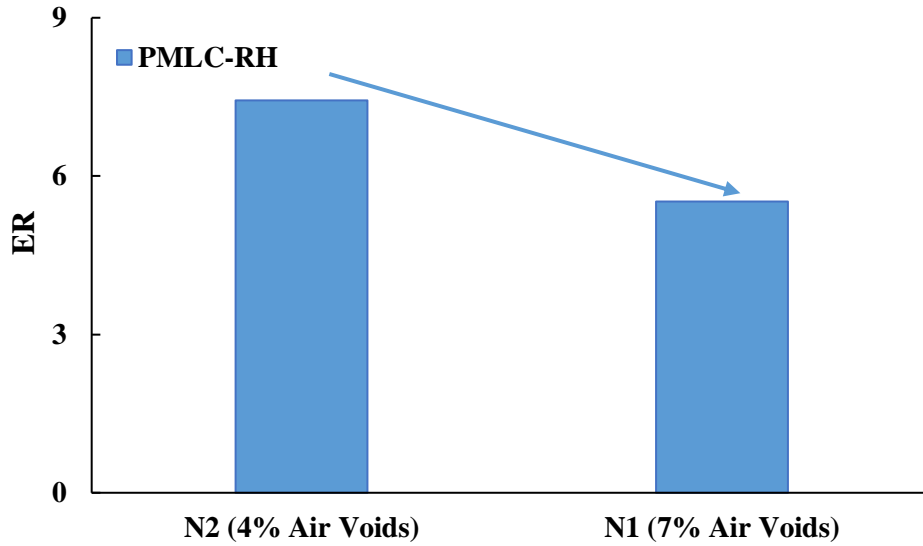
	PMLC-RH Vs. PMLC-CA	LMLC-STOA Vs. LMLC-CA	Statistical Test
DCSE <sub>HMA</sub>	-	+	<i>Paired-t</i> test
DCSE <sub>Min</sub>	+	+	<i>Paired-t</i> test
ER	-	-	<i>Paired-t</i> test
TX-N <sub>f</sub>	+	+	Two-way ANOVA
TX-β	+	+	Two-way ANOVA
NCAT-N <sub>f</sub>	+	+	Two-way ANOVA
NCAT-β	+	+	Two-way ANOVA
J <sub>c</sub>	-	-	<i>Paired-t</i> test
FI	+	+	Two-way ANOVA
CT <sub>Index</sub>	+	+	Two-way ANOVA

#### 6.3.2 Air Voids Sensitivity

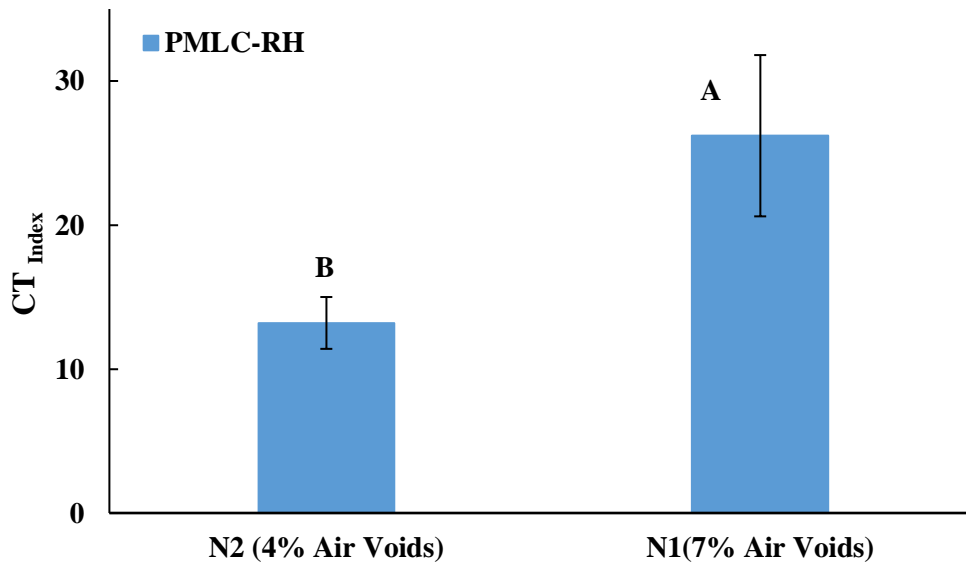
Several laboratory and field studies have investigated the effect of air voids (density) on the fatigue of asphalt mixtures (Harvey et al., 1996; Fisher et al., 2010; Tran et al., 2016). In general, these studies indicate that lower air voids improve fatigue performance of asphalt mixtures by increasing stiffness and possibly reducing the rate of aging.

In this study, the target in-place air voids of mixtures N1 and N2 were used to evaluate sensitivities to air voids. Specimens for N1 were compacted to  $7.0 \pm 0.5\%$  air voids, whereas specimens for N2 were compacted to  $4.0 \pm 0.5\%$  air voids. It was expected that the mix compacted to a lower air void content would have better cracking resistance. For each cracking test and aging condition, if the results of the two mixtures followed the expected trend, that cracking test parameter was considered sensitive to air voids.

Figure 6.26 shows two examples of air voids sensitivity results using PMLC-RH ER and  $CT_{Index}$  results. Both ER and  $CT_{Index}$  values were expected to decrease with the increasing air void contents, so mixture N2 with the lower air voids was expected to yield the higher ER and  $CT_{Index}$  values. The arrow in Figure 6.26 (a) showed that ER results decreased with the increasing air void contents based on the mean value analysis, indicating ER parameter was affected by air voids in the expected trend. Figure 6.26 (b) shows that mixture N2 with lower air void contents yielded a lower mean  $CT_{Index}$  value, meaning that  $CT_{Index}$  parameter is not sensitive to air voids based on mean value analysis. According to the statistical group analysis results,  $CT_{Index}$  value of mixture N2 was statistically lower than the values of mixtures N1, which also indicated  $CT_{Index}$  parameter was not sensitive to air voids based on statistical group analysis.



(a)



(b)

**Figure 6. 26 Examples of Air Voids Sensitivity; (a) ER Results, (b) CT<sub>Index</sub> Results**

Table 6.4 and 6.5 summarizes the sensitivity of the cracking test parameters to air voids using both mean value and statistical analyses for plant mixtures and laboratory mixtures, respectively. A “+” indicates that the parameter matched the expected trend for the two mixtures; a “-” indicates that the parameter did not match the expected trend for the two mixtures; “N/A” indicates that the parameter could not be analyzed statistically.

As shown in Table 6.4, five cracking test parameters were sensitive to air voids at both aging conditions based on the mean values analysis, including ER, TX-N<sub>f</sub>, TX-β, NCAT-N<sub>f</sub>, and NCAT-β. DCSE<sub>HMA</sub> and DCSE<sub>Min</sub>, FI and CT<sub>Index</sub> were not sensitive to air voids at either aging condition. J<sub>c</sub> was sensitive to air voids for reheated samples, but not for critically aged samples. However, the statistical analysis indicated that only NCAT-N<sub>f</sub> and NCAT-β were sensitive to air voids for critically aged samples. For tests with larger variabilities, such as TX-OT, and NCAT-OT, the lack of statistical sensitivities can be attributed to the high test variability.

**Table 6. 4 Summary of Air Voids Sensitivity Analysis for Plant Mixtures**

Cracking test parameters	Mean Value Analysis		Statistical Analysis	
	PMLC-RH	PMLC-CA	PMLC-RH	PMLC-CA
DCSE <sub>HMA</sub>	-	-	N/A	N/A
DCSE <sub>Min</sub>	-	-	N/A	N/A
ER	+	+	N/A	N/A
TX-N <sub>f</sub>	+	+	-	-
TX-β	+	+	-	-
NCAT-N <sub>f</sub>	+	+	-	+
NCAT-β	+	+	-	+
J <sub>c</sub>	+	-	N/A	N/A
FI	-	-	-	-
CT <sub>Index</sub>	-	-	-	-

As shown in Table 6.5, for laboratory mixtures, six cracking test parameters were sensitive to air voids at both aging conditions based on mean value analysis, including ER, TX-N<sub>f</sub>, TX-β, NCAT-N<sub>f</sub>, NCAT-β, and J<sub>c</sub>. DCSE<sub>Min</sub>, FI and CT<sub>Index</sub> were not sensitive to air voids at either aging condition. DCSE<sub>HMA</sub> was only sensitive to air voids for critically aged samples.

However, no parameter was sensitive to air voids based on statistical analysis, which might be caused by high test variability.

**Table 6. 5 Summary of Air Voids Sensitivity Analysis for Laboratory Mixtures**

Cracking test parameters	Mean Value Analysis		Statistical Analysis	
	LMLC-STOA	LMLC-CA	LMLC-STOA	LMLC-CA
DCSE <sub>HMA</sub>	-	+	N/A	N/A
DCSE <sub>Min</sub>	-	-	N/A	N/A
ER	+	+	N/A	N/A
TX-N <sub>f</sub>	+	+	-	-
TX-β	+	+	-	-
NCAT-N <sub>f</sub>	+	+	-	-
NCAT-β	+	+	-	-
J <sub>c</sub>	+	+	N/A	N/A
FI	-	-	-	-
CT <sub>Index</sub>	-	-	-	-

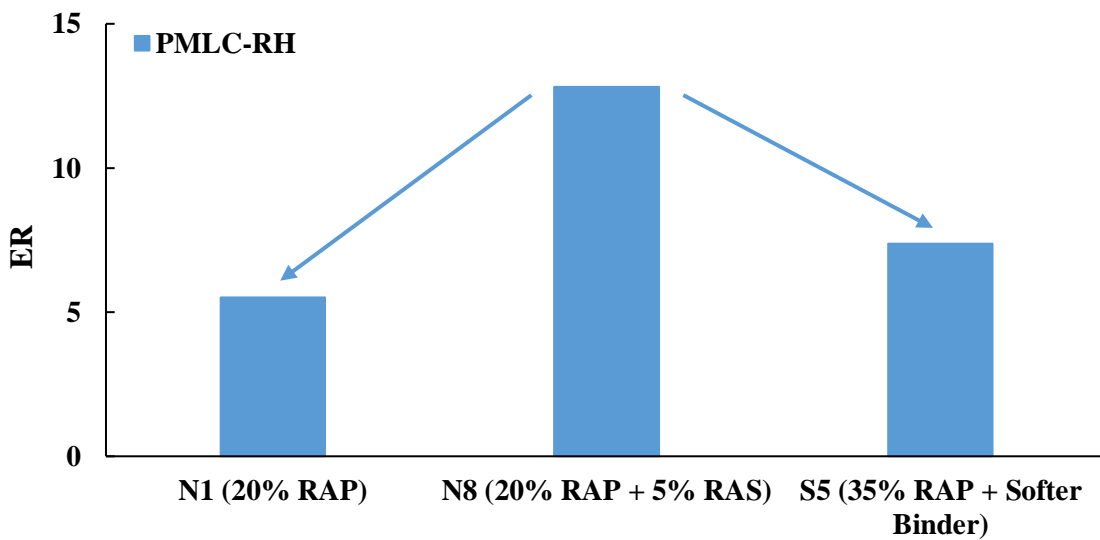
### 6.3.3 Recycled Asphalt Materials Sensitivity

In general, high RAP contents and the addition of RAS reduce the strain tolerance of asphalt mixtures, and, in most cases, reduce their cracking resistance (Huang et al., 2011; Mogawer et al., 2012; West et al., 2016). Although the use of softer virgin binders and rejuvenators is believed to help counteract the stiffening effects of aged recycled binders, volumetric properties oftentimes are unable to provide a meaningful indication regarding the net effects of recycled materials, virgin binders, and additives (Shen et al., 2007; West et al., 2016; Castro, 2017).

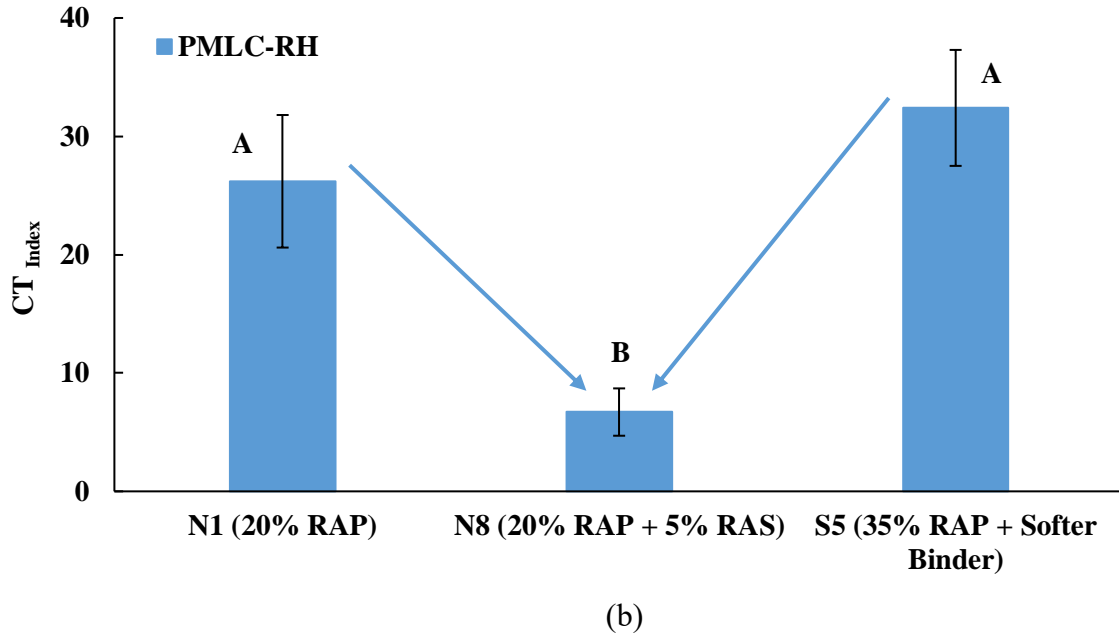
In this study, mixtures N1, N8, and S5, designed with different RAP and RAS contents, provided an opportunity to assess the sensitivity of the cracking tests to these recycled materials. Mixture N1 containing 20% RAP was set as the control mixture, mixture N8 contained 20%

RAP and 5% RAS, and mixture S5 contained 35% RAP and a softer grade of virgin binder were the experimental mixtures. Mixture N1 and S5 were expected to have higher cracking resistance than mixture N8. Therefore, any of the cracking test parameters included in the experimental plan was considered sensitive to RAP/RAS if the results matched the expected trend.

Figure 6.27 shows two examples of recycled asphalt materials sensitivity results using PMLC-RH ER and  $CT_{Index}$  results. Both ER and  $CT_{Index}$  values for mixture N8 were expected to be less than the corresponding values for mixtures N1 and S5. The arrows of Figure 6.27 (a) show that the mean ER values of mixture N1 and mixture S5 are less than the mean value of mixture N8, which is opposite of the expected trend. Thus, ER parameter was not sensitive to recycled asphalt materials based on mean value analysis. The  $CT_{Index}$  results shown in Figure 6.27 (b) indicated that mixtures N1 and S5 yielded better cracking resistance than mixture N8 based on mean value analysis and statistical group analysis, which is consistent with expected trend. Thus,  $CT_{Index}$  was sensitive to recycled asphalt materials using both analysis methods. The results of the recycled asphalt materials sensitivity using both mean value and statistical analyses for plant mixtures and laboratory mixtures are summarized in Table 6.6 and 6.7, respectively.



(a)



(b)  
**Figure 6. 27 Examples of Recycled Asphalt Materials Sensitivity;  
 (a) ER Results, (b) CT<sub>Index</sub> Results**

As shown in Table 6.6, for plant mixtures, it can be seen that the following cracking test parameters were sensitive to recycled asphalt materials at both aging conditions based on mean value analysis: DCSE<sub>HMA</sub>, DCSE<sub>Min</sub>, TX-N<sub>f</sub>, TX-β, NCAT-N<sub>f</sub>, NCAT-β, FI, and CT<sub>Index</sub>. Furthermore, J<sub>c</sub> only showed recycled asphalt materials sensitivity for critically aged samples, and ER was not sensitive to recycled asphalt materials. Based on statistical analysis results, TX-β, NCAT-β, FI, and CT<sub>Index</sub> were sensitive to recycled asphalt materials at both aging conditions, while TX-N<sub>f</sub> was sensitive to recycled materials for critically aged samples only.

**Table 6. 6 Summary of Recycled Asphalt Materials Sensitivity Analysis for Plant Mixtures**

Cracking test parameters	Mean Value Analysis		Statistical Analysis	
	PMLC-RH	PMLC-CA	PMLC-RH	PMLC-CA
DCSE <sub>HMA</sub>	+	+	N/A	N/A
DCSE <sub>Min</sub>	+	+	N/A	N/A
ER	-	-	N/A	N/A
TX-N <sub>f</sub>	+	+	-	+
TX-β	+	+	+	+
NCAT-N <sub>f</sub>	+	+	-	-
NCAT-β	+	+	+	+
J <sub>c</sub>	-	+	N/A	N/A
FI	+	+	+	+
CT <sub>Index</sub>	+	+	+	+

As shown in Table 6.7, for laboratory mixtures, all the parameters were sensitive to recycled asphalt materials based on mean value analysis except for ER. ER was sensitive to critically aged samples only. According to the statistical analysis results, NCAT-N<sub>f</sub>, NCAT-β, FI, and CT<sub>Index</sub> were sensitive to recycled asphalt materials at both aging conditions, while TX-N<sub>f</sub> and TX-β was sensitive to STOA samples only.

**Table 6. 7 Summary of Recycled Materials Sensitivity Analysis for Laboratory Mixtures**

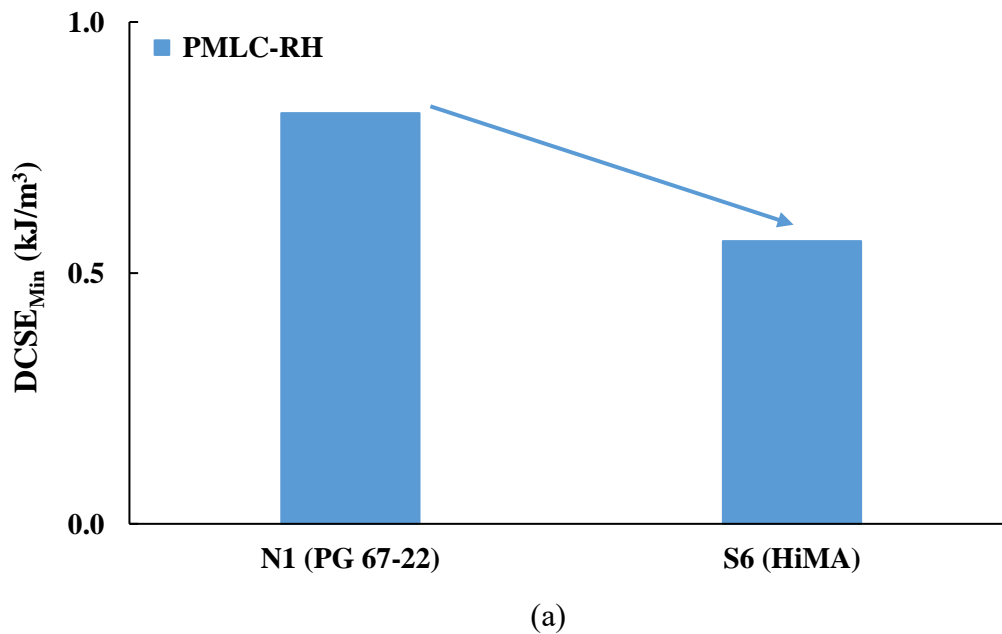
Cracking test parameters	Mean Value Analysis		Statistical Analysis	
	LMLC-STOA	LMLC-CA	LMLC-STOA	LMLC-CA
DCSE <sub>HMA</sub>	+	+	N/A	N/A
DCSE <sub>Min</sub>	+	+	N/A	N/A
ER	-	+	N/A	N/A
TX-N <sub>f</sub>	+	+	+	-
TX-β	+	+	+	-
NCAT-N <sub>f</sub>	+	+	+	+
NCAT-β	+	+	+	+
J <sub>c</sub>	+	+	N/A	N/A
FI	+	+	+	+
CT <sub>Index</sub>	+	+	+	+

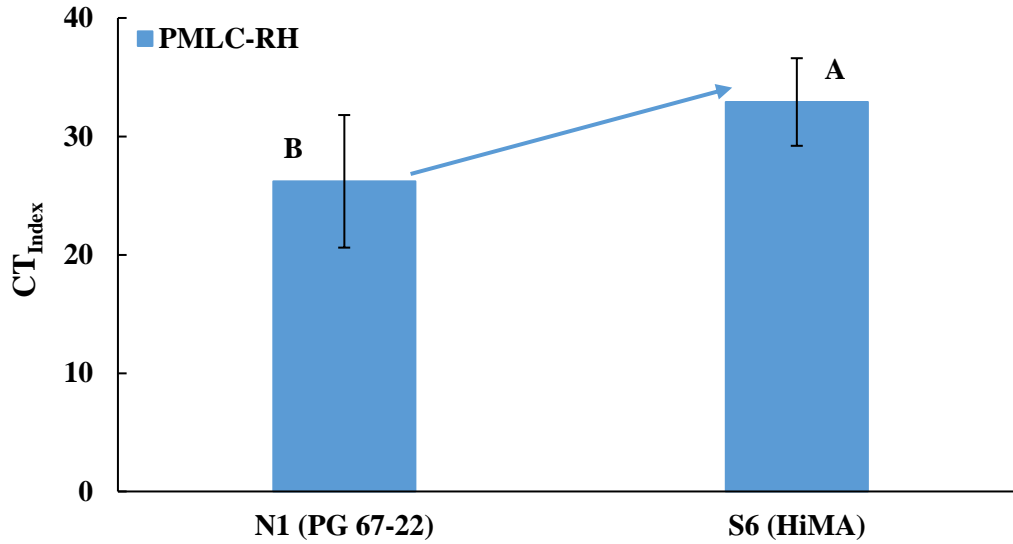
#### 6.3.4 Modified Binder Sensitivity

Polymer-modified binders have been widely used to improve the performance and life cycle cost benefits of asphalt pavements. The polymers used for modification primarily include styrene-butadiene-styrene (SBS), styrene-butadiene rubber (SBR), and crumb rubber (CR) (Bahia et al., 2001; Yildirim, 2007). Mixtures produced with modified binder generally yield better cracking and rutting resistance (Bahia et al., 2001; Kim et al., 2003; Kök and Çolak, 2011).

The effect of modified binders on the cracking resistance of asphalt mixtures was examined by comparing mixture N1 with mixture S6. Mixture N1 with an unmodified PG 67-22 binder and 20% RAP was the control mixture. Mixture S6 used the same mix design as the control mixture except that a HiMA binder with approximately 7% SBS was used instead of the unmodified binder. Considering the components of these two mixtures, mixture S6 was expected to yield better cracking resistance than mixture N1. Cracking test parameters were considered sensitive to modified binders if their results matched the expected trend.

Figure 6.28 shows two examples to illustrate the analysis of modified binder sensitivity using PMLC-RH  $DCSE_{Min}$  and  $CT_{Index}$  results. Both  $DCSE_{Min}$  and  $CT_{Index}$  values of mixture N1 were expected to be less than the corresponding values of mixtures S6. As shown in Figure 6.28 (a), the arrow indicated that the mean  $DCSE_{Min}$  value of mixture N1 was greater than the value of mixture S6, which was opposite of the expected trend. Therefore,  $DCSE_{Min}$  was not sensitive to modified binder based on the mean value analysis. Figure 6.28 (b) shows the mean value and statistical analyses results for the sensitivity of  $CT_{Index}$  to modified binder. Both mean value and statistical analyses indicated that mixture S6 had greater  $CT_{Index}$  value which was consistent with the expected trend. Consequently,  $CT_{Index}$  was considered sensitive to modified binder using both analysis methods. The results of the modified binder sensitivity using both mean value and statistical analyses for plant mixtures and laboratory mixtures are summarized in Table 6.8 and 6.9, respectively.





(b)

**Figure 6. 28 Examples of Modified Binder Sensitivity;  
(a) DCSE<sub>Min</sub> Results, (b) CT<sub>Index</sub> Results**

As shown in Table 6.8, for plant mixtures, the mean value analysis results showed that ER, DCSE<sub>HMA</sub>, NCAT- $\beta$ , FI, and CT<sub>Index</sub> were sensitive to polymer modification at both aging conditions. DCSE<sub>Min</sub>, TX-N<sub>f</sub>, TX- $\beta$ , and NCAT-N<sub>f</sub> were not sensitive to modified binders for reheated samples, but they were sensitive to modified binders for critically aged samples. J<sub>c</sub> was sensitive to modified binders only for reheated samples. However, based on the statistical analysis results, only FI and CT<sub>Index</sub> were found sensitive to modified binders at both aging conditions. All four of OT parameters were sensitive to modified binders for critically aged samples.

**Table 6. 8 Summary of Modified Binder Sensitivity Analysis for Plant Mixtures**

Cracking test parameters	Mean Value Analysis		Statistical Analysis	
	PMLC-RH	PMLC-CA	PMLC-RH	PMLC-CA
DCSE <sub>HMA</sub>	+	+	N/A	N/A
DCSE <sub>Min</sub>	-	+	N/A	N/A
ER	+	+	N/A	N/A
TX-N <sub>f</sub>	-	+	-	+
TX-β	-	+	-	+
NCAT-N <sub>f</sub>	-	+	-	+
NCAT-β	+	+	-	+
J <sub>c</sub>	+	-	N/A	N/A
FI	+	+	+	+
CT <sub>Index</sub>	+	+	+	+

As presented in Table 6.9, for laboratory mixtures, the mean value analysis showed that most of the cracking test parameters were sensitive to modified binder at both aging conditions, including DCSE<sub>HMA</sub>, DCSE<sub>Min</sub>, TX-N<sub>f</sub>, TX-β, NCAT-N<sub>f</sub>, NCAT-β, FI, and CT<sub>Index</sub>. Furthermore, ER was only sensitive to modified binder before critical aging, and J<sub>c</sub> was not sensitive to modified binder. Based on the statistical analysis, all the parameters of TX-OT, NCAT-OT, I-FIT, and IDEAL-CT test were sensitive to modified binder at both aging conditions.

**Table 6. 9 Summary of Modified Binder Sensitivity Analysis for Laboratory Mixtures**

Cracking test parameters	Mean Value Analysis		Statistical Analysis	
	LMLC-STOA	LMLC-CA	LMLC-STOA	LMLC-CA
DCSE <sub>HMA</sub>	+	+	N/A	N/A
DCSE <sub>Min</sub>	+	+	N/A	N/A
ER	+	-	N/A	N/A
TX-N <sub>f</sub>	+	+	+	+
TX-β	+	+	+	+
NCAT-N <sub>f</sub>	+	+	+	+
NCAT-β	+	+	+	+
J <sub>c</sub>	-	-	N/A	N/A
FI	+	+	+	+
CT <sub>Index</sub>	+	+	+	+

#### 6.4 Correlations between Different Laboratory Cracking Tests

Pearson’s correlation coefficients ( $r_p$ ) were calculated using Minitab software to determine the strength and direction of correlations among the ten cracking test parameters. Technically,  $r_p$  can range from -1.0 to + 1.0, and the negative and positive sign of  $r_p$  indicates the direction of correlation. The greater absolute value of  $r_p$  indicates stronger correlation, and  $|r_p|$  of 0.8 - 1.0 implies very strong correlation (Evans, 1996). Note that  $r_p$  can only be used to evaluate linear relationships or correlations, and the calculation of  $r_p$  are based on the mean values.

Table 6.10 presents the summary of the  $r_p$  values among ten cracking test parameters, with  $|r_p|$  values greater than 0.80 highlighted with shaded cells. As can be seen, the  $r_p$  values among NCAT-N<sub>f</sub>, TX-N<sub>f</sub>, FI, and CT<sub>Index</sub> were greater than 0.80 except for the  $r_p$  between TX-N<sub>f</sub> and NCAT-N<sub>f</sub>, and FI. The  $r_p$  between TX-N<sub>f</sub> and NCAT-N<sub>f</sub> was 0.76, which was reasonably close to 0.80. However, the  $r_p$  between TX-N<sub>f</sub> and FI was 0.58, which was caused by the

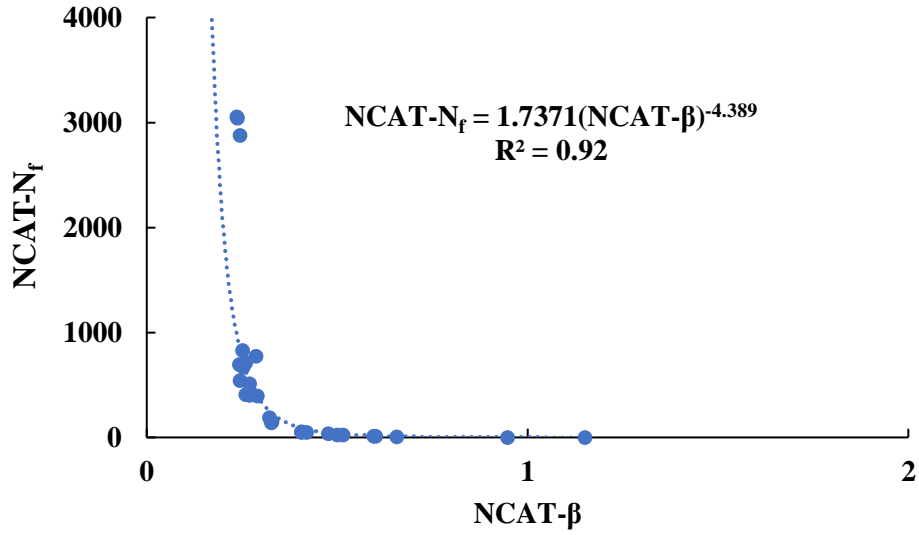
extremely high TX-N<sub>f</sub> value of PMLC-RH S13 mixture. After removing this extremely high value, all the r<sub>p</sub> values among NCAT-N<sub>f</sub>, TX-N<sub>f</sub>, FI, and CT<sub>Index</sub> were greater than 0.80, which were presented under the original value in the corresponding cell. Thus, there are very strong positive linear correlations among NCAT-N<sub>f</sub>, TX-N<sub>f</sub>, FI, and CT<sub>Index</sub> results. Also, the r<sub>p</sub> between NCAT-β and TX-β was 0.87, which indicates that a very strong linear relationship exists between these two parameters.

**Table 6. 10 Summary of Pearson Correlation Coefficients**

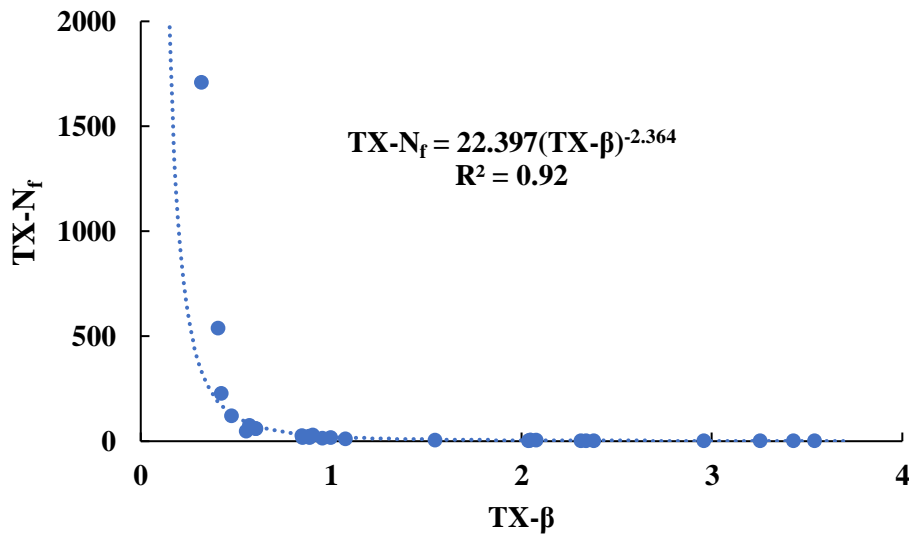
		ER Test			TX-OT		NCAT-OT		J <sub>c</sub>	FI	CT <sub>Index</sub>
		DCSE <sub>HMA</sub>	DCSE <sub>Min</sub>	ER	N <sub>f</sub>	β	N <sub>f</sub>	β			
ER Test	DCSE <sub>HMA</sub>	1									
	DCSE <sub>Min</sub>	0.40	1								
	ER	0.01	-0.73	1							
TX-OT	N <sub>f</sub>	-0.01	0.57	-0.32	1						
	β	-0.60	-0.78	0.45	-0.35	1					
NCAT-OT	N <sub>f</sub>	0.23	0.70	-0.42	0.76 (0.91)	-0.60	1				
	β	-0.61	-0.62	0.27	-0.24	0.87 (0.87)	-0.44	1			
J <sub>c</sub>		0.09	0.37	-0.22	0.37	-0.51	0.42	-0.48	1		
FI		0.37	0.76	-0.48	0.58 (0.86)	-0.69	0.95 (0.96)	-0.53	0.33	1	
CT <sub>Index</sub>		0.10	0.72	-0.47	0.91 (0.91)	-0.58	0.90 (0.90)	-0.42	0.47	0.81 (0.91)	1

Figure 6.29 presents the plots of NCAT-N<sub>f</sub> versus NCAT-β and TX-N<sub>f</sub> versus TX-β results fitted with power relationships. As shown, the coefficients of determination (R<sup>2</sup>) of two

regression equations were 0.92, indicating very strong power relationships between the  $N_f$  and  $\beta$  parameters for both TX-OT and NCAT-OT results.



(a)



(b)

Figure 6. 29 OT  $N_f$  versus  $\beta$  Correlations; (a) NCAT-OT Results, (b) TX-OT Results

## 6.5 Summary

In this Chapter, the potential of six laboratory asphalt mixture cracking tests to identify TDC susceptibilities of seven experimental mixtures was evaluated using plant mixtures and laboratory mixtures at two aging conditions. The seven mixtures, designed to have a wide range of cracking susceptibilities, were constructed as the surface layer on the NCAT Test Track. The cracking test results were first used to conduct the comparison analysis between plant mixtures and laboratory mixtures. Then, the cracking tests were also evaluated for sensitivity to laboratory aging, air voids, recycled materials, and binder modification. Correlations among the results for the six cracking tests were also examined. Based on these analyses, the following conclusions are made:

(1) No significant differences were identified between PMLC-RH and LMLC-STOA mixtures for  $DCSE_{Min}$ ,  $TX-\beta$ ,  $NCAT-\beta$ ,  $J_c$  and  $CT_{Index}$ . After critical aging, no statistical difference was observed between plant mixtures and laboratory mixtures among all the cracking test parameters. This indicates that it is possible to produce laboratory mixtures with similar cracking resistance parameters to plant produced mixtures, especially if the mixtures are laboratory aged to represent a critical amount of field aging.

(2) The sensitivity of six cracking tests to laboratory aging, air voids, recycled materials, and binder modification were evaluated using both mean value and statistical analyses, which is summarized as follows:

- The ER parameter was not sensitive aging and recycled asphalt materials for both plant mixtures and laboratory mixtures. ER was sensitive to air voids and modified binder for plant mixtures and laboratory mixtures at both aging conditions except for the modified binder sensitivity of critically aged laboratory

mixtures. The intermediate parameter of the ER method,  $DCSE_{Min}$  showed sensitivity to aging, recycled asphalt materials, and modified binder for plant mixtures and laboratory mixtures at both aging conditions except for the modified binder sensitivity of reheated plant mixtures. However,  $DCSE_{Min}$  was not sensitive to air voids for both plant and laboratory mixtures.  $DCSE_{HMA}$  was sensitive to recycled asphalt materials and modified binder for the plant and laboratory mixtures at both aging conditions, but it only showed sensitivity to aging and air voids for laboratory mixtures.

- $TX-N_f$  and  $TX-\beta$  were sensitive to aging for both plant mixtures and laboratory mixtures. Based on mean value analysis,  $TX-N_f$  and  $TX-\beta$  were sensitive to air voids, recycled asphalt materials, and modified binder for plant mixtures and laboratory mixtures at both aging conditions except for the modified binder sensitivity of reheated plant mixtures. According to the statistical analysis,  $TX-N_f$  was not sensitive to air voids, and it only showed sensitivity to recycled materials for critically aged plant mixtures and STOA laboratory mixtures. Meanwhile,  $TX-N_f$  was sensitive to modified binder for plant mixtures and laboratory mixtures at both aging conditions except for the reheated plant mixtures.  $TX-\beta$  was not sensitive to air voids, but it was sensitive to recycled asphalt materials and modified binder for plant mixtures and laboratory mixtures at both aging conditions except for critically aged laboratory mixtures and reheated plant mixtures, respectively.
- $NCAT-N_f$  and  $NCAT-\beta$  were sensitive to aging for both plant mixtures and laboratory mixtures. Based on mean value analysis,  $NCAT-N_f$  and  $NCAT-\beta$  were

sensitive to air voids, recycled asphalt materials, and modified binder for plant mixtures and laboratory mixtures at both aging conditions except for the sensitivity of NCAT- $N_f$  to reheated plant mixtures. Based on statistical analysis, NCAT- $N_f$  and NCAT- $\beta$  were only sensitive to air voids for critically aged plant mixtures, and they were also sensitive to modified binder for plant mixtures and laboratory mixtures at both aging conditions except for reheated plant mixtures. Furthermore, NCAT- $\beta$  was sensitive to recycled materials for both plant mixtures and laboratory mixtures, but NCAT- $N_f$  was only sensitive to recycled materials for laboratory mixtures.

- $J_c$  was not sensitive to aging for both plant mixtures and laboratory mixtures, and it was also not sensitive to modified binder except for reheated plant mixtures. Furthermore,  $J_c$  showed sensitivity to air voids and recycled asphalt materials for plant mixtures and laboratory mixtures at both aging conditions except for critically aged plant mixtures and reheated plant mixtures, respectively.
- FI and  $CT_{\text{Index}}$  were sensitive to aging for both plant mixtures and laboratory mixtures. In addition, both mean value and statistical analyses indicated that FI and  $CT_{\text{Index}}$  were sensitive to recycled asphalt materials and modified binder, but they were not sensitive to air voids.

(3) Strong positive linear correlations exist among NCAT- $N_f$ , TX- $N_f$ , FI, and  $CT_{\text{Index}}$  results. Meanwhile, there were strong power relationships between the  $N_f$  and  $\beta$  parameters for both TX-OT and NCAT-OT results, and a strong linear relationship existed between TX- $\beta$  and NCAT- $\beta$ .

## **CHAPTER 7 PRELIMINARY VALIDATION OF LABORATORY CRACKING TESTS**

This chapter summarizes the preliminary field cracking performance of the seven test sections. The six laboratory cracking tests were validated by establishing correlations between laboratory test results and the preliminary field cracking performance.

### **7.1 Preliminary Field Cracking Performance**

The seven test sections were monitored weekly during the trafficking cycle from September 2015 to November 2019. Cracks were traced using a vehicle equipped with a high-resolution camera for pavement scanning. The recorded videos were used to detect and measure the cracking percentage for each test section, and various severity and extent of cracks were observed for the seven test sections after approximately 15 million ESALs and 52 months field aging of 73,728 CDD. Hairline cracks appeared on the surfaces of sections N1, N2, and N5 after approximately 9 million ESALs, and the cracking percentages of sections N1, N2, and N5 were 10.6%, 7.5%, and 9.3%, respectively, after approximately 15 million ESALs and 73,728 CDD. Section N2 yielded the lowest cracking percentage among these three sections, which might be attributed to the highest density of the surface layer. Section N8, the mixture containing 5% RAS, was the first section to crack, with observable cracking beginning after approximately 7 million ESALs. In December 2017, after 10 million ESALs of trafficking, field cores were cut from each of the sections. The cores taken from section N8 confirmed that the entire surface of section N8 was cracked, and the cores showed that the cracks had propagated to the bottom of surface layer, as shown in Figure 7.1. Note that the cracks did not penetrate into the intermediate layer and there were no signs of debonding between layers. Therefore, section N8 was confirmed as having significant TDC. Furthermore, the cracks of section N8 continued developing with traffic and

environmental aging, and the cracking percentage of section N8 was 70.7% after approximately 15 million ESALs and 73,728 CDD.



**Figure 7. 1 Cracks on Section N8 and Field Core**

In November 2019, a small crack was observed in section S5, but the crack severity was too low to be recognized by the high-resolution camera. Therefore, the cracking percentage of section S5 was recorded as 0.0%. As of November 2019, no cracking was evident in sections S6 and S13. The cracking percentages of all seven sections were summarized in Table 7.1. In general, sections N1, N2, N5, and N8 have exhibited significant cracking, with section N8 having by far the highest cracking percentage of 70.7%.

**Table 7. 1 Preliminary Field Cracking Performance Summary**

Experimental Section	N1	N2	N5	N8	S5	S6	S13
Cracking Percentage (%)	10.6	7.5	9.9	70.7	0.0	0.0	0.0

## 7.2 Correlations between Field Cracking Performance and Laboratory Cracking Test Results

In this section, the preliminary field cracking performance was utilized to correlate with the laboratory cracking test results to help identify the best test for determining the TDC susceptibility of asphalt mixtures for possible use in the mixture design and quality assurance. Relationships between each cracking test parameter and field cracking performance were evaluated through three approaches: 1) analysis of Pearson's correlation coefficient; 2) whether or not the cracking test parameter correctly identified mixture N8 as the most susceptible to TDC; and 3) whether or not the cracking test parameter correctly differentiated uncracked sections from cracked sections.

### 7.2.1 Analysis of Pearson's Correlation Coefficient

Pearson's correlation coefficient ( $r_p$ ) between each cracking test parameter and field cracking performance was calculated for both plant mixtures and laboratory mixtures at both aging conditions. As we mentioned previously,  $r_p$  ranged from -1.0 to + 1.0, and a greater  $|r_p|$  value indicates a stronger linear correlation or relationship. In addition,  $|r_p|$  of 0.8 - 1.0 implies very strong correlation (Evans, 1996). Note that the calculation of  $r_p$  is based on the mean values of each cracking test parameter. Table 7.2 presents the summary of  $r_p$  values between each cracking test parameter and field cracking performance, with  $|r_p|$  values greater than 0.80 highlighted with shaded cells. As mentioned previously, for all cracking test parameters, greater value indicates better cracking resistance except for parameters NCAT- $\beta$  and TX- $\beta$ , which means lower cracking percentage. Thus, all the  $r_p$  values should be negative except for the two  $\beta$  parameters.

As shown in Table 7.2, the  $r_p$  values between ER and field cracking performance were positive for PMLC-RH, PMLC-CA, and LMLC-STOA specimens, which was unexpected. Table

7.2 shows that the  $r_p$  values between NCAT- $\beta$  and field cracking performance are greater than 0.90 for both plant mixture and laboratory mixture at both aging condition, which indicates that NCAT- $\beta$  has a very strong linear correlation with field cracking performance. In addition, the  $r_p$  values between TX- $\beta$  and field cracking performance were 0.98 for both PMLC-RH and LMLC-STOA specimens, and the corresponding  $r_p$  values for PMLC-CA and LMLC-CA specimens were 0.75 and 0.74, respectively, which were reasonably close to 0.80. In general, both NCAT- $\beta$  and TX- $\beta$  show a very strong linear correlation with the field cracking performance. Additionally, the  $|r_p|$  value between DCSE<sub>Min</sub> and field cracking performance for LMLC-STOA specimen was greater than 0.80, which also indicates that a very strong linear relationship exists between DCSE<sub>Min</sub> and field cracking performance for LMLC-STOA specimen.

**Table 7. 2 Summary of  $r_p$  between Cracking test parameter and Field Cracking Performance**

Cracking test parameter	PMLC-RH	PMLC-CA	LMLC-STOA	LMLC-CA
DCSE <sub>HMA</sub>	-0.68	-0.57	-0.49	-0.65
DCSE <sub>Min</sub>	-0.76	-0.69	-0.82	-0.45
ER	0.70	0.06	0.53	-0.06
TX-N <sub>f</sub>	-0.26	-0.28	-0.39	-0.32
TX- $\beta$	0.98	0.75	0.98	0.74
NCAT-N <sub>f</sub>	-0.42	-0.44	-0.49	-0.37
NCAT- $\beta$	0.97	0.93	0.91	0.93
J <sub>c</sub>	-0.13	-0.34	-0.40	-0.50
FI	-0.62	-0.53	-0.58	-0.45
CT <sub>Index</sub>	-0.35	-0.41	-0.50	-0.41

### 7.2.2 Identification of the most Susceptible Mixture to TDC

As mentioned previously, section N8 yielded the highest cracking percentage of 70.7%, which indicated that mixture N8 was the most susceptible to TDC. In this section, all of the cracking

test parameters were evaluated to determine if they could identify mixture N8 as the most susceptible to TDC. Note that only the mean values of each cracking test parameter were used. Table 7.3 summarizes the validation results for plant mixtures and laboratory mixtures at both aging conditions. A “+” indicates that the parameter identified mixture N8 as the most susceptible to TDC; a “-” indicates that the parameter did not identify mixture N8 as the most susceptible to TDC.

As shown in Table 7.3, the following parameters correctly identified mixture N8 as the most susceptible to TDC for both plant mixtures and laboratory mixtures at both aging conditions:  $DCSE_{Min}$ ,  $TX-N_f$ ,  $TX-\beta$ ,  $NCAT-N_f$ ,  $NCAT-\beta$ ,  $FI$ , and  $CT_{Index}$ .  $DCSE_{HMA}$  identified mixture N8 as the most susceptible to TDC for PMLC-RH, PMLC-CA, and LMLC-CA specimens, and  $J_c$  only identified mixture N8 as the most susceptible to TDC for laboratory mixture at both aging conditions. ER did not identify mixture N8 as the most susceptible to TDC.

**Table 7. 3 Identification Results of the Most Susceptible Mixture to TDC**

Cracking test parameter	PMLC-RH	PMLC-CA	LMLC-STOA	LMLC-CA
$DCSE_{HMA}$	+	+	-	+
$DCSE_{Min}$	+	+	+	+
ER	-	-	-	-
$TX-N_f$	+	+	+	+
$TX-\beta$	+	+	+	+
$NCAT-N_f$	+	+	+	+
$NCAT-\beta$	+	+	+	+
$J_c$	-	-	+	+
FI	+	+	+	+
$CT_{Index}$	+	+	+	+

### 7.2.3 Discrimination between Cracked Sections and Uncracked Sections

Based on the preliminary field cracking performance, the seven experimental sections were grouped into two categories: 1) cracked sections, including N1, N2, N5, and N8; 2) uncracked sections, including S5, S6 and S13. In this section, all the cracking test parameters were evaluated to determine if they could discriminate uncracked sections from cracked sections.

Figure 7.2 shows an example of the evaluation using LMLC-STOA  $CT_{Index}$  results. As presented in Figure 7.2, the  $CT_{Index}$  values of mixtures S5, S6 and S13 were greater than the corresponding  $CT_{Index}$  values of the remaining five mixtures, which indicated  $CT_{Index}$  was able to differentiate uncracked sections from cracked sections for LMLC-STOA specimens. Note that only the mean values of each cracking test parameter were used in this section.

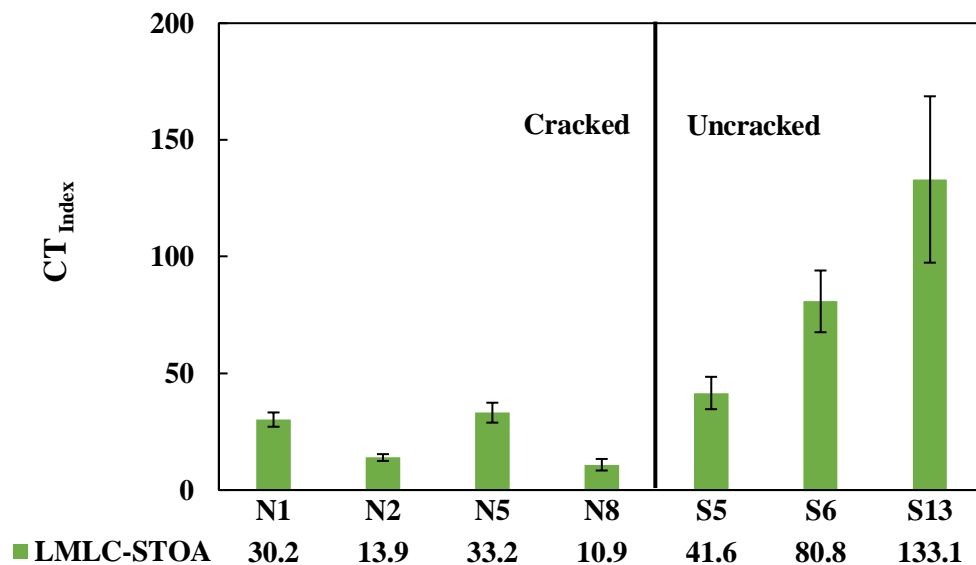


**Figure 7. 2 Example of Discrimination between Cracked and Uncracked Sections**

Table 7.4 summarizes the discrimination evaluations for plant mixtures and laboratory mixtures at both aging conditions. A “+” indicates that the parameter differentiated uncracked sections from cracked sections; a “-” indicates that the parameter did not differentiate uncracked sections from cracked sections. As shown in Table 7.4, FI and  $CT_{Index}$  were able to discriminate

uncracked sections from cracked sections for plant mixtures at both aging conditions and short-term aged laboratory mixtures. In addition, TX-N<sub>f</sub> and TX-β differentiated uncracked sections from cracked sections for critically aged plant mixtures and laboratory mixtures at both aging conditions. NCAT-N<sub>f</sub> only discriminated uncracked sections from cracked sections for critically aged plant mixtures and short-term aged laboratory mixtures. DCSE<sub>HMA</sub>, DCSE<sub>Min</sub>, and NCAT-β only discriminated uncracked sections from cracked sections for critically aged laboratory mixtures. ER and J<sub>c</sub> did not discriminate uncracked sections from cracked sections.

**Table 7. 4 Discrimination Results between Cracked and Uncracked Sections**

Cracking test parameter	PMLC-RH	PMLC-CA	LMLC-STOA	LMLC-CA
DCSE <sub>HMA</sub>	-	+	-	-
DCSE <sub>Min</sub>	-	+	-	-
ER	-	-	-	-
TX-N <sub>f</sub>	-	+	+	+
TX-β	-	+	+	+
NCAT-N <sub>f</sub>	-	+	+	-
NCAT-β	-	+	-	-
J <sub>c</sub>	-	-	-	-
FI	+	+	+	-
CT <sub>Index</sub>	+	+	+	-

### 7.3 Summary

In this chapter, the preliminary field cracking performance of seven test sections as of November 2019 were summarized. The measured field cracking percentage of each test section was compared to the laboratory cracking test results to help identify the best tests for determining the TDC susceptibility of asphalt mixtures for possible use in the mixture design and quality

assurance. Based on the comparisons of lab test results and measured field cracking performance, the following conclusions were obtained:

(1) Sections N1, N2, N5, and N8 exhibited a range of cracking severity and extent after approximately 15 million ESALs and 73,728 CDD. The section N8 with 5% RAS had the highest cracking percentage of 70.7%. No measurable cracks were found in sections S5, S6 and S13.

(2) Based on the  $r_p$  results, NCAT- $\beta$  and TX- $\beta$  showed a very strong linear correlation with the preliminary cracking performance for both plant mixtures and laboratory mixtures at both aging conditions. There was also a very strong linear relationship between DCSE<sub>Min</sub> and field cracking performance for LMLC-STOA specimens.

(3) DCSE<sub>Min</sub>, TX-N<sub>f</sub>, TX- $\beta$ , NCAT-N<sub>f</sub>, NCAT- $\beta$ , FI, and CT<sub>Index</sub> correctly identified mixture N8 as the most susceptible to TDC for both plant mixtures and laboratory mixtures at both aging conditions. DCSE<sub>HMA</sub> identified mixture N8 as the most susceptible to TDC for PMLC-RH, PMLC-CA, and LMLC-CA specimens.  $J_c$  only identified mixture N8 as the most susceptible to TDC for laboratory mixtures at both aging conditions. ER did not identify mixture N8 as the most susceptible to TDC.

(4) FI and CT<sub>Index</sub> were able to discriminate uncracked sections from cracked sections for short-term aged laboratory mixtures and plant mixtures at both aging conditions. TX-N<sub>f</sub> and TX- $\beta$  differentiated uncracked sections from cracked sections for critically aged plant mixtures and laboratory mixtures at both aging conditions. NCAT-N<sub>f</sub> only discriminated uncracked sections from cracked sections for critically aged plant mixtures and short-term aged laboratory mixtures. DCSE<sub>HMA</sub>, DCSE<sub>Min</sub>, and NCAT- $\beta$  only discriminated uncracked sections from cracked sections

for critically aged laboratory mixtures. ER and  $J_c$  did not discriminate uncracked sections from cracked sections.

## CHAPTER 8 CONCLUSIONS AND RECOMMENDATIONS

This study focused on two aspects about TDC: 1) determining a critical aging protocol to condition asphalt mixtures for laboratory cracking tests, and 2) evaluating the ability of laboratory cracking tests to identify mixtures susceptible to TDC. The conclusions and recommendations for each aspect were summarized in this chapter.

### 8.1 Determination of a Critical Aging Protocol

The critical field aging condition for evaluating TDC was first examined from a literature review. An experiment was then conducted using four loose mixture aging protocols on materials from five field projects in the USA. Two candidate CA protocols were proposed based on the binder test results, and the key findings and conclusions of this part are summarized as follows:

- 70,000 CDD was identified as the critical field aging condition for evaluating TDC.
- The 24-hour, 135°C protocol yielded the greatest aging level, followed by the 12-hour, 135°C protocol, the 5-day, 95°C, protocol, and the 6-hour, 135°C protocol, respectively.
- No significant difference in the oxidation-hardening relationship was evident for mixtures aged at 95°C versus 135°C.
- The 5-day, 95°C protocol was most representative of 70,000 CDD of field aging, and 8-hour, 135°C protocol was estimated to yield an equivalent aging level as 5-day, 95°C protocol.

Two candidate CA protocols of loose mixture aging for 5 days at 95°C and 8 hours at 135°C 5-day were further validated using four NCAT TDC experimental mixtures. The correlations between two candidate CA protocols and field aging were evaluated using mixture

and binder tests. Based on the analysis results, following key findings and conclusions were obtained:

- The two candidate CA protocols had a significant impact on reducing the fatigue and cracking resistance of asphalt binder and mixture.
- No significant difference was observed between two CA protocols based on I-FIT test results. The 8-hour, 135°C protocol yielded more aging than the 5-day, 95°C protocol based on IDEAL-CT test results, the G-R parameter, LAS test results, and the  $\Delta T_c$  parameter, but the opposite trend was observed for small-specimen AMPT cyclic fatigue test results.
- The test results of post-construction field cores generally showed an expected trend of increased stiffness and reduced cracking resistance with field aging.
- Most of the asphalt binder and mixture properties indicated that the two candidate CA protocols yielded more severe aging than 4 years field aging in Alabama.

## **8.2 Preliminary Evaluation of Laboratory Cracking Tests**

Six laboratory cracking tests were evaluated for their ability to identify mixtures susceptible to TDC using seven mixtures with a wide range of characteristics including air voids, binder type, and recycled materials. Both plant-produced and laboratory prepared mixtures at both aging conditions were tested in this part. The key findings and conclusions from this evaluation are summarized as followed:

- No significant differences were identified between plant mixtures and the corresponding laboratory mixtures after critical aging for all the cracking test parameters.

- All the cracking test parameters of I-FIT, IDEAL-CT, and both OT tests are sensitive to aging for both plant mixtures and laboratory mixtures. However, ER and  $J_c$  are not sensitive to aging for both plant mixtures and laboratory mixtures.
- No cracking test parameter is statistically sensitive to all influence factors. Based on mean value analysis, only NCAT- $\beta$  is sensitive to all of the influence factors for plant mixtures at both aging conditions. Meanwhile, the cracking test parameters of both OT tests are sensitive to all the influence factors for laboratory mixtures.
- FI and  $CT_{Index}$  are sensitive to recycled asphalt materials and modified binder for both plant mixtures and laboratory mixtures at both aging conditions.
- Strong positive linear correlations exist among NCAT- $N_f$ , TX- $N_f$ , FI, and  $CT_{Index}$  results. Meanwhile, there are strong power relationships between the  $N_f$  and  $\beta$  parameters for both OT tests.

The preliminary field cracking performance of seven test sections were compared to the laboratory cracking test results. The following conclusions were obtained:

- Sections N1, N2, N5, and N8 exhibited a range of cracking severity and extent after approximately 15 million ESALs and 73,728 CDD. Section N8 with 5% RAS had the highest cracking percentage of 70.7% of the lane area. No measurable cracks were found in sections S5, S6 or S13.
- Based on the  $r_p$  results, NCAT- $\beta$  and TX- $\beta$  showed a very strong linear correlation with the field cracking performance for both plant mixtures and laboratory mixtures at both aging conditions.

- $DCSE_{Min}$ ,  $TX-N_f$ ,  $TX-\beta$ ,  $NCAT-N_f$ ,  $NCAT-\beta$ ,  $FI$ , and  $CT_{Index}$  correctly identified mixture N8 as the most susceptible to TDC for both plant mixtures and laboratory mixtures at both aging conditions. ER did not identify mixture N8 as the most susceptible to TDC.
- No cracking test parameter was able to discriminate uncracked section from cracked sections for plant mixtures and laboratory mixtures at both aging conditions. ER and  $J_c$  did not discriminate uncracked sections from cracked sections.

### 8.3 Recommendations for Future Research

This study determined a critical aging protocol for TDC evaluation, and six laboratory cracking tests were evaluated regarding their suitability to identify susceptible mixtures to TDC. The recommendations for the future research regarding critical aging and validation of cracking tests were summarized as follows:

- The preliminary critical field aging condition of 70,000 CDD was identified based on the pavement distress survey results of NCHRP 09-49A. More field TDC data should be further collected and analyzed to validate this critical field aging condition.
- According to the FT-IR CA and G-R parameter results, no significant difference in the oxidation-hardening relationship was observed for mixtures aged at 95°C and 135°C. However, this conclusion was obtained based on the results of five mixtures and one 95°C protocol, which needs to be further validated using more mixtures and 95°C protocols.
- Based on the laboratory cracking test results, both  $FI$  and  $CT_{Index}$  are not sensitive to air voids. Thus, the equations used to calculate these two parameters might need to be corrected or reformed.

- The preliminary aging validation results indicated that two candidate CA protocols yielded a more severe aging level than 4 years field aging in Alabama. Therefore, additional field aging data is needed to help determine the representative CDD of the two candidate CA protocols. The seven experimental sections on the NCAT Test Track will remain in place for additional trafficking and environmental aging through the fall of 2020. This ongoing work will help further validate the aging protocol and identify the best test for determining the TDC susceptibility of asphalt mixtures for possible use in mix design and quality assurance.

## REFERENCES

- Airey, G. D. (2003). State of the art report on ageing test methods for bituminous pavement materials. *International Journal of Pavement Engineering*, 4(3), 165-176.
- Al-Qadi, I. L., Lippert, D. L., Wu, S., Ozer, H., Renshaw, G., Murphy, T. R., Butt, A. Gundapuneni, S., Trepanier, J. S., Vespa, J. W., Said, I. M., Espinoza L., Arturo F., and Safi, F. R. (2017). *Utilizing Lab Tests to Predict Asphalt Concrete Overlay Performance*. Illinois Center for Transportation/Illinois Department of Transportation.
- Al-Qadi, I. L., Ozer, H., & Lambros, J (2019). Development of the Illinois Flexibility Index Test. *Asphalt Mixtures*, 31.
- Anderson, R. M., King, G. N., Hanson, D. I., & Blankenship, P. B. (2011). Evaluation of the relationship between asphalt binder properties and non-load related cracking. *Journal of the Association of Asphalt Paving Technologists*, 80.
- Arabani, M., & Ferdowsi, B. (2009). Evaluating the Semi-Circular Bending Test for HMA Mixtures, *IJE Transactions A: Basics*, Vol. 22, pp. 47-58.
- Arega, Z. A., Bhasin, A., & De Kesel, T. (2013). Influence of extended aging on the properties of asphalt composites produced using hot and warm mix methods. *Construction and Building Materials*, 44, 168-174.
- Bahia, H. U., Hanson, D. I., Zeng, M., Zhai, H., Khatri, M. A., and Anderson, R. M. (2001). *Characterization of modified asphalt binders in Superpave mix design*, NCHRP Report 459, Transportation Research Board.
- Baladi, G. Y., Schorsch, M., & Svasdisant, T. (2003). *Determining the causes of top-down cracks in bituminous pavements* (No. RC-1440).
- Barber, E., Al-Qadi, I. L., Giustozzi, F., & Ozer, H. (2018). Development of Machine Compliance Factor for the Illinois Flexibility Index Test (I-FIT), *Annual Meeting of the Transportation Research Board*, (No. 18-04786).
- Barry, M. K. (2016). *An analysis of impact factors on the Illinois flexibility index test* (Doctoral dissertation).
- Batioja-Alvarez, D., Lee, J., & Haddock, J. E. (2019). Understanding the Illinois Flexibility Index Test (I-FIT) using Indiana Asphalt Mixtures. *Transportation Research Record*, 0361198119841282.
- Bell, C. A., AbWahab, Y., Cristi, M. E., and Sosnovske, D. (1994a). *Selection of laboratory aging procedures for asphalt-aggregate mixtures*, SHRP-A-383, Strategic Highway Research Program.

- Bell, C. A., Sosnovske, D., & Wieder, J. A. (1994b). *Aging: binder validation* (No. SHRP-A-384). Washington, DC: Strategic Highway Research Program, National Research Council.
- Bennert, T., & Maher, A. (2008). Field and laboratory evaluation of a reflective crack interlayer in New Jersey. *Transportation Research Record*, 2084(1), 114-123.
- Bennert, T., Haas, E., & Wass, E. (2018). Indirect tensile test (IDT) to determine asphalt mixture performance indicators during quality control testing in New Jersey. *Transportation Research Record*, 2672(28), 394-403.
- Bowers, B. F., Diefenderfer, B. K., Wollenhaupt, G., Stanton, B., & Boz, I. (2019). Laboratory Properties of a Rejuvenated Cold Recycled Mixture Produced in a Conventional Asphalt Plant. In *Airfield and Highway Pavements 2019: Testing and Characterization of Pavement Materials* (pp. 100-108). Reston, VA: American Society of Civil Engineers.
- Braham, A. F., Buttlar, W. G., Clyne, T. R., Marasteanu, M. O., & Turos, M. I. (2009). The effect of long-term laboratory aging on asphalt concrete fracture energy. *Journal of the Association of Asphalt Paving Technologists*, 78.
- Brown, S., & Scholz, T. V. (2000). Development of laboratory protocols for the ageing of asphalt mixtures. In *Eurasphalt and Eurobitume Congress, 2nd, 2000, Barcelona, Spain*.
- Cao, W., Mohammad, L. N., Barghabany, P., & Cooper, S. B. (2019). Relationship between laboratory and full-scale fatigue performance of asphalt mixtures containing recycled materials. *Materials and Structures*, 52(1), 26.
- Cao, W., Mohammad, L. N., Elseifi, M., Cooper III, S. B., & Saadeh, S. (2018). Fatigue Performance Prediction of Asphalt Pavement Based on Semicircular Bending Test at Intermediate Temperature. *Journal of Materials in Civil Engineering*, 30(9), 04018219.
- Castro, A., *Evaluation of a Surface Mixture with Delta-S Rejuvenator on NCAT Pavement Test Track*, Master Thesis, Auburn University, Auburn, United States, 2017.
- Chen, C., Yin, F., Turner, P., West, R. C., & Tran, N. (2018). Selecting a Laboratory Loose Mix Aging Protocol for the NCAT Top-Down Cracking Experiment. *Transportation Research Record*, 2672(28), 359-371.
- Chen, J. S., Wang, T. J., & Lee, C. T. (2018). Evaluation of a highly-modified asphalt binder for field performance. *Construction and Building Materials*, 171, 539-545.
- Chen, X., & Solaimanian, M. (2019). Effect of Test Temperature and Displacement Rate on Semicircular Bend Test. *Journal of Materials in Civil Engineering*, 31(7), 04019104.
- Chitragar, S. F., & Singh, D. (2016). Evaluation of Fracture Resistance of Asphalt Mixes Containing Recycled Asphalt Pavement Using SCB Test. *Indian Highways*, 44(1).
- Chong, K. P., and Kuruppu, M. D. (1988). New Specimens for Mixed Mode Fracture Investigations of Geomaterials, *Engineering Fracture Mechanics*, Vol. 30, pp. 701-712.

- Cotterell, B., & Reddel, J. K. (1977). The essential work of plane stress ductile fracture. *International journal of fracture*, 13(3), 267-277.
- Dauzats, M., & Rampal, A. (1987). Mechanism of surface cracking in wearing courses. In *International Conference on the Structural Design*.
- Dauzats, M., and Linder, R. (1982). A method for the evaluation of the structural condition of pavements with thick bituminous road bases." In *Fifth international conference on the structural design of asphalt pavements*.
- De Freitas, E. F., Pereira, P., Picado-Santos, L., & Papagiannakis, A. T. (2005). Effect of construction quality, temperature, and rutting on initiation of top-down cracking. *Transportation research record*, 1929(1), 174-182.
- De La Roche, C., Van de Ven, M., Gabet, T., Dubois, V., Grenfell, J., & Porot, L. (2009, May). Development of a laboratory bituminous mixtures ageing protocol.
- Devore, J., & Farnum, N. (2005). *Applied Statistics for Engineers and Scientists (2nd Edition)*, Belmont, CA: Thomson Brooks/Cole.
- Diefenderfer, B. K., Boz, I., & Bowers, B. F. (2019). Evaluating Cracking Tests for Performance-Based Design Concept for Cold Recycled Mixtures. In *Airfield and Highway Pavements 2019: Design, Construction, Condition Evaluation, and Management of Pavements* (pp. 220-229). Reston, VA: American Society of Civil Engineers.
- Diefenderfer, S. D., & Bowers, B. F. (2019). Initial Approach to Performance (Balanced) Mix Design: The Virginia Experience. *Transportation Research Record*, 2673(2), 335-345.
- Domke, C., Davison, R., & Glover, C. (1999). Effect of oxidation pressure on asphalt hardening susceptibility. *Transportation Research Record: Journal of the Transportation Research Board*, (1661), 114-121.
- Dong, W., & Charmot, S. (2018). Proposed tests for cold recycling balanced mixture design with measured impact of varying emulsion and cement contents. *Journal of Materials in Civil Engineering*, 31(2), 04018387.
- Elseifi, M. A., Mohammad, L. N., Ying, H., & Cooper III, S. (2012). Modeling and evaluation of the cracking resistance of asphalt mixtures using the semi-circular bending test at intermediate temperatures. *Road Materials and Pavement Design*, 13(sup1), 124-139.
- Elwardany, M. D., Yousefi Rad, F., Castorena, C., & Kim, Y. R. (2017). Evaluation of asphalt mixture laboratory long-term ageing methods for performance testing and prediction. *Road Materials and Pavement Design*, 18(sup1), 28-61.
- Espinoza-Luque, A. F., Al-Qadi, I. L., & Ozer, H. (2018). Optimizing rejuvenator content in asphalt concrete to enhance its durability. *Construction and Building Materials*, 179, 642-648.

- Estakhri, C. K., Cao, R., Alvarez-Lugo, A., & Button, J. W. (2009). Production, placement, and performance evaluation of warm mix asphalt in texas. In *Material Design, Construction, Maintenance, and Testing of Pavements: Selected Papers from the 2009 GeoHunan International Conference* (pp. 1-8).
- Etheridge, R. A., Wang, Y. D., Kim, S. S., & Kim, Y. R. (2019). Evaluation of Fatigue Cracking Resistance of Asphalt Mixtures Using Apparent Damage Capacity. *Journal of Materials in Civil Engineering*, 31(11), 04019257.
- Evans, J. D. (1996). *Straightforward statistics for the behavioral sciences*, Brooks/Cole.
- Fisher, J., Graves, C., Blankenship, P., Hakimzadeh-Khoei, S., and Anderson, R. M. (2010). *Factors affecting asphalt pavement density and the effect on long term pavement performance*, KTC Report 10-05, Kentucky Transportation Center.
- Freitas, E., P. Pereira, and L. Picado-Santos. (2003). Assessment of top-down cracking causes in asphalt pavements. In *3rd International Symposium on Maintenance and Rehabilitation of Pavements and Technological Control, Guimarães, Portugal*, pp. 555-564.
- Garcia, V. M., & Miramontes, A. (2015). Understanding sources of variability of overlay test procedure. *Transportation Research Record*, 2507(1), 10-18.
- Garcia, V. M., Miramontes, A., Garibay, J., Abdallah, I., Carrasco, G., Lee, R., & Nazarian, S. (2017). Alternative methodology for assessing cracking resistance of hot mix asphalt mixtures with overlay tester. *Road Materials and Pavement Design*, 18(sup4), 388-404.
- Gerritsen, A. H., van Gurp, C. P., van der Heidi, J. J., Molenaar, A. A., and Pronk, A. C. (1987). Prediction and prevention of surface cracking in asphaltic pavements, *Sixth International Conference on Structural Design of Asphalt Pavements*, Vol. 1, pp. 378-391.
- Glover, C. J., Davison, R. R., Domke, C. H., Ruan, Y., Juristyarini, P., Knorr, D. B., & Jung, S. H. (2005). Development of a new method for assessing asphalt binder durability with field validation. Texas Dept Transport, 1872.
- Gu, F., Luo, X., West, R. C., Taylor, A. J., & Moore, N. D. (2018). Energy-based crack initiation model for load-related top-down cracking in asphalt pavement. *Construction and Building Materials*, 159, 587-597.
- Gu, F., Zhang, Y., Luo, X., Luo, R., & Lytton, R. L. (2015). Improved methodology to evaluate fracture properties of warm-mix asphalt using overlay test. *Transportation Research Record*, 2506(1), 8-18.
- Harigan, E. T., Leahy, R. B., & Youtcheff, J. S. (1994). The Superpave mix design system manual of specifications, test methods, and practices. *Strategic Highway Research Program, SHRP-A-379, National Research Council, Washington DC*.
- Harmelink, D., & Aschenbrener, T. (2003). *Extent of top-down cracking in Colorado* (No. CDOT-DTD-R-2003-7).

- Harvey, J. T., & Tsai, B. W. (1996). Effects of asphalt content and air void content on mix fatigue and stiffness. *Transportation Research Record*, 1543(1), 38-45.
- Haslett, K. E. (2018). Evaluation of Cracking Indices for Asphalt Mixtures Using SCB Tests at Different Temperatures and Loading Rates.
- Houston, W. N., Mirza, M. W., Zapata, C. E., & Raghavendra, S. (2007). Simulating the effects of hot mix asphalt aging for performance testing and pavement structural design. *NCHRP Research Results Digest*, 324.
- Houston, W. N., Mirza, M. W., Zapata, C. E., & Raghavendra, S. (2005). Environmental effects in pavement mix and structural design systems. *NCHRP, Project*, 9-23.
- Howard, I. L., & Doyle, J. D. (2015). Durability Indexes via Cantabro Testing for Unaged, Laboratory-Conditioned, and One-Year Outdoor-Aged Asphalt Concrete. In *Transportation Research Board 94th Annual Meeting* (No. 15-1366).
- Huang, B., Shu, X., & Vukosavljevic, D. (2011). Laboratory investigation of cracking resistance of hot-mix asphalt field mixtures containing screened reclaimed asphalt pavement. *Journal of Materials in Civil Engineering*, 23(11), 1535-1543.
- Huang, L., Cao, K., & Zeng, M. (2009). Evaluation of semicircular bending test for determining tensile strength and stiffness modulus of asphalt mixtures. *Journal of Testing and Evaluation*, 37(2), 122-128.
- Hugo, F., and Kennedy, T. W. (1985). Surface cracking of asphalt mixtures in southern Africa, *Journal of the Association of Asphalt Paving Technologists*, Vol. 54, pp. 454-501.
- Im, S., & Zhou, F. (2017). New and Simpler Cracking Test Method for Asphalt Mix Designs. *Transportation Research Record*, 2631(1), 1-10.
- Im, S., Karki, P., & Zhou, F. (2016). Development of new mix design method for asphalt mixtures containing RAP and rejuvenators. *Construction and Building Materials*, 115, 727-734.
- Im, S., Zhou, F., Lee, R., & Scullion, T. (2014). Impacts of rejuvenators on performance and engineering properties of asphalt mixtures containing recycled materials. *Construction and Building Materials*, 53, 596-603.
- Islam, M. R., Hossain, M. I., & Tarefder, R. A. (2015). A study of asphalt aging using Indirect Tensile Strength test. *Construction and Building Materials*, 95, 218-223.
- Jahanbakhsh, H., Hosseini, P., Nejad, F. M., & Habibi, M. (2019). Intermediate temperature fracture resistance evaluation of cement emulsified asphalt mortar. *Construction and Building Materials*, 197, 1-11.
- Jin, X., Han, R., Cui, Y., & Glover, C. J. (2011). Fast-rate-constant-rate oxidation kinetics model for asphalt binders. *Industrial & Engineering Chemistry Research*, 50(23), 13373-13379.

- Kaseer, F., Yin, F., Arámbula-Mercado, E., Martin, A. E., Daniel, J. S., & Salari, S. (2018). Development of an index to evaluate the cracking potential of asphalt mixtures using the semi-circular bending test. *Construction and Building Materials*, 167, 286-298.
- Kassem, E., Masad, E., Lytton, R., & Chowdhury, A. (2011). Influence of air voids on mechanical properties of asphalt mixtures. *Road Materials and Pavement Design*, 12(3), 493-524.
- Kim, B., Roque, R., & Birgisson, B. (2003). Effect of styrene butadiene styrene modifier on cracking resistance of asphalt mixture. *Transportation research record*, 1829(1), 8-15.
- Kim, M., Mohammad, L. N., & Elseifi, M. A. (2012). Characterization of fracture properties of asphalt mixtures as measured by semicircular bend test and indirect tension test. *Transportation Research Record*, 2296(1), 115-124.
- Kim, M., Mohammad, L. N., Phaltane, P., & Elseifi, M. A. (2017). Density and SCB measured fracture resistance of temperature segregated asphalt mixtures. *International Journal of Pavement Research and Technology*, 10(2), 112-121.
- Kim, S. S., Yang, J. J., & Etheridge, R. A. (2018). Effects of mix design variables on flexibility index of asphalt concrete mixtures. *International Journal of Pavement Engineering*, 1-6.
- Kim, Y. R., Castorena, C., Elwardany, M. D., Rad, F. Y., Underwood, S., Akshay, G., Farrar, M. J., and Glaser, R. R. (2018). Long-term aging of asphalt mixtures for performance testing and prediction. *Transportation Research Board*.
- Kök, B. V., and Çolak, H. (2011). Laboratory comparison of the crumb-rubber and SBS modified bitumen and hot mix asphalt. *Construction and Building Materials*, 25(8), 3204-3212.
- Koohi, Y., Luo, R., Lytton, R. L., & Scullion, T. (2012). New methodology to find the healing and fracture properties of asphalt mixes using overlay tester. *Journal of Materials in Civil Engineering*, 25(10), 1386-1393.
- Lee, S. H., Tam, A. B., Kim, J., & Park, D. W. (2019). Evaluation of rejuvenators based on the healing and mechanistic performance of recycled asphalt mixture. *Construction and Building Materials*, 220, 628-636.
- Li, X., and Marasteanu, M. (2004). Evaluation of the low temperature fracture resistance of asphalt mixtures using the semi circular bend test (with discussion). *Journal of the Association of Asphalt Paving Technologists*, 73.
- Li, Y. (1999). *Asphalt Pavement Fatigue Cracking Modeling*. Louisiana State University, Baton Rouge, LA.
- Ling, C., Swiertz, D., Mandal, T., Teymourpour, P., & Bahia, H. (2017). Sensitivity of the Illinois flexibility index test to mixture design factors. *Transportation Research Record*, 2631(1), 153-159.

- Little, D. N., Lytton, R. L., Williams, D., & Chen, C. W. (2001). *Microdamage healing in asphalt and asphalt concrete, Volume 1: microdamage and microdamage healing, project summary report* (No. FHWA-RD-98-141; Research report 7229). Turner-Fairbank Highway Research Center.
- Liu, M., Ferry, M. A., Davison, R. R., Glover, C. J., & Bullin, J. A. (1998). Oxygen uptake as correlated to carbonyl growth in aged asphalts and asphalt Corbett fractions. *Industrial & engineering chemistry research*, 37(12), 4669-46742.
- Luo, S., Lu, Q., & Qian, Z. (2015). Performance evaluation of epoxy modified open-graded porous asphalt concrete. *Construction and Building Materials*, 76, 97-102.
- Lytton, R. L., Uzan, J., Fernando, E. G., Roque, R., Hiltunen, D., & Stoffels, S. M. (1993). *Development and validation of performance prediction models and specifications for asphalt binders and paving mixes* (Vol. 357). Washington, DC: Strategic Highway Research Program.
- Ma, W. (2014). *Proposed Improvements to Overlay Test for Determining Cracking Resistance of Asphalt Mixtures*, Master Thesis, Auburn University, Auburn, AL.
- Ma, W., Tran, N. H., Taylor, A. J., Willis, J. R., & Robbins, M. M. (2015). Comparison of laboratory cracking test results and field performance. *Journal of the Association of Asphalt Paving Technologists*, (84).
- Malan, G. W., Straus, P. J., and Hugo, F. (1989). A field study of premature surface cracking in asphalt (with discussion). In *Association of Asphalt Paving Technologists Proc* (Vol. 58).
- Matsuno, S., and Nishizawa, T. (1992). Mechanism of Longitudinal Surface Cracking in Asphalt Pavement, *Proceedings of the 7th International Conference on Asphalt Pavements*, Vol. 2, pp. 277-291.
- Mensching, D. J., Andriescu, A., DeCarlo, C., Li, X., & Youtcheff, J. S. (2017). Effect of extended aging on asphalt materials containing re-refined engine oil bottoms. *Transportation Research Record*, 2632(1), 60-69.
- Min Baek, C. (2010). *Investigation of Top-Down Cracking Mechanisms Using the Viscoelastic Continuum Damage Finite Element Program*, Doctoral Dissertation, North Carolina State University, Raleigh, NC.
- Mogawer, W. S., Austerman, A. J., Bonaquist, R., & Roussel, M. (2011). Performance characteristics of thin-lift overlay mixtures: High reclaimed asphalt pavement content, recycled asphalt shingles, and warm-mix asphalt technology. *Transportation Research Record*, 2208(1), 17-25.
- Mogawer, W., Austerman, A., Mohammad, L., & Kutay, M. E. (2013). Evaluation of high RAP-WMA asphalt rubber mixtures. *Road Materials and Pavement Design*, 14(sup2), 129-147.

- Mogawer, W., Bennert, T., Daniel, J. S., Bonaquist, R., Austerman, A., & Booshehrian, A. (2012). Performance characteristics of plant produced high RAP mixtures. *Road Materials and Pavement Design*, 13(sup1), 183-208.
- Mohammad, L. N., Kim, M., & Elseifi, M. (2012). Characterization of asphalt mixture's fracture resistance using the semi-circular bending (SCB) test. In *7th RILEM international conference on cracking in pavements* (pp. 1-10). Springer, Dordrecht.
- Mohammad, L. N., Wu, Z., & Aglan, M. A. (2004, May). Characterization of fracture and fatigue resistance on recycled polymer-modified asphalt pavements. In *Proceedings, 5th international conference* (pp. 375-382).
- Mohammed-Ali, U., Rivera-Perez, J. J., Ozer, H., & Al-Qadi, I. L. (2019). Cracking Resistance of Sulfur Extended Asphalt Mixtures Using Illinois Flexibility Index Test. In *Airfield and Highway Pavements 2019: Testing and Characterization of Pavement Materials* (pp. 164-173). Reston, VA: American Society of Civil Engineers.
- Moore, N. (2016). *Evaluation of Laboratory Cracking Tests Related to Top-Down Cracking in Asphalt Pavements*. Auburn University, Auburn. AL.
- Morian, N., Hajj, E. Y., Glover, C. J., & Sebaaly, P. E. (2011). Oxidative aging of asphalt binders in hot-mix asphalt mixtures. *Transportation Research Record*, 2207(1), 107-116.
- Myers, L. A. (2000). *Development and propagation of surface-initiated longitudinal wheel path cracks in flexible highway pavements*, Doctoral dissertation, University of Florida, FL.
- Myers, L. A., & Roque, R. (2002). Top-down crack propagation in bituminous pavements and implications for pavement management. *Journal of the Association of Asphalt Paving Technologists*, 71.
- Myers, L. A., Roque, R., & Ruth, B. E. (1998). Mechanisms of surface-initiated longitudinal wheel path cracks in high-type bituminous pavements. *Journal of the Association of Asphalt Paving Technologists*, 67.
- Nesnas, K., & Nunn, M. (2004). A model for top-down reflection cracking in composite pavements. In *Fifth international RILEM conference on reflective cracking in pavements* (pp. 409-416). RILEM Publications SARL.
- Newcomb, D., Martin, A. E., Yin, F., Arambula, E., Park, E. S., Chowdhury, A., Brown, R., Rodezno, C., Tran, N., Coleri, E., Jones, D., Harvey, J. T., and Jones, D. (2015). *Short-term laboratory conditioning of asphalt mixtures* (No. Project 09-52).
- Nsengiyumva, G., & Kim, Y. R. (2019). Effect of Testing Configuration in Semi-Circular Bending Fracture of Asphalt Mixtures: Experiments and Statistical Analyses. *Transportation Research Record*, 0361198119839343.
- Ouyang, C., Wang, S., Zhang, Y., & Zhang, Y. (2006). Improving the aging resistance of styrene-butadiene-styrene tri-block copolymer modified asphalt by addition of antioxidants.

*Polymer degradation and stability*, 91(4), 795-804.

Ozer, H., Al-Qadi, I. L., Barber, E., Okte, E., Zhu, Z., & Wu, S. (2017). *Evaluation of I-Fit results and machine variability using MnRoad test track mixtures*. Illinois Center for Transportation/Illinois Department of Transportation.

Ozer, H., Al-Qadi, I. L., Lambros, J., El-Khatib, A., Singhvi, P., & Doll, B. (2016). Development of the fracture-based flexibility index for asphalt concrete cracking potential using modified semi-circle bending test parameters. *Construction and Building Materials*, 115, 390-401.

Ozer, H., Al-Qadi, I. L., Singhvi, P., Bausano, J., Carvalho, R., Li, X., & Gibson, N. (2018). Prediction of pavement fatigue cracking at an accelerated testing section using asphalt mixture performance tests. *International Journal of Pavement Engineering*, 19(3), 264-278.

Ozer, H., Al-Qadi, I. L., Singhvi, P., Khan, T., Rivera-Perez, J., & El-Khatib, A. (2016). Fracture Characterization of Asphalt Mixture with RAP and RAS Using the Illinois Semi-Circular Bending Test Method and Flexibility Index. *Transportation Research Record: Journal of the Transportation Research Board*, 2575, 130-137.

Partl, M. N., Bahia, H. U., Canestrari, F., De la Roche, C., Di Benedetto, H., Piber, H., & Sybilski, D. (Eds.). (2012). *Advances in interlaboratory testing and evaluation of bituminous materials: state-of-the-art report of the RILEM technical committee 206-ATB* (Vol. 9). Springer Science & Business Media.

Petersen, J. C. (2009). A review of the fundamentals of asphalt oxidation: chemical, physicochemical, physical property, and durability relationships. *Transportation Research E-Circular*, (E-C140).

Rahbar-Rastegar, R., Daniel, J. S., & Dave, E. V. (2018). Evaluation of viscoelastic and fracture properties of asphalt mixtures with long-term laboratory conditioning. *Transportation Research Record*, 2672(28), 503-513.

Reed, J. X. (2010). *Evaluation of the effects of aging on asphalt rubber* (Master's thesis, Arizona State University).

Reinke, G., Hanz, A., Herlitzka, D., Engber, S., & Ryan, M. (2015, April). Further Investigations into the Impact of REOB and Paraffinic Oils on the Performance of Bituminous Mixtures. In *Asphalt Binder ETG at National Asphalt Pavement Association Meeting, Fall River, Mass.*

Rivera-Perez, J. J. (2017). *Effect of specimen geometry and test configuration on the fracture process zone for asphalt materials*, Master Thesis, University of Illinois at Urbana-Champaign, IL.

Rivera-Perez, J., Ozer, H., & Al-Qadi, I. L. (2018). Impact of Specimen Configuration and Characteristics on Illinois Flexibility Index. *Transportation Research Record*, 2672(28), 383-393.

- Roque, R., Birgisson, B., Drakos, C., & Dietrich, B. (2004). Development and field evaluation of energy-based criteria for top-down cracking performance of hot mix asphalt (with discussion). *Journal of the Association of Asphalt Paving Technologists*, 73.
- Roque, R., Zou, J., Kim, Y. R., Baek, C., Thirunavukkarasu, S., Underwood, B. S., & Guddati, M. N. (2010). *Top-down cracking of hot-mix asphalt layers: Models for initiation and propagation* (No. NCHRP Project 1-42A).
- Rowe, G. M. (2011). Prepared Discussion for the AAPT paper by Anderson et al.: Evaluation of the Relationship between Asphalt Binder Properties and Non-Load Related Cracking. *Journal of the Association of Asphalt Paving Technologists*, 80, 649-662.
- Rowe, G. M., & Bouldin, M. G. (2000, September). Improved techniques to evaluate the fatigue resistance of asphaltic mixtures. In *2nd Eurasphalt & Eurobitume Congress Barcelona* (Vol. 2000).
- Ruan, Y., Davison, R. R., & Glover, C. J. (2003). The effect of long-term oxidation on the rheological properties of polymer modified asphalts. *Fuel*, 82(14), 1763-1773.
- Safaei, F., Castorena, C., & Kim, Y. R. (2016). Linking asphalt binder fatigue to asphalt mixture fatigue performance using viscoelastic continuum damage modeling. *Mechanics of Time-Dependent Materials*, 20(3), 299-323.
- Safaei, F., Lee, J. S., Nascimento, L. A. H. D., Hintz, C., & Kim, Y. R. (2014). Implications of warm-mix asphalt on long-term oxidative ageing and fatigue performance of asphalt binders and mixtures. *Road Materials and Pavement Design*, 15(sup1), 45-61.
- Safi, F. R., Al-Qadi, I. L., Hossain, K., & Ozer, H. (2019). Total Recycled Asphalt Mixes: Characteristics and Field Performance. *Transportation Research Record*, 0361198119849915.
- Santagata, E., Anderson, D. A., & Marasteanu, M. (1996). A rheological investigation on the physical hardening of modified asphalt binders. In *Eurasphalt & Eurobitume Congress*, Strasbourg, 7-10 May 1996. Volume 3. Paper E&E. 5.151.
- Sheehy, E. (2013). Case Study: High RAP Pilot Project, *Presentation from the New Jersey Asphalt Paving Conference*, accessed July 28, 2018, [https://cait.rutgers.edu/system/files/u10/High\\_RAP\\_NJDOT -- Sheehy.pdf](https://cait.rutgers.edu/system/files/u10/High_RAP_NJDOT_-_Sheehy.pdf).
- Shen, J., Amirkhanian, S., & Tang, B. (2007). Effects of rejuvenator on performance-based properties of rejuvenated asphalt binder and mixtures. *Construction and Building Materials*, 21(5), 958-964.
- Shen, S. H., Wen, H. F., Mohammad, L., Lund, N., Faheem, A., Zhang, W. G., & Wu, S. H. (2013). *Performance of WMA technologies: stage II-long-term field performance*. Transportation Research Board of the National Academies, Washington, DC.
- Shu, X., Huang, B., & Vukosavljevic, D. (2008). Laboratory evaluation of fatigue characteristics of recycled asphalt mixture. *Construction and Building Materials*, 22(7), 1323-1330.

- Singh, D., Chitragar, S. F., & Ashish, P. K. (2017). Comparison of moisture and fracture damage resistance of hot and warm asphalt mixes containing reclaimed pavement materials. *Construction and Building Materials*, 157, 1145-1153.
- Sirin, O., Ohiduzzaman, M., Kassem, E., & Paul, D. K. (2018). Comprehensive evaluation of long-term aging of asphalt mixtures in hot climatic condition. *Road Materials and Pavement Design*, 1-23.
- Son, S., Said, I. M., & Al-Qadi, I. L. (2019). Fracture properties of asphalt concrete under various displacement conditions and temperatures. *Construction and Building Materials*, 222, 332-341.
- Song, W., Huang, B., & Shu, X. (2018). Influence of warm-mix asphalt technology and rejuvenator on performance of asphalt mixtures containing 50% reclaimed asphalt pavement. *Journal of Cleaner Production*, 192, 191-198.
- Sun, L., Wang, Y., & Zhang, Y. (2014). Aging mechanism and effective recycling ratio of SBS modified asphalt. *Construction and Building Materials*, 70, 26-35.
- Svasdisant, T., Schorsch, M., Baladi, G., & Pinyosunun, S. (2002). Mechanistic analysis of top-down cracks in asphalt pavements. *Transportation Research Record: Journal of the Transportation Research Board*, (1809), 126-136.
- Tran, N. (2010). Evaluation of Warm Mix Asphalt with High RAP on NCAT Pavement Test Track. NCAT
- Tran, N. H., Taylor, A., & Willis, R. (2012). Effect of rejuvenator on performance properties of HMA mixtures with high RAP and RAS contents. *NCAT Report*, 12-05.
- Tran, N., Turner, P., & Shambley, J. (2016). *Enhanced Compaction to Improve Durability and Extend Pavement Service Life: A Literature Review* (No. NCAT Report No. 16-02).
- Tran, N., Xie, Z., Julian, G., Taylor, A., Willis, R., Robbins, M., & Buchanan, S. (2016). Effect of a recycling agent on the performance of high-RAP and high-RAS mixtures: Field and lab experiments. *Journal of Materials in Civil Engineering*, 29(1), 04016178.
- Turner, F. (2008). WRI Research Related to the Optimal Timing of Preventive Maintenance for Addressing Environmental Aging. Western Research Institute.
- Uhlmeier, J., Willoughby, K., Pierce, L., & Mahoney, J. (2000). Top-down cracking in Washington state asphalt concrete wearing courses. *Transportation Research Record: Journal of the Transportation Research Board*, (1730), 110-116.
- Van den Bergh, W. (2011). The effect of ageing on the fatigue and healing properties of bituminous mortars, Ph.D Dissertation, Delft University of Technology, Delft University.
- Von Quintus, H. L. (1991). *Asphalt-aggregate mixture analysis system, AAMAS* (No. 338). Transportation Research Board.

- Walubita, L. F., Faruk, A. N., Das, G., Tanvir, H. A., Zhang, J., & Scullion, T. (2012). *The overlay tester: a sensitivity study to improve repeatability and minimize variability in the test results* (No. FHWA/TX-12/0-6607-1). Texas Transportation Institute.
- Wang, J., Birgisson, B., & Roque, R. (2007). Windows-based top-down cracking design tool for Florida: using energy ratio concept. *Transportation Research Record*, 2037(1), 86-96.
- Wang, L. B., Myers, L. A., Mohammad, L. N., & Fu, Y. R. (2003). Micromechanics study on top-down cracking. *Transportation Research Record*, 1853(1), 121-133.
- West, R. C., Tran, N. H., Taylor, A. J., & Willis, R. J. (2016). Comparison of Laboratory Cracking Test Results with Field Performance of Moderate and High RAP Content Surface Mixtures on the NCAT Test Track. In *8th RILEM International Symposium on Testing and Characterization of Sustainable and Innovative Bituminous Materials* (pp. 979-991). Springer, Dordrecht.
- West, R. C., Winkle, C. V., Maghsoodloo, S., & Dixon, S. (2017). Relationships between simple asphalt mixture cracking tests using Ndesign specimens and fatigue cracking at FHWA's accelerated loading facility. *Road Materials and Pavement Design*, 18(sup4), 428-446.
- West, R., Timm, D., Powell, B., Heitzman, M., Tran, N., Rodezno, C., ... & Vargas, A. (2019). *Phase VI (2015-2017) NCAT Test Track Findings* (No. NCAT Report 18-04).
- Willis, J. R., Taylor, A. J., & Nash, T. M. (2016). Laboratory and Field Evaluation of Florida Mixtures at the 2012 National Center for Asphalt Technology Pavement Test Track. *Transportation Research Record*, 2590(1), 65-73.
- Willis, R., Timm, D., West, R., Powell, B., Robbins, M., Taylor, A., Smit, A., Tran, N., Heitzman, M., Bianchini, A. (2009). Phase III NCAT test track findings. *NCAT report*, 09-08.
- Wu, S., & Muhunthan, B. (2018). A mechanistic-empirical model for predicting top-down fatigue cracking in an asphalt pavement overlay. *Road Materials and Pavement Design*, 1-32.
- Wu, S., Al-Qadi, I. L., Lippert, D. L., Ozer, H., Luque, A. F. E., & Safi, F. R. (2017). Early-age performance characterization of hot-mix asphalt overlay with varying amounts of asphalt binder replacement. *Construction and Building Materials*, 153, 294-306.
- Wu, Z., Mohammad, L. N., Wang, L. B., & Mull, M. A. (2005). Fracture resistance characterization of superpave mixtures using the semi-circular bending test. *Journal of ASTM International*, 2(3), 1-15.
- Xie, Z., Tran, N., Julian, G., Taylor, A., & Blackburn, L. D. (2017). Performance of asphalt mixtures with high recycled contents using rejuvenators and warm-mix additive: field and lab experiments. *Journal of Materials in Civil Engineering*, 29(10), 04017190.
- Yildirim, Y. (2007). Polymer modified asphalt binders. *Construction and Building Materials*, 21(1), 66-72.

- Yin, F., Kaseer, F., Arámbula-Mercado, E., & Epps Martin, A. (2017c). Characterising the long-term rejuvenating effectiveness of recycling agents on asphalt blends and mixtures with high RAP and RAS contents. *Road Materials and Pavement Design*, 18(sup4), 273-292.
- Yin, F., Martin, A. E., Arámbula-Mercado, E., & Newcomb, D. (2017a). Characterization of non-uniform field aging in asphalt pavements. *Construction and Building Materials*, 153, 607-615.
- Yin, F., West, R. C., Director, P. E., Xie, Z., Taylor, A., & Julian, G. (2017b). *Effects of Loading Rate and Mix Reheating on Indirect Tensile  $N_{flex}$  Factor and Semi-Circular Bend J-integral Test Results to Assess the Cracking Resistance of Asphalt Mixtures* (No. NCAT Report 17-09).
- Zhang, Z., Roque, R., Birgisson, B., & Sangpetngam, B. (2001). Identification and verification of a suitable crack growth law (with discussion). *Journal of the Association of Asphalt Paving Technologists*, 70.
- Zhao, S., Huang, B., Shu, X., Jia, X., & Woods, M. (2012). Laboratory performance evaluation of warm-mix asphalt containing high percentages of reclaimed asphalt pavement. *Transportation Research Record*, 2294(1), 98-105.
- Zhou, F., & Scullion, T. (2003). *Upgraded overlay tester and its application to characterize reflection cracking resistance of asphalt mixtures* (No. FHWA/TX-04/0-4467-1). Texas Transportation Institute, Texas A & M University System.
- Zhou, F., & Scullion, T. (2005). *Overlay tester: A rapid performance related crack resistance test* (Vol. 7). Texas Transportation Institute, Texas A & M University System.
- Zhou, F., Hu, S., Chen, D. H., & Scullion, T. (2007). Overlay tester: simple performance test for fatigue cracking. *Transportation Research Record*, 2001(1), 1-8.
- Zhou, F., Im, S., & Hu, S (2019). Development and Validation of the IDEAL Cracking Test. *Asphalt Mixtures*, 1.
- Zhou, F., Im, S., Hu, S., Newcomb, D., & Scullion, T. (2017a). Selection and preliminary evaluation of laboratory cracking tests for routine asphalt mix designs. *Road Materials and Pavement Design*, 18(sup1), 62-86.
- Zhou, F., Im, S., Sun, L., & Scullion, T. (2017b). Development of an IDEAL cracking test for asphalt mix design and QC/QA. *Road Materials and Pavement Design*, 18(sup4), 405-427.
- Zhou, F., Newcomb, D., Gurganus, C., Banihashemrad, S., Park, E. S., Sakhaeifar, M., & Lytton, R. L. (2016). Experimental design for field validation of laboratory tests to assess cracking resistance of asphalt mixtures. *NCHRP Project*, 9-57.
- Zhou, F., Scullion, T., Nady, R. M., Mahboub, K., Scullion, T., McGinnis, R., Marasteanu, M., Roque, R., & Dunning, R. (2005). Overlay tester: a simple performance test for thermal reflective cracking. In *Asphalt Paving Technology: Association of Asphalt Paving Technologists-*

*Proceedings of the Technical Sessions* (Vol. 74, pp. 443-483). Association of Asphalt Paving Technologist.

Zhu, Z., Singhvi, P., Espinoza-Luque, A. F., Ozer, H., & Al-Qadi, I. L. (2019). Influence of mix design parameters on asphalt concrete aging rate using I-FIT specimens. *Construction and Building Materials*, 200, 181-187.

Zou, J., & Roque, R. (2011). Top-down cracking: Enhanced performance model and improved understanding of mechanisms. *Asphalt paving technology*, (80), 255-288.